March 2018

Synthesis of Novel Zwitterionic Polymers: From Functional Surfactants to Therapeutics

Matthew Skinner

SYNTHESIS OF NOVEL ZWITTERIONIC POLYMERS: FROM FUNCTIONAL SURFACTANTS TO THERAPEUTICS

A Dissertation Presented

by

MATTHEW W. SKINNER

Submitted to the Graduate School of the
University of Massachusetts Amherst in partial fulfillment
of the requirements for the degree of

DOCTOR OF PHILOSOPHY

February 2018

Polymer Science and Engineering

SYNTHESIS OF NOVEL ZWITTERIONIC POLYMERS:
FROM FUNCTIONAL SURFACTANTS TO THERAPEUTICS

A Dissertation Presented

by

MATTHEW W. SKINNER

Approved as to style and content by:

_____
Todd Emrick, Chair

_____
Ryan Hayward, Member

_____
Sarah Perry, Member

_____
E. Bryan Coughlin, Department Head
Polymer Science and Engineering

DEDICATION

To my loving, patient, and devoted parents.

ACKNOWLEDGMENTS

I would like to thank my thesis advisor, Todd Emrick, for his guidance and support throughout my doctoral research, and for continuously challenging me to develop a comprehensive understanding of organic and polymer chemistry, an organized and creative approach to solving research problems, and an impactful rhetoric for communicating scientific findings. I would also like to thank the members of my committee, Ryan Hayward and Sarah Perry, for their guidance and advice, as well as for pushing me to thoroughly probe and comprehend the physical properties and behavior of materials synthesized throughout my doctoral research. This guidance has enriched my dissertation, and has given me an understanding of polymer physics which will continue to serve me in future research endeavors. I also wish to express my gratitude to Bryan Coughlin for his mentorship and support throughout this process.

I wish to acknowledge the funding sources which supported the research comprising this dissertation, including the National Science Foundation (NSF) Materials Research Science & Engineering Center (MRSEC) on Polymers (DMR-0820506), the National Institutes of Health (NIH) under award number R21 CA167674, and the U.S. Department of Education Graduate Assistance in Areas of National Need (GAANN) under award number P200A150276.

I am grateful to Samantha McRae Page, Ryan Selhorst, Sarah Ward, Dr. Banishree Saha, Dr. Kaitlyn Wong, Dr. Maria Mora, Dr. Giovanna Crisi, Dr. Richard Arenas, Dr. Sallie Schneider, and Yalin Liu for collaborating and enhancing my dissertation research. I also thank the faculty and staff of the Polymer Science and Engineering Department for

supporting and enriching my research, as well as for providing invaluable guidance throughout my graduate studies.

Thank you to the members of the Emrick group for providing constructive criticism and inciteful evaluation of my work, as well as for establishing an encouraging, engaging, and entertaining research environment. I would like to acknowledge members of The Drunken Chickens softball team and the memories we shared; summer softball was an experience I looked forward to every year. I am especially grateful for friends and colleagues, including Marcus Cole, Ryan Selhorst, Sarah Ward, Rachel Letteri, Samantha McRae Page, Zak Page, Stephen Rosa, Stephen Strassburgh, Adam Hauser, Ned Burnett, Ari Shapell, Adam Merzel, Andy Webb, John Brody, and Chris Adams. I also wish to express my gratitude to my parents, Kevin and Susan Skinner, my brother Paul Skinner, and my sister-in-law Stephanie Skinner. Your love, support, and willingness to listen was critical to me enduring, enjoying, and ultimately completing this dissertation. I am especially grateful to my parents for helping me realize the importance of scientific pursuits. I wish to acknowledge and thank Finn for greeting me with a smiling face every day and always cheering me up after long days in the lab; you are a blessing. Finally, I would like to thank Katherine Brooks. Thank you for providing me the unwavering love, support, and friendship which allowed me to complete my dissertation and helped me discover a new sense of pride and confidence.

ABSTRACT

SYNTHESIS OF NOVEL ZWITTERIONIC POLYMERS:
FROM FUNCTIONAL SURFACTANTS TO THERAPEUTICS

FEBRUARY 2018

MATTHEW W. SKINNER, B.A., WASHINGTON UNIVERSITY IN ST. LOUIS

M.A., UNIVERSITY OF MASSACHUSETTS AMHERST

Ph.D., UNIVERSITY OF MASSACHUSETTS AMHERST

Directed by: Professor Todd Emrick

This dissertation describes the synthesis, characterization, and investigation of novel zwitterionic polymers containing phosphorylcholine (PC), sulfobetaine (SB), and functional choline phosphate (CP) zwitterions for use as surfactants, self-assembled nanomaterials, and therapeutics. Facile, reproducible, and modular chemistries were utilized for incorporating zwitterions into a range of polymer backbones, and strategies were developed for overcoming difficult challenges encountered in zwitterionic polymer synthesis, especially related to the varying solubility of zwitterions, hydrophobic polymers, and functional comonomers. Synthetic strategies utilized in this work give access to well-defined materials with narrow molecular weight distributions, tunable compositions and architectures, and versatile chemical functionality.

Chapter 2 describes the synthesis of water-soluble PC- and SB-functionalized siloxane polymers. PC- and SB-siloxane homopolymers and block copolymers were synthesized using thiol-ene ‘click’ chemistry, and their assembly in water and at oil-water interfaces was investigated.

Chapter 3 describes the preparation of zwitterionic block copolymer analogues of commercial Pluronic® surfactants. PC-containing triblock copolymers were prepared with tunable zwitterion content (5-47 mole percent) and relatively narrow molecular weight distributions. These block copolymer amphiphiles readily formed nanoparticles in water and served as novel surfactants. Through the copolymerization of PC- and CP-methacrylate monomers, functional mimics of conventional Pluronic structures became amenable to crosslinking and the successful synthesis of nanomaterials and robust gels.

Chapter 4 presents the *in vivo* evaluation of poly(2-methacryloyloxyethyl phosphorylcholine)-doxorubicin (polyMPC-Dox) prodrugs for treating human ovarian tumors (SKOV-3). In human ovarian tumor-bearing mice, polyMPC-Dox prodrugs with an approximate Dox loading of 19 weight percent accumulated in tumor tissue at twice the level of free Dox, and animals treated with polyMPC-Dox exhibited enhanced survival and retarded tumor growth compared to conventional Dox treatment.

Finally, Chapter 5 augments the polyMPC prodrug concept with the development of polymer-temozolomide (TMZ) conjugates intended for glioblastoma treatment. PolyMPC-TMZ prodrugs were prepared by the controlled free radical copolymerization of MPC and novel TMZ-methacrylate monomers, affording copolymers with random and block architectures. Polymer conjugation significantly improved the solution stability of TMZ, and the antitumor activity of polyMPC-TMZ prodrugs was demonstrated in TMZ-sensitive (U87MG) and TMZ-resistant (T98G) glioblastoma cell lines. The impact of drug loading, polymer architecture, and adjuvant co-delivery on the cytotoxicity of polyMPC-TMZ conjugates was investigated.

TABLE OF CONTENTS

Page

LIST OF TABLES

Table Page

LIST OF FIGURES

Figure Page

LIST OF SCHEMES

Scheme Page

CHAPTER 1

POLYMER ZWITTERIONS: SYNTHESIS, SOLUTION PROPERTIES, AND THEIR USE IN SURFACTANTS AND THERAPEUTICS

1.1 Introduction

Polymer zwitterions are hydrophilic polymers utilized in numerous applications, including as commercial surfactants and detergents,[1,2] biocompatible surfaces and matrices,[3-5] antifouling coatings,[6-9] and scaffolds or encapsulants for sustained drug delivery.[10-14] Composed of covalently tethered anion-cation pairs (*i.e.* zwitterions) distributed as pendent groups along or within polymer backbones, zwitterionic polymers are charge-neutral materials which demonstrate excellent aqueous dispersibility, extensive

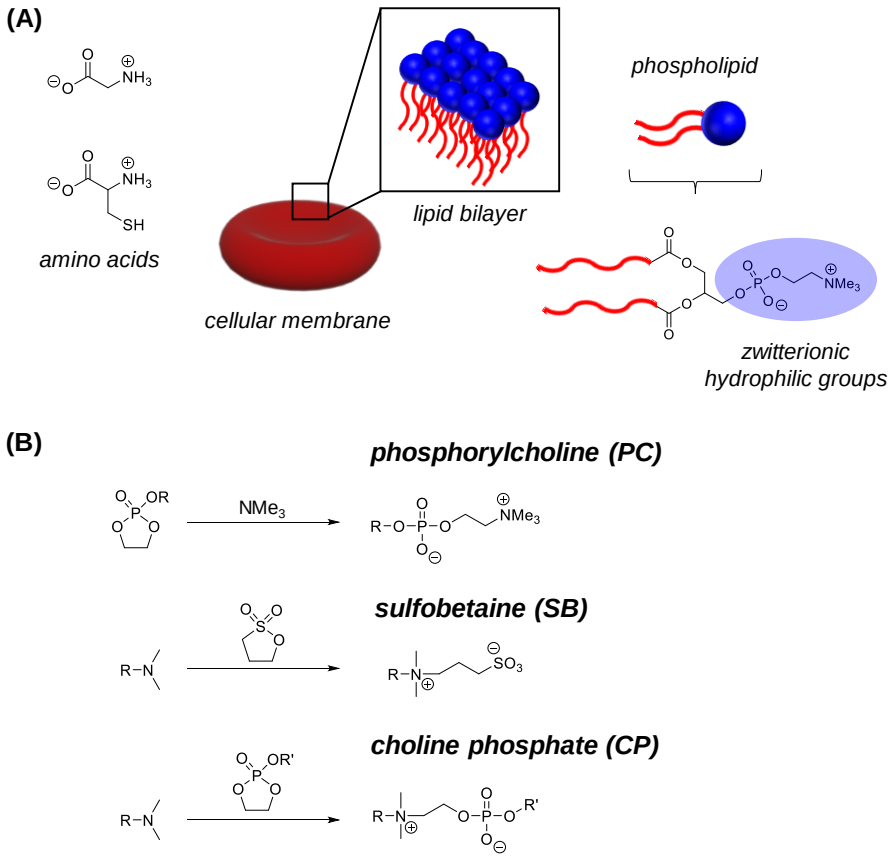

Figure 1.1: (A) Examples of zwitterions found in Nature; (B) synthesis of phosphorylcholine (PC), sulfobetaine (SB), and choline phosphate (CP) zwitterions.

hydration in water,[15-18] and nonfouling properties.[6-9] Additionally, several examples are biomimetic and biocompatible.[3-5] As depicted in Figure 1.1A, zwitterions are pervasive throughout Nature: free amino acids exist as zwitterions at physiological pH, and many of the polar head groups of phospholipids which comprise cellular membranes are zwitterionic moieties.[19] Drawing inspiration from these natural examples, organic and polymer chemists have generated a diverse library of synthetic zwitterionic functionality, preparing analogues composed of varying cationic (*e.g.*, alkylammonium, pyridinium, sulfonium, *etc.*)[20,21] and anionic (*e.g.*, phosphate, sulfonate, or carboxylate)[9] chemical groups. This thesis focuses on three classes of zwitterions—phosphorylcholine (PC), sulfobetaine (SB), and choline phosphate (CP) zwitterions—typically prepared by alkyamine-mediated ring-opening of phosphorous- and sulfur-containing heterocycles (Figure 1.1B).

PC- and SB-functionalized polymers prepared from 2-methacryloyloxyethyl phosphorylcholine (MPC)[22,23] and sulfobetaine methacrylate (SBMA), respectively, represent two of the most extensively utilized and studied zwitterionic polymeric variants.[24,25] As shown in Figure 1.2A, polyMPC and polySBMA are readily prepared using conventional free radical polymerization chemistries, as well as using controlled polymerization techniques (*e.g.*, atom transfer radical polymerization or reversible addition-fragmentation chain transfer)[26-29] which give access to PC- and SB-polymers with narrow molecular weight distributions, functional end groups, and complex architectures. In general, polyMPC-based materials are biocompatible,[3,8,30] resist protein and bacterial adsorption,[6,7,31] and demonstrate excellent aqueous solubility which is unaffected by temperature or salt.[18] PolySBMA, on the other hand, exhibits upper critical solution

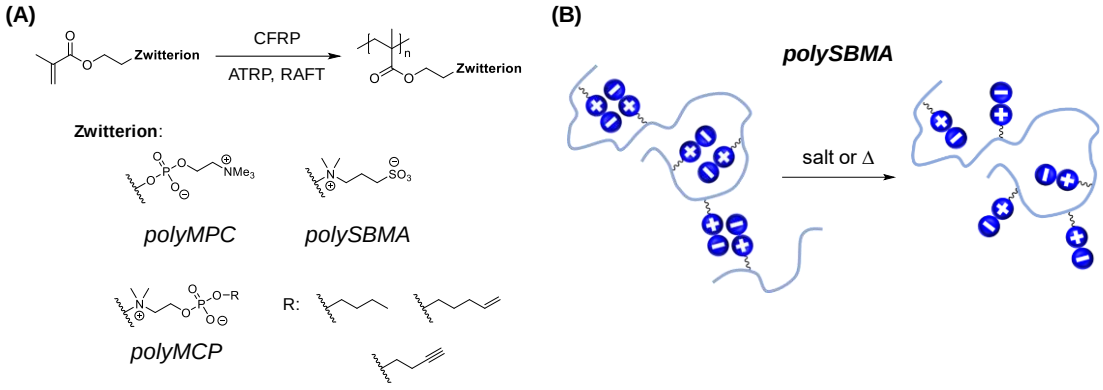

Figure 1.2: (A) Chemical structures of PC-, SB-, and CP-methacrylate monomers and their respective polymers synthesized using various free radical polymerization chemistries; (B) depiction of the salt- and temperature-responsive solubility of polySBMA in water.

temperature miscibility in water and salt-responsive solublity due to intra- and interpolymer Coulombic interactions of pendent SB zwitterions (Figure 1.2B), which are broken upon addition of salt or by increasing solution temperature.[25,32] As a result of this unique aqueous solubility, polySBMA is widely investigated for the synthesis of materials which exhibit responsive assembly in water and at interfaces.[33-35] Methacrylate polymers bearing CP moieties, 'reverse' PC-zwitterions containing reactive chemical handles embedded directly within the zwitterionic functionality (Figure 1.2A), have emerged as functional zwitterionic materials readily synthesized using controlled polymerization techniques and amenable to post-polymerization modification *via* facile and reproducible 'click' chemistries.[36,37] As polyMCP variants have been shown to exhibit biocompatiblity comparable to polyMPC in human cells,[36] these reverse zwitterionic materials hold great promise for drug delivery applications as implantable hydrogels or injectable polymer-drug conjugates.

Owing to the excellent dispersibility of zwitterions in aqueous solutions, zwitterionic functionality is useful as the hydrophilic component of polymer amphiphiles.

Of particular interest is the preparation of well-defined zwitterionic amphiphilic polymers using controlled polymerization methodologies, as these techniques give access to materials with tunable amphiphilicity (*i.e.*, hydrophilic-lipophilic balance), molecular weight, and architecture (*i.e.*, random *vs.* block copolymers). Notable examples which demonstrate the versatility of zwitterionic polymer amphiphiles include work by the Armes and Ishihara groups describing the preparation of novel SB- and PC-functionalized block copolymer surfactants for interfacial stabilization, aqueous self-assembly, and surface modification.[38-41] Armes and workers reported the reversible addition-fragmentation chain transfer (RAFT) polymerization-induced self-assembly of polySBMA-poly(2-hydroxypropyl methacrylate) block copolymer amphiphiles in water.[40] By varying the molecular weight of hydrophobic poly(2-hydroxypropyl methacrylate) polymerized from a hydrophilic polySBMA macro-chain transfer agent (macro-CTA), water-dispersible self-assembled nanoparticles with micellar, worm-like, or vesicular morphologies were readily accessed. Ishihara *et al*. reported the synthesis of polyMPC-poly(dimethylsiloxane)-polyMPC triblock copolymers by macro-initiated atom transfer radical polymerization (ATRP) for the modification of hydrophobic poly(dimethylsiloxane) substrates and preparation of antifouling coatings.[41]

Chapters 2 and 3 of this thesis aim to contribute to the field of zwitterionic polymer amphiphiles through the synthesis and investigation of novel, versatile, and functional surfactants bearing pendent PC, SB, and CP zwitterions. Critical to the preparation of zwitterionic polymer amphiphiles with tunable compositions are chemistries which allow for the modification and controlled polymerization of zwitterionic methacrylate monomers. As such, this thesis takes advantage of facile coupling reactions between thiol nucleophiles

Scheme 1.1: Modification of unsaturated chemical functionality using thiol-Michael addition and thiol-ene/yne 'click' chemistries.

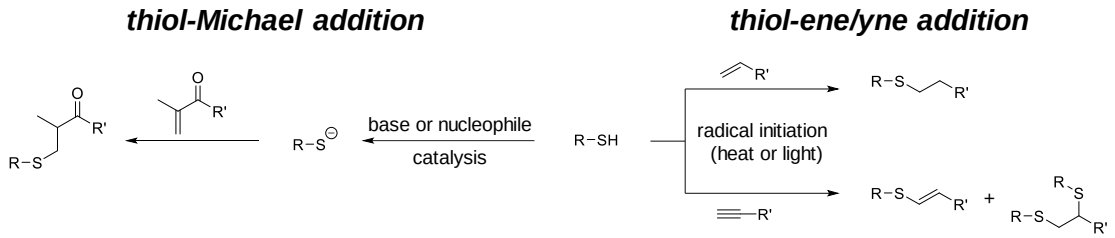

and unsaturated chemical functionality (*i.e.*, thiol-Michael addition, thiol-ene addition, and thiol-yne addition), as well as a controlled free radical polymerization methodology (*i.e.*, ATRP). Thiol-Michael and thiol-ene/yne addition chemistries, depicted in Scheme 1.1, allow for the efficient modification of small molecules and polymers *via* the reaction of thiol groups with α,β-unsaturated carbonyl (thiol-Michael addition) or alkene/alkyne (thiol-ene/yne) moieties.[42-44]

ATRP is a living free radical polymerization methodology discovered simultaneously by Mitsuo Sawamoto[45] and Krzysztof Matyjaszewski[46] which allows for the controlled polymerization of functional vinyl monomers (*i.e.*, (meth)acrylates, (meth)acrylamides, and styrenes) and the preparation of polymeric materials with tunable molecular weight, narrow molecular weight distributions, well-defined polymer end groups, and diverse architectures.[47,48] As shown by the mechanism in Figure 1.3, ATRP is initiated by the reversible homolytic cleavage of an organic halide in the presence of a transition metal catalyst. Suitable organic halide initiating species include alkyl chloride, aryl chloride, alkyl bromide, and aryl bromide species, with cuprous halide salts most commonly employed as catalysts. Upon electron transfer and formation of a carbon-centered radical, the initiating R species adds across the unsaturated functionality of a

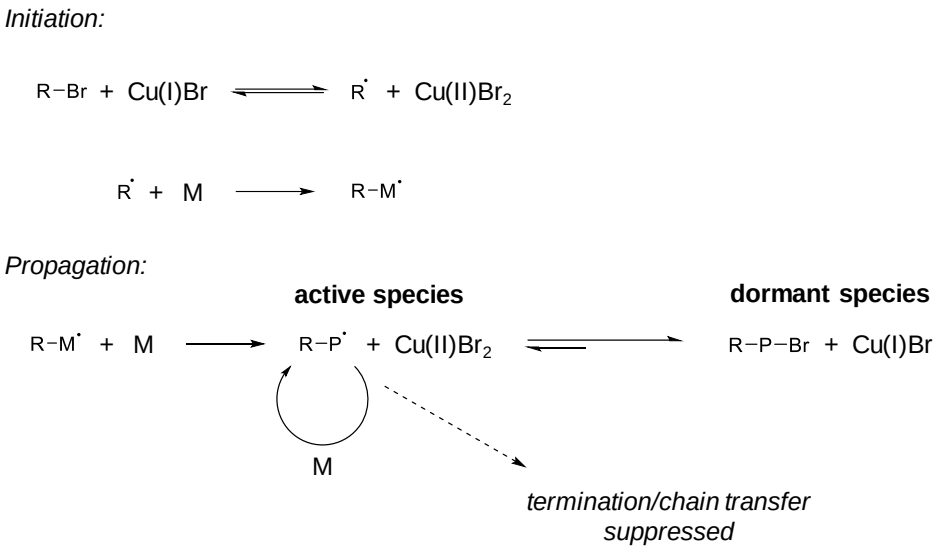

Figure 1.3: Mechanism for the polymerization of vinyl monomers (M) by atom transfer radical polymerization (ATRP).

suitable vinyl monomer, with further monomer propagation ensuing. Terminating and chain transfer reactions, which increase the breadth of the molecular weight distribution of the resulting polymer product, are sufficiently suppressed by a redox equilibrium, established between propagating polymer chains and the oxidized cuprous catalyst, which predominantly favors the dormant species. ATRP of zwitterionic PC-, SB-, and CP-methacrylate monomers has previously been reported in protic solvents (*i.e.*, water, methanol, and 2,2,2-trifluoroethanol),[26,28,36,37] yielding well-defined zwitterionic homopolymers, random copolymers, and block copolymers. Importantly, ATRP allows for the polymerization of vinyl monomers from the backbones or chain ends of halide-functionalized materials (*i.e.*, macro-initiated ATRP), allowing for the synthesis of block copolymer amphiphiles using commercial pre-polymers.[38,41,49,50]

Chapters 4 and 5 of this thesis seek to develop the polymer zwitterion concept further, transitioning from the synthesis and investigation of fundamental materials to the preparation and evaluation of zwitterionic polymers as injectable scaffolds for improving

the chemotherapeutic treatment of solid tumors. While small molecule chemotherapeutics are essential for treating tumors, their efficacy is often hampered by rapid clearance upon administration and non-specific tissue accumulation. The former behavior necessitates recurring dosing regimens to maintain efficacious drug concentrations, while the latter often results in undesired side effects that can impede treatment and reduce patient compliance. Additionally, the hydrophobicity of many chemotherapeutics renders them poorly soluble in physiological solutions, reducing bioavailability and often requiring the use of potentially dangerous excipients.[51-53] Polymer-drug conjugation, which affords soluble prodrugs that exhibit extended *in vivo* circulation, reduced toxicity, and enhanced selectively for tumoral tissue,[54-57] offers a facile solution for augmenting chemotherapy. Poly(ethylene glycol) (PEG) is a hydrophilic polymer often investigated for preparing polymer-drug conjugates,[58-60] and currently utilized in numerous FDA-approved injectable polymer therapeutics.[61-64] Although modification of hydrophobic drugs with PEG (*i.e.*, PEGylation) affords conjugates with enhanced hydrodynamic diameter and improved water-solubility, drug loading is inherently limited, with conjugation only feasible at the chain-end hydroxyl groups. Moreover, recent clinical evaluations suggest PEGylated therapeutics can illicit undesired immunogenicity, leading to a reduction in the efficacy of PEG-based polymer therapeutics.[65-68] As such, safe, non-immunogenic alternatives are desired for developing new polymer-based chemotherapeutics. PolyMPC has emerged as a hydrophilic and biocompatible polymer scaffold well-suited for the preparation of polymer-chemotherapeutic conjugates.[10-12,14,69,70] In addition to its extreme hydrophilicity, which allows for the solubilization of drugs with very poor aqueous solubility at high drug loadings, polyMPC is readily prepared with narrow molecular weight distributions and

tunable functionality using controlled free radical polymerization techniques.[10,26,27,69,70] The tolerance of these polymerization methodologies to various chemical functionalities allows for the preparation of zwitterionic polymer prodrugs by post-polymerization conjugation, or through direct RAFT copolymerization of chemotherapeutic-functionalized monomers.

RAFT is a metal-free living polymerization technique which allows for the polymerization of vinyl-based monomers under free radical conditions.[71,72] Additionally, this methodology is well-suited for generating polymer zwitterions with narrow molecular weight distributions and diverse chemical functionality through copolymerization.[27,29,35-37,70] The mechanism of a typical RAFT polymerization, initiated using a range of commercial free radical initiators under thermal or photolytic conditions, is depicted in Figure 1.4. Critical to the synthesis of polymers with narrow molecular weight distributions is the inclusion of a thiocarbonylthio chain transfer agent (CTA) which establishes an equilibrium between dormant and active polymer chains through reversible chain transfer. The new carbon-centered radical formed through chain transfer initiates a

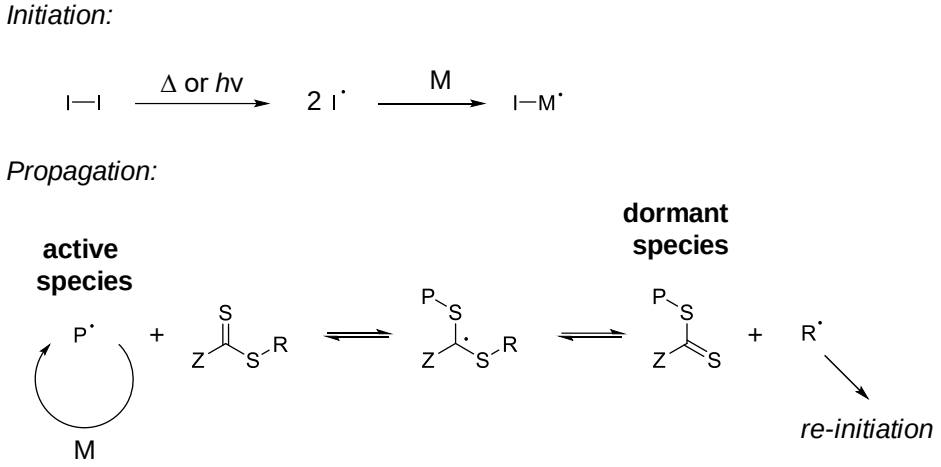

Figure 1.4: Mechanism for the polymerization of vinyl monomers (M) by RAFT methodology.

new polymer chain, and the chain transfer equilibrium suppresses undesired termination events. As RAFT methodology is amenable to polymerizing monomers with a diverse set of chemical functional groups and is conducted without the use of metal catalysts which can be toxic and difficult to remove, RAFT is well-suited for the preparation of polymeric materials intended for *in vivo* applications.

1.2 Thesis Outline

This thesis describes the synthesis, characterization, and application of zwitterionic polymers as novel and functional amphiphiles for aqueous assembly, interfacial stabilization, and nanomaterials synthesis, as well as the development of a zwitterionic polymer prodrug platform for treating ovarian and brain tumors. A particular focus of this work is the design and implementation of facile and modular synthetic strategies which allow zwitterions to be incorporated into diverse polymer compositions and architectures.

Chapter 2 describes the preparation of a series of water-soluble siloxane polymers with pendent PC and SB zwitterions using thiol-ene 'click' chemistry (Journal of Polymer Science Part A: Polymer Chemistry, 2016).[74] Specifically, well-defined vinyl-substituted siloxane homopolymers and block copolymers were functionalized with small molecule zwitterionic thiols at room temperature. Rapid and quantitative substitution of the pendent vinyl groups was achieved, and zwitterionic polysiloxanes of narrow molecular weight distribution were obtained. The PC- and SB-substituted polymers were found to be readily soluble in pure, salt-free water. Critical micelle concentrations (CMCs) of these polymers in water were measured using a pyrene fluorescence probe, with CMC values estimated to be < 0.01 g/L. Polymer aggregates were studied by dynamic light scattering, and micelles

generated from the PC block copolymers were visualized, after drying, by transmission electron microscopy. Aqueous solutions of these zwitterionic polysiloxanes significantly reduced the oil-water interfacial surface tension, functioning as novel polymer amphiphiles that lend stability to oil-in-water emulsions.

Chapter 3 describes novel zwitterionic polymer amphiphiles with chemical structures mimicking Pluronic® block copolymers prepared by ATRP of PC- or CP-methacrylate monomers using a difunctional poly(propylene oxide) (PPO) macroinitiator. Well-defined, water-dispersible zwitterionic triblock copolymers, or 'zwitteronics', were prepared with PC content ranging from 5 to 47 mole percent and composition-independent surfactant properties in water which deviate from the properties of conventional Pluronic amphiphiles. These PC-zwitteronics assembled into nanoparticles in water, with tunable sizes and critical aggregation concentrations based on their hydrophilic-lipophilic balance. Owing to the lower critical solution temperature miscibility of the hydrophobic PPO block in water, PC-zwitteronics exhibited thermoreversible aqueous solubility tuned by block copolymer composition. The versatility of this approach was demonstrated by embedding chemical functionality, in the form of alkyne groups, directly into the zwitterionic moieties. These alkynes proved ideal for crosslinking the zwitteronic nanoparticles and generating nanoparticle-crosslinked hydrogels with tunable elastic properties using UV-initiated thiol-yne 'click' chemistry.

Chapter 4 describes the evaluation of a polymer prodrug composed of doxorubicin (Dox) conjugated covalently to polyMPC for the treatment of human ovarian tumors in animals (Molecular Pharmaceutics, 2016).[12] This work builds upon previous studies which describe the synthesis of polyMPC-Dox prodrugs and their utility for treating solid

tumors.[10-12] PolyMPC-Dox prodrugs were prepared using facile conjugation chemistry to yield conjugates soluble in water and injectable saline, with a Dox weight percent loading of ~19%. Toxicity evaluation showed that polyMPC was well-tolerated in mice at doses up to 800 mg/kg, confirming the biocompatibility of the polymer carrier at high concentration. Additionally, the polyMPC-Dox prodrug was well-tolerated in animals at a Dox equivalent dose of 10 mg/kg, greater than twice the maximum tolerated dose of free Dox (~4 mg/kg) in the same mouse strain. In a human ovarian tumor model (SKOV-3), polyMPC-Dox accumulated in tumors at twice the level of free Dox, with no additional off-target organ uptake, a result of improved pharmacokinetics afforded by the prodrug and passive targeting attributed to an enhanced permeability and retention effect. When administered to human ovarian tumor-bearing mice using a recurring dosing regimen comparable to that used clinically, polyMPC-Dox significantly retarded tumor growth relative to treatment with free Dox. Moreover, animals treated with multiple doses of polyMPC-Dox (eight total doses) exhibited enhanced survival, with a notably reduced incidence of toxicity or adverse events relative to mice treated with free Dox. These *in vivo* results demonstrate advantages of treating human ovarian tumors with polyMPC-Dox, including reduced systemic toxicity, improved drug accumulation in tumors, and enhanced therapeutic efficacy.

Finally, Chapter 5 expands the polyMPC prodrug platform through the development of zwitterionic polymer prodrugs for treating glioblastoma, a highly aggressive malignant brain tumor. A new and versatile synthesis was developed to produce polymer prodrugs composed of polyMPC conjugated covalently to the glioblastoma drug temozolomide (TMZ) (ACS Macro Letters, 2017).[75] Through the development of a novel

TMZ-substituted methacrylate, and its subsequent RAFT copolymerization with MPC or chain-extension from a polyMPC macro-CTA, water-dispersible polyMPC-TMZ conjugates with random and block copolymer architectures were realized with TMZ loadings of approximately 16-50 and 14-35 mole percent, respectively. After polymerization, the structural fidelity of conjugated TMZ, a drug acutely susceptible to undesired hydrolytic decomposition, was confirmed using NMR and UV-Vis spectroscopy, while molecular weight estimation by gel permeation chromatography confirmed the preparation of polymer-TMZ conjugates with narrow molecular weight distributions. The fundamental solution properties of the polyMPC-TMZ copolymers, including their critical aggregation concentrations and hydrodynamic diameters in phosphate-buffered saline, were measured using dynamic light scattering, and nanoparticles formed from the block copolymer prodrugs were visualized using cyrogenic transmission electron microscopy. Using UV-Vis spectroscopy, improvement in the aqueous stability of TMZ afforded through polymer conjugation was investigated, specifically examining effects of drug loading and polymer architecture. The antitumor activity of these novel polyMPC-TMZ prodrugs was assessed in chemosensitive (U87MG) and chemoresistant (T98G) glioblastoma cell lines, and the impact of augmenting polyMPC-TMZ efficacy through co-delivery of a glioblastoma-sensitizing adjuvant was examined. These studies demonstrate that prodrugs with a block copolymer architecture afford the most significant improvements in TMZ stability and anti-glioblastoma efficacy. This synthetic design opens new possibilities for formulating numerous types of polymeric TMZ-based structures, and demonstrates the viability of systemically treating glioblastoma tumors using injectable polyMPC-TMZ prodrugs.

1.3 References

1. FernLey, G. W. Zwitterionic Surfactants: Structure and Performance. *J. Am. Oil Chem. Soc.* **1978**, *55*, 98-103.

2. Dahanayake, M.; Rosen, M. J. *Structure/Performance Relationships in Surfactants*; **1984**; 49-59.

3. Whelan, D. M.; van der Giessen, W. J.; Krabbendam, S. C.; van Vliet, E. A.; Verdouw, P. D.; Serruys, P. W.; van Beusekom, H. M. M. Biocompatibility of Phosphorylcholine Coated Stents in Normal Porcine Coronary Arteries. *Heart* **2000**, *83*, 338-345.

4. Ishihara, K. Highly Lubricated Polymer Interfaces for Advanced Artificial Hip Joints Through Biomimetic Design. *Polymer J.* **2015**, *47*, 585-597.

5. Zhang, Z.; Chao, T.; Liu, L.; Cheng, G.; Ratner, B. D.; Jiang, S. Zwitterionic Hydrogels: An In Vivo Implantation Study. *J. Biomater. Sci. Polym. Ed.* **2009**, *20*, 1845-1859.

6. Ye, S-H.; Johnson, C. A.; Woolley, J. R.; Murata, H.; Gamble, L. J.; Ishihara, K.; Wagner, W. R. Simple Surface Modification of a Titanium Alloy with Silanated Zwitterionic Phosphorylcholine or Sulfobetaine Modifiers to Reduce Thrombogenicity. *Colloids Surf. B Biointerfaces* **2010**, *79*, 357-364.

7. Ishihara, K.; Nomura, H.; Mihara, T.; Kurita, K.; Iwasaki, Y.; Nakabayashi, N. Why Do Phospholipid Polymers Reduce Protein Adsorption? *J. Biomed. Mater. Res.* **1998**, *39*, 323-330.

8. Iwasaki, Y.; Ishihara, K. Phosphorylcholine-Containing Polymers for Biomedical Applications. *Anal. Bioanal. Chem.* **2005**, *381*, 534-546.

9. Zhang, Z.; Chao, T.; Chen, S.; Jiang, S. Superlow Fouling Sulfobetaine and Carboxybetaine Polymers on Glass Slides. *Langmuir* **2006**, *22*, 10072-10077.

10. Chen X, Parelkar S, Henchey E, Schneider S, Emrick T. PolyMPC-Doxorubicin Prodrugs. *Bioconjugate Chem*. **2012**, *23*, 1753-1763.

11. Page, S. M.; Henchey, E.; Chen, X.; Schneider, S.; Emrick, T. Efficacy of PolyMPC-DOX Prodrugs in 4T1 Tumor-Bearing Mice. *Mol. Pharmaceutics*. **2014**, *11*, 1715-1720.

12. Wong, K. E.; Mora, M. C.; Skinner, M.; McRae Page, S.; Crisi, G. M.; Arenas, R. B.; Schneider, S. S.; Emrick, T. Evaluation of PolyMPC-Dox Prodrugs in a Human Ovarian Tumor Model. *Mol. Pharm.* **2016**, *13*, 1679-1687.

13. Yusa, S-i; Fukuda, K.; Yamamoto, T.; Ishihara, K.; Morishima, Y. Synthesis of Well-Defined Amphiphilic Block Copolymers Having Phospholipid Polymer Sequences as a Novel Biocompatible Polymer Micelle Reagent. *Biomacromolecules* **2005**, *6*, 663-670.

14. Konno, T.; Watanabe, J.; Ishihara, K. Enhanced Solubility of Paclitaxel Using Water-Soluble and Biocompatible 2-Methacryloyloxyethyl Phosphorylcholine Polymers. *J. Biomed. Mater. Res.* **2003**, *65A*, 209-214.

15. Morisaku, T.; Watanabe, J.; Konno, T.; Takai, M.; Ishihara, K. Hydration of Phosphorylcholine Groups Attached to Highly Swollen Polymer Hydrogels Studied by Thermal Analysis. *Polymer* **2008**, *49*, 4652-4657.

16. Shao, Q.; White, A. D.; Jiang, S. Difference in Hydration between Carboxybetaine and Sulfobetaine. *J. Phys. Chem. B* **2010**, *114*, 16625-16631.

17. Leng, C.; Hung, H-C.; Sun, S.; Wang, D.; Li, Y.; Jiang, S.; Chen, Z. Probing the Surface Hydration of Nonfouling Zwitterionic and PEG Materials in Contact with Proteins. *ACS Appl. Mater. Interfaces* **2015**, *7*, 16881-16888.

18. Ishihara, K.; Mu, M.; Konno, T.; Inoue, Y.; Fukazawa. The Unique Hydration State of. Poly(2-methacryloyloxyethyl phosphorylcholine). *J. Biomater. Sci. Polym. Ed.* **2017**, *28*, 884-899.

19. Hayward, J. A.; Chapman, D. Biomembrane Surfaces as Models for Polymer Design: The Potential Haemocompatibility. *Biomaterials* **1984**, *5*, 135-142.

20. Gal, Y-S.; Jin, S-H.; Lim, K. T.; Kim, S-H.; Koh, K. Synthesis and Electro-Optical Properties of Self-Doped Ionic Conjugated Polymers: Poly[2-ethynyl-*N*-(4-sulfobutyl)pyridinium betaine]. *Curr. Appl. Phys.* **2005**, *5*, 38-42.

21. Santa Chalarca, C. F.; Emrick, T. Reactive Polymer Zwitterions: Sulfonium Sulfonates. *J. Polym. Sci. A Poly. Chem.* **2017**, *55*, 83-92.

22. Umeda, T.; Nakaya, T.; Imoto, M. The Convenient Preparation of a Vinyl Monomer Containing a Phospholipid Analogue. *Makromol. Chem., Rapid Commun.* **1982**, *3*, 457-459.

23. Ishihara, K.; Ueda, T.; Nakabayashi, N. Preparation of Phospholipid Polymers and Their Properties as Polymer Hydrogel Membranes. *Polym. J.* **1990**, *22*, 355-360.

24. Goda, T.; Ishihara, K.; Miyahara, Y. Critical Update on 2-Methacryloyloxyethyl Phosphorylcholine (MPC) Polymer Science. *J. Appl. Polym. Sci.* **2015**, *132*, 41766.

25. Lowe, A. B.; McCormick, C. L. Synthesis and Solution Properties of Zwitterionic Polymers. *Chem. Rev.* **2002**, *102*, 4177-4189.

26. Ma, I. Y.; Lobb, E. J.; Billingham, N. C.; Armes, S. P.; Lewis, A. L.; Lloyd, A. W. Synthesis of Biocompatible Polymers. 1. Homopolymerization of 2-Methacryloyloxyethyl Phosphorylcholine via ATRP in Protic Solvents: An Optimization Study. *Macromolecules* **2002**, *35*, 9306-9314.

27. Bhuchar, N.; Deng, Z.; Ishihara, K.; Narain, R. Detailed Study of the Reversible Addition-Fragmentation Chain Transfer Polymerization and Co-Polymerization of 2-Methacryloyloxyethyl Phosphorylcholine. *Polym. Chem.* **2011**, *2*, 632-639.

28. Zhang, Q.; Tang, X.; Wang, T.; Yu, F.; Guo, W.; Pei, M. Thermo-Sensitive Zwitterionic Block Copolymers *via* ATRP. *RSC Adv*. **2014**, *4*, 24240-24247.

29. Donovan, M. S.; Sumerlin, B. S.; Lowe, A. B.; McCormick, C. L. Controlled/"Living" Polymerization of Sulfobetaine Monomers Directly in Aqueous Media via RAFT. *Macromolecules* **2002**, *35*, 8663-8666.

30. Takatori, Y.; Moro, T.; Ishihara, K.; Kamogawa, M.; Oda, H.; Umeyama, T.; Kim, Y. T.; Ito, H.; Kyomoto, M.; Tanaka, T. Clinical and Radiographic Outcomes of Total Hip Replacement with Poly(2-methacryloyloxyethyl phosphorylcholine)-Grafted Highly Cross-Linked Polyethylene Liners: Three-Year Results of a Prospective Consecutive Series. *Mod. Rheumatol*. **2015**, *25*, 286-291.

31. Selan, L.; Palma, S.; Scoarughi, G. L.; Papa, R.; Veeh, R.; Clemente, D. D.; Artini, M. Phosphorylcholine Impairs Susceptibility to Biofilm Formation of Hydrogel Contact Lenses. *Am. J. Ophtholmal.* **2009**, *147*, 134-139.

32. Woodfield, P. A.; Zhu, Y.; Pei, Y.; Roth, P. J. Hydrophobically Modified Sulfobetaine Copolymers with Tunable Aqueous UCST through Postpolymerization Modification of Poly(pentafluorophenyl acrylate). *Macromolecules* **2014**, *47*, 750-762.

33. Doncom, K. E. B.; Willcock, H.; O'Reilly, R. K. The Direct Synthesis of Sulfobetaine-Containing Amphiphilic Block Copolymers and Their Self-Assembly Behavior. *Eur. Polym. J.* **2017**, *87*, 497-507.

34. Chen, C-Y.; Wang, H-L. Dual Thermo- and pH-Responsive Zwitterionic Sulfobetaine Copolymers for Oral Delivery System. *Macromol. Rapid Commun.* **2014**, *35*, 1534-1540.

35. Chang, C-C.; Letteri, R.; Hayward, R. C.; Emrick, T. Functional Sulfobetaine Polymers: Synthesis and Salt-Responsive Stabilization of Oil-in-Water Droplets. *Macromolecules* **2015**, *48*, 7843-7850.

36. Hu, G.; Parelkar, S. S.; Emrick, T. A Facile Approach to Hydrophilic, Reverse Zwitterionic, Choline Phosphate Polymers. *Polym. Chem.* **2015**, *6*, 525-530.

37. Hu, G.; Emrick, T. Functional Choline Phosphate Polymers. *J. Am. Chem. Soc.* **2016**, *138*, 1828-1831.

38. Ma, Y.; Tang, Y.; Billingham, N. C.; Armes, S. P. Well-Defined Biocompatible Block Copolymers via Atom Transfer Radical Polymerization of 2-Methacryloyloxyethyl Phosphorylcholine in Protic Media. *Macromolecules* **2003**, *36*, 3475-3484.

39. Lowe, A. B.; Billingham, N. C.; Armes, S. P. Synthesis and Properties of Low-Polydispersity Poly(sulfopropylbetaine)s and Their Block Copolymers. *Macromolecules* **1999**, *32*, 2141-2148.

40. Doncom, K. E. B.; Warren, N. J.; Armes, S. P. Polysulfobetaine-Based Diblock Copolymer Nano-Objects *via* Polymerization-Induced Self-Assembly. *Polym. Chem.* **2015**, *6*, 7264-7273.

41. Seo, J-H.; Matsuno, R.; Konno, T.; Takai, M.; Ishihara, K. Surface Tethering of Phosphorylcholine Groups onto Poly(dimethylsiloxane) Through Swelling-Deswelling Methods with Phospholipids Moiety Containing ABA-Type Block Copolymers. *Biomaterials* **2008**, *29*¸1367-1376.

42. Nair, D. P.; Podgórski, M.; Chatani, S.; Gong, T.; Xi, W.; Fenoli, C. R.; Bowman, C. N. The Thiol-Michael Addition Click Reaction: A Powerful and Widely Used Tool in Materials Chemistry. *Chem. Mater*. **2014**, *26*, 724-744.

43. Hoyle, C. E.; Bowman, C. N. Thiol-Ene Click Chemistry. *Angew. Chem. Int. Ed.* **2010**, *49*, 1540-1573.

44. Lowe, A. B.; Hoyle, C. E.; Bowman, C. N. Thiol-Yne Click Chemistry: A Powerful and Versatile Methodology for Materials Synthesis. *J. Mater. Chem.* **2010**, *20*, 4745-4750.

45. Kato, M.; Kamigaito, M.; Sawamoto, M.; Higashimura, T. Polymerization of Methyl Methacrylate with the Carbon Tetrachloride/Dichlorotris-(Triphenylphosphine)ruthenium(II)/Methylaluminum Bis(2,6-di-tert-butylphenoxide) Initiating System: Possibility of Living Radical Polymerization. *Macromolecules* **1995**, *28*, 1721-1723.

46. Wang, J-S.; Matyjaszewski, K. Controlled/"Living" Radical Polymerization. Atom Transfer Radical Polymerization in the Presence of Transition-Metal Complexes. *J. Am. Chem. Soc.* **1995**, *117*, 5614-5615.

47. Kamigaito, M.; Ando, T.; Sawamoto, M. Metal-Catalyzed Living Radical Polymerization. *Chem. Rev.* **2001**, *101*, 3689-3745.

48. Matyjaszewski, K.; Xia, J. H. Atom Transfer Radical Polymerization. *Chem. Rev.* **2001**, *101*, 2921-2990.

49. Li, Y.; Keefe, A. J.; Giarmarco, M.; Brault, N. D.; Jiang, S. Simple and Robust Approach for Passivating and Functionalizing Surfaces for Use in Complex Media. *Langmuir* **2012**, *1*, 9486-9496.

50. Robinson, K. L.; de Paz-Báñez, M. V.; Wang, X. S.; Armes, S. P. Synthesis of Well-Defined, Semibranched, Hydrophilic-Hydrophobic Block Copolymers Using Atom Transfer Radical Polymerization. *Macromolecules* **2001**, *34*, 5799-5805.

51. Strickley, R. G. Solubilizing Excipients in Oral and Injectable Formulations. *Pharmaceut. Res.* **2004**, *21*, 201-230.

52. Gelderblom, H.; Verwei, J.; Nooter, K.; Sparreboom, A. Cremophor EL: The Drawbacks of Vehicle Selection for Drug Formulation. *Eur. J. Cancer* **2001**, *37*, 1590-1598.

53. Ten Tjie, A. J.; Verweij, J.; Loos, W. J.; Sparreboom, A. Pharmacological Effects of Formulation Vehicles: Implications for Cancer Chemotherapy. *Clin. Pharmacokinet.* **2003**, *42*, 665-685.

54. Ringsdorf, H. Structure and Properties of Pharmacologically Active Polymers. *Journal of Polymer Science: Polymer Symposia* **1975**, *51*, 135-153.

55. Fox, M. E.; Szoka, F. C.; Fréchet, J. M. J. Soluble Polymer Carriers for the Treatment of Cancer: The Importance of Molecular Architecture. *Acc. Chem. Res.* **2009**, *42*, 1141-1151.

56. Liechty, W. B.; Kryscio, D. R.; Slaughter, B. V.; Peppas, N. A. Polymers for Drug Delivery Systems. *Annu. Rev. Chem. Biomol. Eng.* **2010**, *1*, 149-173.

57. Maeda, H.; Nakamura, H.; Fang, J. The EPR Effect for Macromolecular Drug Delivery to Solid Tumors: Improvement of Tumor Uptake, Lowering of Systemic Toxicity, and Distinct Tumor Imaging In Vivo. *Adv. Drug Deliv. Rev.* **2013**, *65*, 71-79.

58. Pasut, G.; Veronese, F. M. PEG Conjugates in Clinical Development or Use as Anticancer Agents: An Overview. *Adv. Drug Deliv. Rev.* **2009**, *61*, 1177-1188.

59. Joralemon, M. J.; McRae, S.; Emrick, T. PEGylated Polymers for Medicine: From Conjugation to Self-Assembled Systems. *Chem. Commun.* **2010**, *46*, 1377-1393.

60. Kurzrock, R.; Goel, S.; Wheler, J.; Hong, D.; Fu, S.; Rezai, K.; Morgan-Linnell, S. K.; Urien, S.; Mani, S.; Chaudhary, I.; Ghalib, M. H.; Buchbinder, A.; Lokjec, F.; Mulcahy, M. Safety, Pharmacokinetics, and Activity of EZN-2208, a Novel Conjugate of Polyethylene Glycol and SN38, in Patients with Advanced Malignancies. *Cancer* **2012**, *118*, 6144-6151.

61. Youngster, S.; Wang, Y. S.; Grace, M.; Bausch, J.; Bordens, R.; Wyss, D. F. Structure, Biology and Therapeutic Implications of Pegylated Interferon Alpha-2b. *Curr. Pharm. Des.* **2002**, *8*, 2139-2157.

62. Reddy, K. R.; Modi, M. W.; Pedder, S. Use of Peginterferon Alfa-2a (40KD) (Pegasys®) for the Treatment of Hepatitis C. *Adv. Drug Deliv. Rev.* **2002**, *54*, 571-586.

63. Filpula, D.; Zhao, H. Releasable PEGylation of Proteins with Customized Linkers. *Adv. Drug Deliv. Rev.* **2008**, *60*, 29-49.

64. Barenholtz, Y. Doxil®—The First FDA-Approved Nano-Drug: Lessons Learned. *J. Control. Release* **2013**, *160*, 117-134.

65. Armstrong, J. K.; Hempel, G.; Koling, S.; Chan, L. S.; Fisher, T.; Meiselman, H. J.; Garratty, G. Antibody Against Poly(ethylene glycol) Adversely Affects PEG-Asparginase Therapy in Acute Lymphoblastic Leukemia Patients. *Cancer* **2007**, *110*, 103-111.

66. Sundy, J. S.; Baraf, H. S. B.; Yood, R. A.; Edwards, N. L.; Gutierrez-Urena, S. R.; Treadwell, E. L.; Vázquez-Mellado, J.; White, W. B.; Lipsky, P. E.; Horowitz, Z.; Huang, W.; Maroli, A. N.; Waltrip, R. W.; Hamburger, S. A.; Becker, M. A. Efficacy and Tolerability of Pegloticase for the Treatment of Chronic Gout in Patients Refractory to Conventional Treatment: Two Randomized Controlled Trials. *JAMA* **2011**, *306*, 711-720.

67. Garay, R.P.; El-Gewely, R.; Armstrong, J. K.; Garratty, G.; Richette, P. Antibodies Against Polyethylene Glycol in Healthy Subjects and in Patients Treated with PEG-Conjugated Agents. *Expert Opin. Drug Deliv.* **2012**, *9*, 1319-1323.

68. Zhang, P.; Sun, F.; Liu, S.; Jiang, S. Anti-PEG Antibodies in the Clinic: Current Issues and Beyond PEGylation. *J. Control. Release* **2016**, *244*, 184-193.

69. Chen, X.; McRae, S.; Parelkar, S.; Emrick, T. Polymeric Phosphorylcholine-Camptothecin Conjugates Prepared by Controlled Free Radical Polymerization and Click Chemistry. *Bionconjug. Chem.* **2009**, *20*, 2331-2341.

70. McRae Page, S.; Martorella, M.; Parelkar, S.; Kosif, I.; Emrick, T. Disulfide Cross-Linked Phosphorylcholine Micelles for Triggered Release of Camptothecin. *Mol. Pharmaceutics* **2013**, *10*, 2684-2692.

71. Moad, G.; Rizzardo, E.; Thang, S. H.; Toward Living Radical Polymerization. *Acc. Chem. Res.***2008**, *41*, 1133-1142.

72. Moad, G.; Rizzardo, E.; Thang, S. H. Radical Addition-Fragmentation Chemistry in Polymer Synthesis. *Polymer* **2008**, *49*, 1079-1131.

73. Skinner, M.; Selhorst, R.; Emrick, T. Synthesis of Water-Soluble Zwitterionic Polysiloxanes. *J. Polym. Sci. A Polym. Chem.* **2016**, *54*, 127-134.

74. Wong, K. E.; Mora, M. C.; Skinner, M.; McRae Page, S.; Crisi, G. M.; Arenas, R. B.; Schneider, S. S.; Emrick, T. Evaluation of PolyMPC-Dox Prodrugs in a Human Ovarian Tumor Model. *Mol. Pharmaceutics* **2016**, *13*, 1679-1687.

75. Skinner, M.; Ward, S. M.; Emrick, T. Versatile Synthesis of Polymer-Temozolomide Conjugates. *ACS Macro Lett.* **2017**, *6*, 215-218.

CHAPTER 2

WATER-SOLUBLE ZWITTERIONIC POLYSILOXANES

2.1 Introduction

Polysiloxanes exhibit distinct properties from carbon-based polymers, most notably their flexibility and low temperature fluidity owing to the long Si—O and Si—C bonds in the structure.[1] Siloxane polymers have excellent thermal stability, high gas permeability, and biocompatibility,[2] and are important in applications ranging from microfluidic device fabrication[3,4] to coatings, sealants, medical devices,[5] and contact lenses.[6]

In siloxane-containing polymers, the "R" groups of the $–R_2Si–O–$ repeat unit are typically small, hydrophobic moieties such as methyl or phenyl groups. The hydrophobicity and aqueous insolubility inherent to conventional siloxane polymers precludes their use in aqueous assembly and deposition processes. Recent work seeking to improve the surface hydrophilicity and physiological properties of crosslinked silicones include methods to prepare water-soluble polysiloxanes as polymer surfactants, drug delivery vehicles, and polymer nanoreactors.[7-14] For example, low molecular weight oligosiloxane surfactants with pendent zwitterions were prepared by successive hydrosilylation and SB formation,[15] affording water-dispersible oligomers. Cationic water-soluble polysiloxanes with pendent ammonium and imidazolium groups were prepared and studied as antimicrobial materials.[16,17] Random copolymers of poly(dimethylsiloxane) (PDMS) and poly(azidopropylmethylsiloxane) gave access to PEGylated polysiloxanes by azide-alkyne cycloaddition.[18] Additional examples include amphiphilic block copolymers with mixed siloxane-hydrocarbon backbones, such as block

copolymers of PDMS with poly(ethylene glycol),[19,20] poly(2-alkyloxazolines),[21,22] and polyMPC.[23]

The work described herein focuses on the preparation of water-soluble zwitterionic polysiloxanes with relatively high molecular weight and no hydrocarbon-containing block. This requires integrating useful functionality into the siloxane backbone, achieved, for example, by polymerization of 1,3,5-trivinyl-1,3,5-trimethylcyclotrisiloxane ($D3^v$) or 1,3,5,7-tetravinyl-1,3,5,7-tetramethylcyclotetrasiloxane ($D4^v$). For example, hexamethylcyclotrisiloxane (D3) polymerization initiated by *n*-butyllithium is followed by addition of $D3^v$ or $D4^v$ to generate PDMS-*b*-poly(vinylmethylsiloxane (PDMS-*b*-PVMS) block copolymers. The pendent vinyl groups are then available for modification by platinum-catalyzed hydrosilylation with alkyl-, epoxy-, and alkoxy-silanes, or by thiol-ene chemistry using any of a variety of thiols.[24,25] Common to both strategies is the similar organic solubility of the polymer and the groups selected for grafting, making functionalization straightforward relative to efforts to integrate strictly hydrophilic groups into the structure.

Successful syntheses of low polydispersity polysiloxanes functionalized with pendent zwitterions would provide new opportunities for siloxane polymers in aqueous assembly and interfacial science. As such, polysiloxanes incorporating PC and SB zwitterions were targeted for their hydrophilicity,[26,27] biocompatibility,[28-30] and nonfouling properties.[9,31-33] PVMS homopolymers and PDMS-*b*-PVMS block copolymers were prepared as functional precursors, and through facile thiol-ene addition,[34] PC- and SB-thiols were attached to the siloxane backbone. Optimizing reaction conditions overcame solubility differences between the vinyl polysiloxanes and zwitterionic thiols.

Homopolymers having the pendent PC or SB groups on each monomer unit and block copolymers with zwitterion incorporations of 10-50 mole percent were synthesized. Percent vinyl conversion and polymer purity were confirmed by NMR spectroscopy, while molecular weight distribution was characterized by gel permeation chromatography (GPC). The zwitterionic polysiloxanes displayed considerable surfactant properties, as determined by pendant drop interfacial tensiometry (IFT), while aqueous assembly characteristics of these novel polymers were examined by determining their critical micelle concentration (CMC) and measuring the size of structures formed in water by dynamic light scattering (DLS) and subsequently by transmission electron microscopy (TEM).

2.2 Synthesis of PC- and SB-Polysiloxanes

Siloxane polymers with pendent vinyl groups were prepared by *n*-butyllithium-initiated anionic ring-opening polymerization (ROP) using a procedure similar to that described by Frey and coworkers.[24] Vinyl-bearing PVMS homopolymer **P1** was synthesized by the room temperature polymerization of $D3^{v}$ in THF, as shown in Figure 2.1A. Kinetics of the $D3^{v}$ polymerization were monitored by analyzing aliquots of the reaction solution at various times using GPC eluting in THF and calibrated against polystyrene standards. As shown in Figure 2.1B, the $D3^{v}$ monomer was consumed rapidly and the number-average molecular weight (M_n) of **P1** approached a constant value within approximately 8 minutes of initiating polymerization. Importantly, the polydispersity index (PDI) of **P1** remained low throughout the polymerization. **P1** was purified by dialysis to remove unreacted monomer, and was isolated as a clear, colorless oil in 75% yield. Polymer **P1** was prepared with an M_n of 7,500 g/mol, as estimated using ^{1}H-NMR

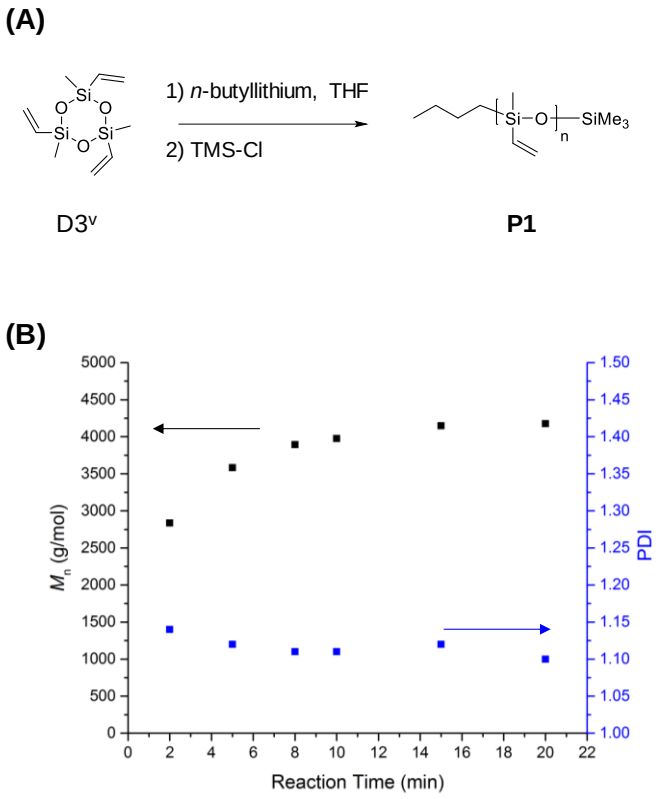

Figure 2.1: (A) Synthesis of PVMS homopolymer **P1** by anionic ROP; (B) changes in the estimated M_n and PDI values for the room temperature, *n*-butyllithium-initiated anionic ROP of D3^v in THF as a function of time.

spectroscopy, and a PDI of 1.07, as estimated using GPC eluting in THF relative to polystyrene standards.

PDMS-PVMS block copolymers were synthesized by anionic ring-opening polymerization using the sequential monomer addition strategy shown in Figure 2.2A. D3 polymerization was initiated with *n*-butyllithium, and the polymerization kinetics were monitored using GPC eluting in THF. As shown in Figure 2.2B, the polymerization of D3 was significantly slower than vinyl-functionalized D3^v, with estimated M_n values for the PDMS homopolymer approaching a constant value after approximately 2 hours. Following D3 consumption, D3^v was added to initiate the second block from the chain-end silanoate, affording PDMS-*b*-PVMS copolymers with vinylsiloxane incorporation of 50 (polymer

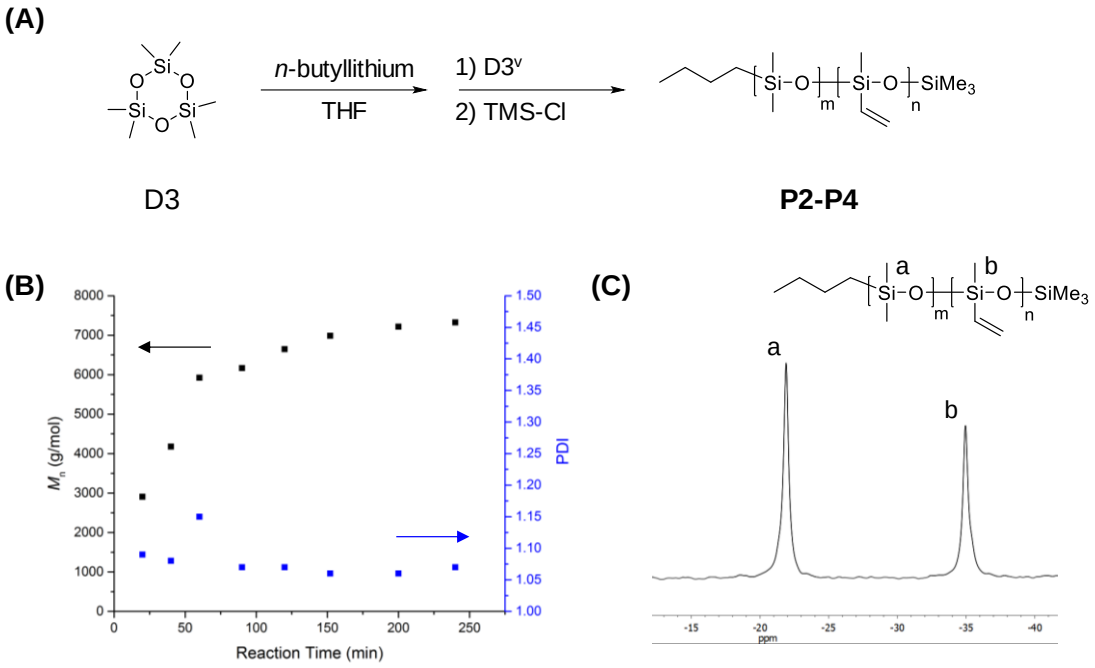

Figure 2.2: (A) One-pot synthesis of PDMS-*b*-PVMS copolymers **P2**-**P4** by sequential monomer addition; (B) changes in the estimated M_n and PDI values for the room temperature, *n*-butyllithium-initiated anionic ROP of D3 in THF as a function of time; (C) representative ^{29}Si-NMR spectrum of PDMS-*b*-PVMS. Single resonances were observed for the PDMS and PVMS segments, confirming block purity.

P2), 32 (polymer **P3**), and 10 (polymer **P4**) mole percent as clear, viscous oils in 70-80% yield. The order of monomer addition was crucial for obtaining copolymers with excellent block purity, due to the faster rate of propagation of D3^v relative to D3.[35] In the ^{29}Si-NMR spectra of block copolymers **P2**-**P4**, singlets were observed at -21.81 and -34.64 ppm (Figure 2.2C), representing Si resonances from the D3 and D3^v block, respectively.

Values of the number-average degree of polymerization (X_n) of vinyl-substituted polysiloxanes **P1**-**P4**, summarized in Table 2.1**,** were determined by ^{1}H-NMR spectroscopy by comparing the relative signal intensities of the dimethylsiloxane (δ = -0.06-0.10 ppm) and vinylmethylsiloxane (δ = 5.73-6.06 ppm) groups against that of the *n*-butyl (δ = 0.89 ppm) chain end. Molecular weight distributions (*i.e.*, PDI values) of polymers **P1**-**P4** were characterized by GPC eluting in THF and calibrated against polystyrene standards.[24,25]

Table 2.1: Molecular weight data for vinyl-substituted polysiloxanes **P1**-**P4**.

Polymer	X_n^{Theor} PDMS[a]	X_n^{NMR} PDMS[b]	X_n^{Theor} PVMS[c]	X_n^{NMR} PVMS[d]	M_n^{Theor} (g/mol)	M_n^{NMR} (g/mol)[e]	M_n^{GPC} (g/mol)[f]	PDI[f]
P1	N/A	N/A	117	87	10,000	7,500	8,400	1.07
P2	63	42	63	42	10,000	6,700	7,300	1.09
P3	90	69	45	33	10,000	8,000	5,200	1.08
P4	180	84	15	9	15,000	7,000	9,900	1.05

[a,c]Theoretical number-average degree of polymerization (X_n) determined from the molar feed ratio of monomer to initiator.
[b,d]X_n measured using ^{1}H-NMR spectroscopy.
[e]Number-average molecular weight (M_n) measured using ^{1}H-NMR spectroscopy.
[f]M_n and PDI estimated by GPC eluting in THF relative to polystyrene standards.

Reasonable agreement was seen between the molecular weights given by NMR and GPC, and the isolated polysiloxanes had low PDI values (<1.1) with vinyl incorporation (100, 50, 32, and 10 mole percent) in excellent agreement with targeted amounts. Although the measured degrees of polymerization and molecular weights were somewhat lower than targeted, the functional polysiloxanes were isolated with narrow molecular weight distributions in high yield and purity, suitable for post-polymerization modification with zwitterionic moieties.

As shown in Figure 2.3, polysiloxanes **P1**-**P4** were modified by thiol-ene addition of zwitterionic thiols to the pendent vinyl groups on the polymer. PC-thiol **PC-SH**, a known small molecule zwitterion from the work of Iwasaki and Miyahara,[36] and newly synthesized SB-thiol **SB-SH**, were prepared by the Michael addition of 1,3-propanedithiol to the commercially available PC- and SB-methacrylates, respectively. The zwitterionic methacrylates were reacted with excess dithiol to promote formation of monothiol

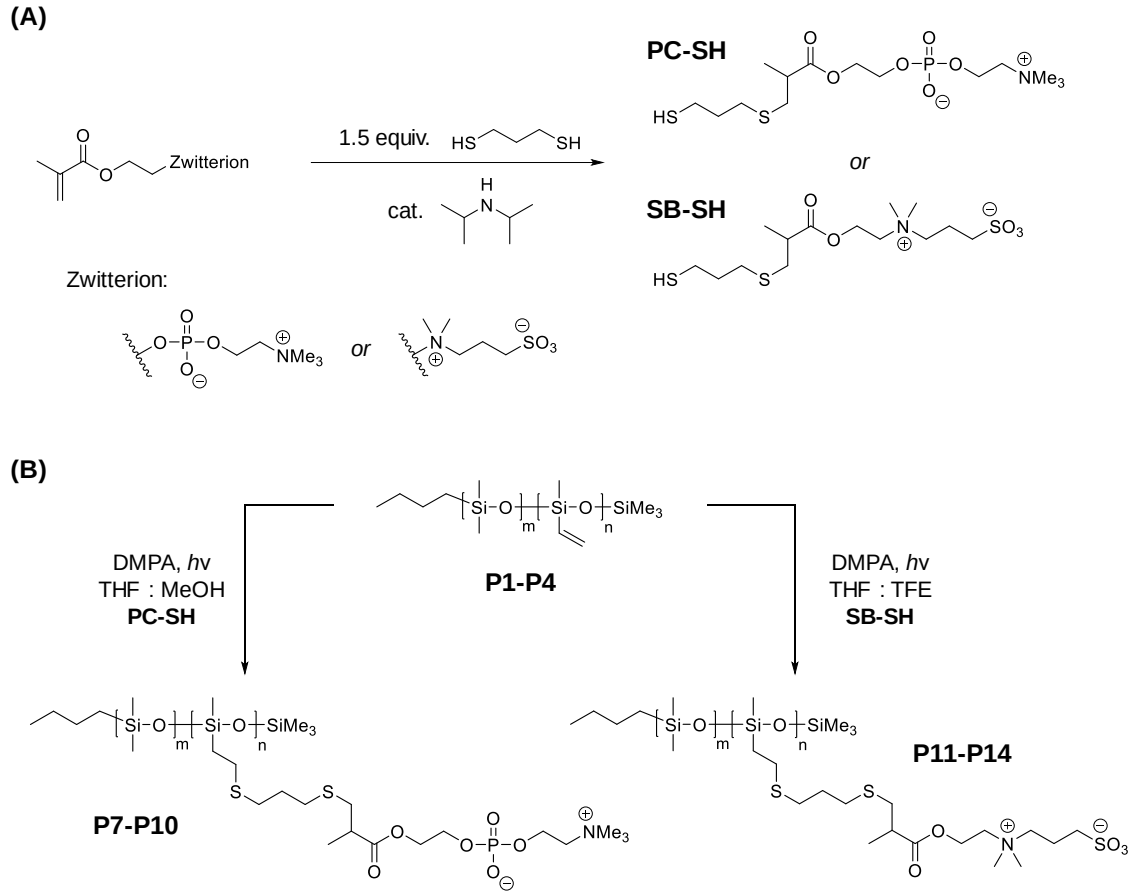

Figure 2.3: (A) Synthesis of zwitterionic thiols **PC-SH** and **SB-SH** by the thiol-Michael addition of 1,3-propanedithiol to PC- and SB-methacrylate, respectively; (B) preparation of PC- (**P7-P10**) and SB- (**P11-P14**) polysiloxanes. Zwitterionic thiols **PC-SH** and **SB-SH** were introduced to PVMS-based precursors by thiol-ene addition to the pendent vinyl groups, affording homopolymers (m = 0) and block copolymers with zwitterion incorporation of 10, 32, or 50 mole percent.

substituted structures as the major product, and the zwitterionic thiols were isolated as hygroscopic solids by precipitation then purified by trituration in THF and/or diethyl ether to remove unreacted dithiol. NMR characterization of **PC-SH** and **SB-SH**, shown in Figure 2.4, as well as electrospray ionization high-resolution mass spectrometry (ESI-HRMS) analysis confirmed the expected structure of **PC-SH** ($[M+H]^+$: 404.131 g/mol) and **SB-SH** ($[M+H]^+$: 388.131 g/mol). The zwitterionic thiols were soluble only in water, methanol (MeOH), and 2,2,2-trifluoroethanol (TFE), typical of small molecule zwitterions.

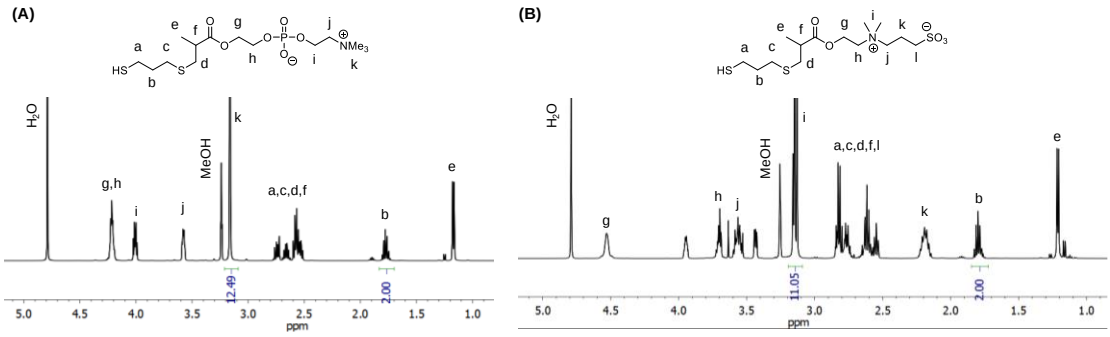

Figure 2.4: ^{1}H-NMR (500 MHz) spectra of **PC-SH** (A) and **SB-SH** (B) in MeOD-d_4.

In the mass spectra of **PC-SH** and **SB-SH**, signals were identified corresponding to disulfide dimers and bis-zwitterion sulfides of **PC-SH** and **SB-SH**. Formation of such side products is expected, and was previously noted in the preparation of **PC-SH**.[36] Comparing integral values in the ^{1}H-NMR spectra of **PC-SH** and **SB-SH** corresponding to the trimethylammonium (peak k, δ = 3.16 ppm) and dimethylammonium (peak i, δ = 3.08-3.20 ppm) protons, respectively, with the integral value for the methylene protons from the propane thiol chain (peak b, $\delta_{\mathbf{PC\text{-}SH}}$ = 1.78 ppm, $\delta_{\mathbf{SB\text{-}SH}}$ = 1.80 ppm), the formation of the mono-zwitterion as the major product (72% for **PC-SH** and 54% for **SB-SH**) was confirmed for each zwitterionic thiol. Importantly, these additional products are nonproblematic with respect to polymer functionalization, and are removed from the polymer product by dialysis.

UV-assisted thiol-ene reactions of the vinyl-substituted polymers and zwitterionic thiols were conducted at room temperature using 2,2-dimethoxy-2-phenylacetophenone (DMPA) photoinitiation.[37] The marked solubility differences between the zwitterionic thiols and vinyl-substituted polysiloxanes (the polymers are insoluble in water, MeOH, and TFE) led to an initial examination of biphasic thiol-ene reaction conditions[38] in immiscible solvents such as MeOH/TFE. However, no significant zwitterionic functionalization was

achieved under these conditions. Homogenous solvent mixtures proved more successful: for example, adding a solution of **PC-SH** in MeOH to a THF solution of polymer resulted in full conversion of the vinyl groups to the corresponding sulfide product. A similar strategy was used for the SB substitution, using TFE to solubilize **SB-SH**. Room temperature thiol-ene addition of **PC-SH** and **SB-SH** to vinyl-substituted polymers was initiated by homolytic decomposition of DMPA at 365 nm, affording rapid and quantitative substitution in one hour. Figure 2.5 shows ^{1}H-NMR spectra of vinyl-substituted polysiloxane block copolymer **P2** (50 mole percent vinylsiloxane), and the corresponding PC (**P8**) and SB (**P12**) copolymers.

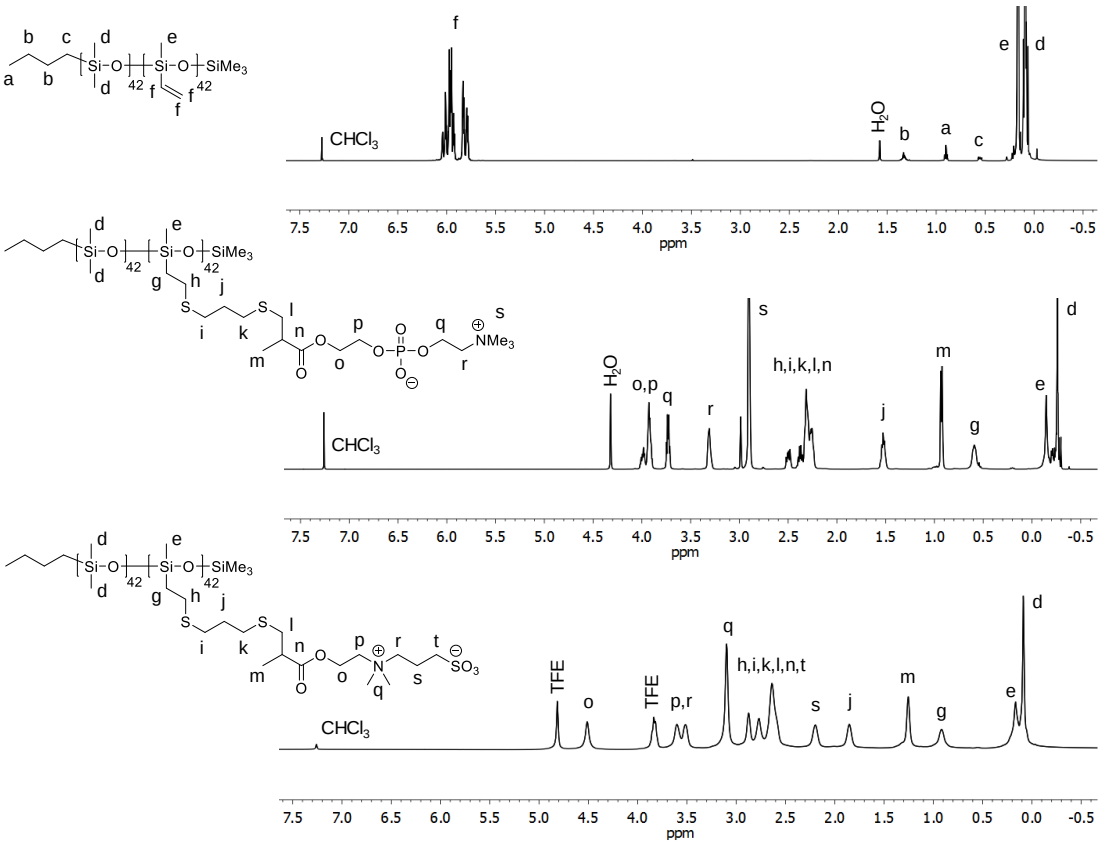

Figure 2.5: ^{1}H-NMR (500 MHz) spectra of **P2** in $CDCl_3$ (top), **P8** in 1:1 $CDCl_3$:MeOD-d_4 (middle), and **P12** in 1:2 $CDCl_3$:TFE-d_3 (bottom).

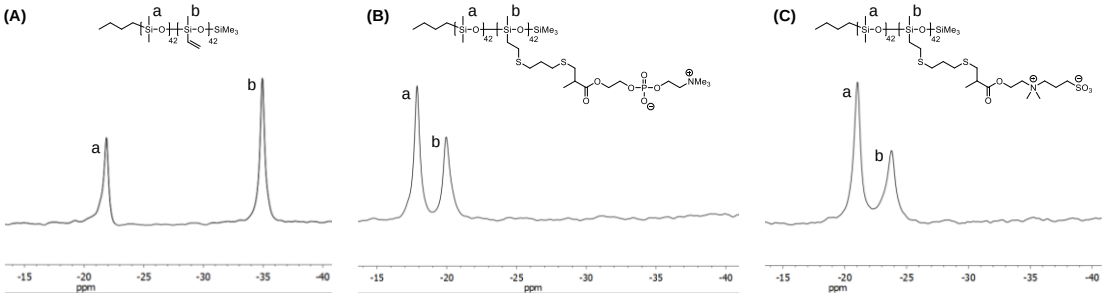

Figure 2.6: Representative ^{29}Si-NMR (99 MHz) spectra of vinyl-substituted polysiloxanes (A), PC-containing polysiloxanes (B), and SB-containing polysiloxanes (C).

In the ^{1}H-NMR spectra of the zwitterion-substituted polymers, vinyl proton signals (region f, δ = 5.73-6.06 ppm) of the siloxane polymer starting material are notably absent, and characteristic signals of the PC and SB groups are introduced. A new resonance is seen at δ = 0.59 ppm for the PC-polysiloxanes, and at δ = 0.92 ppm for the SB-polysiloxanes, corresponding to the alpha methylene protons of each structure (donoted as g). In the ^{29}Si-NMR spectra, following thiol-ene substitution, a shift was observed in the Si resonance from the original vinyl-substituted polymers (δ = -34.97 ppm for **P1**, δ = -34.64 ppm for **P2**-**P4**) (Figure 2.6A) to -19.94 and -23.93 ppm for PC- (Figure 2.6B) and SB-substitution (Figure 2.6C), respectively. These spectra confirm an excellent conversion of the pendent alkenyl moieties to the desired sulfide-tethered zwitterions.

Molecular weight distributions for the zwitterion-substituted polysiloxanes were characterized by GPC in TFE, with calibration against poly(methyl methacrylate) (PMMA) standards. GPC chromatograms of polymers **P7**-**P10** and **P11**-**P14** are shown in Figures 2.7A and 2.7B, respectively. As summarized in Figure 2.7C, the polymers were isolated with low PDI values and estimated M_n values in reasonable agreement with theoretical values. Notably, for polymers **P10** and **P14**, having the lowest percent zwitterion substitution of the samples prepared, a signal at low retention volume was observed in the

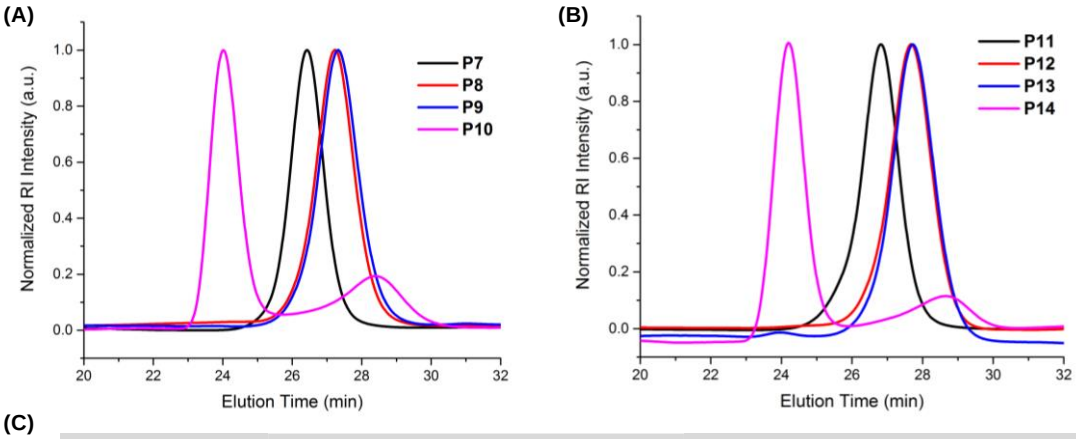

(C)

Polymer	Zwitterion Content (mol %)	M_n^{Theor} (g/mol)	M_n^{GPC} (g/mol)[a]	PDI[a]
P7	100 (PC)	42,600	31,400	1.07
P8	50 (PC)	23,700	20,900	1.11
P9	32 (PC)	21,300	19,800	1.10
P10	10 (PC)	10,600	11,900	1.16
P11	100 (SB)	41,200	26,300	1.11
P12	50 (SB)	23,000	17,100	1.12
P13	32 (SB)	20,800	16,300	1.11
P14	10 (SB)	10,500	11,300	1.15

[a]M_n and PDI values estimated by GPC against PMMA standards.

Figure 2.7: GPC chromatograms of PC-substituted polysiloxanes **P7**-**P10** (A) and SB-substituted polysiloxanes **P11**-**P14** (B) eluting in TFE; (C) molecular weights of zwitterionic polysiloxanes estimated by GPC eluting in TFE.

chromatograms attributed to aggregate formation in this solvent environment. Aggregation of polymers **P10** and **P14** in TFE was confirmed by DLS, which showed the formation of monomodal aggregates with hydrodynamic diameters of approximately 24 nm. Single unimodal peaks were observed in the chromatograms of the other six PC- and SB-substituted polysiloxanes having 32, 50, and 100 mole percent zwitterion. Moreover, for all of the zwitterionic polysiloxanes, no low molecular weight species were observed in the chromatograms, confirming polymer purity and successful removal of unreacted small molecule zwitterions.

These zwitterionic polysiloxanes are amphiphilic and are expected to exhibit aqueous assembly and surfactant properties in water and at fluid-fluid interfaces. The PC-containing polysiloxanes are highly water-soluble, with **P7**-**P10** dissolving in water at ≥ 5 mg/mL. In contrast, the only SB-containing polysiloxane having water solubility at comparable concentrations was homopolymer **P11**. The pure water solubility of the SB-substituted polysiloxane homopolymer contrasts that of other SB-substituted homopolymers in which inter-zwitterion interactions lead to insolubility in pure (salt-free) water.[39] It is reasonable to hypothesize that the solubility of **P11** benefits from weaker SB-SB interactions due to the greater conformational and rotational flexibility of the siloxane backbone relative to hydrocarbon-based polymer zwitterions.[40]

CMC measurements of the zwitterionic polysilxoanes were performed using a pyrene fluorescence assay. 5 μL of a dilute pyrene solution in acetone was added to serial dilutions of the polymers in pure water. The solutions were incubated at room temperature for approximately 18 hours, then analyzed by fluorescence spectroscopy. As pyrene transitions from a hydrophilic to hydrophobic environment at the CMC, a distinct shift in fluorescence intensity from 334 to 339 nm is typically observed. CMC is then estimated by plotting fluorescence intensity ratios (I_{339}/I_{334}) as a function of the log of the polymer concentration. CMC for polymers **P7**-**P11** were similar, with all estimated values < 0.01 g/L. DLS was employed to measure the size of these amphiphiles after dissolution in water at concentrations above the CMC ([polymer] = 1 g/L). In water, the block copolymers may be expected to form micelles having a PDMS core and zwitterionic polysiloxane corona. These polymers have similar degrees of polymerization, such that as zwitterion content increases, the molecular weight of the PDMS segment decreases. As shown in Figure 2.8,

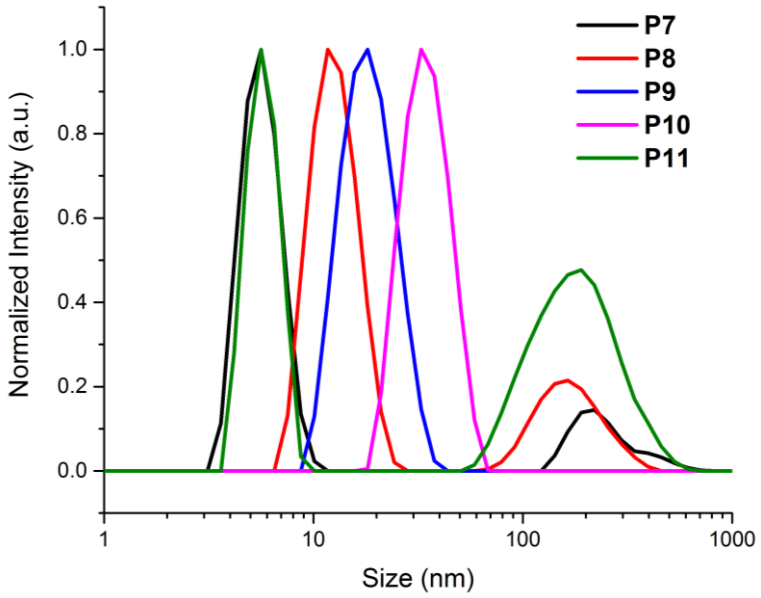

Figure 2.8: Normalized DLS curves for aqueous solutions of **P7**-**P11** at a concentration of 1 mg/mL.

this relationship is reflected in DLS: hydrodynamic diameters of the aggregates decreased with increasing zwitterion content, from 33 nm for **P10** (10 mole percent PC) to 12 nm for **P8** (50 mole percent PC). The zwitterionic homopolymers **P7** and **P11** formed structures in water with small hydrodynamic diameters (< 7 nm) and readily encapsulated the pyrene fluorescence probe. The homopolymers are likely solubilized polymer chains that collapse in water due to the hydrophobicity of the siloxane backbone. For polymers exhibiting bimodal size distributions (**P7**, **P8**, and **P11**), number-based DLS plots confirmed the smaller aggregates as the predominant species.

Self-assembled structures formed by PC-containing polysiloxane block copolymers were visualized by TEM in collaboration with Ryan Selhorst. Aqueous solutions of polymers **P9** and **P10** were prepared at concentrations above the CMC, dropcast onto grids and allowed to dry under ambient conditions. Representative micrographs of assemblies formed from solutions of PC-substituted polysiloxanes are shown in Figure 2.9. High

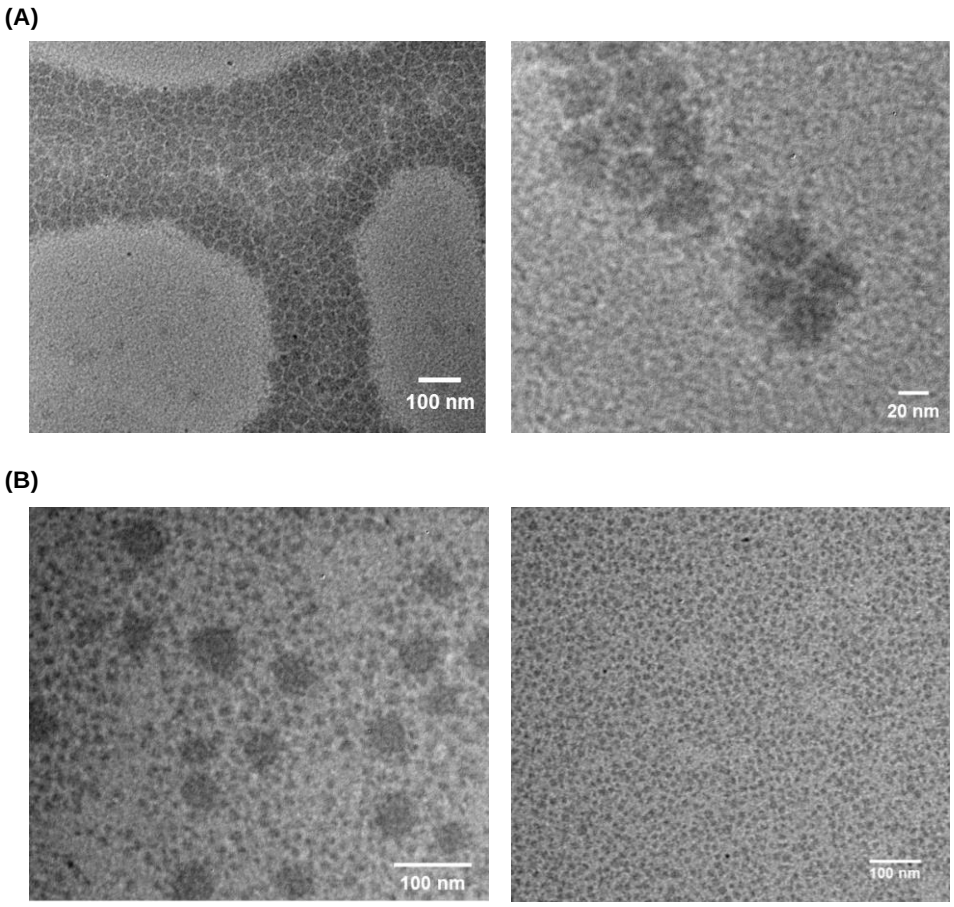

Figure 2.9: Representative TEM images of structures formed from aqueous solutions of **P10** (A) and **P9** (B) after casting on carbon-coated TEM grids.

densities of spherical objects with relatively low size distributions (30-45 nm diameter) and distinct boundaries were formed from **P10** (Figure 2.9A). For aqueous solutions of **P9**, two size populations were observed, consisting of smaller (12-18 nm diameter) and larger objects (35-55 nm) diameter (Figure 2.9B). Since light scattering analysis of aqueous solutions of **P9** shows a single size population (Figure 2.8), the appearance of two size populations by electron microscopy may be the result of drying and solvent evaporation.

The surfactant properties of these novel polysiloxane amphiphiles were evaluated by pendant drop interfacial surface tension (IFT) at room temperature. IFT values (γ) of

Table 2.2: Mean interfacial surface tension (γ_{eq}) values for aqueous solutions of polymers **P7**-**P11** and TCB measured using pendant drop tensiometry.

Polymer	γ_{eq} (mN/m)
P7	17.3 ± 0.1
P8	20.2 ± 0.1
P9	16.2 ± 0.1
P10	13.1 ± 0.1
P11	10.7 ± 0.1

P7-**P11** in water were measured over a 30 minute period by immersing a 1,2,4-trichlorobenzene (TCB) droplet in 1 mg/mL aqueous solutions of the zwitterionic polysiloxanes. Equilibrium surface tension values (γ_{eq}), summarized in Table 2.2, were determined by averaging the values of γ observed at the conclusion of each measurement, and compared to the γ_{eq} of TCB at room temperature in pure water ($\gamma_{eq,TCB}$ = 42.2 ± 0.3 mN/m). The equilibrium interfacial tension of TCB in aqueous solutions of PC-substituted polysiloxanes was reduced at least two-fold (γ_{eq} = 13.1-20.6 mN/m), relative to TCB-H_2O. The most dramatic change was observed for the solution of **P11**, in which the interfacial tension for TCB was reduced to $\gamma_{eq,\mathbf{P11}}$ = 10.7 mN/m. In collaboration with Dr. Rachel Letteri, the room temperature γ_{eq} values of TCB in aqueous solutiosn of **P7**-**P11** were compared to γ_{eq} values for aqueous solutions of methacrylate-based polyMPC or polySBMA homopolymers ([polymer] = 1 mg/mL). In contrast to the amphiphilic zwitterionic polysiloxanes, the PC- and SB-polymethacrylate analogues produced little change in the interfacial tension (γ_{eq} = 39-40 mN/m).[41] The excellent surfactant properties of water-soluble zwitterionic polysiloxanes—qualities not exhibited by conventional

methacrylate-based polymer zwitterions—may prove useful for a wide variety of surfactant emulsion applications.

2.3. Synthesis of Functional Zwitterionic Polysiloxanes

The versatility of the zwitterionic polysiloxane platform was further augmented by synthesizing functional copolymers bearing residual pendent vinyl moieties. Such latent chemical functionality affords materials suitable for the post-polymerization modification of water-soluble polysiloxanes, as well as the production of robust self-assembled nanomaterials (*i.e.*, crosslinked micelles) and networks (*i.e.*, films, hydrogels, and elastomers). Furthermore, the thiol-ene addition chemistry allows for the preparation of functional zwitterionic polysiloxanes with tunable zwitterion content and copolymer architecture (*i.e.*, random and block copolymers).

Initial investigations explored the synthesis of functional PC-polysiloxane copolymers using the UV-mediated thiol-ene strategy depicted in Scheme 2.1. Thiol-ene modification of vinyl-containing polysiloxanes was performed in THF:MeOH mixtures using the conditions summarized in Table 2.3. Following thiol-ene reactions, vinyl content remaining in the isolated copolymers was estimated using ^{1}H-NMR spectroscopy by comparing the integral values of signals corresponding to newly formed alpha methylene

Scheme 2.1: Synthesis of functional PC-polysiloxane copolymers by thiol-ene modification.

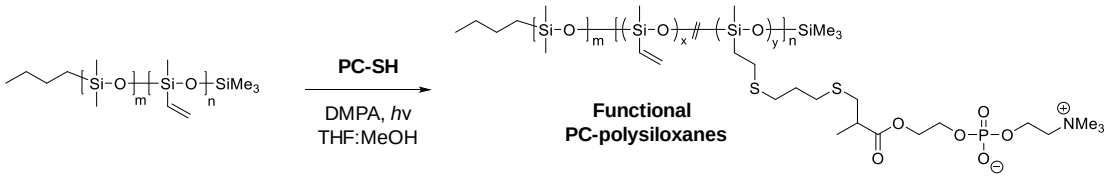

Table 2.3: Thiol-ene conditions investigated for the preparation of functional PC-polysiloxanes.

Reaction Conditions	[vinyl][a] (M)	[PS-SH]:[vinyl]	Irradiation Time[b] (min)	Residual Vinyl Content[c] (mol %)	PDI[d]
1	2.9	0.3	60	70[e]	crosslinked
2	1.9	0.7	60	54[e]	crosslinked
3	0.4	0.9	30	50	1.44
4	0.2	0.9	30	49	1.21
5	0.08	0.9	30	52	1.16
6	0.1	1.5	10	23	1.13
7	0.1	1.5	20	17	1.12
8	0.1	1.5	30	13	1.12

[a]Initial concentration of vinylsiloxane moieties.
[b]Irradiation at $\lambda = 365$ nm.
[c]Residual vinyl content estimated by ^{1}H-NMR spectroscopy in 1:1 $CDCl_3$:MeOD-d_4.
[d]PDI values estimated using GPC eluting in TFE relative to PMMA standards.
[e]Estimated for the soluble fraction.

protons of PC-modified segments (δ = 0.40-0.69 ppm) and residual vinyl protons (δ = 5.37-5.84 ppm). Additionally, PDI values for the PC-substituted copolymers were estimated using GPC eluting in TFE relative to PMMA standards. Thiol-ene reactions performed at high vinylsiloxane concentrations (reactions 1 and 2) led to undesired polymer crosslinking, which was attributed to radical coupling of pendent vinyl moieties following **PC-SH** consumption. Reactions performed at lower vinylsiloxane concentrations (conditions 3-8), on the other hand, yielded soluble PC-polysiloxanes with residual vinyl groups, narrow molecular weight distributions, and low PDI values. As shown by the results obtained for the thiol-ene conditions of reactions 3-5, the PDI values for the vinyl-containing PC-polysiloxanes were found to decrease with decreasing intial vinylsiloxane concentration. Notably, reducing the starting vinyl concentration had a negligible effect

on the content of pendent vinyl groups remaining following thiol-ene functionalization. Varying the UV irradiation time (λ = 365 nm) for the thiol-ene modification of the vinyl-functionalized polysiloxane precursors at a similar vinyl concentration (reactions 6-8) afforded copolymers with similarly low PDI values and tunable latent vinyl content. These results provide a proof-of-principle for synthesizing water-soluble, functional zwitterionic polysiloxanes.

2.4. Conclusions

In summary, the work presented in this chapter described the preparation of novel polysiloxane homopolymers and block copolymers containing pendent PC and SB zwitterions, enabled by facile thiol-ene addition chemistry. These zwitterionic polysiloxanes exhibit aqueous solubility, mediation of fluid-fluid interfaces, and micelle formation, all useful properties for advancing the chemistry and applications of polysiloxanes in aqueous media. Adjusting thiol-ene modification conditions, polysiloxanes bearing pendent zwitterions and residual reactive functionality were readily prepared. Future studies will utilize functional zwitterionic polysiloxane compositions for the preparation of novel biomaterials, with suitable applications ranging from crosslinked micelles for sustained drug delivery to hydrogel networks for ocular therapeutic applications. Additionally, latent vinyl functionality allows for covalent incorporation of these zwitterionic polysiloxane structures into silicone elastomers through conventional hydrosilylation chemistry. Such zwitterion-containing elastomers hold potential as novel antifouling coatings and hydrophilic substrates for microfluidic device fabrication.

2.5 References

1. Yilgör, E.; Yilgör, I. Silicone Containing Copolymers: Synthesis, Properties and Applications. *Prog. Polym. Sci.* **2014**, *39*, 1165-1195.

2. Jerschow, P. *Silicone Elastomers*; Smithers Rapra: Schrewsbury, 2001; Vol. 12; p 5.

3. Duffy, D. C.; McDonald, J. C.; Schueller, O. J.; Whitesides, G. M. Rapid Prototyping of Microfluidic Systems in Poly(dimethylsiloxane). *Anal. Chem.* **1998**, *70*, 4974-4984.

4. Kane, R. S.; Takayama, S.; Ostuni, E.; Ingber, D. E.; Whitesides, G. M. Patterning Proteins and Cells Using Soft Lithography. *Biomaterials* **1999**, *20*, 2363-2376.

5. Yoda, R. Elastomers for Biomedical Applications. *J. Biomater. Sci. Polym. Ed.* **1998**, *9*, 561-626.

6. Nicolson, P. C.; Vogt, J. Soft Contact Lens Polymers: An Evolution. *Biomaterials* **2001**, *22*, 3273-3283.

7. Özçam, A. E.; Efimenko, K.; Genzer, J. Effect of Ultraviolet/Ozone Treatment on the Surface and Bulk Properties of Poly(dimethylsiloxane) and Poly(vinylmethylsiloxane) Networks. *Polymer* **2014**, *55*, 3107-3119.

8. Nguyen, L.; Hang, M.; Wang, W.; Tian, Y.; Wang, L.; McCarthy, T. J.; Chen, W. Simple and Improved Approaches to Long-Lasting, Hydrophilic Silicones Derived from Commercially Available Precursors. *ACS Appl. Mater. Interfaces* **2014**, *6*, 22876-22883.

9. Ye, S-H.; Johnson, C. A.; Woolley, J. R.; Murata, H.; Gamble, L. J.; Ishihara, K.; Wagner, W. R. Simple Surface Modification of a Titanium Alloy with Silanated Zwitterionic Phosphorylcholine or Sulfobetaine Modifiers to Reduce Thrombogenicity. *Colloids Surf. B Biointerfaces* **2010**, *79*, 357-364.

10. Yuan, Y.; Zang, X.; Ai, F.; Zhou, J.; Shen, J.; Lin, S. Grafting Sulfobetaine Monomer onto Silicone Surface to Improve Haemocompatibility. *Polym. Int.* **2004**, *53*, 121-126.

11. Goda, T.; Konno, T.; Takai, M.; Moro, T.; Ishihara, K. Biomimetic Phosphorylcholine Polymer Grafting from Polydimethylsiloxane Surface Using Photo-Induced Polymerization. *Biomaterials* **2006**, *27*, 5151-5160.

12. Gonçalves, S.; Leirós, A.; van Kooten, T.; Dourado, F.; Rodrigues, L. R. Physicochemical and Biological Evaluation of Poly(ethylene glycol) Methacrylate Grafted Onto Poly(dimethylsiloxane) Surfaces for Prosthetic Devices. *Colloids Surf. B Biointerfaces* **2013**, *109*, 228-235.

13. Halila, S.; Manguian, M.; Fort, S.; Cottaz, S.; Hamaide, T.; Fleury, E.; Driguez, H. Syntheses of Well-Defined Glyco-Polyorganosiloxanes by "Click" Chemistry and Their Surfactant Properties. *Macromol. Chem. Phys.* **2008**, *209*, 1282-1290.

14. Du, Z.; Qin, J.; Wang, W.; Zhu, Y.; Wang, G. Synthesis, Surface Activities, and Aggregation Behaviors of Butynediol-ethoxylate Modified Polysiloxanes. *J. Phys. Chem. B* **2015**, *119*, 14180-14187.

15. Snow, S. A.; Fenton, W. N.; Owen, M. J. Synthesis and Characterization of Zwitterionic Silicone Sulfobetaine Surfactants. *Langmuir* **1990**, *6*, 385-391.

16. Sauvet, G.; Fortuniak, W.; Kazmierski, K.; Chojnowski, J. Amphiphilic Block and Statistical Siloxane Copolymers with Antimicrobial Activity. *J. Polym. Sci. A Polym. Chem.* **2003**, *41*, 2939-2948.

17. Mizerska, U.; Fortuniak, W.; Chojnowski, J.; Halasa, R.; Konopacka, A.; Werel, W. Polysiloxane Cationic Biocides with Imidazolium Salt (ImS) Groups, Synthesis and Antibacterial Properties. *Eur. Polym. J.* **2009**, *45*, 779-787.

18. Rambarran, T.; Gonzaga, F.; Brook, M. A. Multifunctional Amphiphilic Siloxane Architectures Using Sequential, Metal-Free Click Ligations. *J. Polym. Sci. A Polym. Chem.* **2013**, *51*, 855-864.

19. Li, D.; Li, C.; Wan, G.; Hou, W. Self-Assembled Vesicles of Amphiphilic Poly(dimethylsiloxane)-*b*-Poly(ethylene glycol) Copolymers as Nanotanks for Hydrophobic Drugs. *Colloids Surf. A* **2010**, *372*, 1-8.

20. Rheingans, O.; Hugenberg, N.; Harris, J. R.; Fischer, K.; Maskos, M. Nanoparticles Built of Cross-Linked Heterotelechelic, Amphiphilic Poly(dimethylsiloxane)-*b*-Poly(ethylene oxide) Diblock Copolymers. *Macromolecules* **2000**, *33*, 4780-4790.

21. Nardin, C.; Hirt, T.; Leukel, J.; Meier, W. Polymerized ABA Triblock Copolymer Vesicles. *Langmuir* **2000**, *16*, 1035-1041.

22. Choi, H-J.; Brooks, E.; Montemagno, C. D. Synthesis and Characterization of Nanoscale Biomimetic Polymer Vesicles and Polymer Membranes for Bioelectronic Applications. *Nanotechnology* **2005**, *16*, S143-S149.

23. Seo, J-H.; Matsuno, R.; Takai, M.; Ishihara, K. Cell Adhesion on Phase-Separated Surface of Block Copolymer Composed of Poly(2-methacryloyloxyethyl Phosphorylcholine) and Poly(dimethylsiloxane). *Biomaterials* **2009**, *30*, 5330-5340.

24. Boehm, P.; Mondeshki, M.; Frey, H. Polysiloxane-Backbone Block Copolymers in a One-Pot Synthesis: A Silicone Platform for Facile Functionalization. *Macromol. Rapid Commun.* **2012**, *33*, 1861-1867.

25. Lunn, D. J.; Boott, C. E.; Bass, K. E.; Shuttleworth, T. A.; McCreanor, N. G.; Papadouli, S.; Manners, I. Controlled Thiol-Ene Functionalization of Polyferrocenylsilane-*block*-Polyvinylsiloxane Copolymers. *Macromol. Chem. Phys.* **2013**, *214*, 2813-2820.

26. Laughlin, R. G. Fundamentals of the Zwitterionic Hydrophilic Group. *Langmuir* **1991**, *7*, 842-847.

27. Chen, M.; Briscoe, W. H.; Armes, S. P.; Klein, J. Lubrication at Physiological Pressures by Polyzwitterionic Brushes. *Science* **2009**, *323*, 1698-1701.

28. Whelan, D. M.; van der Giessen, W. J.; Krabbendam, S. C.; van Vliet, E. A.; Verdouw, P. D.; Serruys, P. W.; van Beusekom, H. M. M. Biocompatibility of Phosphorylcholine Coated Stents in Normal Porcine Coronary Arteries. *Heart* **2000**, *83*, 338-345.

29. Chen, X.; Parelkar, S. S.; Henchey, E.; Schneider, S.; Emrick, T. PolyMPC-Doxorubicin Prodrugs. *Bioconjugate Chem.* **2012**, *23*, 1753-1763.

30. Zhang, Z.; Chao, T.; Liu, L.; Cheng, G.; Ratner, B. D.; Jiang, S. Zwitterionic Hydrogels: An In Vivo Implantation Study. *J. Biomater. Sci. Polym. Ed.* **2009**, *20*, 1845-1859.

31. Ishihara, K.; Nomura, H.; Mihara, T.; Kurita, K.; Iwasaki, Y.; Nakabayashi, N. Why Do Phospholipid Polymers Reduce Protein Adsorption? *J. Biomed. Mater. Res.* **1998**, *39*, 323-330.

32. Iwasaki, Y.; Ishihara, K. Phosphorylcholine-Containing Polymers for Biomedical Applications. *Anal. Bioanal. Chem.* **2005**, *381*, 534-546.

33. Zhang, Z.; Chao, T.; Chen, S.; Jiang, S. Superlow Fouling Sulfobetaine and Carboxybetaine Polymers on Glass Slides. *Langmuir* **2006**, *22*, 10072-10077.

34. Hoyle, C. E.; Bowman, C. N. Thiol-Ene Click Chemistry. *Angew. Chem. Int. Ed.* **2010**, *49*¸1540-1573.

35. Chojnowski, J.; Cypryk, M.; Fortuniak, W.; Rózga-Wijas, K.; Ścibiorek, M. Controlled Synthesis of Vinylmethylsiloxane-Dimethylsiloxane Gradient, Block and Alternate Copolymers by Anionic ROP of Cyclotrisiloxanes. *Polymer* **2002**, *43*, 1993-2001.

36. Goda, T.; Tabata, M.; Sanjoh, M.; Uchimura, M.; Iwasaki, Y.; Miyahara, Y. Thiolated 2-Methacryloyloxyethyl Phosphorylcholine for an Antifouling Biosensor Platform. *Chem. Commun.* **2013**, *49*, 8683-8685.

37. Uygun, M.; Tasdelen, M.; Yagci, Y. Influence of Type of Initiation on Thiol-Ene "Click" Chemistry. *Macromol. Chem. Phys.* **2010**, *211*, 103-110.

38. Jasinski, F.; Lobry, E.; Tarablsi, B.; Chemtob, A.; Croutxé-Barghorn, C.; Nouen, D. L.; Criqui, A. Light-Mediated Thiol-Ene Polymerization in Miniemulsion: A Fast Route to Semicrystalline Polysulfide Nanoparticles. *ACS Macro. Lett.* **2014**, *3*, 958-962.

39. Lowe, A. B.; McCormick, C. L. Synthesis and Solution Properties of Zwitterionic Polymers. *Chem. Rev.***2002**, *102*, 4177-4189.

40. Woodfield, P. A.; Zhu, Y.; Pei, Y.; Roth, P. J. Hydrophobically Modified Sulfobetaine Copolymers with Tunable Aqueous UCST through Postpolymerization Modification of Poly(pentafluorophenyl acrylate). *Macromolecules* **2014**, *47*, 750-762.

41. Chang, C-C.; Letteri, R.; Hayward, R.; Emrick, T. Functional Sulfobetaine Polymers: Synthesis and Salt-Responsive Stabilization of Oil-in-Water Droplets. *Macromolecules* **2015**, *48*, 7843-7850.

CHAPTER 3

ZWITTERIONIC PLURONIC MIMICS

3.1 Introduction

Poly(ethylene oxide)-poly(propylene oxide)-poly(ethylene oxide) (PEO-PPO-PEO) triblock copolymers comprise a family of versatile surfactants utilized commercially as emulsifiers, antifoaming agents, detergents, dispersants, coatings, and pharmaceutical excipients.[1-7] Known commonly under the trade name Pluronic®, these water-dispersible block copolymer amphiphiles are prepared by the sequential ring-opening polymerization of propylene oxide and ethylene oxide,[1] affording copolymers with narrow molecular weight distributions and varying hydrophilic-lipophilic balance (HLB). In aqueous solution, Pluronics exhibit complex assembly behavior, including micelle formation above a critical concentration with aggregation and morphological properties dependent on copolymer HLB, concentration, solution conditions, and processing.[3,7-15] For most Pluronic compositions, aqueous micelle formation is thermoreversible, a behavior which arises from the lower critical solution temperature (LCST) miscibility of PPO in water. Additionally, several Pluronic copolymers undergo thermally induced physical gelation at high polymer concentrations,[16] a characteristic mediated by micellar aggregation. Owing to their aqueous assembly properties, Pluronics are used as templates for mesoporous and nanomaterials synthesis and are investigated extensively for drug delivery.[6,7,16-19]

Synthetic modifications of Pluronics alter their solution properties in water,[20,21] produce bioconjugates,[22] and enhance their stability *via* covalent crosslinking.[23-25] Due to the inert nature of the polyether backbone, functionalization is restricted to the chain-end hydroxyl groups. Strategies currently employed in Pluronic functionalization are generally

tedious and inefficient, requiring long reaction times to approach complete chain-end modification. Alternative approaches that produce chemical compositions mimicking conventional PEO-PPO-PEO copolymers will allow access to amphiphiles with tunable chemical functionality, while retaining the desirable surfactant qualities of Pluronics. Notable examples include biodegradable compositions which incorporate hydrolytically labile ester, phosphoester, or acetal moieties,[26-28] as well as analogs that exhibit aqueous assembly behavior and present pendent moieties amenable to post-polymerization modification.[29-32]

Zwitterionic polymers, containing polar moieties composed of covalently tethered anion-cation pairs, are of interest as the hydrophilic components of polymer amphiphiles.[33-38] Typical examples incorporate the zwitterions as pendent or chain-end groups and serve as novel materials for controlled release, aqueous assembly, antifouling coatings, and interfacial stabilization. Though numerous amphiphiles have been reported, only two examples of zwitterionic materials which mimic conventional Pluronics have been reported.[37,38] Li, *et al*. described poly(carboxybetaine methacrylate)-PPO-poly(carboxybetaine methacrylate) triblock copolymers as functional antifouling coatings for hydrophobic surfaces.[37] While these zwitterionic triblock copolymers produced nonfouling surfaces amenable to protein conjugation through the pendent carboxybetaines, the chemical characterization of these block copolymer amphiphiles was not reported, and their aqueous solution properties were not investigated. Jeong and coworkers reported the chain-end modification of PPO with PC groups, affording PC-PPO-PC amphiphiles which exhibited aqueous assembly and thermal gelation.[38] Although this PPO derivative is well-suited as a thermoreversible matrix, accessing water-dispersible polymer amphiphiles with

tunable critical aggregation concentrations (CACs), aggregate size, and LCST values is precluded using this strategy. As such, this work set out to prepare and investigate poly(2-methacryloyloxyethyl phosphorylcholine)-*b*-PPO-*b*-poly(2-methacryloyloxyethyl phosphorylcholine) (polyMPC-*b*-PPO-*b*-PPO) as Pluronic analogs with a modular and functional amphiphilic design.

This section focuses on a new class of Pluronic mimics incorporating PC groups as naturally occurring zwitterions to impart antifouling properties, biocompatibility,[39-41] and excellent aqueous dispersibility.[36] These novel 'zwitteronics' were prepared by atom transfer radical polymerization (ATRP) of zwitterionic methacrylates initiated from the chain-ends of homotelechelic PPO macroinitiators. Upon discovering optimal polymerization conditions, a series of triblock copolymers was prepared by the macroinitiated polymerization of MPC. These polyMPC-PPO-polyMPC triblock copolymers were synthesized with narrow molecular weight distributions (PDI = 1.14-1.32), as characterized by gel permeation chromatography (GPC), and with MPC incorporation ranging from 5-47 mole percent. Owing to the exceptional hydrophilicity of the pendent zwitterions, the PC-zwitteronic amphiphiles were readily dispersed in water and exhibited surfactant behavior, which by surface tensiometry proved distinct from Pluronics. These triblock copolymers self-assembled in water into soft nanoparticles, and several compositions exhibited thermoreversible aggregation. Their aqueous assembly properties, including critical aggregation concentration (CAC), nanoparticle size, and LCST miscibility, were assessed using a pyrene fluorescence assay, dynamic light scattering (DLS), and UV-Vis spectroscopy, respectively. Importantly, the block copolymer assembly parameters were tuned readily by varying zwitterion content and

block copolymer HLB. Seeking to demonstrate the versatility of this novel materials platform, functional zwitteronics were prepared by copolymerizing MPC with an alkyne-substituted choline phosphate methacrylate (MCP), a 'reverse' zwitterionic monomer that embeds alkynes directly within the choline phosphate moieties.[42] Functional zwitteronics with 15-17 mole percent alkyne incorporation were prepared, and their amenability to post-polymerization thiol-yne modification was utilized for nanoparticle crosslinking and the formation of robust, covalently crosslinked nanoparticle networks.

3.2 Synthesis of Zwitterionic Pluronic Mimics

A homotelechelic PPO macroinitiator bearing chain-end alkyl halides suitable for initiating ATRP of methacrylate monomers was synthesized following a modified procedure.[30] As shown in Scheme 3.1, macroinitiator **P15** was prepared by esterification of commercial PPO with 2-bromoisobutyrylbromide in dry tetrahydrofuran (THF). Macroinitiator purification—critical for preparing block copolymer samples devoid of homopolymer contaminants—was performed by washing with aqueous sodium hydroxide (NaOH) and stirring over decolorizing carbon. This procedure afforded **P15** as a viscous orange oil in excellent purity and good yield (~70-75%).

Scheme 3.1: Synthesis of PPO macroinitiator **P15**.

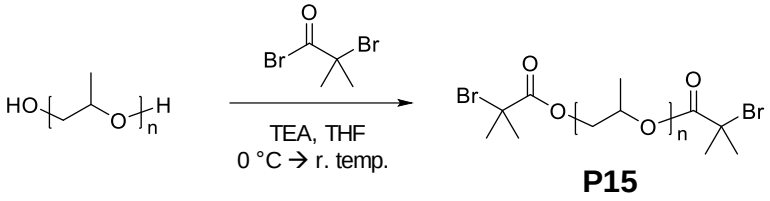

P15

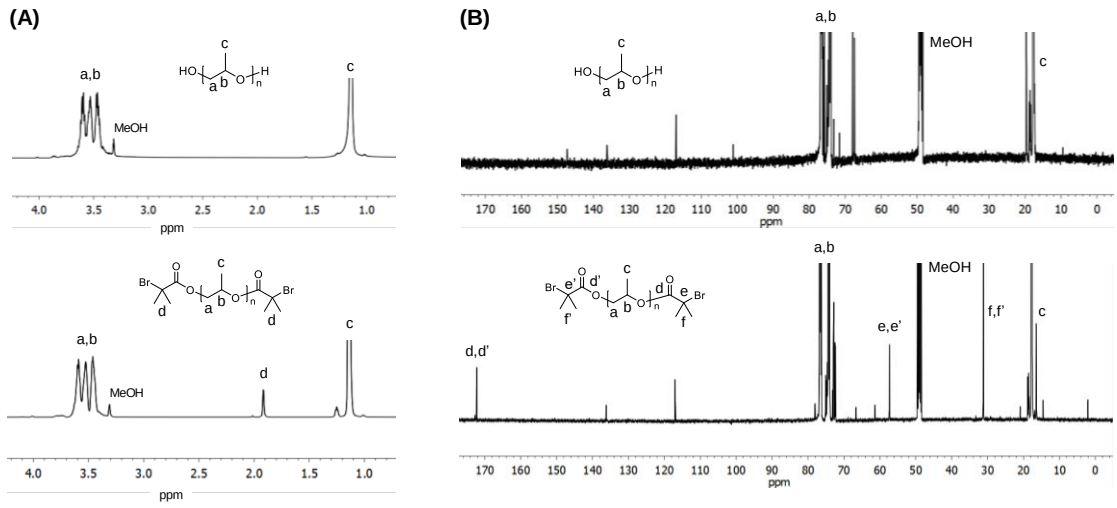

Figure 3.1: (A) ^{1}H-NMR (500 MHz) spectra of the PPO starting material (top) and macroinitiator **P15** (bottom) in MeOD-d_4; (B) ^{13}C-NMR (125 MHz) of the PPO starting material (top) and macroinitiator **P15** (bottom) in MeOD-d_4.

Macroinitiator **P15** was characterized by NMR spectroscopy to confirm esterification at each chain end. In the ^{1}H-NMR spectrum of **P15**, a singlet at 1.92 ppm corresponded to the methyl protons of the bromoisobutyrates; this signal was notably absent in the spectrum of the PPO starting material (Figure 3.1A). Additionally, ^{13}C-NMR resonances of **P15** (Figure 3.1B) at 172.26/172.25 and 57.36/57.33 ppm were attributed to the carbonyl and quaternary alkyl bromide moieties, respectively, of each esterified chain-end. Matrix-assisted laser desorption/ionization time-of-flight (MALDI-TOF) mass spectrometry provided additional confirmation of the macroinitiator chain-end identity, with spectra of the PPO starting material and polymer **P15** shown in Figure 3.2. In each spectrum, major and minor signals are attributed to sodiated and potassiated analytes, respectively; the most intense signals corresponding to analytes with number-average degree of polymerization (X_n) of 79-82 are magnified. Differences in mass-to-charge ratio (m/z) values for structures of similar X_n ranged from 297.3 to 298.9, with a mean difference of 298.3, in excellent agreement with the change expected following the addition of two

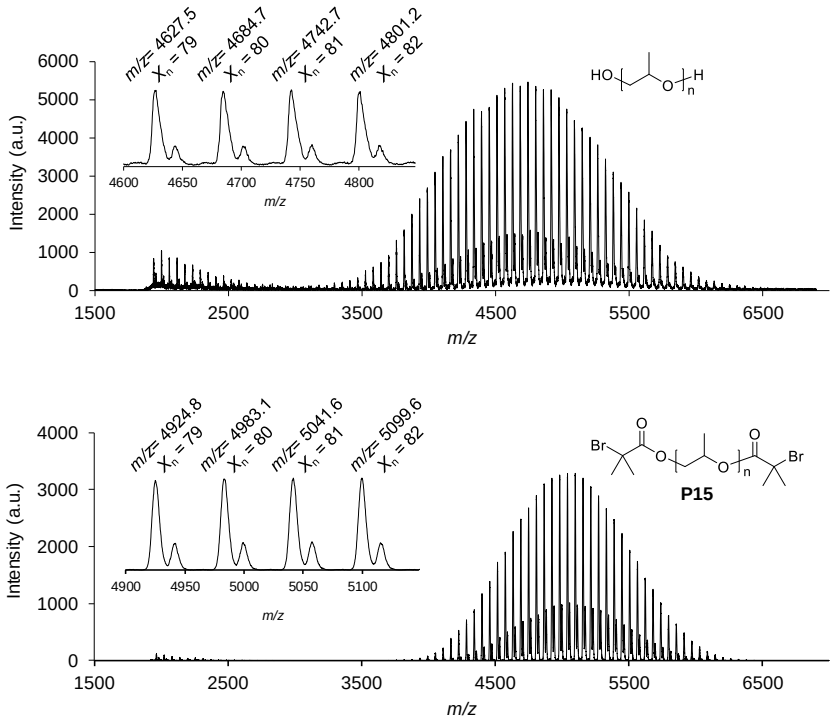

Figure 3.2: MALDI-TOF mass spectra of the commercial PPO starting material (top) and macroinitiator **P15** (bottom). Signals attributed to analytes with X_n values of 79-82 for each polymer are inset with corresponding *m*/*z* values.

α,ω-bromoisobutyrate groups (Δ *m*/z = 298.0). MALDI-TOF measured the absolute molecular weight of PPO macroinitiator **P15** as 5,060 g/mol with a PDI value of 1.01, with a lower molecular weight fraction attributed to oligomeric species (this was also observed in the spectrum of the commercial PPO starting material). Characterization of both polymer samples using gel permeation chromatography (GPC), eluting in 2,2,2-trifluoroethanol (TFE), showed similar evidence of oligomeric impurities, suggesting that these structures did not arise from ionization-induced fragmentation during MALDI-TOF analysis. Importantly, this minor oligomeric component did not interfere with the block copolymer syntheses.

Scheme 3.2: Synthesis of PC-zwitterions **P16-P20** by macroinitiated-ATRP.

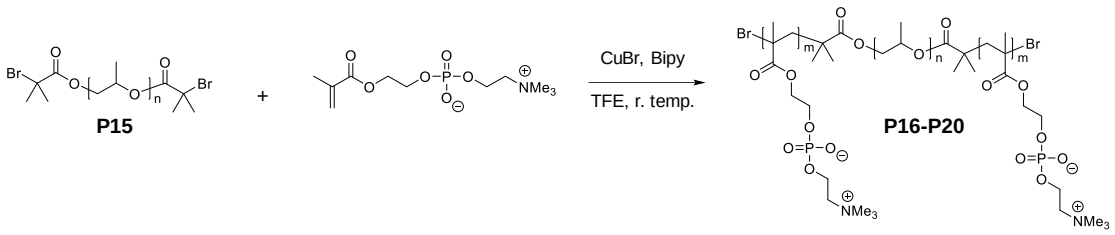

PC-zwitteronics, termed **P16-P20**, were prepared by ATRP of MPC from the chain ends of macroinitiator **P15**, as shown in Scheme 3.2. Polymerizations were conducted at room temperature at a monomer concentration of 0.5 M in TFE, mediated with a copper(I) bromide (CuBr)/2,2'-bipyridyl (Bipy) catalyst system. When targeting MPC incorporations of 7-46 mole percent, monomer conversions of 83-97% were achieved, as estimated by ^{1}H-NMR spectroscopy. Polymerizations were quenched by exposure to air and residual copper was removed by elution through a short plug of silica gel. The polymers were purified further by dialysis in water, followed by lyophilization to afford **P16-P20** in 42-78% yield. **P16**, containing the shortest polyMPC blocks, was isolated as a semi-solid, while **P17-P20** were obtained as white powders.

Successful incorporation of polyMPC into block copolymers **P16-P20** was confirmed and quantified by NMR spectroscopy. As shown in the representative ^{1}H-NMR spectrum of **P20** in Figure 3.3A, characteristic resonances for both the polyMPC and PPO blocks were observed, including signals attributed to the trimethylammonium group (peak k, δ = 3.32 ppm) and PPO methylene protons (peaks a and b, δ = 3.41-3.67 ppm). A single resonance corresponding to the phosphate moieties of the PC groups was observed in the ^{31}P-NMR spectrum of **P20** at -0.51 ppm (Figure 3.3B), confirming successful polymerization of MPC from the macroinitiator. As summarized in Figure 3.3C, polymerization stoichiometries targeted MPC incorporations of 7, 16, 28, 38, and 46 mole

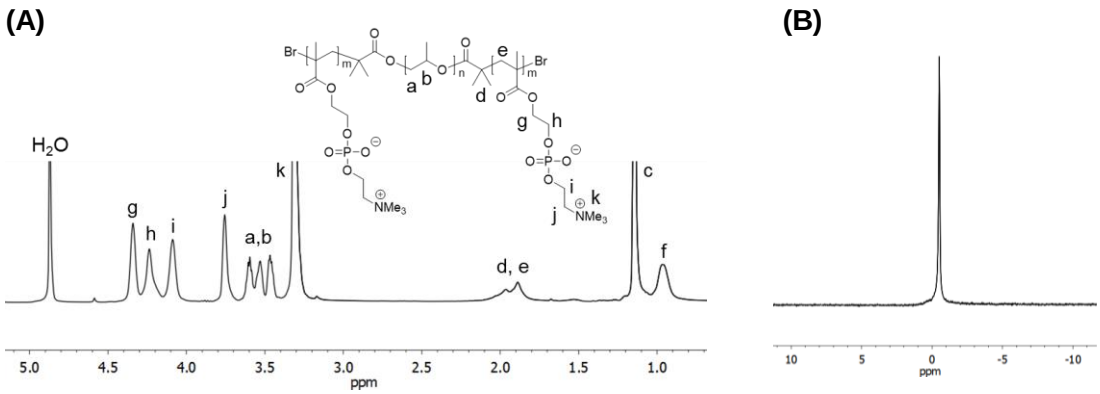

(C)

Polymer	Targeted MPC incorporation (mol %)	Measured MPC incorporation (mol %)[a]	Copolymer composition
P16	7	5	polyMPC$_2$-PPO$_{82}$-polyMPC$_2$
P17	16	15	polyMPC$_7$-PPO$_{82}$-polyMPC$_7$
P18	23	20	polyMPC$_{11}$-PPO$_{82}$-polyMPC$_{11}$
P19	38	35	polyMPC$_{22}$-PPO$_{82}$-polyMPC$_{22}$
P20	46	47	polyMPC$_{36}$-PPO$_{82}$-polyMPC$_{36}$

[a]Measured using ^{1}H-NMR spectroscopy (500 MHz, MeOD-d$_4$)

Figure 3.3: (A) Representative ^{1}H-NMR spectrum (500 MHz) of PC-zwitteronic **P20** in MeOD-d$_4$; (B) representative ^{31}P-NMR spectrum (202 MHz) of **P20** in MeOD-d$_4$; (C) targeted and estimated copolymer compositions of block copolymers **P16**-**P20**.

percent for **P16**-**P20**, respectively. MPC incorporations in the block copolymers were estimated by integration of ^{1}H-NMR signal intensities of PC methylene (peaks g-i, δ = 4.01-4.41 ppm) *vs*. PPO methylene resonances (peaks a and b, δ = 3.41-3.67 ppm). In general, these NMR-estimated values were in excellent agreement with targeted incorporations. Using the X_n value for polymer **1** obtained by MALDI-TOF analysis (X_n = 82), the compositions of the PC-zwitteronic block copolymers were estimated. As shown in Figure 3.3C, PC-zwitteronics were prepared with varying solution properties due to the polyMPC X_n values, ranging from 2 to 36.

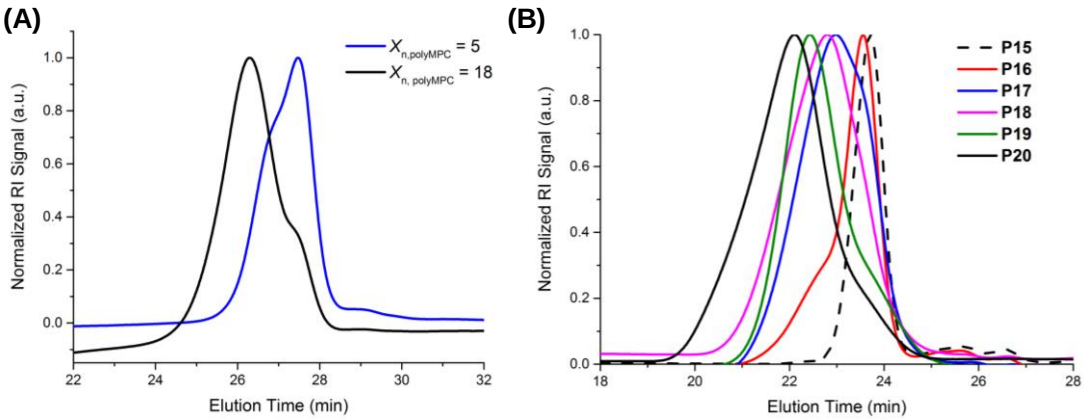

(C)

Polymer	M_n (g/mol)[a]	PDI[a]
P15	19,850	1.01
P16	20,850	1.14
P17	25,180	1.18
P18	26,530	1.17
P19	29,200	1.16
P20	34,670	1.32

[a]M_n and PDI values estimated by GPC eluting in TFE relative to PMMA standards.

Figure 3.4: (A) GPC chromatograms of PC-zwitteronics eluting in TFE prepared using MeOH as the polymerization solvent with polyMPC segments having X_n values of 5 or 18; (B) GPC chromatograms of polymers **P15**-**P20** eluting in TFE; (C) values of M_n and PDI for **P15**-**P20** estimated by GPC eluting in TFE relative to PMMA standards.

Selecting a suitable polymerization solvent proved crucial for preparing PC-zwitteronic block copolymers with narrow molecular weight distributions. Polymerization in methanol (MeOH) gave block copolymer products with bimodal molecular weight distributions, as characterized by GPC (Figure 3.4A). This lack of control over polymerization kinetics was attributed to phase separation that occurred upon mixing homogenous solutions of MPC and **P15**. In contrast, polymerizations performed in TFE, a good solvent for polymer zwitterions,[36,43] led to well-defined triblock copolymers. Molecular weight distributions of polymers **P15**-**P20**, shown in Figure 3.4B, were characterized by GPC eluting in TFE, with M_n and PDI values estimated relative to PMMA

calibration standards (Figure 3.4C). As anticipated, M_n values for **P16-P20** increased with polyMPC X_n, and all block copolymers were isolated with reasonably low PDI values. High and low molecular weight shoulders were noted in the chromatograms of **P16** and **P19**, respectively. Although these features suggest varying rates of MPC initiation from the PPO macroinitiator chain ends, they were at low intensity relative to the main polymer peaks. Moreover, the macroinitiated ATRP of MPC in TFE affords polyMPC-PPO-polyMPC triblock copolymers with precisely tunable compositions and narrow molecular weight distributions.

Owing to the orthogonal solubility of the PPO and zwitterionic blocks, the PC-zwitteronics readily aggregated into nanoparticles in water with hydrodynamic diameters ranging from 16 to 164 nm. CAC values of block copolymers **P16-P20** were estimated in pure water using a pyrene fluorescence assay in which photoluminescence (PL) emission of the hydrophobic fluorophore is sensitive to its local chemical environment.[44] In aqueous surfactant-containing solutions, the ratio of the PL peak intensities corresponding to the first (I_1, λ_{em} ~ 374 nm) and third (I_3, λ_{em} ~ 385 nm) vibronic bands decreases sharply as pyrene is encapsulated in the nanoparticle core. To estimate CAC values for the PC-zwitteronic block copolymers, pyrene was added at ~0.6 μM in serial aqueous dilutions of polymers **P16-P20**. After incubating at room temperature for 16-18 hours, PL emission spectra were collected at an excitation wavelength of 336 nm. Figure 3.5A shows a representative plot of I_1/I_3 values for **P19** at different polymer concentrations. Above a critical concentration, the I_1/I_3 value decreased rapidly, indicating pyrene solubilization into the nanoparticle core. Similar behavior was noted for the other PC-zwitteronics, and the CAC of each block copolymer was estimated from the onset of the I_1/I_3 reduction. The

(A)

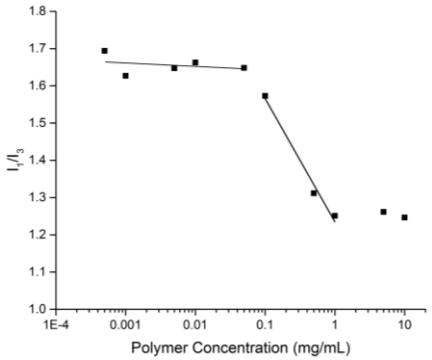

(B)

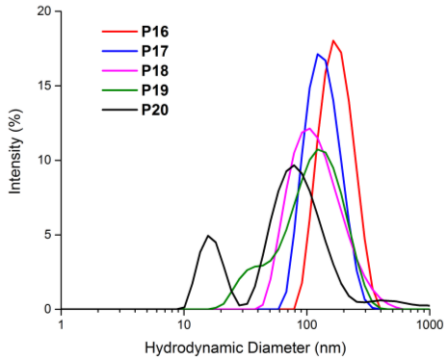

(C)

Polymer	CAC[a] (mg/mL)	Pluronic Equivalent CAC[45] (mg/mL)	Hydrodynamic Diameter[e] (nm)
P16	0.0017	-	164
P17	0.0055	0.0044[b]	122
P18	0.011	-	106
P19	0.058	0.025[c]	38, 122
P20	0.062	0.035[d]	16, 79

[a]Aqueous CAC values estimated using a pyrene fluorescence assay fluorescence assay. [b]Pluronic L121 (PEO_5-PPO_{68}-PEO_5). [c]Pluronic P123 (PEO_{20}-PPO_{69}-PEO_{20}). [d]Pluronic F127 (PEO_{100}-PPO_{65}-PEO_{100}). [e]Hydrodynamic diameters of PC-zwitteronics measured by DLS analysis of 1 mg/mL aqueous suspensions.

Figure 3.5: (A) A representative plot of the relative fluorescence intensity of the first (I_1) and third (I_3) vibronic bands for pyrene in aqueous solutions at varying **P19** concentrations; (b) DLS plots for **P16**-**P20** in water above CAC at 25 °C; (c) CAC values for **P16**-**P20** and Pluronics L121, P123, and F127 estimated using a pyrene fluorescence assay, as well as corresponding aggregate hydrodynamic diameters measured using DLS.

estimated CACs, summarized in Figure 3.5C, decreased with polyMPC block length. Relative to comparable Pluronic compositions (*i.e.*, Pluronic L121, P123, and F127), PC-zwitteronics exhibited higher CACs, evident by comparing values determined for **P17** and **P19** with those of commercial Pluronics having hydrophilic segments with similar X_n values (L121 and P123, respectively).[45] Furthermore, **P19** and **P20** exhibited higher CAC values than F127, a Pluronic having X_n for each PEO segment of 100. These higher CAC

values suggest a greater hydrophilicity of the zwitterionic blocks relative to PEO, findings consistent with investigations demonstrating greater hydration and hydrophilicity of zwitterionic *vs.* EO-based surfactants, hydrogels, and films.[46-49]

The hydrodynamic diameters of these zwitteronic nanoparticles, comprising hydrophobic PPO cores and hydrophilic polyMPC coronae, were assessed by DLS at concentrations well above the CAC of each polymer (1 mg/mL). DLS plots and hydrodynamic diameters for **P16**-**P20**, after filtration through 0.45 μm membranes, are shown in Figure 3.5B. Block copolymers **P16**-**P18** formed monomodal particles with mean diameters ranging from 106-164 nm which decreased with zwitterion content. In contrast, the more hydrophilic block copolymers **P19** and **P20** formed bimodal nanoparticles consisting predominantly of the smaller (38 and 16 nm, respectively) aggregates, as confirmed by number-based DLS analysis.

In addition to exhibiting concentration-dependent assembly properties, PC-zwitteronics exhibited thermoresponsive aqueous miscibility and clouding behavior analogous to conventional Pluronics. Aqueous solubility was assessed by measuring visible light transmission (λ = 550 nm) through 10 mg/mL suspensions of PC-zwitteronics in water as a function of temperature. As shown in Figure 3.6, block copolymers **P16**-**P18** exhibited sharp LCST transitions ranging from -2.6 to 0.5 °C, increasing with PC content. On the other hand, the more hydrophilic **P19** showed a weak cloud point transition at 9.9 °C, while the triblock copolymer with the longest polyMPC block, **P20**, demonstrated no LCST behavior. Surprisingly, the PC-zwitteronic block copolymers did not undergo the thermally induced physical gelation characteristic of conventional Pluronics, even at polymer concentrations approaching 200 mg/mL (17 weight percent) in water and at

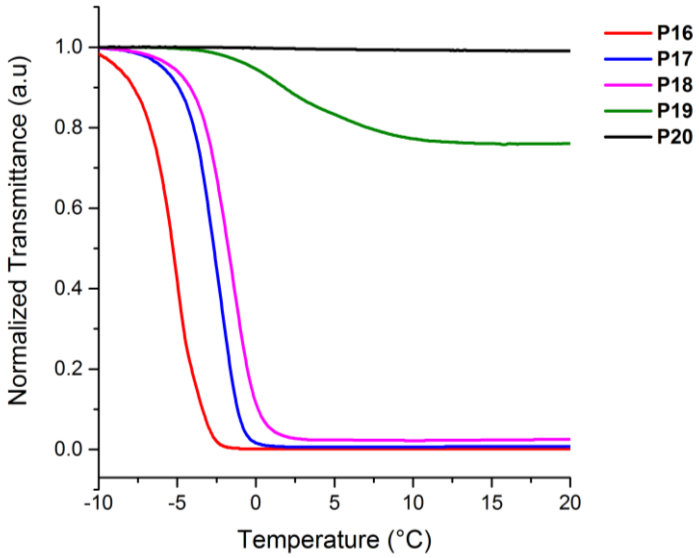

Figure 3.6: Cloud point curves for **P16**-**P20** suspensions (10 mg/mL in water).

temperatures up to 95 °C. In comparison, Pluronic F127 gelled at 200 mg/mL and 36 °C. As physical crosslinking of Pluronics solutions is induced by hydrophobic interactions and micellar aggregation,[16] the absence of thermal gelation behavior exhibited by the zwitteronic block copolymers suggests that the pendent zwitterions are sufficiently hydrated so as to prevent aggregation, even at high concentrations.

Surface tension measurements of aqueous suspensions of **P16**-**P20**, above their CAC values, were performed using a Langmuir instrument equipped with cylindrical glass troughs (0.2 cm depth, 1.5 cm diameter) and a metal probe (0.51 mm diameter). Measurements were conducted by inserting the tip of the probe into the polymer suspensions (~350 µL), allowing the block copolymer amphiphiles to spread from the air-water interface to the probe surface. The probe was equilibrated in each polymer solution for at least 10 minutes, and equilibrium surface tension values (γ_{eq}) were obtained by averaging the observed γ values at the end of each measurement. Values of γ_{eq} for **P16**-**P20** are shown in Figure 3.7A, along with γ_{eq} obtained for the PPO starting material, a

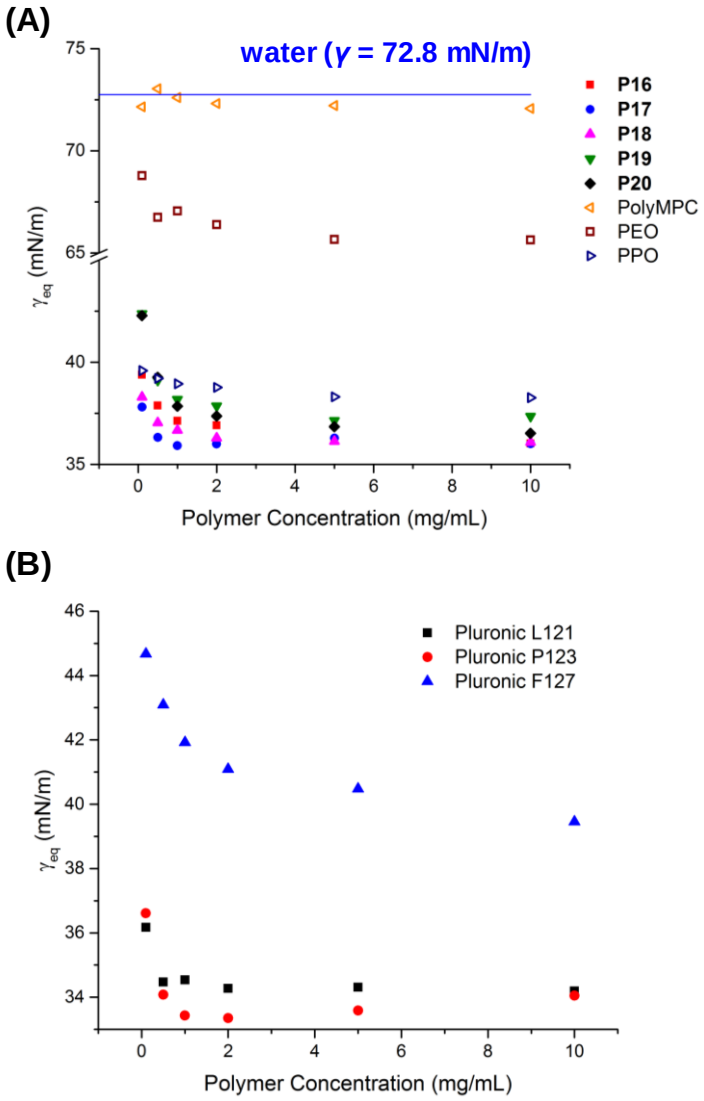

Figure 3.7: (A) Room temperature γ_{eq} values for aqueous suspensions of PC-zwitterionics **P16-P20**, polyMPC **P21**, PEO, and PPO at varying polymer concentrations. The blue line shows γ_{eq} for pure water (72.8 mN/m); (B) room temperature γ_{eq} values measured for Pluronics L121, P123, and F127 at varying polymer concentrations in pure water.

polyMPC homopolymer sample prepared by reversible addition-fragmentation chain-transfer (RAFT) polymerization (**P21**, M_n = 38,500 g/mol, PDI = 1.08), and a commercial sample of PEO (M_n ~ 1,500 g/mol). While the PEO homopolymer showed a slight reduction in aqueous surface tension (γ_{eq} = 68.8-65.6), water-soluble polyMPC **P21**

exhibited γ_{eq} values comparable to pure water (72.1-73.0 mN/m), demonstrating its hydrophilic, non-surface-active nature. The PC-zwitteronics, on the other hand, markedly altered the aqueous surface tension, reducing γ_{eq} to 37.8-42.4 and 36.0-37.4 mN/m at concentrations of 0.1 and 10 mg/mL, respectively. Values of γ_{eq} for **P16**-**P20** were nearly equivalent to that of the PPO starting material at all concentrations. Pluronics L121 and P123 showed similar surface activity in water, reducing γ_{eq} to values of 36.2 and 36.6 mN/m respectively, at a concentration of 0.1 mg/mL, and 34.2 and 34.1 mN/m at 10 mg/mL (Figure 3.7B). In comparison, the more hydrophilic Pluronic F127 was less surface active, reducing γ_{eq} to values of 44.7 and 39.5 mN/m at concentrations of 0.1 and 10 mg/mL, respectively. This diminished surface activity is characteristic of Pluronics, for which aqueous surface tension values of compositions with similar PPO molecular weight generally increase with increasing PEO molecular weight.[3,50] In contrast, PC-zwitteronics **P16**-**P20** exhibited a non-monotonic change in γ_{eq} with increasing polyMPC X_n and demonstrated composition-independent surfactant properties.

3.3 Synthesis of Functional Zwitterionic Pluronic Mimics

Seeking to expand the scope of the zwitteronics platform by introducing reactive functionality, zwitteronic block copolymers bearing pendent alkyne moieties distributed randomly throughout the hydrophilic blocks were synthesized by macroinitiated-ATRP. Alkyne groups, amenable to modification using azide-alkyne cycloaddition or thiol-yne chemistries, were incorporated into the hydrophilic segments by copolymerization of trimethylsilyl (TMS) alkyne-substituted choline phosphate methacrylate **1** with MPC.[42] As shown in Figure 3.8A, alkyne-substituted **P22** and **P23** were synthesized by

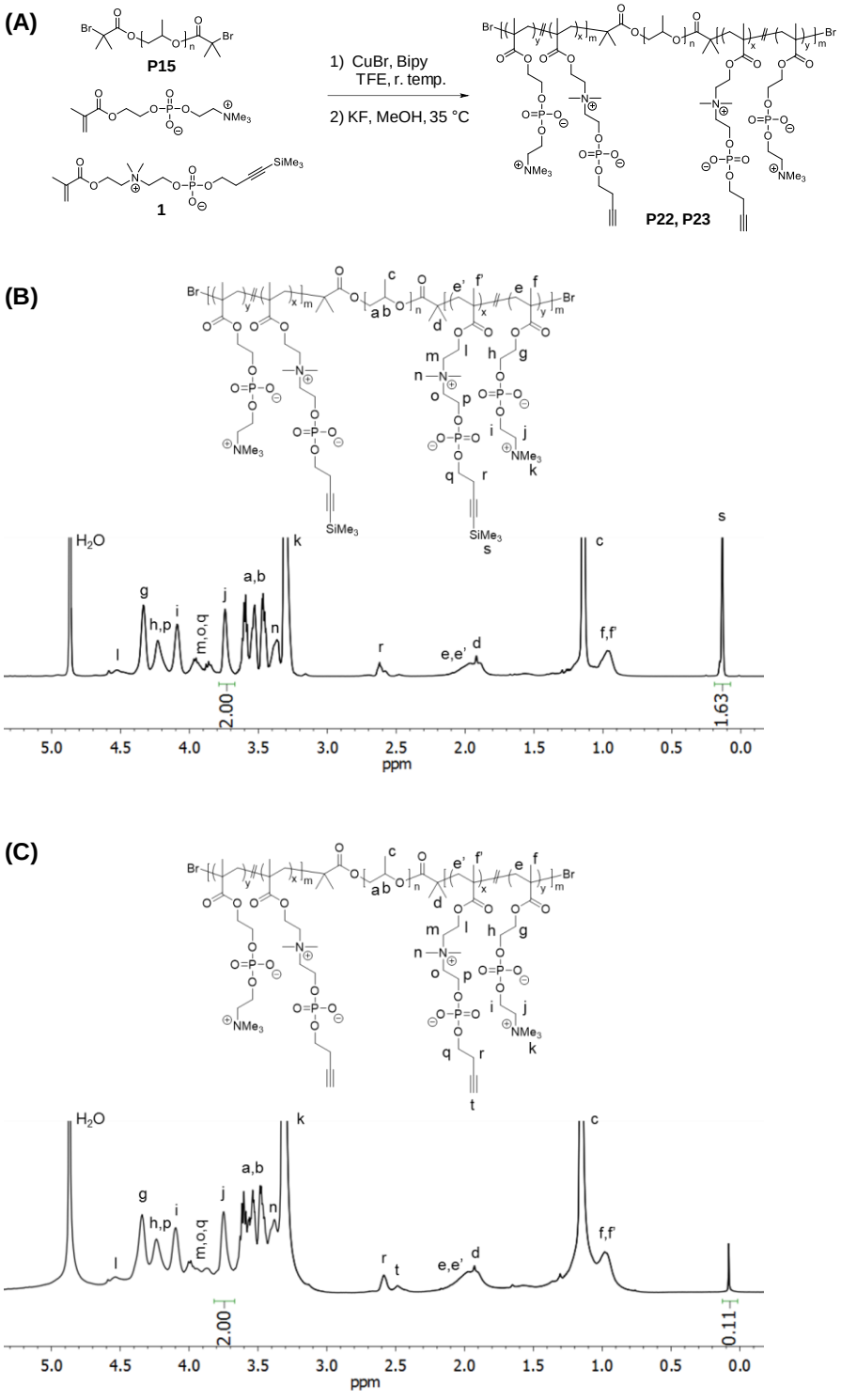

Figure 3.8: (A) Synthesis of functional zwitteronic block copolymers **P22** and **P23** bearing pendent alkyne moieties by the macroinitiated-ATRP of MPC and monomer **1**, with subsequent TMS-deprotection performed using KF in MeOH; representative ^{1}H-NMR spectra of TMS-protected (B) and deprotected (C) functional PC-zwitteronic **P23** obtained in MeOD-d_4.

copolymerization of MPC and monomer **1** in TFE using macroinitiator **P15** and a CuBr/bipyridine catalyst system. Syntheses targeted TMS-alkyne incorporations of 20 mole percent and zwitterionic blocks with X_n values of 12 and 24. Monomer conversions reaching >90% were achieved and the TMS-protected polymers were purified in similar fashion as **P16**-**P20**. Silyl deprotection was achieved by stirring the functional block copolymers at 35 °C in a methanolic solution of potassium fluoride (KF), and the deprotected polymers were purified by dialysis against water then isolated by lyophilization to afford functional zwitteronics **P22** and **P23** as white powders.

Figure 3.8 shows representative ^{1}H-NMR spectra of **P23** before (Figure 3.8B) and after (Figure 3.8C) TMS deprotection. In both spectra, characteristic resonances of pendent PC and alkyne-CP moieties were observed, including signals corresponding to trimethylammonium (peak k, δ = 3.22-3.34 ppm) and dimethylammonium (peak n, δ = 3.34-3.43 ppm) protons of the PC and CP zwitterions, respectively. In the spectrum of the protected block copolymers, a sharp singlet for protons of the TMS protecting groups was seen at 0.14 ppm. Comparing integral values for signals corresponding to the TMS and PC methylene protons (peak j, δ = 3.67-3.79 ppm) before (Figure 3.8B) and after treatment with KF (Figure 3.8C), deprotection afforded polymers **P22** and **P23** with ~95 of the TMS protecting groups removed. Copolymer compositions for the functional zwitteronics, summarized in Table 3.1, were estimated prior to TMS removal using ^{1}H-NMR spectroscopy by comparing relative intensities of the CP, PC, and PPO resonances. The estimated compositions of **P22** and **P23** were in excellent agreement with targeted values. Functional block copolymers **P22** and **P23** were prepared with monomodal molecular

Table 3.1: Composition and molecular weight data for functional zwitteronics **P22** and **P23**.

Polymer	Targeted X_n (MPC, MCP)	Measured X_n[a] (MPC, MCP)	M_n[b] (g/mol)	PDI[c]
P22	10, 2	11, 2	23,450	1.16
P23	19, 5	19, 4	31,310	1.31

[a]Estimated by ^{1}H-NMR spectroscopy (500 MHz) in MeOD-d_4.
[b]Estimated using GPC eluting in TFE and calibrated against PMMA standards.

weight distributions and reasonably low PDI values (Table 3.1), as estimated using GPC eluting in TFE.

Possessing hydrophilic segments with reactive alkynes embedded directly within the zwitterion, block copolymers **P22** and **P23** are functional amphiphiles well-suited for nanomaterials synthesis using facile click reactions. To demonstrate the versatility of these functional Pluronic mimics, thiol-yne chemistry was employed to covalently crosslink nanoparticles and hydrogels. Such crosslinked structures are of particular interest as robust or even injectable materials and for encapsulation and release of hydrophobic moieties (*i.e.*, therapeutics, dyes, *etc.*)[51,52]; notably, nanoparticle-crosslinked hydrogels have been examined as mechano-responsive networks and biocompatible matrices for tunable drug delivery.[53-56]

As shown in Scheme 3.3, UV-mediated crosslinking of aqueous **P22** or **P23** nanoparticle suspensions afforded shell-crosslinked nanoparticles or nanoparticle-crosslinked hydrogels depending on the composition of the thiol crosslinker. Thiol-yne crosslinking of nanoparticle coronae to give stable zwitteronic nanoparticles was carried out by irradiation of aqueous polymer suspensions using 365 nm light in the presence of dithiothreitol (DTT) as a difunctional crosslinker and Irgacure 2959 as the photoinitiator.

Scheme 3.3: Synthesis of shell-crosslinked nanoparticles by aqueous thiol-yne crosslinking of functional zwitteronics.

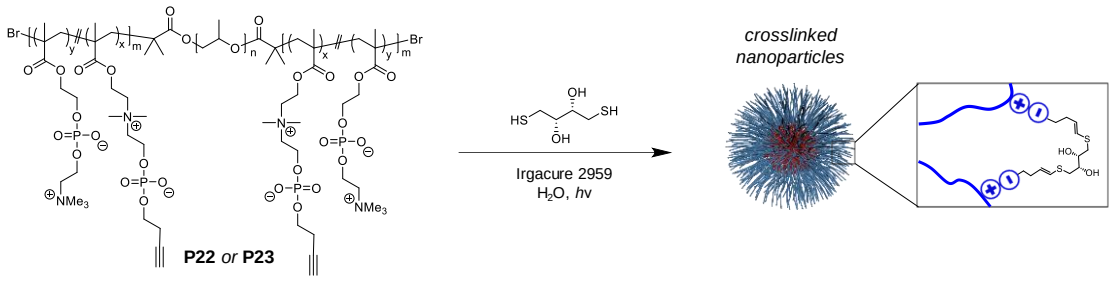

The thiol-yne reactions were performed at 1:2 alkyne:thiol ratio and polymer concentration of either 50 or 100 mg/mL. DLS curves of **P22** and **P23** in MeOH at 1 mg/mL are shown in Figure 3.9A. Prior to UV exposure, the pristine **P22** and **P23** formed well-dispersed unimers with mean hydrodynamic diameters of ~14 and 21 nm in MeOH, respectively, a good solvent for both the PPO and zwitterionic segments. Following irradiation in the presence of DTT, the **P22** nanoparticles remained intact in MeOH and exhibited a significantly larger average hydrodynamic diameter (*ca*. 44 nm) than did the MeOH-soluble **P22** prior to the reaction. Similar results confirming DTT nanoparticle crosslinking were also observed for **P23**. Aqueous suspensions of the DTT-crosslinked **P22** and **P23** nanoparticles, diluted to a concentration of 1 mg/mL, were cast on carbon-coated grids, allowed to dry at room temperature under ambient conditions, and visualized by transmission electron microscopy (TEM). As shown in the representative TEM micrographs in Figure 3.9B, spherical **P22** (left) and **P23** (right) nanoparticles were observed, with estimated diameters of 80 ± 30 nm and 51 ± 22 nm, respectively. Though the nanoparticles exhibited relatively broad size distributions, they were observed as well-dispersed structures with discrete and intact coronae, suggesting a minimal degree of inter-particle coupling.

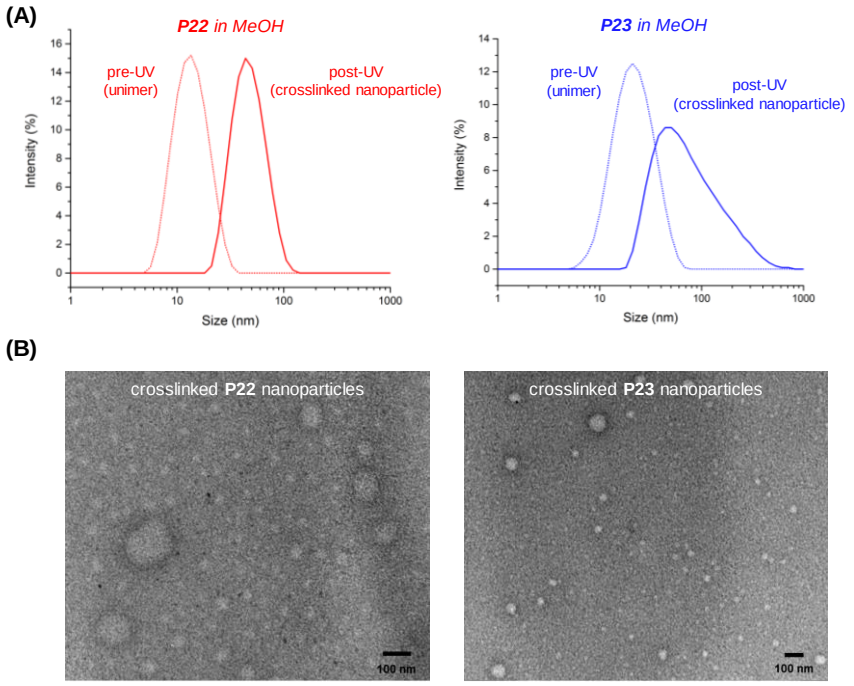

Figure 3.9: (A) DLS curves of **P22** (left) and **P23** (right) in MeOH (1 mg/mL) before and after UV exposure, confirming thiol-yne crosslinking; (B) TEM images of **P22** (left) and **P23** (right) DTT-crosslinked nanoparticles cast on carbon-coated TEM grids.

Substituting DTT with a tetra-functional PEO thiol (alkyne:thiol molar ratio of 1:1) and using a similar UV-initiated thiol-yne strategy afforded hydrogels crosslinked through alkyne-bearing zwitteronic nanoparticles. Figure 3.10 shows images of 10, 25, 50, and 100 mg/mL **P23** aqueous suspensions before and after irradiation at 365 nm. Following irradiation, the 25, 50, and 100 mg/mL suspensions no longer flowed upon vial inversion, demonstrating network formation. Reactions performed at zwitteronic concentrations of 10 mg/mL failed to yield macroscopic hydrogels, suggesting a critical concentration of alkyne functionality is necessary to afford robust covalent hydrogels from the functional zwitteronics.

In collaboration with Yalin Liu, hydrogels prepared from functional zwitteronics **P22** and **P23** at concentrations of 50 and 100 mg/mL were allowed to swell in water at room temperature for 18-24 hours and were characterized by rheology at 37 °C. A

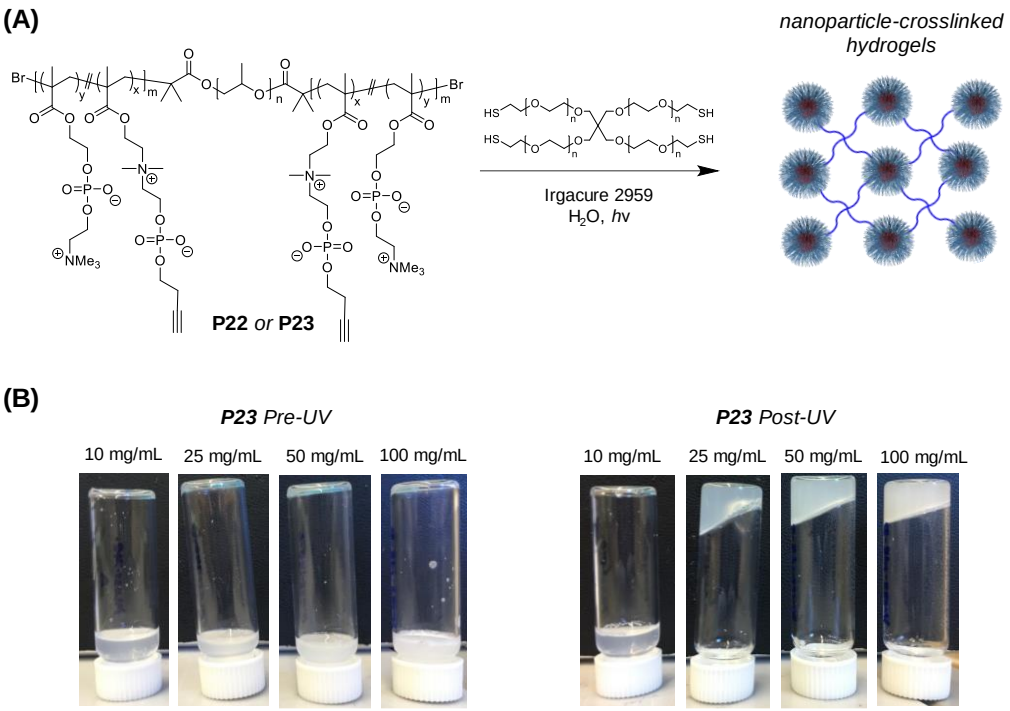

Figure 3.10: (A) Preparation of nanoparticle-crosslinked hydrogels by thiol-yne crosslinking of **P22** or **P23** in water using tetrafunctional PEO thiol; (B) images of **P23** suspensions before and after UV-mediated thiol-yne crosslinking at polymer concentrations of 10, 25, 50, and 100 mg/mL.

representative plot of the elastic modulus (G'), viscous modulus (G"), and tan(delta) for the 100 mg/mL **P23** hydrogel are shown in Figure 3.11A. Values of G' and tan(delta) remained relatively constant at varying frequencies, confirming crosslinking of the nanoparticle network; similar behavior was noted for the **P22** hydrogels and the **P23** network prepared at a zwitteronic concentration of 50 mg/mL. Values of G' measured at nearly all frequencies for the **P22** and **P23** gels were more than an order of magnitude greater than corresponding G" values, demonstrating that the thiol-yne crosslinked hydrogels exhibit predominantly elastic behavior. Elastic moduli of the nanoparticle-crosslinked hydrogels were estimated from G' values obtained at the lowest frequency tested (1 rad/s). As shown in the table in Figure 3.11B, hydrogels prepared from polymers **P22** and **P23** exhibited elastic moduli of 1.03-3,950 Pa and 1,110-14,800 Pa, respectively.

(A)

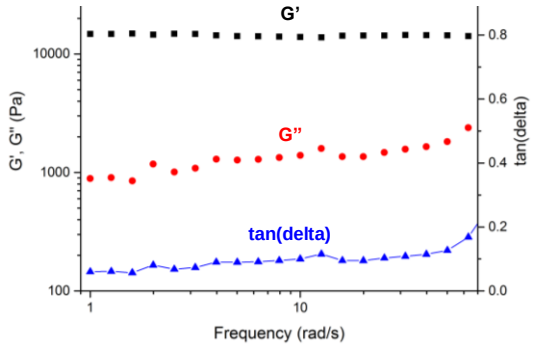

(B)

Polymer	Concentration (mg/mL)	Elastic modulus[a] (Pa)
P22	50	1.03
P22	100	3,950
P23	50	1,110
P23	100	14,800
Pluronic F127	200	10,200

[a]Elastic modulus values estimated from G' values measured at a frequency of 1 rad/s.

Figure 3.11: (A) representative plots of the elastic modulus (G'), viscous modulus (G"), and tan(delta) measured for the 100 mg/mL **P23** hydrogel; (B) elastic moduli of **P22**, **P23**, and Pluronic F127 hydrogels measured by rheology.

For both **P22** and **P23** hydrogels, the gel stiffness increased with functional zwitteronic concentration. Additionally, hydrogels prepared from **P23** exhibited higher elastic moduli than comparable **P22** gels, suggesting that the stiffness of these nanoparticle-crosslinked hydrogels can readily be tuned over four orders of magnitude through changes in polymer concentration and functional group incorporation. Notably, the elastic modulus estimated for the 100 mg/mL **P23** gel was comparable to that of a Pluronic F127 thermogel prepared at concentration of 200 mg/mL. As Pluronic F127 thermogels have been examined for controlled drug delivery,[57-62] the results of this rheological characterization suggest that matrices prepared from functional zwitteronic block copolymers possess elastic properties potentially suitable for therapeutic applications.

3.4 Conclusions

To summarize, a novel and versatile platform of zwitterionic Pluronic mimics, or zwitteronics, was prepared by ATRP methodology starting from a difunctional PPO macroinitiator. Optimized polymerization conditions afforded polyMPC-*b*-PPO-*b*-polyMPC copolymers with narrow molecular weight distributions and compositions in

which X_n of the polymer zwitterion block ranged from 2 to 36. Upon dispersion in water, PC-zwitteronics formed nanoparticles with CAC values and hydrodynamic diameters readily tuned *via* zwitterion content. PC-zwitteronics are surfactants which reduce aqueous surface tension values similar to those of conventional Pluronics, while also exhibiting unique composition-independent surface activity. Furthermore, PC-zwitteronics demonstrated similar LCST miscibility as Pluronics while requiring significantly lower hydrophilic block content to form homogenous, non-clouding suspensions. Interestingly, the zwitteronic block copolymers did not form physical gels at high concentrations; this behavior was attributed to the extreme hydrophilicity of the pendent zwitterions which precludes intermicellar aggregation. By copolymerizing MPC with an alkyne-substituted choline phosphate methacrylate, functional zwitteronic block copolymers amenable to post-polymerization modification were prepared with functional group incorporations of 20 mole percent. As an initial demonstration, the functional Pluronic mimics were used to generate robust, crosslinked nanoparticles and hydrogels *via* thiol-yne coupling.

The modular synthetic strategy presented in this work gives access to amphiphiles with tunable composition and properties. As such, future syntheses aim to incorporate diverse chemical functionality (*e.g.*, alkyl or alkene moieties) through pendent choline phosphate groups, as well as temperature and salt-responsive sulfobetaine (SB) zwitterions. Additionally, future studies will examine zwitteronic amphiphiles as dispersants, and investigate crosslinked zwitteronic nanoparticles and networks for sustained release applications.

3.5 References

1) Schmolka, I. R. A Review of Block Polymer Surfactants. *J. Am. Oil Chem. Soc.* **1977**, *54*, 110-116.

2) Bahadur, P.; Riess, G. Block Copolymers: A Special Class of Surfactants. *Tenside Surfact. Det.* **1991**, *28*, 173-179.

3) Alexandridis, P.; Hatton, T. A. Poly(ethylene oxide)-Poly(propylene oxide)-Poly(ethylene oxide) Block Copolymer Surfactants in Aqueous Solutions and at Interfaces: Thermodynamics, Structure, Dynamics, and Modeling. *Colloids Surfaces A: Physicochem. Eng. Aspects* **1995**, *96*, 1-46.

4) Amiji, M.; Park, K. Prevention of Protein Adsorption and Platelet Adhesion on Surfaces by PEO/PPO/PEO Triblock Copolymers. *Biomaterials* **1992**, *13*, 682-692.

5) Lv, C.; Su, Y.; Wang, Y.; Ma, X.; Sun, Q.; Jiang, Z. Enhanced Permeation Performance of Cellulose Acetate Ultrafiltration Membrane by Incorporation of Pluronic F-172. *J. Membrane Sci*. **2007**, *294*, 68-74.

6) Chiappetta, D. A.; Sosnik, A. Poly(ethylene oxide)-Poly(propylene oxide) Block Copolymer Micelles as Drug Delivery Agents: Improved Hydrosolubility, Stability and Bioavailability of Drugs. *Eur. J. Pharm. Biopharm.* **2007**, *66*, 303-317.

7) Kabanov, A. V.; Lemieux, P.; Vinogradov, S.; Alakhov, V. Pluronic® Block Copolymers: Novel Functional Molecules for Gene Therapy. *Adv. Drug Deliv. Rev.* **2002**, *54*, 223-233.

8) Kozlov, M. Y..; Melik-Nubarov, N. S.; Batrakova, E. V.; Kabanov, A. V. Relationship Between Pluronic Block Copolymer Structure, Critical Micellization Concentration and Partitioning Coefficients of Low Molecular Mass Solutes. *Macromolecules* **2000**, *33*, 3305-3313.

9) Mortensen, K. Structural Studies of Aqueous Solutions of PEO-PPO-PEO Triblock Copolymers, Their Micellar Aggregates and Mesophases; a Small-Angle Neutron Scattering Study. *J. Phys.: Condens. Matter* **1996**, *8*, A103-A124.

10) Nolan, S. L.; Phillips, R. J.; Cotts, P. M.; Dungan, S. R. Light Scattering Study on the Effect of Polymer Composition on the Structural Properties of PEO-PPO-PEO Micelles. *J. Colloid Interface Sci.* **1997**, *191*, 291-302.

11) Almgren, M.; Brown, W.; Hvidt, S. Self-Aggregation and Phase-Behavior of Poly(ethylene oxide)-Poly(propylene oxide)-Poly(ethylene oxide) Block Copolymers in Aqueous Solution. *Colloid Polym. Sci.* **1995**, *273*, 2-15.

12) Duval, M.; Waton, G.; Schosseler, F. Temperature-Induced Growth of Wormlike Copolymer Micelles. *Langmuir* **2005**, *21*, 4904-4911.

13) Landazuri, G.; Fernandez, V. V. A.; Soltero, J. F. A.; Rharbi, Y. Kinetics of the Sphere-to-Rod like Micelle Transition in a Pluronic Triblock Copolymer. *J. Phys. Chem. B.* **2012**, *116*, 11720-11727.

14) King, S. M.; Heenan, R. K.; Cloke, V. M.; Washington, C. Neutron Scattering from a Poly(oxyethylene)-Poly(oxypropylene)-Poly(oxyethylene) Copolymers in Dilute Aqueous Solution under Shear Flow. *Macromolecules* **1997**, *30*, 6215-6222.

15) Prhashanna, A.; Khan, S. A.; Chen, S. B. Micelle Morphology and Chain Conformation of Triblock Copolymers Under Shear: LA-DPD Study. *Colloids Surf., A* **2016**, *506*, 457-466.

16) Bromberg, L. E.; Ron, E. S. Temperature-Responsive Gels and Thermogelling Polymer Matrices for Protein and Peptide Delivery. *Adv. Drug Deliv. Rev.* **1998**, *31*, 197-221.

17) Meng, Y.; Gu, D.; Zhang, F. Q.; Shi, Y. F.; Cheng, L.; Feng, D.; Wu, Z. X.; Chen, Z. X.; Wang, Y.; Stein, A.; Zhao, D. Y. A Family of Highly Ordered Mesoporous Polymer Resin and Carbon Structures from Organic-Organic Self-Assembly. *Chem. Mater.* **2006**, *18*, 4447-4464.

18) Wang, L.; Yamauchi, Y. Block Copolymer Mediated Synthesis of Dendritic Platinum Nanoparticles. *J. Am. Chem. Soc.* **2009**, *131*, 9152-9153.

19) Batrakova, E. V.; Kabanov, A. V. Pluronic Block Copolymers: Evolution of Drug Delivery Concept from Inert Nanocarriers to Biological Response Modifiers. *J. Control. Release* **2008**, *130*, 98-106.

20) Xiong, X. Y.; Tam, K. C.; Gan, L. H. Synthesis and Thermally Responsive Properties of Novel Pluronic F87/Polycaprolactone (PCL) Block Copolymers with Short PCL Blocks. *J. Appl. Polym. Sci.* **2006**, *100*, 4163-4172.

21) Custers, J. P. A.; van den Broeke, L. J. P.; Keurentjes, J. T. F. Phase Behavior and Micellar Properties of Carboxylic Acid End Group Modified Pluronic Surfactants. *Langmuir* **2007**, *23*, 12857-12863.

22) Hassanzadeh, S.; Feng, Z.; Pettersson, T.; Hakkarainen, M. A Proof-of-Concept for Folate-Conjugated and Quercetin-Anchored Pluronic Mixed Micelles as Molecularly Modulated Polymeric Carriers for Doxorubicin. *Polymer* **2015**, *74*, 193-204.

23) Choi, W. I.; Tae, G.; Kim, Y. H. One Pot, Single Phase Synthesis of Thermo-Sensitive Nano-Carriers by Photo-Crosslinking of a Diacrylated Pluronic. *J. Mater. Chem.* **2008**, *18*, 2769-2774.

24) Tao, Y.; Han, J.; Ye, C.; Thomas, T.; Dou, H. Reduction-Responsive Gold-Nanoparticle-Conjugated Pluronic Micelles: an Effective Anti-Cancer Drug Delivery System. *J. Mater. Chem.* **2012**, *22*, 18864-18871.

25) Yang, T-F.; Chen, C-N.; Chen, M-C. Lai, C-H.; Liang, H-F.; Sung, H-W. Shell-Crosslinked Pluronic L121 Micelles as a Drug Delivery Vehicle. *Biomaterials* **2007**, *28*, 725-734.

26) Jeong, B.; Bae, Y. H.; Kim, S. W. Thermoreversible Gelation of PEG-PLGA-PEG Triblock Copolymer Aqueous Solutions. *Macromolecules* **1999**, *32*, 7064-7069.

27) Wang, Y-C.; Xia, H.; Yang, X-Z.; Wang, J. Synthesis and Thermoresponsive Behaviors of Biodegradable Pluronic Analogs. *J. Polym. Sci. A Polym. Chem*. **2009**, *47*, 6168-6179.

28) Worm, M.; Kang, B.; Dingels, C.; Wurm, F. R. Acid-Labile Amphiphilic PEO-*b*-PPO-*b*-PEO Copolymers: Degradable Poloxamer Analogs. *Macrmol. Rapid Commun*. **2016**, *37*, 775-780.

29) Petrov, P.; Tsvetanov, C. B.; Jérôme, R. Two-Component "Onionlike" Micelles with a PPO Core, a PDMAEMA Shell and a PEO Corona: Formation and Crosslinking. *Polym. Int.* **2008**, *57*, 1258-1264.

30) Robinson, K. L.; de Paz-Báñez, M. V.; Wang, X. S.; Armes, S. P. Synthesis of Well-Defined, Semibranched, Hydrophilic—Hydrophobic Block Copolymers Using Atom Transfer Radical Polymerization. *Macromolecules* **2001**, *34*, 5799-5805.

31) Halacheva, S.; Rangelov, S.; Tsvetanov, C. Poly(glycidol)-Based Analogues to Pluronic Block Copolymers. Synthesis and Aqueous Solution Properties. *Macromolecules* **2006**, *39*, 6845-6852.

32) Amado, E.; Augsten, C.; Mäder, K.; Blume, A.; Kressler, J. Amphiphilic Water Soluble Triblock Copolymers Based on Poly(2,3-dihydroxypropyl methacrylate) and Poly(propylene oxide): Synthesis by Atom Transfer Radical Polymerization and Micellization in Aqueous Solutions. *Macromolecules* **2006**, *39*, 9486-9496.

33) Seo, J-H.; Matsuno, R.; Takai, M.; Ishihara, K. Cell Adhesion on Phase-Separated Surface of Block Copolymer Composed of Poly(2-methacryloyloxyethyl phosphorylcholine) and Poly(dimethylsiloxane). *Biomaterials* **2009**, *30*, 5330-5340.

34) Ma, Y.; Tang, Y.; Billingham, N. C.; Armes, S. P. Well-Defined Biocompatible Block Copolymers via Atom Transfer Radical Polymerization of 2-Methacryloyloxyethyl Phosphorylcholine in Protic Media. *Macromolecules* **2003**, *36*, 3475-3484.

35) Kratz, K.; Breitenkamp, K.; Hule, R.; Pochan, D.; Emrick, T. PC-Polyolefins: Synthesis and Assembly Behavior in Water. *Macromolecules* **2009**, *42*, 3227-3229.

36) Skinner, M.; Selhorst, R.; Emrick, T. Synthesis of Water-Soluble Zwitterionic Polysiloxanes. *J. Polym. Sci. A Polym. Chem.* **2016**, *1*, 127-134.

37) Li, Y.; Keefe, A. J.; Giarmarco, M.; Brault, N. D.; Jiang, S. Simple and Robust Approach for Passivating and Functionalizing Surfaces for Use in Complex Media. *Langmuir* **2012**, *28*, 9707-9713.

38) Ko, D. Y.; Patel, M.; Jung, B. K.; Park, J. H.; Jeong, B. Phosphorylcholine-Based Zwitterionic Biocompatible Thermogel. *Biomacromoelcules* **2015**, *16*, 3853-3862.

39) Whelan, D. M.; van der Giessen, W. J.; Krabbendam, S. C.; van Vliet, E. A.; Verdouw, P. D.; Serruys, P. W.; van Beusekom, H. M. M. Biocompatibility of Phosphorylcholine Coated Stents in Normal Porcine Coronary Arterties. *Heart* **2000**, *83*, 338-345.

40) Iwasaki, Y.; Ishihara, K. Phosphorylcholine-Containing Polymers for Biomedical Applications. *Anal. Bioanal. Chem.* **2005**, *381*, 534-546.

41) Iwasaki, Y.; Ishihara, K. Cell Membrane-Inspired Phospholipid Polymers for Developing Medical Devices with Excellent Biointerfaces. *Sci. Tech. Adv. Mater.* **2012**, *13*, 064101.

42) Hu, G.; Emrick, T. Functional Choline Phosphate Polymers. *J. Am. Chem. Soc.* **2016**, *138*, 1828-1831.

43) Wong, K. E.; Mora, M .C.; Skinner, M.; Page, S. M.; Crisi, G. M.; Arenas, R. B.; Schneider, S. S.; Emrick, T. Evaluation of PolyMPC-Dox Prodrugs in a Human Ovarian Tumor Model. *Mol. Pharmaceutics* **2016**, *13*, 1679-1687.

44) Kalyanasundaram, K.; Thomas, J. K. Environmental Effects on Vibronic Band Intensities in Pyrene Monomer Fluorescence and Their Application in Studies of Micellar Systems. *J. Am. Chem. Soc.* **1977**, *99*, 2039-2044.

45) Kabanov, A. V.; Batrakova, E. V.; Miller, D. W. Pluronic® Block Copolymers as Modulators of Drug Efflux Transporter Activity in the Blood-Brain Barrier. *Adv. Drug Deliv. Rev.* **2003**, *55*, 151-164.

46) Yaseen, M.; Lu, J. R. The Structure of Zwitterionic Phosphocholine Surfactant Monolayers. *Langmuir* **2006**, *22*, 5825-5832.

47) Morisaku, T.; Watanabe, J.; Konno, T.; Takai, M.; Ishihara, K. Hydration of Phosphorylcholine Groups Attached to Highly Swollen Polymer Hydrogels Studied by Thermal Analysis. *Polymer* **2008**, *49*, 4652-4657.

48) Chen, M.; Briscoe, W. H.; Armes, S. P.; Klein, J. Lubrication at Physiological Pressures by Polyzwitterionic Brushes. *Science* **2009**, *323*, 1698-1701.

49) Kobayashi, M.; Terayama, Y.; Yamaguchi, H.; Terada, M.; Murakami, D.; Ishihara, K.; Takahara, A. Wettability and Antifouling Behavior on the Surfaces of Superhydrophilic Polymer Brushes. *Langmuir* **2012**, *28*, 7212-7222.

50) Alexandridis, P.; Athanassiou, V.; Fukuda, S.; Hatton, T. A. Surface Activity of Poly(ethylene oxide)-*block*-Poly(propylene oxide)-*block*-Poly(ethylene oxide) Copolymers. *Langmuir* **1994**, *10*, 2604-2612.

51) O'Reilly, R. K.; Hawker, C. J.; Wooley, K. L. Cross-linked Block Copolymer Micelles: Functional Nanostructures of Great Potential and Versatility. *Chem. Soc. Rev.* **2006**, *35*, 1068-1083.

52) Zhang, X.; Dong, H.; Fu, S.; Zhong, Z.; Zhuo, R. Redox-Responsive Micelles with Cores Crosslinked via Click Chemistry. *Macromol. Rapid Commun*. **2016**, *37*, 993-997.

53) Xiao, L.; Liu, C.; Zhu, J.; Pochan, D. J.; Jia, X. Hybrid, Elastomeric Hydrogels Crosslinked by Multifunctional Block Copolymer Micelles. *Soft Matter* **2010**, *6*, 5293-5297.

54) Xiao, L.; Zhu, J.; Londono, J. D.; Pochan, D. J.; Jia, X. Mechano-responsive Hydrogels Crosslinked by Block Copolymer Micelles. *Soft Matter* **2012**, *8*, 10233-10237.

55) Lu, C.; Mikhail, A. S.; Wang, X.; Brook, M. A.; Allen, C. Hydrogels Containing Core Cross-Linked Block Co-Polymer Micelles. *I. Biomater. Sci. Polym. Ed.* **2012**, *23*, 1069-1090.

56) Wei, L.; Cai, C.; Lin, J.; Chen, T. Dual-Drug Delivery System Based on Hydrogel/Micelle Composites. *Biomaterials* **2009**, *30*, 2606-2613.

57) Johnston, T. P.; Punjabi, M. A.; Froelich, C. J. Sustained Delivery of Interleukin-2 from a Poloxamer 407 Gel Matrix Following Intraperitoneal Injection in Mice. *Pharm. Res.* **1992**, *9*, 425-434.

58) Veyries, M. L.; Couarraze, G.; Geiger, S.; Agnely, F.; Massias, L.; Kunzil, B.; Faurisson, F.; Rouveix, B. Controlled Release of Vancomycin from Poloxamer 407 Gels. *Int. J. Pharm.* **1999**, *192*, 183-193.

59) El-Kamel, A. H. In Vitro and In Vivo Evaluation of Pluronic F127-based Ocular Delivery Systems for Timolol Maleate. *Int. J. Pharm.* **2002**, *241*, 47-55.

60) Liu, Y.; Lu, W-L.; Wang, J-C.; Zhang, X.; Zhang, H.; Wang, X-Q.; Zhou, T-Y.; Zhang, Q. Controlled Delivery of Recombinant Hirudin Based on Thermo-Sensitive Pluronic® F127 Hydrogel for Subcutaneous Administration: In Vitro and In Vivo Characterization. *J. Control. Release* **2007**, *117*, 387-395.

61) Lin, Z.; Gao, W.; Hu, H.; Ma, K.; He, B.; Dai, W.; Wang, X.; Wang, J.; Zhang, X.; Zhang, Q. Novel Thermo-Sensitive Hydrogel System with Paclitaxel Nanocrystals: High Drug-loading, Sustained Drug Release and Extended Local Retention Guaranteeing Better Efficacy and Lower Toxicity. *J. Control. Release* **2014**, *174*, 161-170.

62) Silveira, C. P.; Apolinário, L. M.; Fávaro, W. J.; Paula, A. J.; Durán, N. Doxorubicin-Functionalized Silica Nanoparticles Incorporated into a Thermoreversible Hydrogel and Intraperitoneally Administered Result in High Prostate Antitumor Activity and Reduced Cardiotoxicity of Doxorubicin. *ACS Biomater. Sci. Eng.* **2016**, *2*, 1190-1199.

CHAPTER 4

POLYMER PRODRUGS FOR TREATING OVARIAN TUMORS

4.1 Introduction

Ovarian cancer is the most lethal gynecological malignancy among women in the United States, and remains a leading cause of death with approximately 22,000 diagnoses and 14,000 deaths annually.[1] Early tumor detection is challenging, and patients often present advanced, metastatic, or disseminated disease at diagnosis. Conventional treatment involves surgical de-bulking of solid tumor accompanied by chemotherapy. Doxorubicin (Dox), an anthracycline chemotherapeutic, remains a prominent treatment option for various hematologic cancers and solid tumors, including malignant ovarian neoplasms.[2,3] While Dox is a powerful antitumor agent, its efficacy is limited by rapid clearance kinetics and non-specific accumulation in healthy tissue. This poor specificity leads to off-target toxicity resulting in myelosuppression, gastrointestinal irritation, and cardiotoxicity, thus limiting Dox dosing even when otherwise effective for tumor reduction.[2,4]

To improve the therapeutic efficacy of Dox, specifically its pharmacokinetics, toxicity, and tumor accumulation, conjugation to polymers offers a convenient and attractive strategy. Polymer-drug conjugation affords prodrugs of larger hydrodynamic size than the drug alone. This lengthens renal clearance half-life and prolongs *in vivo* circulation.[5] Coupling this improved pharmacokinetic profile with the enhanced permeability and retention (EPR) effect, whereby polymer-drug conjugates penetrate into the leaky vasculature of tumors and become entrapped due to poor tumoral lymphatic drainage, drug uptake in solid tumors is enhanced and off-target organ accumulation reduced.[6-8] For ease of delivery, hydrophilic polymers solvate otherwise water insoluble

drugs at high loadings,[9-15] and are potential replacements for excipients (*i.e.*, ethanol or Cremophor® EL) which prove problematic in some patient populations for causing severe or even fatal anaphylactic reactions.[16,17]

Emrick and coworkers previously reported the synthesis and *in vivo* evaluation of a polymer-Dox prodrug prepared from poly(2-methacryloyloxyethyl phosphorylcholine) (polyMPC),[18,19] a hydrophilic polymer noted for its exceptional water solubility and biocompatibility.[20-22] Using a polyMPC copolymer containing pendant acyl hydrazines, Dox conjugation was achieved by formation of hydrazone bonds, which are acid-sensitive and thus cleavable *in vivo* in the acidic microenvironment of solid tumors,[23,24] or intracellularly in acidic endosomes and lysosomes.[25] PolyMPC-Dox prodrugs exhibited an *in vivo* circulation half-life of greater than 2 hours, and in an aggressive mouse breast tumor model (4T1 cell line) administration of polyMPC-Dox reduced the mean tumor size and afforded a two-fold increase in survival time over Dox-treated mice. Dox in the prodrug animal group accumulated in tumors at twice the level of free Dox, with a corresponding reduction in off-target organ uptake.

To gauge the therapeutic breadth and clinical relevance of polyMPC-based chemotherapeutics (*i.e.*, polyMPC-Dox), work presented in this section sought to test the effectiveness of polyMPC-Dox in a human tumor line, specifically the SKOV-3 ovarian tumor model. SKOV-3 tumors are Dox-resistant at dosing levels tolerated by animals,[3] and thus this model allows evaluation of polymer-Dox conjugates in a challenging human tumor model. Experiments were performed with polyMPC and polyMPC-Dox to evaluate *in vivo* biocompatibility and establish a maximum tolerated dose (MTD) of the prodrug. Mice with subcutaneously established SKOV-3 xenografts were treated with Dox or

polyMPC-Dox using a recurring dosing schedule resembling that employed for human patients.[26] Animals were monitored for symptoms of treatment-associated toxicity, change in tumor size, and survival. The overall accumulation of Dox and polyMPC-Dox in solid ovarian tumors was compared, as was the specificity for uptake in tumor tissue versus off-target organs. *In vivo* experiments discussed in this section were performed in collaboration with researchers at the Pioneer Valley Life Sciences Institute (Springfield, MA).

4.2 Evaluation of PolyMPC-Dox Prodrugs in Human Ovarian Tumors

PolyMPC **P24** was prepared for *in vivo* biocompatibility evaluation by the room temperature atom transfer radical polymerization (ATRP) of MPC in methanol (MeOH) using copper(I) bromide (CuBr) and 2,2'-bipyridyl (Bipy) as the catalyst and ligand, respectively (Figure 4.1A).[18] Following the polymerization, residual reagents were removed by passing the product mixture through a plug of silica gel, then dialyzing against pure water. Polymer **P24** was isolated by lyophilization as a granular, white solid in up to 75% yield, and its purity was confirmed by NMR spectroscopy (Figure 4.1B). Number-average molecular weights (M_n) of polymer **P24** were estimated by gel permeation chromatography (GPC) in 2,2,2-trifluoroethanol (TFE) to be 41,900-43,500 g/mole,

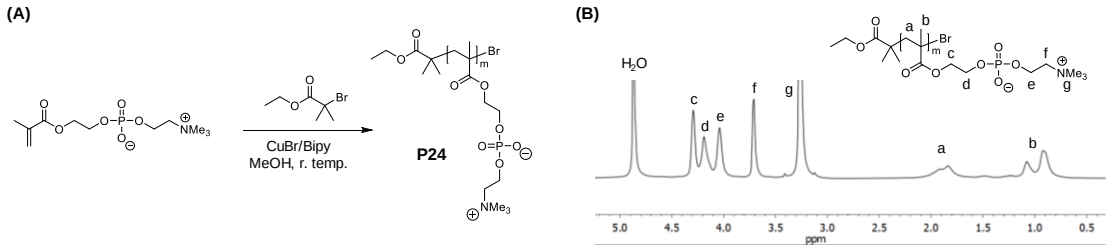

Figure 4.1: (A) Synthesis of polyMPC **P24** by ATRP of MPC in MeOH; (B) ^{1}H-NMR (500 MHz) spectra of polymer **P24** in MeOD-d_4.

relative to poly(methyl methacrylate) (PMMA) calibration standards, with polydispersity index (PDI) values of 1.17-1.25. Given its similarity in chemical structure, PMMA, for which TFE is a good solvent, is a useful GPC standard for **P24**. These M_n estimates for **P24** were in general agreement with targeted values (~35,000 g/mole). It should be noted that the zwitterionic structure of the polymer precludes molecular weight evaluation by mass spectrometry such as matrix-assisted laser desorption time-of-flight (MALDI-TOF) techniques.

Three batches of polyMPC-Dox **P26** were synthesized to gauge its *in vivo* toxicity, biodistribution, and tumor efficacy. Functional polyMPC-hydrazine **P25**, with randomly incorporated pendent acyl hydrazine moieties, was prepared by ATRP and post-polymerization modification using a strategy described by Emrick and coworkers (Figure 4.2A).[18,19] A 22 mole percent hydrazine content in polymer **P25** was estimated by ^{1}H-NMR spectroscopy (Figure 4.2B). As shown in Figure 4.2A, polymer prodrug **P26** was prepared by reacting **P25** with Dox•HCl in acidified methanol (MeOH), affording covalent conjugation by acyl hydrazone formation. Residual Dox•HCl was removed by passing the prodrug solution through size exclusion media eluting with MeOH and then pure water. Following lyophilization, polymer prodrug **P26** was isolated as a dark red powder in yields greater than 84%. The purity of **P26** was assessed by GPC in TFE, with detection by UV absorbance. In chromatograms of polymer **P26** (Figure 4.2C), a single unimodal peak was observed, with a notable absence of low molecular weight components, demonstrating the successful removal of residual Dox•HCl from the prodrug. UV-Vis analysis of aqueous solutions of different batches of **P26** (Figure 4.2D) confirmed Dox conjugation and gave calculated Dox weight percent loadings of 16.7-20.6%, comparable loading to the prodrug

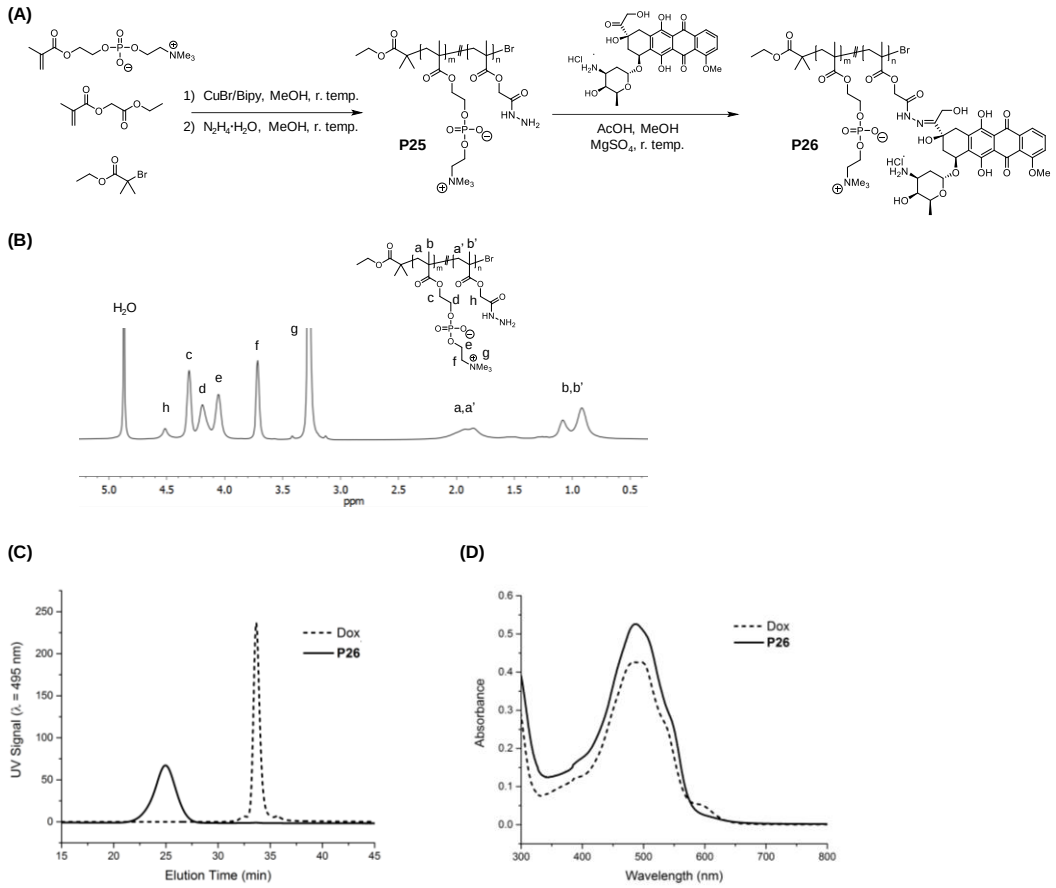

Figure 4.2: (A) Synthesis of polyMPC-Dox prodrug **P26** by conjugation of polyMPC-hydrazine **P25** and Dox•HCl; (B) ^{1}H-NMR spectrum of polymer **P25** in MeOD-d_4; (C) TFE GPC chromatograms of Dox and polyMPC-Dox **P26**. For prodrug **P26**, a single polymer fraction was observed (24.8 minutes), with a notable absence of any residual Dox (33.6 minutes); (D) UV-Vis absorbance spectra of Dox (0.05 mg/mL, λ_{max} = 494 nm) and **P26** (0.25 mg/mL, λ_{max} = 487 nm) in pure water.

assessed by Emrick and coworkers in the 4TI mouse breast cancer model.[19] PolyMPC-Dox **P26** was found to have an average hydrodynamic size in phosphate-buffered saline (PBS) of 13.9 ± 0.2 nm, as determined by dynamic light scattering (DLS). The formation of a very minor population of self-associated aggregates was noted, behavior which was similarly observed for solutions of polymer **P24** in PBS. In both cases, unimers were the predominant population, suggesting that polymers **P24** and **P26** are well-dispersed in injectable saline.

The *in vivo* biocompatibility of **P24** was assessed using a dosing study to establish an MTD of polyMPC, or the lowest dose at which systemic toxicity is observed. Non-obese diabetic severe combined immunodeficient (NOD SCID) mice, commonly used for xenograft tumor models,[27,28] received solutions of **P24** in Hank's balanced salt solution (HBSS) at doses of 50, 100, 200, 400, or 800 mg/kg. Two intravenous injections of these doses were administered, at Day 0 and 17, and the weight, physical appearance and behavior of the animals were monitored daily and compared to a control group administered HBSS. Polymer **P24** was well-tolerated with no noted physical or behavioral indication of toxicity. As shown in Figure 4.3A, mice given polymer **P24** at all doses exhibited weight gains similar to those of control mice, indicating excellent biocompatibility of injected polyMPC. Histological evaluation of the heart, kidneys, spleen, and lungs resected from mice treated with polymer **P24** showed no differences from the organs of the control animals. The livers of mice administered polymer **P24** exhibited a minor increase in lymphocyte concentration at higher polymer doses with no corresponding effect on the health of the hepatocytes, as shown in Figure 4.3B. While this work initially sought to establish a definitive MTD for polymer **P24**, solutions of the polymer at doses greater than 800 mg/kg were exceedingly viscous and unsuitable for intravenous administration. Nonetheless, these experiments suggest polyMPC to be non-toxic even at high doses and indicate a general suitability of polyMPC as an injectable drug carrier.

The toxicity of polymer prodrug **P26** was evaluated in NOD SCID mice to determine appropriate doses for subsequent biodistribution and tumor efficacy studies. While prodrug **P26** was tolerated in athymic nude mice at Dox equivalent doses greater

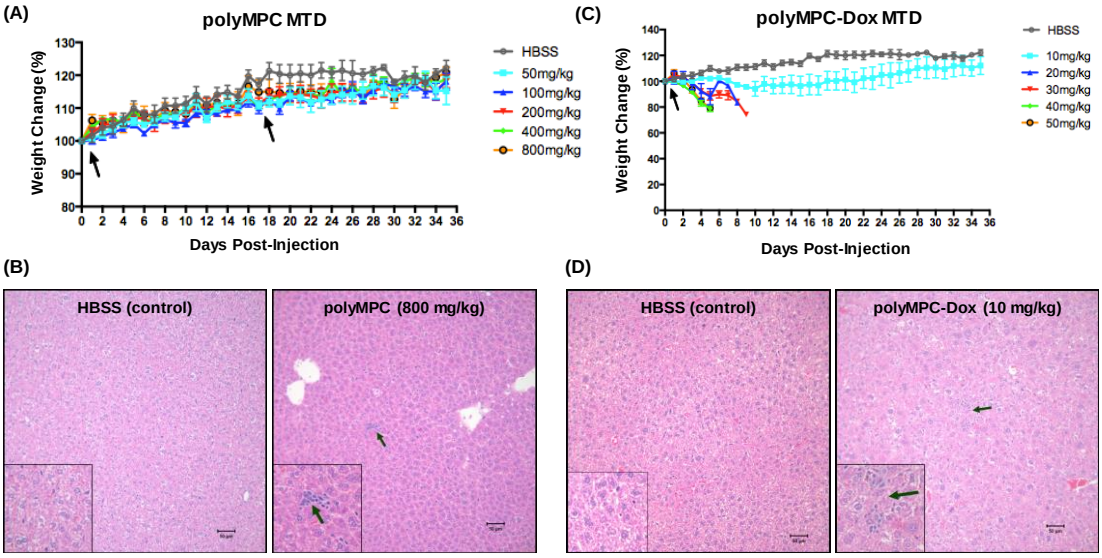

Figure 4.3: (A) Percent change in the weight of mice administered two injections of HBSS (control) or polymer **P24** at doses of 50-800 mg/kg. Black arrows indicate days of administration (Day 0 and 17). Error bars represent ± the standard error the mean (SEM); (B) representative hematoxylin and eosin (H&E) staining of liver sections of mice administered HBSS (left) and 800 mg/kg polyMPC **P24** (right). Generalized increased inflammation, indicated by green arrows, was observed in the livers of mice administered polyMPC **P24** at a dose of 800 mg/kg. Images were taken at 20X magnification with 40X magnification inlay images. Scale bars represent 50 µm; (C) percent change in the weight of mice administered a single injection of HBSS (control) or polyMPC-Dox **P26** at Dox equivalent doses of 10-50 mg/kg. The black arrow indicates the day of administration (Day 0). Error bars represent ± the SEM. (D) representative H&E staining of liver sections of mice administered HBSS (left) and polyMPC-Dox **P26** (right) at a Dox equivalent dose of 10 mg/kg. Green arrows indicate evidence of increased lymphocytes and enlarged hepatocytes in the livers of mice administered **P26**. Images were taken at 20X magnification with 40X magnification inlay images. Scale bars represent 50 µm.

than three-fold the reported MTD of 8 mg/kg for free Dox,[18,29] NOD SCID mice are uniquely sensitive to Dox,[30] with systemic toxicity to Dox observed at doses as low as 4 mg/kg, necessitating a re-establishment of the prodrug MTD. NOD SCID mice were administered a single tail vein injection of **P26** in injectable saline at Dox equivalent doses of 10, 20, 30, 40 or 50 mg/kg, with control animals given a single injection of HBSS. As shown in Figure 4.3C, mice given the prodrug at doses of 20-50 mg/kg experienced weight loss and required removal from the study by euthanasia. However, mice administered **P26**

at a Dox equivalent dose of 10 mg/kg maintained healthy weights, and aside from minor injection site irritation in one animal, exhibited no overt signs of systemic toxicity. Histopathologic analysis of liver sections of mice administered prodrug **P26** demonstrated evidence of lymphocytic infiltration and hepatocyte enlargement, as indicated in Figure 4.3D. However, as Dox treatment is commonly accompanied by hepatotoxicity, these changes are attributed to Dox itself.[31,32] From these results, the Dox equivalent MTD of polymer prodrug **P26** in NOD SCID mice was estimated to be 10 mg/kg, although the actual value might be higher, since dosing between 10 and 20 mg/kg was not performed. Similar to our previous findings, the MTD of the polyMPC-Dox prodrug was significantly higher than that of the drug alone, confirming the capacity of polyMPC to mask dose-limiting Dox toxicity, and enable dosing at higher levels.

The *in vivo* biodistribution of both polymer-drug conjugate **P26** and free Dox was assessed in mice bearing human ovarian tumors, comparing drug accumulation in tumor

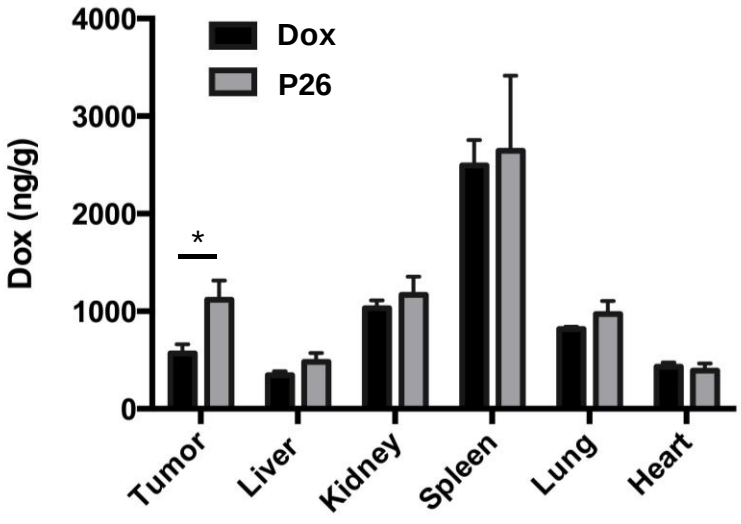

Figure 4.4: Biodistribution results following a single injection of free Dox (6 mg/kg) or polyMPC-Dox **P26** (6 mg/kg, Dox equivalent weight) in SKOV-3 tumor-bearing mice. Accumulation, expressed as ng Dox/g of tissue, was measured in tumors and major organs using HPLC. Error bars represent ± the SEM (*$p \leq 0.1$).

tissue and off-target organs (*i.e.*, liver, kidney, spleen, lung, and heart). Subcutaneous SKOV-3 tumors were established in the right flanks of NOD SCID mice, and single doses of free Dox, at 6 mg/kg, or prodrug **P26** at a Dox equivalent dose of 6 mg/kg, were administered by tail vein injection (n=3 mice per group). These selected doses were consistent with the previous biodistribution analysis of prodrug **P26** in a breast tumor model.[19] As a control, three tumor-bearing mice were given a single injection of HBSS. Three days post-injection, the mice were euthanized, and the tumors and organs removed, weighed, and homogenized in acidified isopropanol. The extracts were analyzed by high-performance liquid chromatography (HPLC), and using the fluorescence and UV-Vis absorbance of Dox the concentration of accumulated drug was measured in each tissue, with data shown in Figure 4.4.[19] Three days after introduction of the drug, mean tumor tissue accumulation of Dox from prodrug **P26**, and from free Dox, was 1120 ng/g and 567 ng/g, respectively. The accumulation of Dox from prodrug **P26** in the solid tumors was nearly two-fold that of free Dox after a single injection, a significant difference at $\alpha = 0.10$ ($p = 0.064$). However, no significant differences were observed for prodrug and Dox accumulation in off-target organs. The greater Dox accumulation found in tumors resulting from the prodrug delivery system mirrors biodistribution analysis of polyMPC-Dox in a mouse breast cancer model.[19]

The efficacy of polymer prodrug **P26** for treating human ovarian cancer was assessed using a SKOV-3 tumor model. NOD SCID mice, with subcutaneously established SKOV-3 tumors, were divided into groups of eight and treated with HBSS saline (control), free Dox at 2 mg/kg (~ ½ MTD),[30] or prodrug **P26** at a Dox equivalent dose of 5 mg/kg (~ ½ MTD). Following tumor establishment, one mouse from the polyMPC-Dox group was

excluded due to formation of an intramuscular tumor (precluding accurate tumor volume measurements). Dosing at approximately one-half of the MTD was selected in an attempt to minimize dose-limiting toxicity during the weekly dosing schedule designed to mimic current clinical dosing practice.[26] Throughout the study, mice were monitored every 24-48 hours, as were tumor volumes, weights, and overall health of the animals. Animals were removed from the study when tumor volume exceeded 1,500 mm^3, weight decreased by more than 20%, or signs of distress in appearance or behavior were evident. Mice administered HBSS alone and prodrug **P26** received a total of eight doses, while mice given free Dox received six or seven treatments (the seventh injection was withheld from several animals due to ulcer formation at the injection site). By Day 50, seven of eight control animals were euthanized due to excessive tumor growth. As a result of losing the control animals, final treatments were administered to all groups at Day 53. An attempt to treat a set of animals with 5 mg/kg of Doxil, the liposomal formulation of Dox, failed due to a rapid systemic toxicity observed in these NOD SCID animals at that dosing level.

A summary of the efficacy study, shown in Figure 4.5, plots survival curves (Figure 4.5A) and the percent change in mean tumor volumes (Figure 4.5B) following treatment with HBSS (control), free Dox, and polyMPC-Dox **P26**. As shown in Figure 4.5A, mice treated with prodrug **P26** exhibited mean survival time of 79 days, almost twice that of the control mice (~47 days) and 15 days longer than mice treated with free Dox (~64 days). Moreover, by Day 60, when all control mice had been euthanized, 86% of the animals treated with prodrug **P26** were alive, while only 50% of the mice from the free Dox group had survived. Overall survival for mice treated with prodrug **P26** was 121 days, greater than two-fold the overall survival of the control mice, and 35 days longer than the free Dox

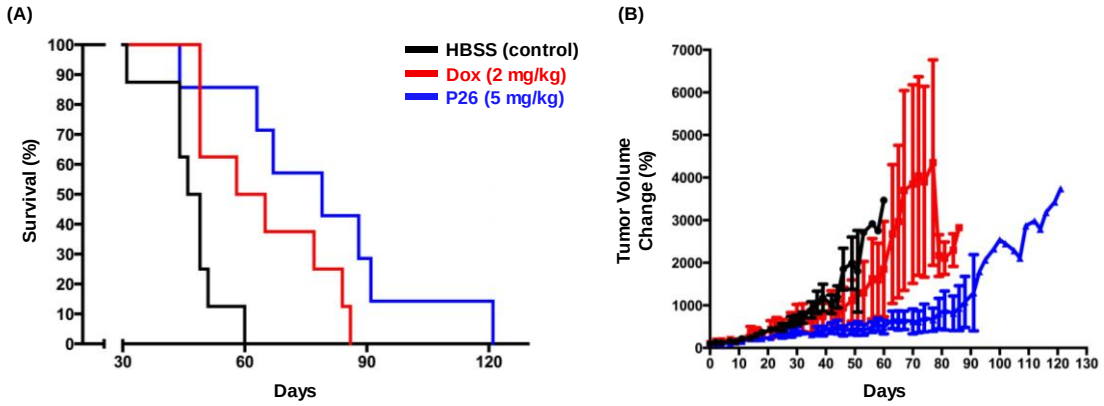

Figure 4.5: Survival curves (A) and percent change in mean tumor volumes (B) for SKOV-3 tumor-bearing mice treated with HBSS (control), free Dox (2 mg/kg), or polyMPC-Dox (5 mg/kg Dox equivalent dose). The last treatment day for all groups was Day 53. Error bars represent ± SEM.

group. It should be noted that survival curves were found to be significantly different ($p = 0.006$) using log-rank analysis. Additionally, the survival of mice treated with prodrug **P26** was significant compared to control animals ($p = 0.0016$), and approached significance relative to the survival of mice treated with free Dox ($p = 0.107$).

In addition to improved survival, treatment with prodrug **P26** reduced tumor growth compared to the free Dox and control groups, as shown in Figure 4.5B. At Day 30, prior to euthanizing any animals, the average tumor volumes for HBSS, free Dox, and prodrug mice were 888 mm^3, 660 mm^3, and 588 mm^3, respectively. Tumors in mice administered HBSS or free Dox grew slowly for 40 days, after which the tumor growth rate in both groups rapidly increased. At Day 79, the mean tumor volume for the free Dox group dropped sharply, a result of seven of eight mice requiring euthanasia due to tumor volumes exceeding the established maximum values. Mean tumor growth in the prodrug **P26** group, on the other hand, remained comparatively stagnant for approximately 80 days. Moreover, the therapeutic effects of prodrug **P26** lasted well beyond the end of the treatment schedule

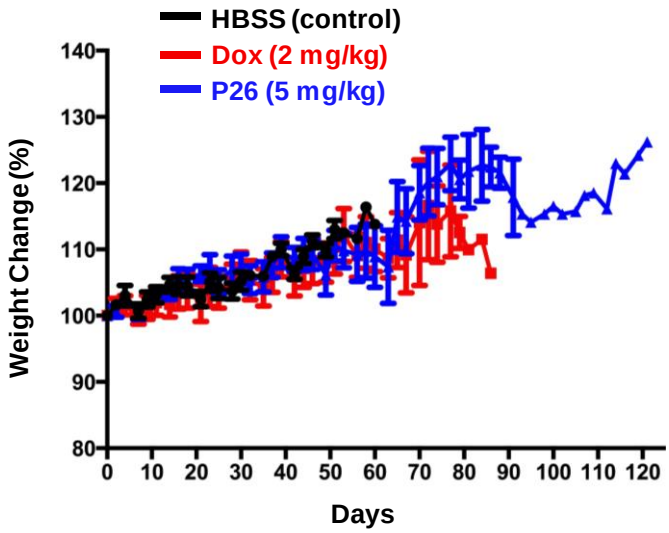

Figure 4.6: Percent change in mean weights of SKOV-3 tumor-bearing mice treated with HBSS (control), free Dox (2 mg/kg), or polyMPC-Dox (5 mg/kg Dox equivalent dose).

(Day 53), as the change in mean tumor volume was suppressed continuously for nearly 4 weeks following the final dose.

The systemic effects of free Dox and polyMPC-Dox treatments were gauged by measuring animal weight throughout the study, and monitoring their general appearance and behavior. As shown in Figure 4.6, the mean weight of mice treated with prodrug **P26** and free Dox increased similarly to the control group, suggesting that treatments were well-tolerated. This is an impressive result, as mice were administered high cumulative doses of either free Dox (12-14 mg/kg) or prodrug **P26** (40 mg/kg) without experiencing systemic toxicity. Evidence of tail necrosis (manifested as ulcers at injection sites) was observed in several mice treated with free Dox, as well as in one mouse treated with prodrug **P26**, necessitating euthanasia. While wounds observed in mice treated with free Dox eventually resolved, several ulcers were severe enough to prevent additional injections.

To assess the physiological effects of the recurring treatment regimen, animal organs were harvested, weighed, and evaluated (Figure 4.7A). For the heart, lungs, and

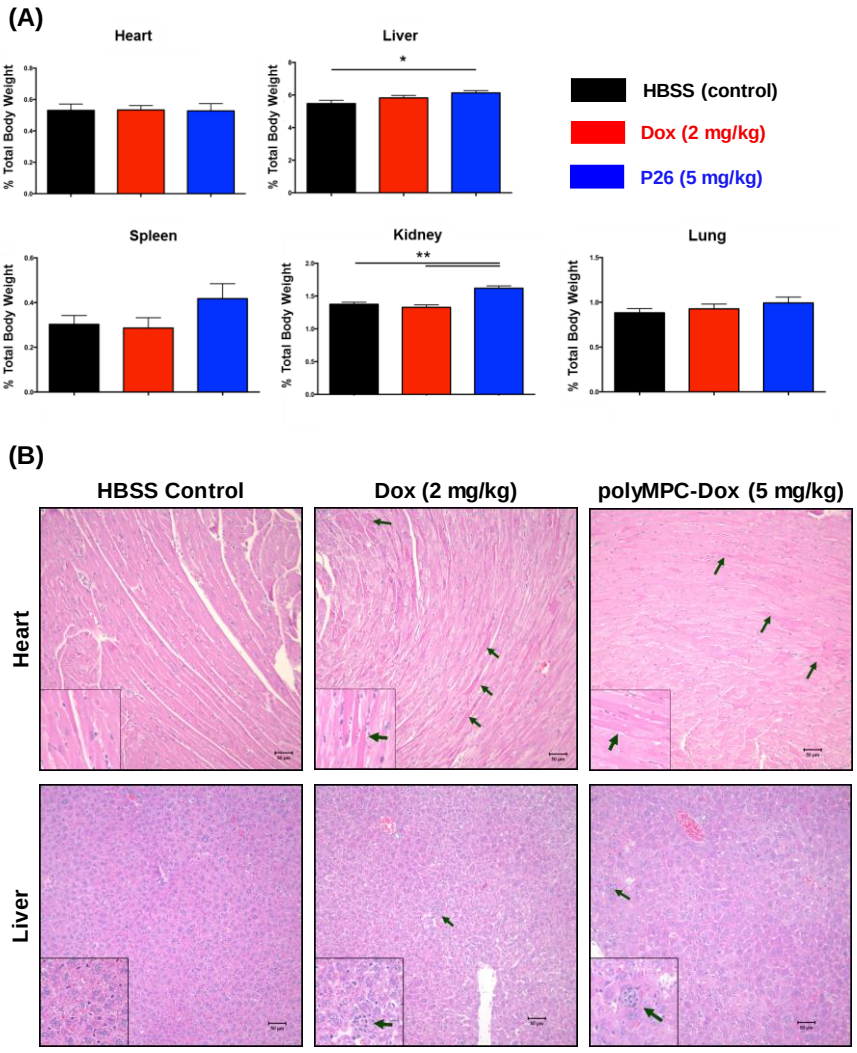

Figure 4.7: (A) Proportional organ weights at time of euthanasia for NOD SCID mice, bearing subcutaneous SKOV-3 human ovarian tumors, treated with multiple administrations of HBSS (control), Dox (2 mg/kg), or polyMPC-Dox **P26** (5 mg/kg Dox equivalent dose). * and ** represent statistically significant differences at $\alpha = 0.05$ and $\alpha = 0.01$, respectively. Error bars represent ± SEM; (B) representative H&E staining of heart (left) and liver (right) sections of mice administered HBSS, Dox (2 mg/kg), and polyMPC-Dox **P26** (5 mg/kg Dox equivalent dose) in a SKOV-3 human ovarian tumor efficacy study. Green arrows indicate eosinophilic fibers observed in the hearts of mice treated with free Dox and polyMPC-Dox **P26**. Livers of mice treated with free Dox and polyMPC-Dox **P26** exhibited generalized increased inflammation and hepatocyte enlargement relative to the livers of mice administered HBSS, as indicated by green arrows. Images were obtained at 20X magnification with 40X inlay images. Scale bars represent 50 µm.

spleen, no significant differences in mean proportional weights were observed among treatment groups. Histological analysis of heart sections for mice treated with free Dox

and prodrug **26** showed evidence of minor myocyte eosinophilic fibers indicative of ischemic changes in the cardiac tissue, as depicted in Figure 4.7B. However, these findings were variable and no consistent quantitative measure or trend was identified among treatment groups. Differences were noted between the proportional weights of the liver and kidneys of control mice and mice treated with prodrug **26**. As shown in Figure 4.7B, histology of liver sections from mice treated with free Dox and the prodrug revealed evidence of enlarged hepatocytes, increased mitotic activity, and lymphocytic infiltration indicative of hepatotoxic injury. These findings were even more striking within the liver sections of mice treated with free Dox, which is consistent with the known hepatotoxic nature of Dox.[31,32] The changes observed in liver tissue, therefore, are attributable to Dox itself, and not the prodrug or polymer carrier. Moreover, given the serial administration of drug used in this efficacy study, accumulation of Dox in organs involved in drug clearance would be expected. Further research is thus warranted to examine polyMPC-Dox clearance, especially under treatment conditions that resemble current clinical regimens.

4.3 Conclusions

This work described the first evaluation of a polyMPC cancer prodrug in a human tumor model. The polyMPC-Dox conjugates employed are water-soluble polymer prodrugs, with an average Dox weight percent loading of ~19%. The performance of the prodrug was compared to that of free Dox in a human ovarian tumor model (SKOV-3) to assess its toxicity, tumor accumulation properties, and therapeutic efficacy. Toxicity and efficacy studies demonstrated that polyMPC-Dox could be administered to mice at greater than twice the dose of free Dox without causing systemic toxicity. Moreover, polyMPC

itself was well-tolerated in these animals, even at very high doses (i.e., 800 mg/kg), demonstrating its utility in injectable polymer therapeutics. *From a single injection biodistribution study, Dox accumulation from the prodrug group in tumor tissue was nearly two-fold that of free Dox, without observation of enhanced uptake in off-target organs.* In an efficacy study, ovarian tumor-bearing mice receiving weekly prodrug dosing exhibited improved survival time and reduced tumor growth relative to free Dox treatment. These results demonstrate the advantages of treating human ovarian tumors using the polyMPC-Dox prodrug, including enhanced tumor uptake with reduced off-target toxicity, higher dosing capabilities, and improved therapeutic efficacy. *In vivo* evaluation in human ovarian tumors suggests that the polyMPC-Dox prodrug is safer and more effective in the treatment of solid tumors compared to Dox. Moreover, treatment with polyMPC-Dox did not elicit evidence of severe cardiotoxicity, even with recurring doses. This study thus demonstrates the viability of polyMPC-Dox cancer therapy, and that a simple water-soluble polymer-drug conjugate is useful for improving drug delivery to tumors, even without the presence of targeting groups or biorecognition sequences in the delivery vehicle.

4.4 References

1. National Cancer Institute. A Snapshot of Ovarian Cancer. http://www.cancer.gov/research/progress/snapshots/ovarian (accessed Sep 28, 2015).

2. Rahman, A. M.; Yusuf, S. W.; Ewer, M. S. Anthracycline-induced Cardiotoxicity and the Cardiac Sparing Effect of Liposomal Formulation. *Int. J. Nanomedicine*. **2007**, *2*, 567-583.

3. Shim, G-s.; Manandhar, S.; Shin, D.; Kim, T-H.; Kwak, M-K. Acquisition of Doxorubicin Resistance in Ovarian Carcinoma Cells Accompanies Activation of the NRF2 Pathway. *Free Radic. Biol. Med.* **2009**, *47*, 1619-1631.

4. Singal, P.K.; Iliskovic, N. Doxorubicin-Induced Cardiomyopathy. *N. Engl. J. Med.* **1998**, *339*, 900-905.

5. Fox, M. E.; Szoka, F. C.; Fréchet, J. M. J. Soluble Polymer Carriers for the Treatment of Cancer: The Importance of Molecular Architecture. *Acc. Chem. Res.* **2009**, *42*, 1141-1151.

6. Matsumura, Y.; Maeda, H. A New Concept for Macromolecular Therapeutics in Cancer Chemotherapy: Mechanism of Tumor Tropic Accumulation of Proteins and Antitumor Agents SMANCS. *Cancer Res.* **1986**, *46*, 6387-6392.

7. Maeda, H.; Wu, J.; Sawa, T.; Matsumura, Y.; Hori, K. Tumor Vascular Permeability and the EPR Effect in Macromolecular Therapeutics: a Review. *J. Control. Release*. **2000**, *65*, 271-284.

8. Maeda, H.; Nakamura, H.; Fang, J. The EPR Effect for Macromolecular Drug Delivery to Solid Tumors: Improvement of Tumor Uptake, Lowering of Systemic Toxicity, and Distinct Tumor Imaging In Vivo. *Adv. Drug Deliv. Rev.* **2013**, *65*, 71-79.

9. Khandare, J.; Minko, T. Polymer-Drug Conjugates: Progress in Polymeric Prodrugs. *Prog. Polym. Sci.* **2006**, *31*, 359-397.

10. Larson, N.; Ghandehari, H. Polymeric Conjugates for Drug Delivery. *Chem. Mater.* **2012**, *24*, 840-853.

11. Luxenhofer, R.; Schulz, A.; Li, S.; Bronich, T. K.; Batrakova, E. V.; Jordan, R.; Kabanov A. V. Doubly Amphiphilic Poly(2-oxazoline)s as High-Capacity Delivery Systems for Hydrophobic Drugs. *Biomaterials*. **2010**, *31*, 4972-4979.

12. Gou, P.; Liu, W.; Mao, W.; Tang, J.; Shen, Y.; Sui, M. Self-Assembling Doxorubicin Prodrug Forming Nanoparticles for Cancer Chemotherapy: Synthesis and Anticancer Study *In Vitro* and *In Vivo*. *J. Mater. Chem. B.* **2013**, *1*, 284-292.

13. She, W.; Li, N.; Luo, K.; Guo, C.; Wang, G.; Geng, Y.; Gu, Z. Dendronized Heparin-Doxorubicin Conjugate Based Nanoparticle as pH-Responsive Drug Delivery System for Cancer Therapy. *Biomaterials*. **2013**, *34*, 2252-2264.

14. Li, H.; Bian, S.; Huang, Y.; Liang, J.; Fan, Y.; Zhang, X. High Drug Loading pH-Sensitive Pullulan-DOX Conjugate Nanoparticles for Hepatic Targeting. *J. Biomed. Mater. Res. A*. **2014**, *102*, 150-159.

15. Song, H.; Zhang, J.; Wang, W.; Huang, P.; Zhang, Y.; Liu, J.; Li, C.; Kong, D. Acid-Responsive PEGylated Doxorubicin Prodrug Nanoparticles for Neuropilin-1 Receptor-Mediated Targeted Drug Delivery. *Colloids Surf., B*. **2015**, *136*, 365-374.

16. Gelderblom, H.; Verweij, J.; Nooter, K.; Sparreboom, A. Cremophor EL: the Drawbacks of Vehicle Selection for Drug Formulation. *Eur. J. Cancer.* **2001**, *37*, 1590-1598.

17. Ten Tjie, A. J.; Verweij, J.; Loos, W. J.; Sparreboom A. Pharmacological Effects of Formulation Vehicles: Implications for Cancer Chemotherapy. *Clin. Pharmacokinet.* **2003**, *42*, 665-685.

18. Chen X, Parelkar S, Henchey E, Schneider S, Emrick T. PolyMPC-Doxorubicin Prodrugs. *Bioconjugate Chem*. **2012**, *23*, 1753-1763.

19. Page, S. M.; Henchey, E.; Chen, X.; Schneider, S.; Emrick, T. Efficacy of PolyMPC-DOX Prodrugs in 4T1 Tumor-Bearing Mice. *Mol. Pharmaceutics*. **2014**, *11*, 1715-1720.

20. Ishihara, K. New Polymeric Biomaterials—Phospholipid Polymers with a Biocompatible Surface. *Front Med. Biol. Eng.* **2000**, *10*, 83-95.

21. Iwasaki, Y.; Ishihara, K. Phosphorylcholine-Containing Polymers for Biomedical Applications. *Anal. Bioanal. Chem*. **2005**, *381*, 534-546.

22. Ishihara, K. Highly Lubricated Polymer Interfaces for Advanced Artificial Hip Joints through Biomimetic Design. *Polym. J.* **2015**, *47*, 585-597.

23. Tannock, I. F.; Rotin, D. Acid pH in Tumors and Its Potential for Therapeutic Exploitation. *Cancer Res.* **1989**, *49*, 4374-4384.

24. Engin, K.; Leeper, D. B.; Cater, J. R.; Thistlethwaite, A. J.; Tupchong, L.; McFarlane, J. D. Extracellular pH Distribution in Human Tumors. *Int. J. Hyperthermia*. **1995**, *11*, 211-216.

25. Mellman, I.; Fuchs, R.; Helenius, A. Acidification of the Endocytic and Exocytic Pathways. *Annu. Rev. Biochem.* **1986**, *55*, 663-700.

26. Rose, P. G. Pegylated Liposomal Doxorubicin: Optimizing the Dosing Schedule in Ovarian Cancer. *Oncologist*. **2005**, *10*, 205-214.

27. Hasan, N.; Ohman, A. W.; Dinulescu, D. M. The Promise and Challenge of Ovarian Cancer Models. *Transl. Cancer. Res.* **2015**, *4*, 14-28.

28. Richmond, A.; Su, Y. Mouse Xenograft Models vs GEM Models for Human Cancer Therapeutics. *Dis. Model Mech.* **2008**, *1*, 78-72.

29. Houba, P. H. J.; Boven, E.; van der Meulen-Muileman, I. H.; Leenders, R. G. G.; Scheeren, J. W.; Pinedo, H. M.; Haisma, H. J. Pronounced Antitumor Efficacy of Doxorubicin When Given as the Prodrug DOX-GA3 in Combination with a Monoclonal Antibody β-Glucuronidase Conjugate. *Int. J. Oncol.* **2001**, *91*, 550-554.

30. Kratz, F.; Mansour, A.; Soltau, J.; Warnecke, A.; Fichtner, I.; Unger, C.; Drevs, J. Development of Albumin-Binding Doxorubicin Prodrugs that are Cleaved by Prostate-Specific Antigen. *Arch. Pharm.* **2005**, *338*, 462-472.

31. Injac, R.; Strukelj, B. Recent Advances in Protection Against Doxorubicin-Induced Toxicity. *Technol. Cancer Res. Treat.* **2008**, *7*, 497-516.

32. Joshi, M.; Sodhi, K. S.; Pandey, R.; Singh, J.; Goyal, S.; Prasad, S.; Kaur, H.; Bhaskar, N.; Mahajan. Cancer Chemotherapy and Hepatotoxicity: An Update. *IAJPS*. **2014**, *4*, 2976-2984.

CHAPTER 5

POLYMER PRODRUGS FOR TREATING GLIOBLASTOMA

5.1 Introduction

Glioblastoma is a solid neoplasm which originates from non-neuronal glial cells of the brain and represents the most commonly diagnosed central nervous system tumor in the United States.[1] Due to its highly aggressive and infiltrative nature, the current prognosis for glioblastoma patients is poor: with combined neurosurgery, radiation therapy, and chemotherapy, median survival is 12-15 months.[2-5] For complete eradication of infiltrative cells in surrounding healthy tissue, chemotherapy is critical to treatment. However, selection of appropriate drugs—typically alkylating agents such as temozolomide, carmustine, lomustine, and procarbazine (Figure 5.1)—is challenging, as the blood-brain barrier (BBB) generally only allows passage of lipophilic small molecules and essential nutrients from the bloodstream to the brain.[6,7] This, combined with issues typical of most small molecule chemotherapeutics (*i.e.*, off-target toxicity, rapid clearance following administration, and poor tumor selectivity), drives the development of new strategies for efficacious treatment of glioblastoma.

Local treatment immediately following surgical resection has been pursued as a potential alternative to systemic tumor treatment as a means of bypassing the BBB and

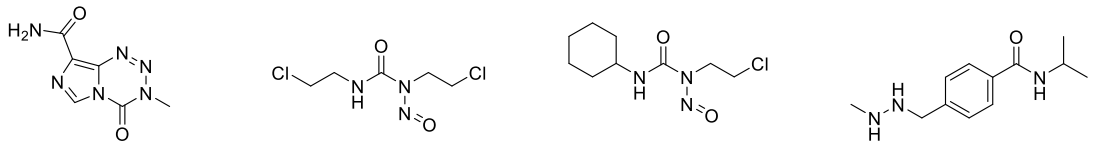

Figure 5.1: Chemical structures of small molecule chemotherapeutics commonly utilized in treating glioblastoma.

delivering chemotherapeutics to invasive cells in a sustained and targeted fashion. To date, Gliadel®, a biodegradable carmustine-loaded polymeric wafer, remains the only approved local glioblastoma treatment. While effective for carmustine delivery, the clinical use of Gliadel® is limited by severe side effects, including seizures, cerebral edemas, and intracranial bleeding, as well as wafer migration and incomplete degradation.[8] Though 'softer' matrices, such as drug-loaded hydrogels,[9] may prove to be safe alternatives to Gliadel®, noninvasive systemic treatments which can cross the BBB have the potential to improve glioblastoma chemotherapy without the side effects of implantable materials.

Temozolomide (TMZ), a bis(imidazotetrazine) heterocycle, is the first-line drug used for treating glioblastoma, and, as such, current research efforts predominantly focus on enhancing its delivery and efficacy. Administered orally, TMZ is a prodrug which releases a DNA alkylating methyldiazonium cation upon decomposition at physiological pH, as shown in Figure 5.2.[10,11] Alkylation occurs primarily at O^6 positions on guanine residues, generating apoptotic DNA mismatch errors.[11] Owing to the slightly alkaline microenvironment of brain tumors,[12] this pH- induced mechanism confers selective cytoxicity for malignant *vs*. healthy brain tissue, resulting in limited off-target toxicity.[2]

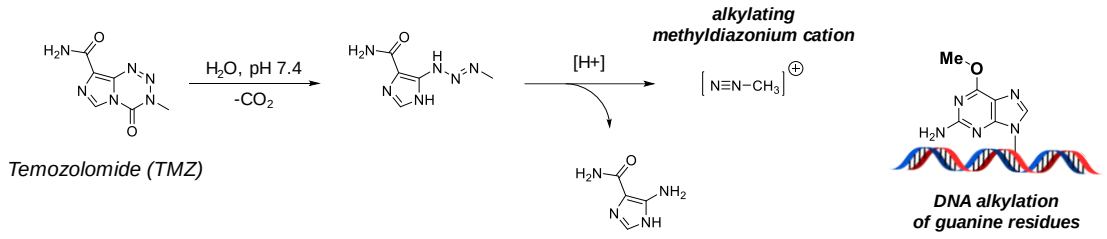

Figure 5.2: Temozolomide (TMZ) decomposition at physiological pH affords 5-(3-methyltriazen-1-yl)imidazole-4-carboxamide (MTIC), and subsequent acid-catalyzed degradation yields 5-aminoimidazole-4-carboxamide (AIC) and the methyldiazonium cation which alkylates DNA (shown at the O^6 position of guanine).

While TMZ effectively crosses the BBB, its efficacy is impeded by hydrolytic instability: TMZ rapidly degrades *in vivo* and exhibits a plasma half-life < 2 hours.[10] As such, frequent dosing is required to maintain suitable antitumor activity.[10,11,13] This hydrolytic instability also complicates clinical TMZ administration, as TMZ degrades over time if not stored under dry conditions.[14-16] In addition to poor stability and a short *in vivo* half-life, TMZ efficacy is hampered by chemoresistance induced by O^6-methylguanine-DNA methyl transferase (MGMT), a native enzyme that repairs damaged DNA following methylation.[10,11] MGMT activity in glioblastoma tumors can be depleted by sustained TMZ exposure,[17,18] and recurrent glioblastoma treated with dose-dense TMZ regimens improves tumor response.[18-22] As these dose-dense treatments can increase occurrence of dose-limiting hematoxicity, new synthetic designs are needed which extend TMZ circulation and allow for delivery of high concentrations of drug, while simultaneously masking undesired off-target toxicity.

Previously investigated strategies to improve TMZ delivery include its co-crystallization with organic acids,[16] encapsulation in injectable nanomaterials,[23,24] and conjugation to biocompatible polymer backbones.[25,26] Covalent polymeric conjugation offers significant advantages, including extending TMZ lifetime *in vivo*, improving drug pharamacokinetics, allowing for high drug loading while retaining aqueous solubility, and masking drug-related toxicity.[27-29] This section extends the poly(2-methacryloyloxyethyl phosphorylcholine) (polyMPC) prodrug platform[30,31] discussed in Chapter 4 to TMZ, and presents the development of water-soluble polyMPC-TMZ conjugates for treating glioblastoma. Through a novel TMZ-methacrylate derivative,[32] TMZ was incorporated as pendent moieties in polyMPC-based random and block copolymers using reversible

addition-fragmentation chain-transfer (RAFT) polymerization. The polymerization experiments afforded polyMPC-TMZ conjugates with tunable drug incorporation and narrow molecular weight distribution. Polymerization conditions were optimized to ensure fidelity of the TMZ structure such that the conjugates would retain the efficacy of TMZ. Solutions properties of the polyMPC-TMZ copolymers were examined, and the effect of polymer architecture on the stability of pendent drug moieties was probed. The antitumor activity of the prodrugs was tested in chemosensitive and chemoresistant glioblastoma cell lines, and their uptake by glioblastoma cells was assessed using confocal microscopy and flow cytometry. Finally, this polymer prodrug platform was expanded through co-delivery of TMZ and O^6-benzylguanine (O^6-BG), an alkylating agent which shows promise for sensitizing TMZ-resistant glioblastoma tumors.[33-36]

5.2 Synthesis of TMZ-Methacrylate

Scheme 5.1: Synthesis of TMZ-methacrylate (**TMZ-MA**).

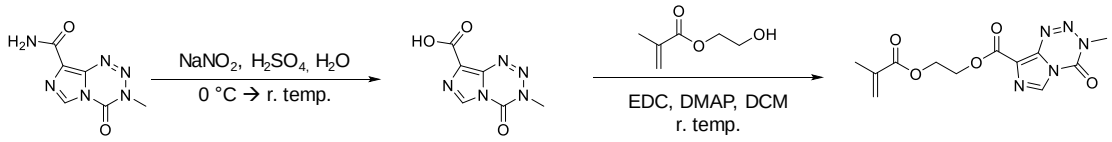

TMZ-methacrylate (**TMZ-MA**), the key monomer in this work, was prepared as shown in Scheme 5.1. TMZ-carboxylic acid (**TMZ-COOH**) was synthesized by diazotization and hydrolysis of pristine TMZ in nitrous acid, generated *in situ* from sodium nitrite ($NaNO_2$) and sulfuric acid (H_2SO_4), using a procedure similar to that described by Stevens and co-workers.[37] Precipitation over ice afforded **TMZ-COOH** as a fine white solid in yields of up to 75%. The absence of TMZ amide resonances in the ^{1}H-NMR spectrum of **TMZ-COOH** (Figure 5.3) indicated complete carbamoyl hydrolysis and

electron ionization high-resolution mass spectrometry (HRMS-EI) confirmed the expected structure of **TMZ-COOH** ($[M]^+$ calculated for $C_6H_5N_5O_3$: 195.0392 g/mol, found: 195.0395 g/mol).

Esterification of **TMZ-COOH** with 2-hydroxyethyl methacrylate (HEMA) was initially attempted *via* the corresponding acid chloride by reaction of **TMZ-COOH** with thionyl chloride,[38] resulting in imidazotetrazine degradation. The comparatively mild carbodiimide-mediated esterification proved more effective. As shown in Scheme 5.1, **TMZ-MA** was synthesized from **TMZ-COOH** and HEMA in the presence of 1-(3-(dimethylamino)propyl)-3-ethylcarbodiimide hydrochloride (EDC) and catalytic 4-(dimethylamino)pyridine (DMAP). **TMZ-MA** was purified simply by aqueous extraction and isolated in 71% yield as a flaky white solid, with the expected molar mass confirmed by fast-atom bombardment HRMS (HRMS-FAB) ($[M+H]^+$ calculated for $C_{12}H_{14}N_5O_5$: 308.0995, found: 308.0989). Spectroscopic characterization of **TMZ-MA** confirmed

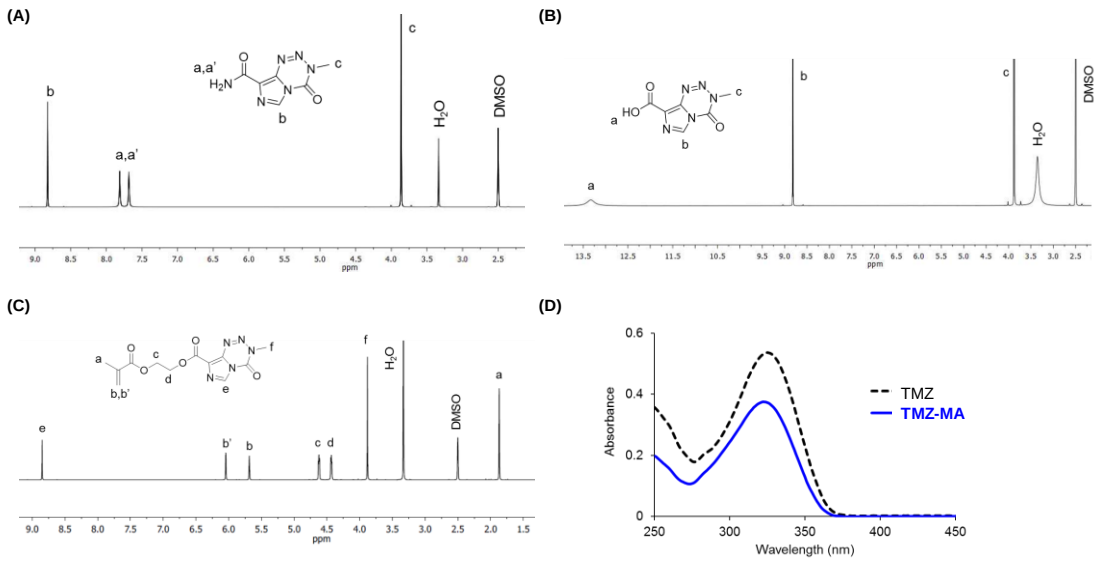

Figure 5.3: ^{1}H-NMR (500 MHz) spectra of TMZ (A), **TMZ-COOH** (B), and **TMZ-MA** (C) obtained in DMSO-d_6; (D) UV-Vis absorption spectra of TMZ and **TMZ-MA** in 2,2,2-trifluoroethanol (TFE) at a concentration of 0.01 mg/mL.

retention of the intact TMZ-moiety. In the ^{1}H-NMR spectrum of **TMZ-MA** (Figure 5.3C), resonances corresponding to the imidazole (δ = 8.85 ppm) and methyltriazene (δ = 3.88 ppm) protons were observed; the UV-Vis absorption spectra of TMZ (λ_{max} = 325 nm) and **TMZ-MA** (λ_{max} = 323 nm) were nearly identical (Figure 5.3D).

5.3 PolyMPC-TMZ Prodrugs: Synthesis, Solution Properties, and *In Vitro* Evaluation

The RAFT-mediated copolymerization of MPC and **TMZ-MA** was attempted initially in a methanol (MeOH)/dimethyl sulfoxide (DMSO) solvent mixture to ensure homogeneity. Although monomer conversion was high (87%), UV-Vis characterization of the isolated copolymer showed a signfiicant absorption at λ_{max} = 287 nm, indicative of TMZ decomposition to the AIC byproduct.[38] This observation prompted an investigation of the stability of TMZ in organic solvents, findings not reported previously. Solutions of TMZ in 1:1 MeOH/DMSO, DMSO, acetonitrile, and 2,2,2-trifluoroethanol (TFE) were incubated at room temperature, 50 °C, and 70 °C. UV-Vis spectroscopy showed the absorption spectrum of TMZ to remain unchanged after 24 hour incubation in DMSO and acetonitrile at all temperature, as shown in Figure 5.4. In contrast, TMZ heated to 50 or 70 °C in 1:1 MeOH/DMSO degraded completely in 1 hour; significant degradation was observed even at room temperature. Importantly, TMZ proved stable in TFE, a generally good solvent for polymer zwitterions, at temperature up to 70 °C for >24 hours. The marked difference in TMZ stability in MeOH versus TFE is attributed to the weaker nucleophilicity of the latter, which slows or precludes imidazotetrazine solvolysis.[39]

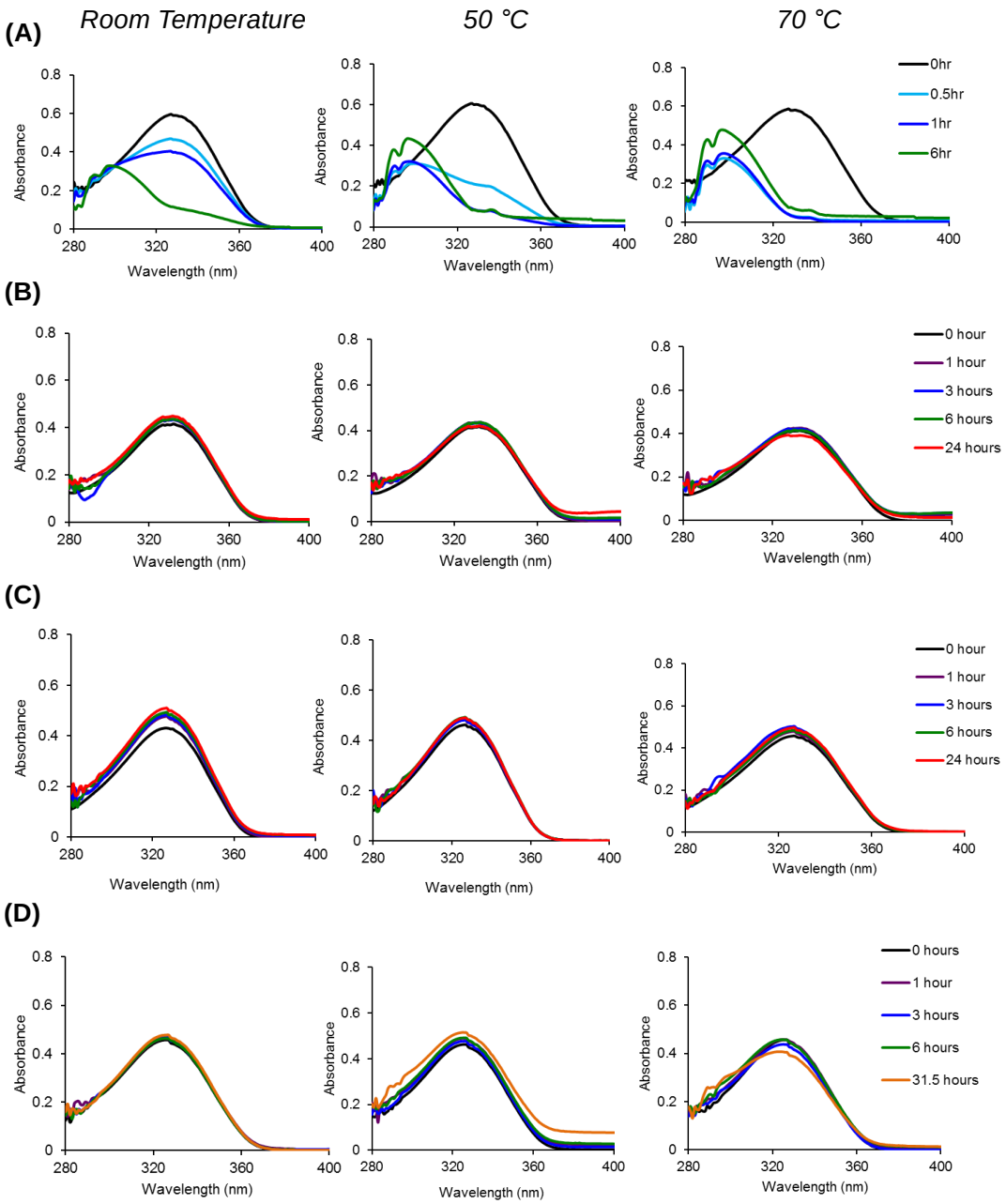

Figure 5.4: UV-Vis absorption spectra of TMZ solutions incubated at room temperature (left), 50 °C (middle), and 70 °C (right) in 1:1 MeOH/DMSO (A), DMSO (B), acetonitrile (C), and TFE (D).

Given the insight derived from this TMZ stability analysis, polyMPC-TMZ prodrugs with random and block copolymer architectures were prepared by RAFT polymerization methodology in TFE. As shown in Figure 5.5, random copolymers **P27**-

P30 were prepared by the copolymerization of MPC and **TMZ-MA** at 70 °C, utilizing 4-cyano-4-phenyl(carbonothioylthio)pentanoic acid and 4,4'-azobis(4-cyanovaleric acid) (ACVA) as chain transfer agent (CTA) and initiator, respectively. Reagent stoichiometries were adjusted to target copolymers with approximate number-average molecular weight (M_n) values of 30,000 g/mol, and monomer feed ratios were intended to afford 20, 25, 35, and 50 mol percent incorporation of **TMZ-MA** into polymers **P27-P30**, respectively. Monomer conversions >85% were achieved in polymerization times of 6-9 hours. Polymerizations were terminated by exposure to air, and the polymer products were purified by repeated precipitation into tetrahydrofuran (THF), followed by centrifugal dialysis against aqueous 0.1 M HCl. The conjugates were then lyophilized, giving **P27-P30** in yields of 70-80% as pink solids that readily dispersed in water at concentrations >20 mg/mL.

PolyMPC-TMZ prodrugs with a diblock architecture were synthesized starting from a polyMPC macro-CTA bearing a dithioester chain-end suitable for RAFT chain extension with **TMZ-MA** (Figure 5.5). PolyMPC macro-CTA **P31** was prepared by homopolymerization of MPC in TFE, targeting an approximate M_n of 15,000 g/mol and quenching the polymerization at < 80% conversion (estimated using ^{1}H-NMR spectroscopy). Following purification by precipitation into THF and dialysis in water,

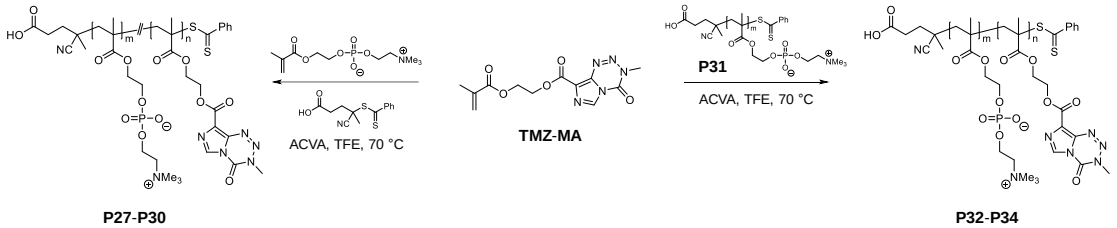

Figure 5.5: Synthesis of polyMPC-TMZ copolymers with random (**P27-P30**) and block (**P32-P34**) copolymer architectures by RAFT polymerization of **TMZ-MA**.

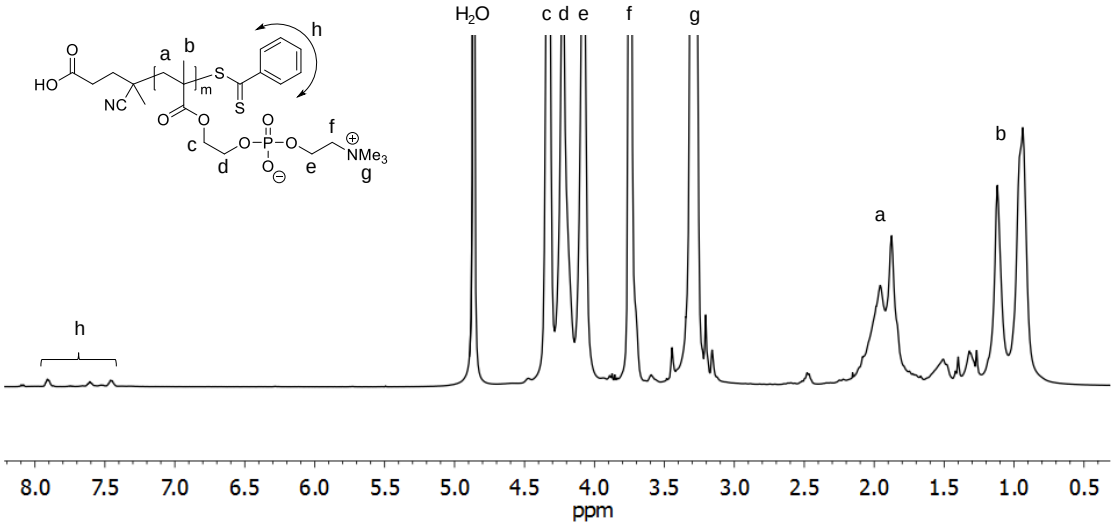

Figure 5.6: ^{1}H-NMR (500 MHz) spectrum of polyMPC macro-CTA **P31** obtained in MeOD-d_4.

polymer **P31** was isolated by lyophilization in 80% yield. ^{1}H-NMR spectroscopy of **P31** (Figure 5.6) showed resonances corresponding to chain-end phenyl protons at 7.45-7.90 ppm (region h), confirming a high degree of retention of the dithioester chain end. Comparing the integrations of the phenyl end group *vs*. PC methylene (δ = 3.75 ppm, region f) resonances, the M_n of polymer **P31**, prepared in numerous batches, was estimated as 20,900-21,900 g/mol. Characterization of **P31** by GPC eluting in TFE gave estimated polydispersity index (PDI) values of 1.05-1.13 (relative to poly(methyl methacrylate) (PMMA) standards). As shown in Figure 5.5, TMZ-functionalized block copolymers, **P32**-**P34**, targeting drug loadings of 20, 26, and 36 mole percent, respectively, were prepared by polymerizing **TMZ-MA** in TFE at 70 °C using macro-CTA **P31** and ACVA as a radical initiator. Monomer conversions of >90% were achieved in approximately 4-8 hour reaction times, and the block copolymers were purified in similar fashion to the random copolymers and isolated as pink solids in >50% yield.

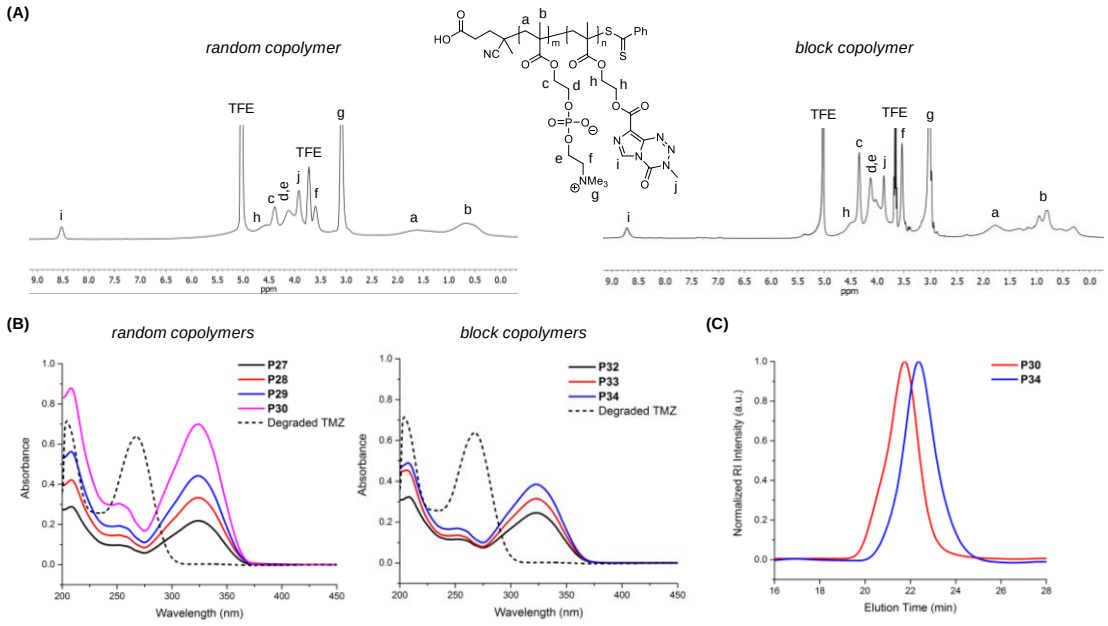

Figure 5.7: (A) Representative ^{1}H-NMR (500 MHz) spectra of **P30** (left) and **P34** (right) obtained in TFE-d_3; UV-Vis spectra of polyMPC-TMZ random copolymers **P27**-**P30** (left) and block copolymers **P32**-**P34** (right) in TFE at a concentration of 0.05 mg/mL in TFE. A representative spectrum of degraded TMZ is shown for each compilation; (C) representative GPC chromatograms of polyMPC-TMZ copolymers **P30** and **P34** eluting in TFE.

NMR and UV-Vis spectroscopy confirmed the structural integrity of the pendent TMZ moieties in copolymers **P27**-**P30** and **P32**-**P34**. In representative ^{1}H-NMR spectra of the polyMPC-TMZ prodrugs, resonances corresponding to TMZ imidazole protons were observed at 8.53 and 8.72 ppm for the random (Figure 5.7A, left) and block (Figure 5.7A, right) copolymers, respectively. Additional resonances at 3.92 (random) and 3.88 (block) ppm are attributed to the TMZ methyltriazene protons. Importantly, these signals for the polymer-bound TMZ are single resonances for both copolymer architectures, with no additional resonances indicative of undesired degradation to the AIC by-product. ^{13}C-NMR spectroscopy of the polyMPC-TMZ copolymers further confirmed retention of the TMZ structure, with characteristic resonances of the urea, imidazole, and methyltriazene groups observed at 140.81/140.01, 131.28/131.34, and 38.22/38.51 ppm for the

Table 5.1: Incorporation of **TMZ-MA** and molecular weight characterization of polyMPC-TMZ copolymers **P27**-**P30** and **P32**-**P34**.

Polymer	Targeted TMZ-MA incorporation (mol %)	Measured TMZ -MA incorporation[a] (mol %)	M_n[b] (g/mol)	PDI[b]
P27	17-20	16-17	38,600-42,800	1.20-1.22
P28	25	23-26	39,400-42,100	1.21
P29	35	32-33	36,200-40,500	1.14-1.20
P30	50	47-50	40,600-46,400	1.15-1.28
P32	20	14-16	23,600-24,800	1.14-1.15
P33	26	24-25	22,600-24,100	1.09-1.15
P34	36	31-35	24,900-31,500	1.09-1.21

[a]Molar incorporation estimated by ^{1}H-NMR spectroscopy in TFE-d_3.
[b]Values of M_n and PDI estimated using GPC eluting in TFE relative to PMMA standards.

random/block architectures, respectively. Figure 5.7B shows the UV-Vis absorption spectra of solutions of polymer **P27**-**P30** (left) and **P32**-**P34** (right) in TFE, as well as the spectrum of TMZ which was allowed to decompose fully. Each copolymer possessed an absorption maximum at 323 nm characteristic of the urea of intact TMZ, as well as a notable absence of any spectral features to suggest TMZ degradation.

TMZ incorporations for polyMPC-TMZ copolymers **P27**-**P30** and **P32**-**P34** were estimated using ^{1}H-NMR spectroscopy by comparing the integrations of TMZ imidazole and PC trimethylammonium (δ_{random} = 2.86-3.29 ppm, δ_{block} = 2.78-3.22 ppm) protons. For each copolymer, numerous samples were prepared for *in vitro* evaluation in glioblastoma cell lines. Characterized drug loading in these samples, summarized in Table 5.1, were in excellent agreement with targeted values and exhibited minimal variation. Additional syntheses targeted TMZ loadings of 65 and 50 mole percent for copolymers with random and block architecuters, respectively. While copolymers with these very high drug loads were synthetically accessible, these materials were poorly soluble in water, even at

concentrations <1 mg/mL, making them unsuitable for further evaluation as polymer prodrugs.

The molecular weights of polyMPC-TMZ copolymers were estimated by GPC, eluting in TFE and calibrated against PMMA standards. Representative chromatograms for random and block copolymers **P30** and **P34**, shown in Figure 5.7C, were relatively narrow and monomodal. As shown in Table 5.1, polyMPC-TMZ random and block copolymers were isolated with M_n values of 36,200-46,400 and 22,600-31,500 g/mol, respectively, and PDI values of 1.09-1.28. Copolymers of the same architecture were found to possess similar estimated M_n across multiple samples, demonstrating the reproducibility of this synthetic approach. Importantly, GPC chromatograms of polyMPC-TMZ copolymers obtained with UV detection at $\lambda = 323$ nm showed a notable absence of residual **TMZ-MA** or other small molecule impurities. This molecular weight characterization confirmed that RAFT methodology is amenable to preparing well-defined polymer-TMZ conjugates using the **TMZ-MA** monomer.

Possessing both hydrophilic PC zwitterions and hydrophobic TMZ moieties, polyMPC-TMZ copolymers were anticipated to form aqueous assemblies with larger hydrodynamic sizes relative to TMZ itself, which in turn would extend TMZ circulation half-life *in vivo*. The critical aggregation concentration (CAC) of the polyMPC-TMZ copolymers was estimated in pH 7.4 phosphate-buffered saline (PBS) at 37 °C using dynamic light scattering (DLS);[40] the absorption characteristics of TMZ preclude using fluorescent (*e.g.*, pyrene)[41] or absorption (*e.g.*, 1,6-diphenyl-1,3,5-hexatriene)[42] assays. Representative plots of DLS scattering intensty for solutions of **P30** and **P34** in PBS at polymer concentrations ranging from 0.005-5 mg/mL are shown in Figure 5.8A.

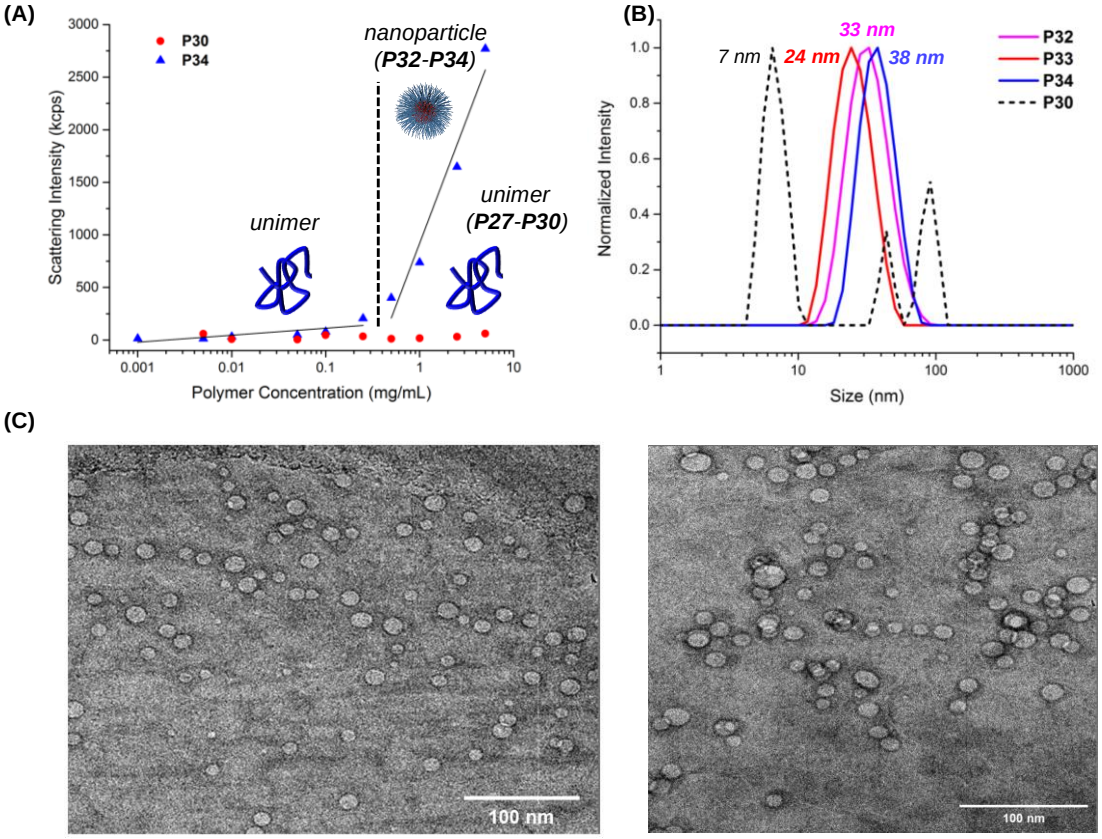

Figure 5.8: (A) Representative scattering intensities for suspensions of polymers **P30** and **P34** with varying polymer concentrations in pH 7.4 PBS at 37 °C measured using DLS. For block copolymers **P32**-**P34**, the CAC (represented by the dotted black line) was estimated as the onset of increasing scattering intensity; (B) DLS plots of polymers **P32**-**P34** and **P30** in pH 7.4 PBS (37 °C) at a concentration of 1 mg/mL; (C) representative cryo-TEM image of **P34** nanoparticles in water at a concentration of 1 mg/mL.

Copolymer **P34** exhibited a sharp increase in scattering intensty at a critical concentration of approximately 0.48 mg/mL, indicating copolymer aggregation. Similar behavior was observed for polymers **P32** and **P33** at concentrations of 0.70 and 0.45 mg/mL. In contrast, the scattering intensity values for solutions of **P30** remained relatively constant at each polymer concentration, suggesting an indiscernible CAC for polyMPC-TMZ random copolymers.

The hydrodynamic diameters (d_h) of structures formed from **P32**-**P34** in PBS at 37 °C were estimated using DLS above the CAC of each polymer at a concentration of 1

mg/mL. The DLS plots in Figure 5.8B show polyMPC-TMZ block copolymers to form monomodal nanoparticles (d_h = 24-38 nm) with no evidence of particle aggregation. Importantly, these block copolymers readily assembled in water into well-defined and narrowly dispersed aggregates without using intricate procedures (*e.g.*, solvent-directed assembly or thin film hydration).[43-45] In contrast, a bimodal size distribution was observed for random copolymer **P30**, dominated by the smaller structures (d_h ~ 7 nm). As expected, the hydrodynamic diameters of **P27**-**P29** were similarly small (d_h ~ 6-9 nm). Suspensions of block copolymer **P34** in pure water were cast on carbon-coated copper grids, vitrified in liquid ethane, and visualized using cryogenic transmission electron microscopy (cryo-TEM). As shown in Figure 5.8C, **P34** nanoparticles were obsersved in high density as spherical aggregates with discrete coronae. The nanoparticles exhibited a narrow size distribution and a mean estimated diameter of 12.6 ± 2.8 nm. The larger diameter estimated using DLS relative to cryo-TEM is attributed to hydration layer of the hydrophilic corona; similar overestimation by DLS has been observed for other polymeric nanoparticles.[46]

The hydrolytic instability of TMZ leads to rapid decomposition in physiological conditions, with reported half-lives in pH 7 PBS and blood plasma of approximately 1 and 1.8 hours, respectively.[47] Premature degradation to methyldiazonium cations (Figure 5.2) leads to off-target hematoxicity and reduces the concentration of TMZ available to glioblastoma cells. As such, frequent dosing is required to maintain efficacious drug concentrations. Developing TMZ formulations which stabilize the drug and extend its half-life in solution is critical to augmenting efficacy. The decomposition of TMZ is readily monitored using UV-Vis spectroscopy: as TMZ degrades, the absorption corresponding to the urea moiety of pristine TMZ (λ = 328-330 nm) decreases in intensity, as shown in

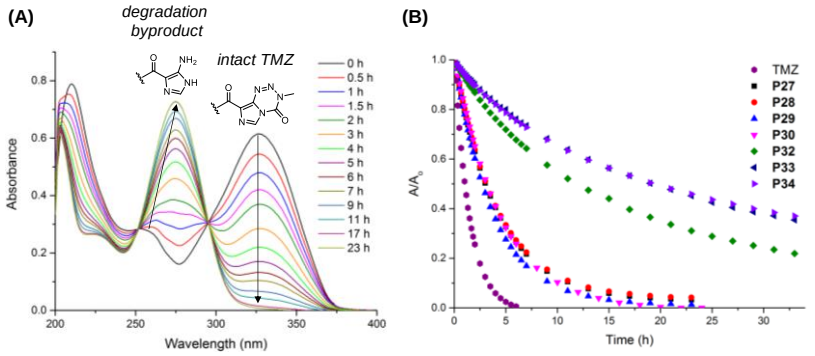

(C)

Sample	$t_{1/2}$ (h)	Residual TMZ (%)
TMZ	1.0	0.6
P27	3.1	3.3
P28	3.2	4.2
P29	2.7	1.3
P30	3.2	0
P32	12.8	18.6
P33	18.9	35.5
P34	19.1	37

Figure 5.9: (A) Representative UV-Vis cascade curves showing the degradation of TMZ (evidenced by a decrease in peak intensity at λ = 328-330 nm, corresponding to the intact TMZ urea) to the AIC byproduct (evidenced by an increase in peak intensity at λ = 265-267 nm, corresponding to the AIC amide); (B) degradation profiles for TMZ, **P27**-**P30**, and **P32**-**P34** incubated in pH 7.4 PBS at 37 °C; (C) values of $t_{1/2}$ estimated for TMZ, **P27**-**P30**, and **P32**-**P34** estimated from exponential fitting of decay curves, as well as percentages of TMZ remaining at the conclusion of each incubation experiment.

Figure 5.9A, and a new absorption attributed to the amide group of the AIC byproduct is observed at λ = 265-267 nm.[16,38]

In collaboration with Sarah Ward, the impact of polyMPC conjugation, drug loading, and copolymer architecture on the hydrolytic stability of TMZ was investigated by UV-Vis spectroscopy. PolyMPC-TMZ random copolymers **P27**-**P30** and block copolymers **P32**-**P34** were incubated at 37 °C in pH 7.4 PBS and compared to TMZ itself. UV-Vis absorption spectra were recorded over time, and degradation profiles constructed from the absorption decrease at λ = 328-330 nm (Figure 5.9B). Half-life ($t_{1/2}$) values for TMZ and the polyMPC-TMZ copolymers, summarized in Figure 5.9C, were obtained from exponential decay curves generated by plotting the normalized absorbance (A/A_0) as a function of incubation time. As shown in Figure 5.9, TMZ degraded quickly in PBS, exhibiting a $t_{1/2}$ of only 1.0 hours. Conjugation to the random copolymers improved TMZ lifetime 2- to 3-fold, extending $t_{1/2}$ to values of 2.7-3.2 hours. Notably, this $t_{1/2}$ increase

was independent of mole percent TMZ incorporation for the random copolymers. Polymer architecture also had a significant effect on TMZ solution stability, with block copolymers **P32**, **P33**, and **P34** exhibiting $t_{1/2}$ values of 12.8, 18.9, and 19.1 hours, respectively. In contrast to the random copolymers, increasing TMZ incorporation from 16-17 to 23-26 mole percent significantly increased the TMZ $t_{1/2}$; however, additional TMZ incorporation beyond 26 mole percent did not further improve solution stability. While TMZ conjugated to **P27**-**P30** degraded almost entirely within 24 hours, significant amounts of TMZ (18-37%) incorporated into the block copolymers remained intact, even after incubation at pH 7.4 and 37 °C for 33 hours. These results suggest that polymer architecture plays a more significant role than drug loading in improving TMZ solution stability. The improvements in TMZ stability exhibited by the polyMPC-TMZ platform are comparable, if not superior, to other delivery systems,[25,26] while also retaining synthetic practicality.

In addition to investigating TMZ stabilization by polymer conjugation, stabilization by uptake into block copolymer surfactants was explored. Aqueous suspensions of block copolymer amphiphiles—polyMPC-TMZ block copolymer **P33** and a polyMPC-*b*-poly(butyl methacrylate) (polyMPC-BMA) (**P35**) copolymer with 28 mole percent BMA—were used to solubilize free TMZ in pH 7.4 PBS at polymer concentrations of 5 mg/mL. By eye, TMZ-contaning polymer **P33** solubilized TMZ more rapidly than the common polyMPC-BMA surfactant. Furthermore, the polyMPC-TMZ block copolymer suspended free TMZ completely at a drug concentration of 4 mg/mL, while the corresponding polyMPC-BMA suspension showed residual undissolved TMZ. These TMZ-block copolymer suspensions were diluted approximately 400 times and incubated at 37 °C monitoring TMZ structural stability by UV-Vis spectroscopy. Under these

conditions, the solution stability was not significantly extended in comparison to free TMZ—half-lives of 1.3 and 1.4 hours were measured for TMZ suspensions prepared using polyMPC-TMZ **P33** and polyMPC-BMA **P35**, respectively. TMZ stability was also examined at a **P35** concentration of 1 mg/mL, well above the estimated CAC of **P35** in water ($CAC_{\mathbf{P35}}$ ~ 0.02 mg/mL, estimated using a pyrene fluorescence assay[41]). Despite solublization and encapsulation of TMZ into the hydrophobic core of the block copolymer aggregates, the TMZ $t_{1/2}$ was only extended to 1.8-2.7 hours; owing to the high absorbance of TMZ-containing block copolymers at a concentration of 1 mg/mL, a comparable experiment was not feasible for the polyMPC-TMZ prodrugs. These results suggest that polymer-TMZ conjugation is superior to encapsulation for significantly enhancing TMZ solution stability.

To investigate the uptake of polyMPC-TMZ copolymers into glioblastoma cells, fluorescent random copolymers with 16 and 51 mole percent TMZ (**P36** and **P37**, respectively) and block copolymers with 11 and 33 mole percent TMZ loadings (**P39** and **P40**, respectively) were synthesized by RAFT integrating fluorescein *O*-methacrylate in low (<1 mole percent) incorporations (Figure 5.10). Fluorescein *O*-methacrylate incorporations in polymers **P36**-**P40** were estimated by fluorescence spectroscopy to be 0.067 (**P36**), 0.068 (**P37**), 0.32 (**P38**), 0.032 (**P39**), and 0.021 (**P40**) weight percent. In collaboration with Dr. Banishree Saha, cellular uptake was investigated by treating U87MG glioblastoma cells with solutions of fluorescent polyMPC-TMZ copolymers in Dulbecco's Modified Eagle's Medium (DMEM) supplemented with 10% fetal bovine

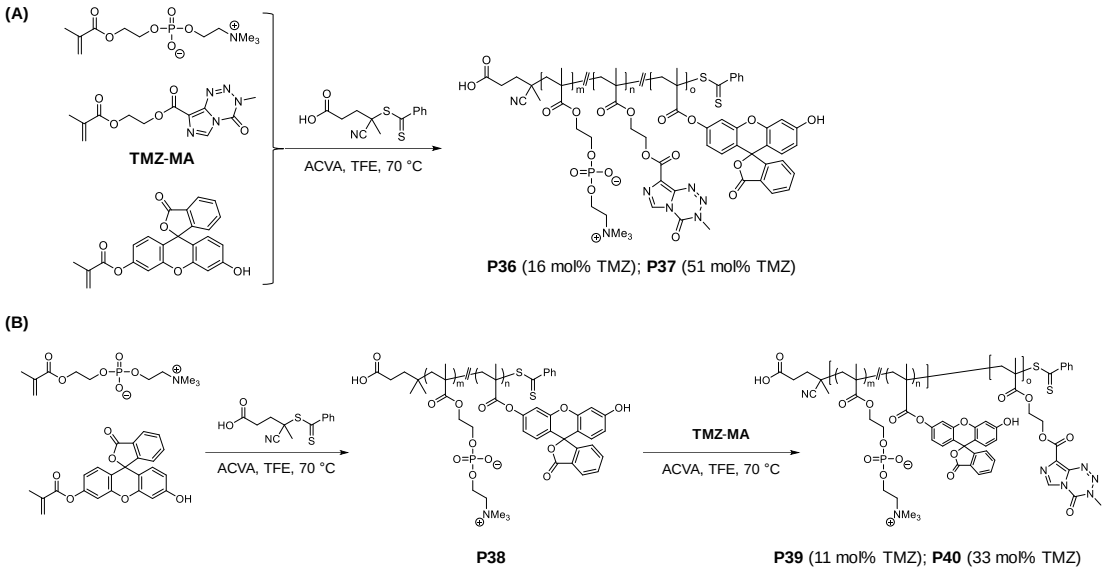

Figure 5.10: Synthesis of fluorescent polyMPC-TMZ random (A) and block (B) copolymers by RAFT polymerization methodology.

serum (FBS) at a TMZ-equivalent concentration of 200 µM. U87MG cells were also treated with a 0.35 mg/mL solution of fluorescein-labeled polyMPC **P38**. Cells were incubated at 37 °C for 2 hours, washed with PBS, treated with solutions of Lysotracker® Red and 4'-6-diamidino-2-phenylindole (DAPI) to stain cellular lyosomes and nuclei, respectively, and fixed with paraformaldehyde. The cells were then imaged by fluorescence confocal microscopy. As shown in the fluorescent micrographs in Figure 5.11, polymers **P36**-**P40** were internalized in the glioblastoma cells and were observed as green puncate spots in the perinuclear region of the cytoplasm. Signficant co-localization of the fluorescein and Lysotracker® Red signals was seen, suggesting polyMPC and polyMPC-TMZ copolymers are uptaken into glioblastoma cells through endocytosis.

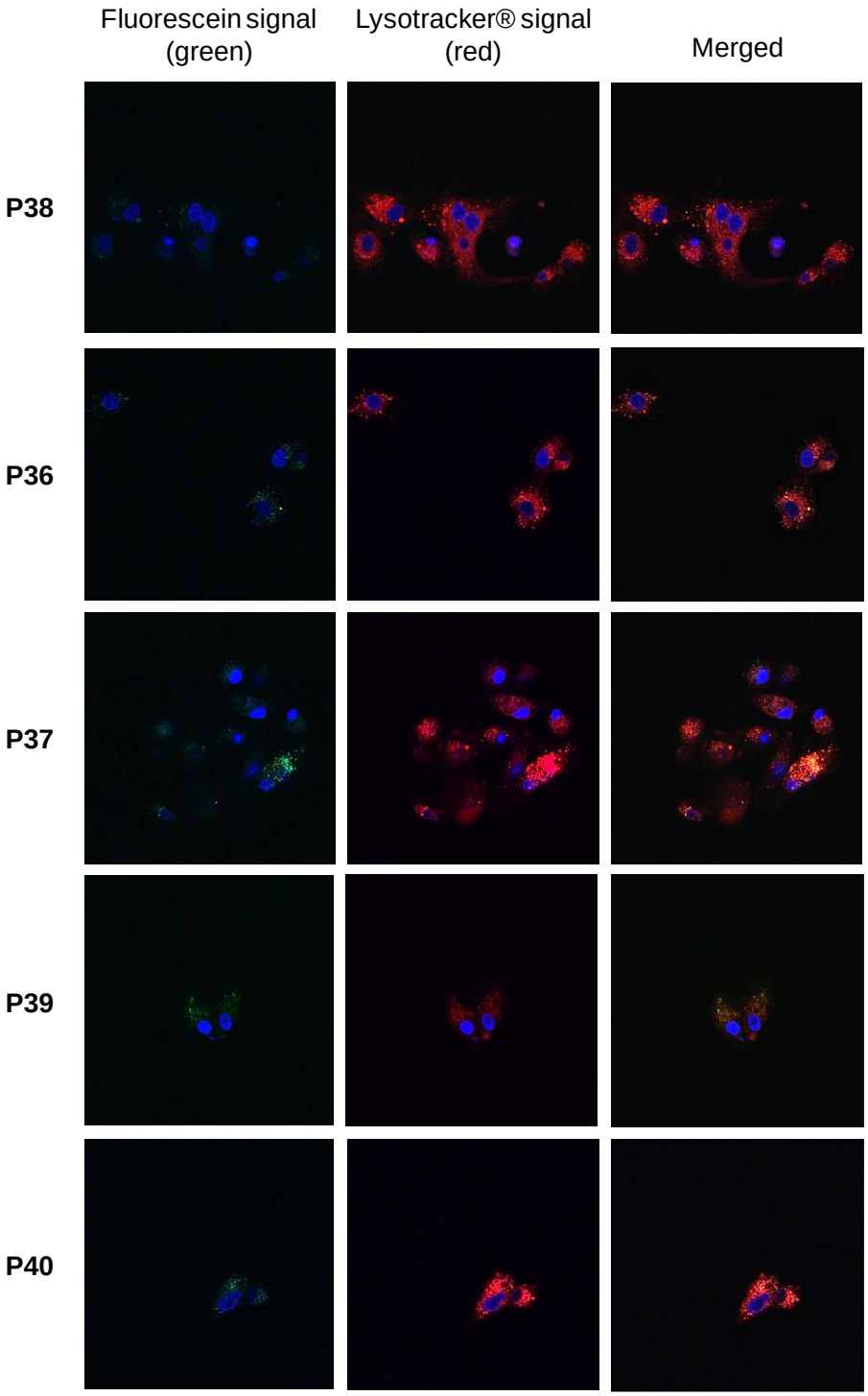

Figure 5.11: Fluorescent confocal micrographs of U87MG glioblastoma cells incubated with fluorescein-labeled (green) polyMPC **P38**, polyMPC-TMZ random copolymers **P36**/**P37**, and polyMPC-TMZ block copolymers **P39**/**P40.** Following a 2-hour incubation at 37 °C, the cells were treated with solutions of DAPI and Lysotracker® Red to stain the nuclei (blue) and lysozomes (red).

The internalization of polymers **P36**-**P40** by U87MG glioblastoma cells was quantified using flow cytometry. Cells were incubated at 37 °C with fluorescein-labeled polyMPC-TMZ copolymers **P36**, **P37**, **P39**, and **P40** at a TMZ-equivalent concentration of 200 μM for 2 hours at 37 °C, and were then washed with PBS to residual non-internalized polymer. Cells were also treated with a solution of fluorescent polyMPC **P38** ([polymer] = 0.35 mg/mL). Polymer uptake into the glioblastoma cells was measured by flow cytometry, detecting fluorescence from pendent fluorescein moieties. As shown in Figure 5.12, the polyMPC-TMZ block copolymers exhibited greater uptake than random copolymers **P36** and **P37**, with block copolymer **P40** (33 mole percent TMZ) exhibiting the greatest degree of internalization. While greater TMZ mole percent incorporation led to enhanced cellular internalization for the polyMPC-TMZ block copolymers, TMZ incorporation in polymer prodrugs with a random architecture did not affect cellular uptake. Notably, minimal cellular internalization was observed for polyMPC **P38**, a result which is consistent with a previous report by Ishihara and coworkers demonstrating that polyMPC does not effectively cross cellular membranes.[48] These cellular internalization assays demonstrate that polyMPC-TMZ conjugates are effectively uptaken by

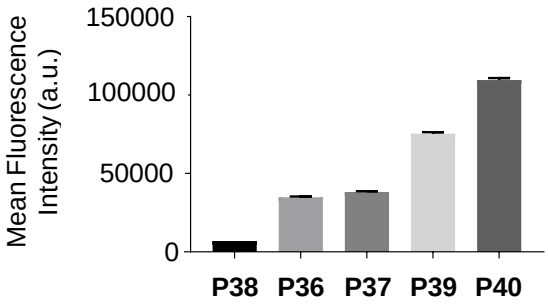

Figure 5.12: Mean fluorescence intensity measured by flow cytometry for U87MG glioblastoma cells treated with fluorescein-labeled polyMPC-TMZ random (**P36**, **P37**) copolymers, block (**P39**, **P40**) copolymers, and polyMPC (**P38**).

glioblastoma cells, and suggest that prodrugs prepared with a block copolymer architecture are advantageous for efficient uptake, which is enhanced by increasing TMZ incorporation.

In collaboration with Dr. Banishree Saha, the antitumor activity of polyMPC-TMZ copolymers was investigated in TMZ-senstive (*i.e.*, U87MG) and TMZ-resistant (*i.e.*, T98G) glioblastoma cells. These cell lines have been utilized extensively for testing the cytotoxicity of TMZ,[49-53] and its delivery systems.[26,54,55] In dose-response assays in the literature, a broad range of reported IC_{50} values are reported for pristine TMZ: approximately 10-500 μM for U87MG cells and 250-1600 μM for T98G cells.[53] This wide variation in IC_{50} values arises from differences in experimental protocols; such inconsistencies have also been noted for other small molecule chemotherapeutics (*e.g.*, doxorubicin).[56-59] Moreover, the poor aqueous solubility and hydrolytic instability of TMZ add a layer of complexity which increases variability in cell culture experiments, as aqueous TMZ solutions must be added to cells immediately after preparation. As such, recognizing the challenges in handling TMZ and accurately measuring its cytotoxicity, great care was taken to limit aqueous exposure and degradation in the *in vitro* anti-glioblastoma assays.

To evaluate cytotoxicity in glioblastoma cells, free TMZ and polyMPC-TMZ copolymers **P27**-**P30** and **P32**-**P34** were incubated at TMZ-equivalent concentrations with U87MG or T98G cells for 6 days, with polyMPC ([polymer] = 25.9 mg/mL) serving as a negative control. Cell viability was measured using a CellTiter-Glo® assay to generate the dose-response curves shown in Figure 5.13. As summarized in Table 5.2, free TMZ exhibited IC_{50} values of 192 ± 72 μM and 418 ± 116 μM in U87MG and T98G cells, respectively; these values are consistent with those previously reported.[53] The IC_{50} values

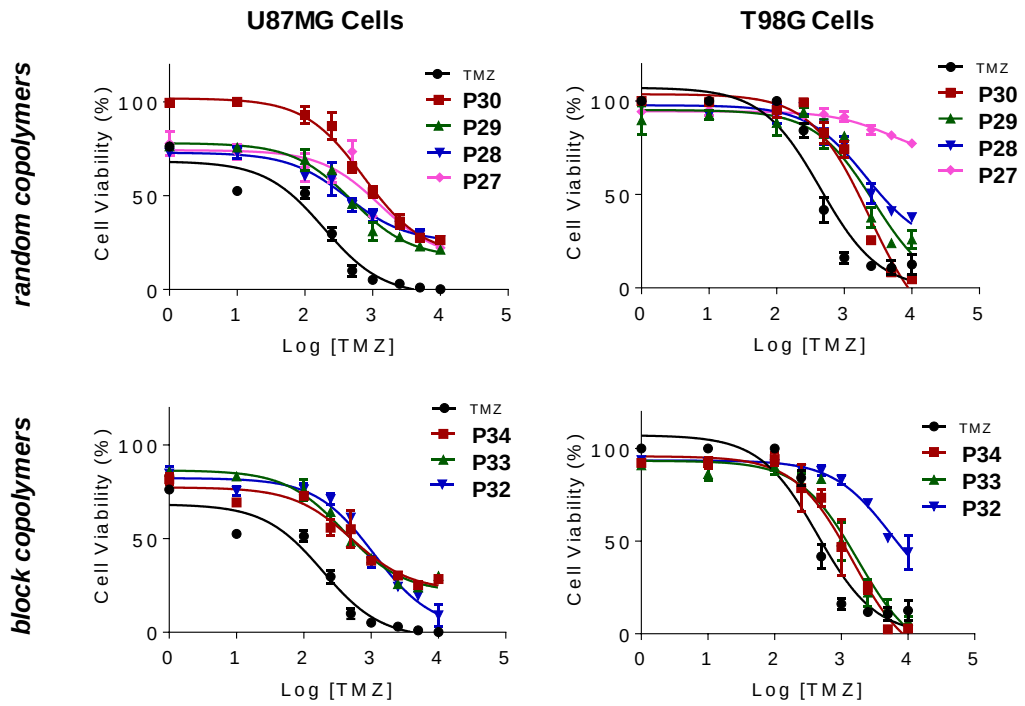

Figure 5.13: Cell viability of polyMPC-TMZ random and block copolymers in U87MG and T98G glioblastoma cells.

for the polyMPC-TMZ copolymers were approximately 7- to 10-fold higher than the free TMZ values in both cell lines. The reduced cytotoxicity of conjugated TMZ relative to free TMZ is typical of polymer prodrugs,[60,61] and is behavior we have noted previously in evaluating polymer-doxorubicin and polymer-camptothecin conjugates.[62-64] As expected, the IC_{50} values measured for the polyMPC-TMZ random and block copolymers were lower in the TMZ-sensitive U87MG cells than those measured in the TMZ-resistant T98G cells. For both cell lines, IC_{50} values plateaued above a critical TMZ incorporation (>20 mole percent): **P27** and **P32** had significantly higher IC_{50} values, as compared to **P28**-**P30** and **P33**-**P34**, respectively. While polymer architecture did not significantly affect the cytotoxicity of polyMPC-TMZ copolymers in chemosensitive U87MG cells, block copolymers with sufficiently high TMZ loading (>20 mole percent) exhibited significantly lower IC_{50} values (approximately 54-82% lower) in the resistant T98G cells, relative to

Table 5.2: IC_{50} values for U87MG and T98G glioblastoma cells treated with TMZ and polyMPC-TMZ copolymers (± indicates standard deviation).

IC_{50} (μM)	U87MG	T98G
TMZ	192 ± 72	418 ± 116
P27	1282 ± 58	4987 ± 26
P28	426 ± 48	2119 ± 77
P29	495 ± 61	2719 ± 98
P30	738 ± 84	2281 ± 132
P32	1095 ± 81	5529 ± 79
P33	396 ± 65	1748 ± 107
P34	517 ± 55	1477 ± 113

comparable random copolymer prodrugs. The potentiated cytotoxicity observed for polyMPC-TMZ block copolymers in the TMZ-resistant T98G cells was attributed to the enhanced TMZ solution stability and cellular internalization afforded by the block copolymer architecture.

A critical challenge in treating glioblastoma tumors is resistance to alkylating agents mediated by O^6-methylguanine-DNA methyltransferase (MGMT), an enzyme found within the cellular cytoplasm and nucleus which repairs cytotoxic methylated guanine lesions *via* methyl abstraction by a highly active cysteine residue (Cys145) (Figure 5.14A).[11] The Cys145 methylation is irreversible and leads to inactivation of the MGMT enzyme. Reduced MGMT activity through promoter gene silencing,[65-67] as well as depletion of MGMT concentration in tumors by hyperalkylation,[17] has been associated with improved outcomes and more effective treatment of glioblastoma tumors with chemotherapeutics such as TMZ. O^6-benzylguanine (O^6-BG), shown in Figure 5.14A, is an MGMT inhibitor which effectively alkylates MGMT enzymes, and has been examined as an adjuvant therapeutic for augmenting TMZ potency.[68-70] Despite promising *in vitro* and *in vivo* results which show that O^6-BG can reduce the IC_{50} value of TMZ in

(A)

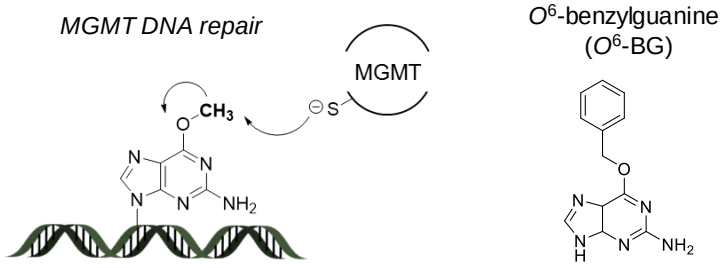

(B)

IC_{50} (μM)	U87MG	T98G
TMZ	471 ± 65	707 ± 106
TMZ + O^6-BG	88 ± 56	194 ± 87
P33	5084 ± 1004	10778 ± 1627
P33 + O^6-BG	606 ± 330	2986 ± 1660

Figure 5.14: (A) Mechanism for the repair of methylated guanine nucleobases by the MGMT enzyme, and the chemical structure of the MGMT inhibitor O^6-benzylguanine (O^6-BG); (B) IC_{50} values of U87MG and T98G glioblastoma cells treated with TMZ or polyMPC-TMZ block copolymer **P33** in conjunction with O^6-BG (100 μM).

glioblastoma cells by more than an order of magnitude, the poor aqueous solubility and severe off-target toxicity exhibited by O^6-BG has limited its successful translation to clinical treatments.[34] As polyMPC-based delivery systems impart aqueous solubility to hydrophobic therapeutics and have been shown to reduce undesired off-target toxicity,[71-73] the solubilization and co-delivery of TMZ and O^6-BG to glioblastoma cells was investigated through its encapsulation into a polyMPC-TMZ block copolymer.

U87MG and T98G glioblastoma cells were treated with aqueous suspensions of polyMPC-TMZ block copolymer **P33** containing O^6-BG at a constant concentration of 100 μM; this dose has previously been investigated for sensitizing U87MG and T98G cell lines to TMZ.[74] As controls, cells were treated with free TMZ, a mixture of TMZ and 100 μM

O^6-BG, and polyMPC-TMZ **P33** alone. Dose-response curves were generated, giving IC_{50} values for free TMZ alone in U87MG and T98G cells of 471 and 707 μM, respectively (Figure 5.14B). As observed previously, the IC_{50} values measured for **P33** were more than an order of magnitude higher in both cell lines than free TMZ. Co-treatment with O^6-BG significantly potentiated the cytotoxicity of the free and polymer-bound TMZ, reducing the **P33** IC_{50} values to 606 and 2986 μM in the U87MG and T98G cells, respectively. Notably, O^6-BG alone at a concentration of 100 μM was well-tolerated in both cell lines, with U87MG and T98G cells exhibiting viabilities of 84% and 78%, respectively, relative to untreated cells. These results suggest a synergistic benefit to treating glioblastoma tumor cells with a combination of a cytotoxic polymer-TMZ surfactant and an MGMT inhibitor.

5.4 Conclusions

In summary, TMZ, a first-line glioblastoma chemotherapeutic, was incorporated successfully into a series of polyMPC conjugates by RAFT copolymerization of a novel TMZ-methacrylate monomer. TMZ was integrated into copolymers with random and block copolymer architectures at tunable drug loadings, and the conjugates were obtained with narrow molecular weight distributions. This method for preparing well-defined polymer-TMZ prodrugs uses simple and effective polymerizations that are metal-free, avoid the need for post-polymerization drug conjugation, and preserve the potent chemical structure of TMZ. The results of this work suggest that polymer conjugation to the water-soluble polyMPC backbone significantly improves the physiological stability of TMZ, with block copolymer prodrugs affording the most profound improvement. Notably, conjugation was found to be much more effective for enhancing TMZ stability than

encapsulation in self-assembled aggregates. Cellular uptake, investigated using confocal microscopy and flow cytometry, suggested that polyMPC-TMZ copolymers are readily internalized in glioblastoma cells by endocytosis, and that block copolymer prodrugs undergo more efficient endocytosis than comparable random copolymer conjugates. Through *in vitro* cell viability experiments, the antitumor activity of these novel polyMPC-TMZ copolymers was demonstrated in chemosensitive and chemoresistant glioblastoma cell lines. PolyMPC-TMZ prodrugs exhibited higher IC_{50} values than free TMZ, a feature characteristic of polymer-drug conjugates, and TMZ incorporation and copolymer architecture were found to impact the efficacy of polymer-TMZ prodrugs. Specifically, drug loadings >20 mole percent were necessary to achieve suitable cytotoxicity, and the block copolymer prodrugs were more efficacious in killing TMZ-resistant glioblastoma cells than the comparable random copolymer prodrugs. Finally, the *in vitro* antitumor activity of a polyMPC-TMZ block copolymer was shown to be significantly enhanced through the co-delivery of the MGMT inhibitor O^6-BG.

Owing to the versatile reactivity of the TMZ-methacrylate derivative, opportunities for introducing TMZ into a variety of biocompatible polymer compositions and networks are now available, providing access to a polymer-TMZ therapeutic platform suitable for systemic and local chemotherapy. Going forward, effective use of such polymers by systemic administration will require retention of the blood-brain barrier crossing properties inherent to TMZ itself, which may require biorecognition with small molecules (*i.e.*, thiamine)[75] or peptides (*i.e.*, glutathione)[76,77] to facilitate transcytosis. Future studies aim to further augment this novel therapeutic platform by incorporating TMZ-sensitizing

molecules, such as O^6-BG, as pendent moieties in the polyMPC-TMZ backbone for overcoming the TMZ-resistance exhibited by many glioblastoma tumors.

5.5 References

1. Ostrom, Q. T.; Gittleman, H.; Fulop, J.; Liu, M.; Blanda, R.; Kromer, C.; Wolinsky, Y.; Kruchko, C.; Barnholtz-Sloan, J. S. CBTRUS Statistical Report: Primary Brain and Central Nervous System Tumors Diagnosed in the United States in 2008-2012. *Neuro Oncol*. **2015**, *17*, iv1-iv62.

2. Omuro, A.; DeAngeli, L. M. Glioblastoma and Other Malignant Gliomas. *JAMA* **2013**, *310*, 1842-1850.

3. Stupp, R.; Mason, W. P.; van den Bent, M. J.; Weller, M.; Fisher, B.; Taphoorn, M. J. B.; Belanger, K.; Brandes, A. A.; Marosi, C.; Bogdahn, U.; Curschmann, J.; Janzer, R. C.; Ludwin, S. K.; Gorlia, T.; Allgeier, A.; Lacombe, D.; Cairncross, G.; Eisenhauer, E.; Mirimanoff, R. O. Radiotherapy Plus Concomitant and Adjuvant Temozolomide for Glioblastoma. *N. Engl. J. Med.* **2005**, *352*, 987-996.

4. Adamson, C.; Kanu, O. O.; Mehta, A. I.; Di, C.; Lin, N.; Mattox, A. K.; Bigner, D. D. Glioblastoma Multiforme: A Review of Where We Have Been and Where We Are Going. *Expert. Opin. Investig. Drugs* **2009**, *18*, 1061-1083.

5. Wen, P. Y.; Kesari, S. Malignant Gliomas in Adults. *N. Engl. J. Med.* **2008**, *359*, 492-507.

6. Karim, R.; Palazzo, C.; Evrard, B.; Piel, G. Nanocarriers for the Treatment of Glioblastoma Multiforme: Current State-of-the-Art. *J. Control. Release* **2016**, *227*, 23-37.

7. Ballabh, P.; Braun, A.; Nedergaard, M. The Blood-Brain Barrier: An Overview: Structure, Regulation, and Clinical Implications. *Neurobiol. Dis.* **2004**, *16*, 1-13.

8. De Bonis, P.; Anile, C.; Pompucci, A.; Fiorentino, A.; Balducci, M.; Chiesa, S.; Maira, G.; Mangiola, A. Safety and Efficacy of Gliadel Wafers fo Newly Diagnosed and Recurrent Glioblastoma. *Acta Neurochir*. **2012**, *154*, 1371-1378.

9. Fourniols, T.; Randolph, L. D.; Staub, A.; Vanvarenberg, K.; Leprince, J. G.; Préat, V.; des Rieux, A.; Danhier, F. Temozolomide-Loaded Photopolymerizable PEG-DMA-Based Hydrogel for the Treatment of Glioblastoma. *J. Control. Release* **2015**, *210*, 95-104.

10. Newlands, E. S.; Stevens, M. F. G.; Wedge, S. R.; Wheelhouse, R. T.; Brock, C. Temozolomide: A Review of its Discovery, Chemical Properties, Pre-Clinical Development and Clinical Trials. *Cancer Treat. Rev.* **1997**, *23*, 35-61.

11. Zhang, J.; Stevens, M. F. G.; Bradshaw, T. D. Temozolomide: Mechanisms of Action, Repair and Resistance. *Curr. Mol. Pharmacol.* **2012**, *5*, 102-114.

12. Rottenberg, D. A.; Ginos, J. Z.; Kearfott, K. J.; Junck, L.; Bigner, D. D. In Vivo Measurement of Regional Brain Tissue pH Using Positron Emission Tomography. *Ann. Neurol.* **1984**, *15*, S98-102.

13. Stevens, M. F. G.; Hickman, J. A.; Langdon, S. P.; Chubb, D.; Vickers, L.; Stone, R.; Baig, G.; Goddard, C.; Gibson, N. W.; Slack, J. A.; Newton, C.; Lunt, E.; Fizames, C.; Lavelle, F. Antitumor Activity and Pharmacokinetics in Mice of 8-Carbamoyl-3-Methyl-Imidazo[5,1,*d*]-1,2,3,5-Tetrazin-4(3*H*)-One (CCRG 81045; M & B 39831), a Novel Drug with Potential as an Alternative to Dacarbazine. *Cancer Res*. **1987**, *47*, 5846-5852.

14. Braverman, O.; Feinshtein, R.; Weisman, A.; Kaspi, J. Temozolomide Storage System. U.S. Patent 20060222792 A1, October 5, 2006.

15. Mirzaei, S.; Khalilian, M. H.; Taherpour, A A. Mechanistic Study of the Hydrolytic Degradation and Protonation of Temozolomide. *RSC Adv.* **2015**, *5*, 41112-41119.

16. Babu, N. J.; Sanphui, P.; Nangia, A. Crystal Engineering of Stable Temozolomide Cocrystals. *Chem. Asian J*. **2012**, *7*, 2274-2285.

17. Tolcher, A. W.; Gerson, S. L.; Denis, L.; Geyer, C.; Hammond, L. A.; Patnaik, A.; Goetz, A. D.; Schwartz, G.; Edwards, T.; Reyderman, L.; Statkevich, P.; Cutler, D. L.; Rowkinsky, E. K. *Br. J. Cancer* **2003**, *88*, 1004-1011.

18. Wick, W.; Platten, M.; Weller, M. New (Alternative) Temozolomide Regimens for the Treatment of Glioma. *Neuro Oncol*. **2009**, *11*, 69-79.

19. Wick, W.; Steinbach, J. P.; Küker, W. M.; Dichgans, J.; Bamberg, M.; Weller, M. *Neurology* **2004**, *62*, 2113-2115.

20. Jauch, T.; Hau, P.; Bogdahn, U. Re-challenge with Temozolomide (TMZ) at Recurrence in High-Grade Gliomas (HGG). *J. Clin. Oncol*. **2007**, *25*, 2034.

21. Wick, A.; Felsberg, J.; Steinbach, J. P.; Herrlinger, U.; Platten, M.; Blaschke, B.; Meyermann, R.; Reifenberger, G.; Weller, M.; Wick, W. Efficacy and Tolerability of Temozolomide in an Alternating Weekly Regimen in Patients with Recurrent Glioma. *J. Clinc. Oncol.* **2007**, *25*, 3357-3361.

22. Berrocal, A.; Perrez Segura, P.; Gil, M.; Balanã, C.; Garcia Lopez, J.; Yaya, R.; Rodríguez, J.; Reynes, G.; Gallego, O.; Iglesias, L. Extended-schedule Dose-dense Temozolomide in Refractory Gliomas. *J. Neuro-Oncol*. **2010**, *96*, 417-422.

23. Appel, E. A.; Rowland, M. J.; Loh, X. J.; Heywood, R. M.; Watts, C.; Scherman, O. A. Enhanced Stability and Activity of Temozolomide in Primary Glioblastoma Multiforme Cells with Cucurbit[*n*]uril. *Chem. Commun.* **2012**, *48*, 9843-9845.

24. Martino, A. D.; Kucharczyk, P.; Capakova, Z.; Humpolicek, P.; Sedlarik, V. Enhancement of Temozolomide Stability by Loading in Chitosan-Carboxylated Polylactice-Based Nanoparticles. *J. Nanopart. Res.* **2017**, *19*, 71-86.

25. Patil, R.; Portilla-Arias, J.; Ding, H.; Inoue, S.; Konda, B.; Hu, J.; Wawrowsky, K. A.; Shin, P. K.; Black, K. L.; Holler, E.; Ljubimova, J. Y. Temozolomide Delivery to Tumor Cells by a Multifunctional Nano Vehicle Based on Poly(β-L-malic acid). *Pharm. Res.* **2010**, *27*, 2317-2329.

26. Fang, C.; Wang, K.; Stephen, Z. R.; Mu, Q.; Kievit, F. M.; Chiu, D. T.; Press, O. W.; Zhang, M. Temozolomide Nanoparticles for Targeted Glioblastoma Therapy. *ACS Appl. Mater. Interfaces* **2015**, *7*, 6674-6682.

27. Larson, N.; Ghandehari, H. Polymeric Conjugates for Drug Delivery. *Chem. Mater*. **2012**, *24*, 840-853.

28. Fox, M. E.; Szoka, F. C.; Fréchet, J. M. J.; Soluble Polymer Carriers for the Treatment of Cancer: The Importance of Molecular Architecture. *Acc. Chem. Res.* **2009**, *42*, 1141-1151.

29. Maeda, H.; Nakamura, H.; Fang, J. The EPR Effect for Macromolecular Drug Delivery to Solid Tumors: Improvement of Tumor Uptake, Lowering of Systemic Toxicity, and Distinct Tumor Imaging In Vivo. *Adv. Drug Delivery Rev*. **2013**, *65*, 71-79.

30. Wong, K. E.; Mora, M. C.; Skinner, M.; McRae Page, S.; Crisi, G. M.; Arenas, R. B.; Schneider, S. S.; Emrick, T. Evaluation of PolyMPC-Dox Prodrugs in a Human Ovarian Tumor Model. *Mol. Pharm.* **2016**, *13*, 1679-1687.

31. McRae Page, S.; Henchey, E.; Chen, X.; Schneider, S.; Emrick, T. Efficacy of PolyMPC-DOX Prodrugs in 4T1 Tumor-Bearing Mice. *Mol. Pharm.* **2014**, *11*, 1715-1720.

32. Skinner, M.; Ward, S. M.; Emrick, T. Versatile Synthesis of Polymer-Temozolomide Conjugates. *ACS Macro Lett*. **2017**, *6*, 215-218.

33. Dolan, M. E.; Pegg, A. E. O^6-Benzylguanine and Its Role in Chemotherapy. *Clin. Cancer Res.* **1997**, *3*, 837-847.

34. Quinn, J. A.; Jiang, S. X.; Reardon, D. A.; Desjardins, A.; Vredenburgh, J. J.; Rich, J. N.; Gururangan, S.; Friedman, A. H.; Bigner, D. D.; Sampson, J. H.; McLendon, R. E.; Herndon II, J. E.; Walker, A.; Friedman, H. S. Phase II Trial of Temozolomide Plus O^6-Benzylguanine in Adults with Recurrent, Temozolomide-Resistant Malignant Glioma. *J. Clin. Oncol.* **2009**, *27*, 1262-1267.

35. Stephen, Z. A.; Kievit, F. M.; Chiarelli, P. A.; Fang, C.; Wang, K.; Hatzinger, S. J.; Ellenbogen, R. G.; Silber, J. R.; Zhang, M. Redox-Responsive Magnetic Nanoparticle for Targeted Convection-Enhanced Delivery of O^6-Benzylguanine to Brain Tumors. *ACS Nano* **2014**, *8*, 10383-10395.

36. Stephen, Z. R.; Gebhart, R. N.; Jeon, M.; Blair, A. A.; Ellenbogen, R. G.; Silber, J. R.; Zhang, M. pH-Sensitive O6-Benzylguanosine Polymer Modified Magnetic Nanoparticles for Treatment of Glioblastomas. *Bioconjugate Chem*. **2017**, *28*, 194-202.

37. Arrowsmith, J.; Jennings, S. A.; Clark, A. S.; Stevens, M. F. G. Antitumor Imidazotetrazines. 41. Conjugation of the Antitumor Agents Mitozolomide and Temozolomide to Peptides and Lexitropsins Bearing DNA Major and Minor Groove-Binding Structural Motifs. *J. Med. Chem.* **2002**, *45*, 5458-5470.

38. Arrowsmith, J.; Jennings, S. A.; Langnel, D. A. F.; Wheelhouse, R. T.; Stevens, M. F. G. Antitumor Imidazotetrazines. Part 39. Synthesis of Bis(imidazotetrazine)s with Saturated Spacer Groups. *J. Chem. Soc., Perkin Trans. 1* **2000**, *1*, 4432-4438.

39. Kevill, D. N.; Anderson, S. W. An Improved Scale of Solvent Nucleophilicity Based on the Solvolysis of the S-methyldibenzothiophenium Ion. *J. Org. Chem.* **1991**, *56*, 1845-1850.

40. Topel, O.; Çakir, A.; Budama, L.; Hoda, N. Determination of Critical Micelle Concentration of Polybutadiene-*block*-Poly(etheylene oxide) Diblock Copolymer by Fluorescence Spectroscopy and Dynamic Light Scattering. *J. Mol. Liq.* **2013**, *177*, 40-43.

41. Kalyanasundaram, K.; Thomas, J. K. Environmental Effects on Vibronic Band Intensities in Pyrene Monomer Fluorescence and Their Application in Studies of Micellar Systems. *J. Am. Chem. Soc.* **1977**, *99*, 2039-2044.

42. Ko, D.Y.; Patel, M.; Jung, B. K.; Park, J. H.; Jeong, B. Phosphorylcholine-Based Zwitterionic Biocompatible Thermogel. *Biomacromolecules* **2015**, *16*, 3853-3862.

43. Kita-Tokarczyk, K.; Grumelard, J.; Haefele, T.; Meier, W. Block Copolymer Vesicles—Using Concepts from Polymer Chemistry to Mimic Biomembranes. *Polymer* **2005**, *46*, 3540-3569.

44. Du, J.; O'Reilly, R. K. Advances and Challenges in Smart and Functional Polymer Vesicles. *Soft Matter* **2009**, *5*, 3544-3561.

45. Zhang, L.; Eisenberg, A. Multiple Morphologies and Characteristics of "Crew-Cut" Micelle-Like Aggregates of Polystyrene-*b*-Poly(acrylic acid) Diblock Copolymers in Aqueous Solutions. *J. Am. Chem. Soc.* **1996**, *118*, 3168-3181.

46. Patil, N.; Falentin-Daudré, C.; Jérôme, C.; Detrembleur, C. Mussel-Inspired Protein-Repelling Ambivalent Block Copolymers: Controlled Synthesis and Characterization. *Polym. Chem.* **2015**, *6*, 2919-2933.

47. Newlands, E. S.; Blackledge, G. R. P.; Slack, J. A.; Rustin, G. J. S.; Smith, D. B.; Stuart, N. S. A.; Quarterman, C. P.; Hoffman, R.; Stevens, M. F. G.; Brampton, M. H.; Gibson, A. C. Phase I Trial of Temozolomide (CCRG 81045: M&B 39831: NSC 362856). *Br. J. Cancer* **1992**, *65*, 287-291.

48. Goda, T.; Goto, Y.; Ishihara, K. Cell-Penetrating Macromolecules: Direct Penetration of Amphiphatic Phospolipid Polymers Across Plasma Membrane of Living Cells. *Biomaterials* **2010**, *31*, 2380-2387.

49. Alonso, M. M.; Gomez-Manzano, C.; Bekele, B. N.; Yung, W. K.; Fueyo, J. Adenovirus-Based Strategies Overcome Temozolomide Resistance by Silencing the O6-Methylguanine-DNA Methyltransferase Promoter. *Cancer Res.* **2007**, *67*, 11499-11504.

50. Baer, J. C.; Freeman, A. A.; Newlands, E. S.; Watson, A. J.; Rafferty, J. A.; Marglson, G. P. Depletion of O6-Alkylguanine-DNA Alkyltransferase Correlates with Potentiation of Temozolomide and CCNU Toxicity in Human Tumour Cells. *Br. J. Cancer* **1993**, *67*, 1299-1302.

51. Kanzawa, T.; Bedwell, J.; Kondo, Y.; Kondo, S.; Germano, I. M. Inhibition of DNA Repair for Sensitizing Resistant Glioma Cells to Temozolomide. *J. Neurosurg*. **2003**, *99*, 1047-1052.

52. Kanzawa, T.; Germano, I. M.; Kondo, Y.; Ito, H.; Kyo, S.; Kondo, S. Inhibition of Telomerase Activity in Malignant Glioma Cells Correlates with Their Sensitivity to Temozolomide. *Br. J. Cancer***2003**, *89*, 922-929.

53. Lee, S. Y. Temozolomide Resistance in Glioblastoma Multiforme. *Genes & Diseases* **2016**, *3*, 198-210.

54. Kim, S-S.; Rait, A.; Kim, E.; DeMarco, J.; Pirollo, K. F.; Chang, E. H. Encapsulation of Temozolomide in a Tumor-Targeting Nanocomplex Enhances Anti-Cancer Efficacy and Reduces Toxicity in a Mouse Model of Glioblastoma. *Cancer Lett.* **2015**, *369*, 250-258.

55. Bertucci, A.; Prasetyanto, E. A.; Septiadi, D.; Manicardi, A.; Brognara, E.; Gambari, R.; Corradini, R.; De Cola, L. Combined Delivery of Temozolomide and Anti-miR221 PNA Using Mesoporous Silica Nanoparticles Induces Apoptosis in Resistant Glioma Cells. *Small* **2015**, *11*, 5687-5695.

56. Wu, A.; Loutherback, K.; Lambert, G.; Estévez-Salmerón, L.; Tlsty, T. D.; Austin, R. H.; Sturm, J. C. Cell Motility and Drug Gradients in the Emergence of Resistance to Chemotherapy. *Proc. Natl. Acad. Sci. U.S.A.* **2013**, *110*, 16103-16108.

57. Smith, L.; Watson, M. B.; O'Kane, S. L.; Drew, P. J.; Lind, M. J.; Cawkwell, L. The Analysis of Doxorubicin Resistance in Human Breast Cancer Cells Using Antibody Microarrays. *Mol. Cancer Ther.* **2006**, *5*, 2115-2120.

58. Gouazé-Andersson, V.; Yu, J. Y.; Kreitenberg, A. J.; Bielawska, A.; Giuliano, A. E.; Cabot, M. C. Ceramide and Glucosylceramide Upregular Expression of the Multidrug Resistance Gene MDR1 in Cancer Cells. *Biochim. Biophys. Acta* **2007**, *1171*, 1407-1417.

59. Aroui, S.; Ram, N.; Appaix, F.; Ronjat, M.; Kenani, A.; Pirollet, F.; De Waard, M. Maurocalcin as a Non Toxic Drug Carrier Overcomes Doxorubicin Resistance in the Cancer Cell Line MDA-MB 231. *Pharm. Res.* **2009**, *26*, 836-845.

60. Wang, D.; Kopečková, P.; Minko, T.; Nanayakkara, V.; Kopeček. Synthesis of Starlike *N*-(2-Hydroxypropyl)methacrylamide Copolymers: Potential Drug Carriers. *Biomacromolecules* **2000**, *1*, 313-319.

61. Veronese, F. M.; Schiavon, O.; Pasut, G.; Mendichi, R.; Andersson, L.; Tsirk, A.; Ford, J.; Wu, G.; Kneller, S.; Davies, J.; Duncan, R. PEG-Doxorubicin Conjugates: Influence of Polymer Structure on Drug Release, In Vitro Cytotoxicity, Biodistribution, and Antitumor Activity. *Bioconjugate Chem.* **2005**, *16*, 775-784.

62. Chen, X.; Parelkar, S. S.; Henchey, E.; Schneider, S.; Emrick, T. PolyMPC-Doxorubicin Prodrugs. *Biconjugate Chem*. **2012**, *23*, 1753-1763.

63. Chen, X.; McRae, S.; Parelkar, S.; Emrick, T. Polymeric Phosphorylcholine-Camptothecin Conjugates Prepared by Controlled Free Radical Polymerization and Click Chemistry. *Bioconjugate Chem*. **2009**, *20*, 2331-2341.

64. McRae Page, S.; Martorella, M.; Parelkar, S.; Kosif, I.; Emrick, T. Disulfide Cross-Linked Phosphorylcholine Micelles for Triggered Release of Camptothecin. *Mol. Pharmaceutics* **2013**, *10,* 2684-2692.

65. Hegi, M. E.; Diserens, A-C.; Gorlia, T.; Hamou, M-F.; de Tribolet, N.; Weller, M.; Kros, J. M.; Hainfellner, J. A.; Mason, W.; Mariani, L.; Bromberg, J. E. C.; Hau, P.; Mirimanoff, R. O.; Cairncross, J. G.; Janzer, R. C.; Stupp, R. *MGMT* Gene Silencing and Benefit from Temozolomide in Glioblastoma. *N. Engl. J. Med.* **2005**, *352*, 997-1003.

66. Rivera, A. L.; Pelloski, C. E.; Gilbert, M. R.; Colman, H.; De La Cruz, C.; Sulman, E. P.; Bekele, B. N.; Aldape, K. D. MGMT Promoter Methylation is Predictive of Response to Radiotherapy and Prognostic in the Absence of Adjuvant Alkylating Chemotherapy for Giloblastoma. *Neuro Oncol*. **2010**, *12*, 116-121.

67. Gilbert, M. R.; Wang, M.; Aldape, K. D.; Stupp, R.; Hegi, M. E.; Jaeckle, K. A.; Armstrong, T. S.; Wefel, J. S.; Won, M.; Blumenthanl, D. T.; Mahajan, A.; Schultz, C. J.; Erridge, S.; Baumert, B.; Hopkins, K. I.; Tzuk-Shina, T.; Brown, P. D.; Chakravarti, A.; Curran Jr., W. J.; Mehta, M. P. Dose-Dense Temozolomide for Newly Diagnosed Glioblastoma: A Randomized Phase III Clinical Trial. *J. Clin. Oncol*. **2013**, *31*, 4085-4091.

68. Bobola, M. S.; Tseng, S. H.; Blank, A.; Berger, M. S.; Silber, J. R. Role of O6-Methylguanine-DNA Methyltransferase in Resistance of Human Brain Tumor Cell Lines to the Clinically Relevant Methylating Agents Temozolomide and Streptozotocin. *Clin. Cancer Res.* **1996**, *2*, 735-741.

69. Wedge, S. R.; Porteous, J. K.; Newland, E. S. 3-Aminobenzamide and/or O^6-Benzylguanine Evaluated as an Adjuvant to Temozolomide or BCNU Treatment in Cell Lines of Variable Mismatch Repair Status and O^6-Alkylguanine-DNA Alkyltransferase Activity. *Br. J. Cancer* **1996**, *74*, 1030-1036.

70. Wedge, S. R.; Porteous, J. K.; May, B. L.; Newlands, E. S. Potentiation of Temozolomide and BCNU Cytotoxicity by O^6-Benzylguanine: A Comparative Study *In Vitro*. *Br. J. Cancer* **1996**, *73*, 482-490.

71. Konno, T.; Watanabe, J.; Ishihara, K. Enhanced Solubility of Paclitaxel Using Water-Soluble and Biocompatible 2-Methacryloyloxyethyl Phosphorylcholine Polymers. *J. Biomed. Mater. Res.* **2003**, *65A*, 209-214.

72. Yusa, S-i.; Fukuda, K.; Yamamoto, T.; Ishihara, K.; Morishima, Y. Synthesis of Well-Defined Amphiphilic Block Copolymers Having Phospholipid Polymer Sequences as a Novel Biocompatible Polymer Micelle Reagent. *Biomacromolecules* **2005**, *6*, 663-670.

73. Miyata, R.; Ueda, M.; Jinno, H.; Konno, T.; Ishihara, K.; Ando, N; Kitagawa, Y. Selective Targeting by PreS1 Domain of Hepatitis B Surface Antigen Conjugated with Phosporylcholine-Based Amphiphilic Block Copolymer Micelles as a Biocompatible, Drug Delivery Carrier for Treatment of Human Hepatocellular Carcinoma with Paclitaxel. *Int. J. Cancer* **2009**, *15*, 2460-2467.

74. Aghi, M.; Rabkin, S.; Martuza, R. L. Effect of Chemotherapy-Induced DNA Repair on Oncolytic Herpes Simplex Viral Replication. *J. Natl. Cancer Inst.* **2006**, *98*, 38-50.

75. Lockman, P. R.; Oyewumi, M. O.; Koziara, J. M.; Roder, K. E.; Mumper, R. J.; Allen, D. D. Brain Uptake of Thiamine-Coated Nanoparticles. *J. Control. Release* **2003**, *93*, 271-282.

76. Geldenhuys, W.; Mbimba, T.; Bui, T.; Harrison, K.; Sutariya, V. Brain-Targeted Delivery of Paclitaxel Using Glutathione-Coated Nanoparticles for Brain Cancers. *J. Drug Target* **2011**, *19*, 837-845.

77. Kannan, R.; Kuhlenkamp, J. F.; Jeandidier, E.; Trinh, H.; Ookhtens, M.; Kaplowitz, N. Evidence for Carrier-Mediated Transport of Glutathione Across the Blood-Brain Barrier in the Rat. *J. Clin. Invest.* **1990**, *85*, 2009-2013.

CHAPTER 6

OUTLOOK

6.1 Functional, Water-Dispersible Polysiloxanes

Chapter 2 presented the synthesis of water-dispersible, zwitterionic siloxane polymers through the thiol-ene modification of vinyl-functionalized precursors with phosphorylcholine (PC)- and sulfobetaine (SB)-thiols. Preliminary syntheses investigated the preparation of functional zwitterionic polysiloxanes *via* non-stoichiometric conversion of pendent vinylsiloxane moieties. Proof-of-principle demonstrations suggested these structures could be accessed with tunable vinyl incorporations while retaining the well-defined characteristics of the polymer precursors (*i.e.*, narrow molecular weight distributions). These water-dispersible materials are amenable to further post-polymerization modification, including crosslinking to afford robust self-assembled nanoparticles or zwitterionic silicone hydrogels. Additionally, these vinyl-containing zwitterionic polysiloxanes could be bleneded commercial silicone formulations (*i.e.*, Sylgard 184), affording hydrophilic silicone elastomers through metal-catalyzed hydrosilylation crosslinking chemistries. Such elastomers are potentially of interest for microfluidic device fabrication, as well as antifouling coatings. In contrast to conventional hydrocarbon-based polymers, polysiloxanes undergo depolymerization and rearrangement in the presence of silanol nucleophiles and metal oxides.[1,2]. As PC- and SB-functionalized siloxane polymers readily assemble at interfaces, these materials hold utilty for synthesizing covalent antifouling coatings through water-borne deposition and subsequent depolymerization/rearrangement at a range of liquid/solid interfaces. As such, the

zwitterionic polysiloxanes described in this dissertation hold promise as versatile and functional polymer amphiphiles.

6.2 Zwitterionic Pluronic Mimics

In Chapter 3, the synthesis of novel PC-functionalized zwitterionic Pluronic mimics, termed 'zwitteronics', was described. These triblock copolymers were prepared by the macroinitiated atom transfer radical polymerization (ATRP) of 2-methacryloyloxyethyl phosphorylcholine (MPC), affording polymer amphiphiles with tunable hydrophilic-hydrophobic balance and relative narrow molecular weight distributions. Aqueous suface tensiomery suggested that these water-dispersble polymer surfactants exhibited composition-independent surface activity, behavior which is unique to the surfactant properties of commercial Pluronics. Future studies should probe this behavior further, specifically by preparing PC-zwitteronic block copolymers with higher polyMPC number-average degree of polymerization (X_n) values (*i.e.*, > 36). Such studies would provide a richer understanding of the fundamental properties of these novel zwitterionic surfactants, especially as they compare to commercial Pluronics.

Future syntheses of zwitterionic Pluronic mimics should seek to develop novel compositions, including analogs bearing pendent SB and choline phosphate (CP) zwitterions. Owing to the temperature- and salt-responsive solubility of SB polymers in water, poly(sulfobetaine methacrylate)-*b*-poly(propylene oxide)-b-poly(sulfobetaine methacrylate) (polySBMA-PPO-polySBMA) are of interest as a Pluronic mimics for triggered aqueous nanomaterials assembly. The CP-containing zwitteronic block copolymers afford functional polymer amphiphiles, which were shown to provide a facile

strategy for nanomaterials crosslinking. Future investigations will look to utilize these self-assembled materials for the encapsulation and relase of various hydrophobic and hydrophilic moleucles, as well as aim to incorporate additional chemical moetiies through pendent CP zwitterions, including diol functionality[3] amenable to boronic ester crosslinking and the generation of biocompatible, self-healing networks.[4,5]

6.3 Expanding the PolyMPC-Doxorubicin Prodrug Platform

Chapter 4 expanded upon previous investigations of the polyMPC-Doxorubicin (polyMPC-Dox) prodrug platform,[6,7] presenting the first *in vivo* assessment of a polyMPC-chemotherapeutic conjugate in a human tumor model. This evaluation represents a significant step towards realizing the utilization of polyMPC as a biocompatible scaffold for injectable polymeric medicines, and as a potential replacement for poly(ethylene glycol) (PEG) in the synthesis of polymer-drug and polymer-protein conjugates. Utilized in numerous approved treatments, PEG remains the gold standard for polymer-based therapies, serving as a biocompatible scaffold which can improve the pharmacokinetics, physiological stability, and aqueous solubility of hydrophobic drugs and therapeutically active proteins.[8] Despite its demonstrated benefits, PEGylation has shortcomings, including inherently limited drug loading, as well as immunogenic effects which can reduce therapeutic efficacy following repeated administration.[9-12] As MPC is readily copolymerized with a variety of functional monomers, the polyMPC platform allows for high drug loadings not achieved through conventional PEGylation. Investigations probing the maximum tolerated dose (MTD) of polyMPC suggest this material is well-tolerated in animals at very high doses. Future studies will continue to examine the safety of polyMPC

as an injectable scaffold, specifically assessing the immunogenicity of aqueous polyMPC solutions *in vitro* and *in vivo*. These studies are critical for demonstrating the suitability of polyMPC as a PEG replacement. Additional work will look to further expand the polyMPC-Dox platform through the preparation of multi-drug therapeutics which allow for the treatment of tumors using chemotherapeutic cocktails, potentially overcoming challenges related to chemoresistance and augmenting antitumor efficacy.

6.4 New Polymer-Temozolomide Therapeutics

Chapter 5 described the preparation of polyMPC-temozolomide (polyMPC-TMZ) conjugates for the treatment of glioblastoma. A critical discovery resulting from this work was the development of a TMZ-methacrylate monomer which allows, for the first time, TMZ to be directly incorporated into polymer backbones using free radical polymerization chemistries. Optimized polymerization conditions gave polyMPC-TMZ therapeutics with narrow molecular weight distributions, tunable drug loadings, and varying architecture (*i.e.*, random and block copolymers). Moreover, polymerization conditions were developed which preserve the labile chemical structure of pendent TMZ moieties. Conjugation was found to significantly enhance the stability of TMZ at physiological conditions, and the polyMPC-TMZ therapeutics exhibited antitumor activity in chemosensitive and chemoresistant human glioblastoma tumor cells.

TMZ-methacrylate is a versatile monomer which gives access to a range of new polymer-TMZ therapeutics. Future studies aiming to advance the polymer-TMZ therapeutic platform will focus on novel systemic and local modes of TMZ delivery. For injectable medicines, the impact of polymer molecular weight and composition on

antitumor activity will be evaluated. Additionally, syntheses will be developed for generating prodrugs with functionality which can overcome clinical challenges of treating glioblastoma, including blood-brain barrier crossing and chemoresistance. In addition to water-soluble polymer prodrugs, the TMZ-methacrylate monomer allows for the preparation of TMZ-containing networks and wafers, including implantable hydrogels and thermoplastics for local drug delivery following surgical tumor resection.

6.5 References

1. Krumpfer, J. W.; McCarthy, T. J. Rediscovering Silicones: "Unreactive" Silcones React with Inorganic Surfaces. *Langmuir* **2011**, *27*, 11514-11519.

2. Zheng, P.; McCarthy, T. J. A Surprise from 1954: Siloxane Equilibration Is a Simple, Robust, and Obvious Polymer Self-Healing Mechanism. *J. Am. Chem. Soc.* **2012**, *134*, 2024-2027.

3. Hu, G.; Emrick, T. Functional Choline Phosphate Polymers. *J. Am. Chem. Soc.* **2016**, *138*, 1828-1831.

4. Wei, Z.; Yang, J. H.; Zhou, J.; Xu, F.; Zrinyi, M.; Dussault, P. H.; Osada, Y.; Chen, Y. M. Self-Healing Gels Based on Constitutional Dynamic Chemistry and Their Potential Applications. *Chem. Soc. Rev.* **2014**, *43*, 8114-8131.

5. Deng, C. C.; Brooks, W. L. A.; Abboud, K. A.; Sumerlin, B. S. Boronic Acid-Based Hydrogels Undergo Self-Healing at Neutral and Acidic pH. *ACS Macro Lett*. **2015**, *4*, 220-224.

6. Chen X, Parelkar S, Henchey E, Schneider S, Emrick T. PolyMPC-Doxorubicin Prodrugs. *Bioconjugate Chem*. **2012**, *23*, 1753-1763.

7. Page, S. M.; Henchey, E.; Chen, X.; Schneider, S.; Emrick, T. Efficacy of PolyMPC-DOX Prodrugs in 4T1 Tumor-Bearing Mice. *Mol. Pharmaceutics*. **2014**, *11*, 1715-1720.

8. Joralemon, M. J.; McRae, S.; Emrick, T. PEGylated Polymers for Medicine: From Conjugation to Self-Assembled Systems. *Chem. Commun*. **2010**, *46*, 1377-1393.

9. Garay, R. P.; El-Gewely, R.; Armstrong, J. K.; Garratty, G.; Richette, P. Antibodies Against Polyethylene Glycol in Healthy Subjects and in Patients Treated with PEG-Conjugated Agents. *Expert Opin. Drug Deliv.* **2012**, *9*, 1319-1323.

10. Armstrong, J. K.; Hempel, G.; Koling, S.; Chan, L. S.; Fisher, T.; Meiselman, H. J.; Garratty, G. Antibody Against Poly(ethylene glycol) Adversely Affects PEG-Asparginase Therapy in Acute Lymphoblastic Leukemia Patients. *Cancer*. **2007**, *110*, 103-111.

11. Zhang, P.; Sun, F.; Liu, S.; Jiang, S. Anti-PEG Antibodies in the Clinic: Current Issues and Beyond PEGylation. *J. Control. Release*. **2016**, *244*, 184-193.

12. Sundy, J. S.; Baraf, H. S. B.; Yood, R. A.; Edwards, N. L.; Gutierrez-Urena, S. R.; Treadwell, E. L.; Vázquez-Mellado, J.; White, W. B.; Lipsky, P. E.; Horowitz, Z.; Huang, W.; Maroli, A. N.; Waltrip, R. W.; Hamburger, S. A.; Becker, M. A. Efficacy and Tolerability of Pegloticase for the Treatment of Chronic Gout in Patients Refractory to Conventional Treatment: Two Randomized Controlled Trials. *JAMA*. **2011**, *306*, 711-720.

CHAPTER 7

EXPERIMENTAL SECTION

7.1 Materials

2-Methacryloyloxyethyl phosphorylcholine (MPC), [2-(methacryloyloxy)ethyl]dimethyl-(3-sulfopropyl)ammonium hydroxide (SBMA), 1,3-propanedithiol, diisopropylamine, 2,2-dimethoxy-2-phenylacetophenone (DMPA), chlorotrimethylsilane, 1,2,4-trichlorobenzene (TCB), pyrene, sodium trifluoroacetate, calcium hydride, sodium benzophenone, pentane, poly(propylene oxide) (PPO), poly(ethylene oxide) (PEO) (M_n ~ 1,500 g/mol), 2-bromoisobutyryl bromide, triethylamine (TEA), activated carbon, copper(I) bromide (CuBr), 2,2'-bipyridyl (Bipy), 2-(dimethylamino)ethyl methacrylate, potassium fluoride (KF), Pluronic® F127, Pluronic® P123, Pluronic® L121, anhydrous acetonitrile, Irgacure 2959, 2-(4'-hydroxybenzeneazo)benzoic acid (HABA), dithiothreitol (DTT), 4,4'-azobis(4-cyanovaleric acid) (ACVA), and 4-cyano-4-(phenylcarbonothioylthio)pentanoic acid, ethyl α-bromoisobutyrate (EBiB), trifluoroacetic acid, sodium nitrate, anhydrous methanol (MeOH), sodium nitrite, 2-hydroxyethyl methacrylate (HEMA), 4-(dimethylamino)pyridine (DMAP), dimethylsulfoxide (DMSO), and fluorescein *O*-methacrylate were purchased from Sigma-Aldrich. 2,2,2-Trifluoroethanol (TFE), *n*-butyllithium (2.5M in hexanes), and ethylene chlorophosphate were purchased from Alfa Aesar. Chloroform, MeOH, tetrahydrofuran (THF), dichloromethane (DCM), hexanes, anhydrous diethyl ether, sodium sulfate anhydrous, sodium chloride (NaCl), sodium hydroxide (NaOH), acetic acid, high performance liquid chromatography (HPLC) grade acetonitrile, magnesium sulfate, HPLC grade water, ethyl acetate, concentrated sulfuric

acid, dichloromethane (DCM), and hydrochloric acid (HCl) were purchased from Fisher Scientific. 4-Methoxyphenol was purchased from Acros Organic. 4-Trimethylsilyl-3-butyn-2-ol was purchased from GFS Chemicals. Deuterated solvents were purchased from Cambridge Isotope Laboratories, Inc. Tetra-functional PEO thiol (M_n ~ 5,000 g/mol) was obtained from JenKem Technology USA. Doxorubicin hydrochloride (Dox•HCl) was purchased from 21CEC. Sodium azide was purchased from EMD Millipore. Sephadex LH-20 and G-25 size exclusion media were purchased from GE Healthcare and were swollen in appropriate solvent overnight prior to use. Temozolomide (TMZ) and 1-(3-dimethylaminopropyl)-3-ethylcarbodiimide hydrochloride (EDC) were purchased from TCI America. O^6-benzylguanine (O^6-BG) was purchased from Santa Cruz Biotechnology. Deuterated solvents were purchased from Cambridge Isotope Laboratories, Inc., and Sigma-Aldrich. Amicon® Ultra-15 regenerated cellulose centrifugal filters with a nominal molecular weight cutoff of 10,000 Da were purchased from Merck Millipore Ltd. Unless otherwise stated, all chemicals were used as received without further purification. HEMA was purified by short-path vacuum distillation using a Kugelrohr apparatus. Anhydrous THF and TEA were obtained by distillation over sodium/benzophenone and calcium hydride, respectively. D3 and $D3^v$ were obtained from Gelest and purified by vacuum distillation over calcium hydride. Prior to polymerization, inhibitor was removed from MPC following a previously described procedure.[1] Human epithelial ovarian (SKOV-3) adenocarcinoma cells and human glioblastoma (U87MG and T98G) cells were purchased from the American Type Culture Collection (ATCC). Hank's balanced salt solution (HBSS), RPMI-1640 medium, Dulbecco's Modified Eagle Medium (DMEM), fetal bovine serum (FBS), pH 7.4 phosphate-buffered saline (PBS), penicillin, streptomycin, and

antiobiotic-antimycotic solution were purchased from Life Technologies (Gibco). FBS used for culturing glioblastoma cells was purchased from GE Healthcare Life Sciences. NOD SCID mice were purchased from Charles River Laboratories and handled according to the guidelines of the Institutional Animal Care Use Committee. The CellTiter-Glo® luminescent cell viability assay was purchased from Promega. The Lysotracker® Red and 4',6-diamidino-2-phenylindole (DAPI) stains were purchased from ThermoFisher Scientific, respectively. The 35 mm glass dishes used in confocal microscopy experiments were obtained from MatTek Corporation.

7.2 Instrumentation

^{1}H-NMR (500 MHz), ^{13}C-NMR (125 MHz), ^{29}Si-NMR (99 MHz), and ^{31}P-NMR (202 MHz) spectra were obtained using a Bruker Ascend™ 500 spectrometer equipped with a Prodigy cryoprobe. High-resolution mass spectral (HRMS) data were obtained on a Bruker MicrOTOF-II spectrometer. Matrix-assisted laser desorption/ionization time-of-flight (MALDI-TOF) mass spectra were obtained using a Bruker MicroFlex working in linear mode and a HABA matrix. Gel permeation chromatography (GPC) eluting in THF was performed against polystyrene standard, operating at 1.0 mL/min and 40 °C with an Agilent 1260 isocratic pump, an autosampler, a PLgel guard column (50 x 7.8 mm^2), two PLgel Mixed C columns (300 mm x 7.8 mm x 5 μm), one PLgel mixed D column (300 mm x 7.8 mm x 5 μm), and an Agilent 1260 refractive index detector. GPC eluting in TFE containing 0.02 M trifluoroacetate was performed against poly(methyl methacrylate) standards, operating at 40 °C with a flow rate of 1.0 mL/min using an Agilent 1200 system equipped with an isocratic pump, a degasser, an autosampler, one 50 x 8 mm^2 Polymer

Standards Service (PSS) PFG guard column, three 300 x 7.5 mm^2 PSS PFG analytical linear M columns with 7 µm particle size, and Agilent 1200 refractive index and UV detectors. Molecular weight and polydispersity of polymer **25** were estimated by GPC in aqueous buffer (0.1 M sodium nitrate, 0.02 weight percent sodium azide) against poly(ethylene oxide) (PEO) standards, operated at 1.0 ml/min and 40 °C with an Agilent 1260 isocratic pump, a Waters Ultrahydrogel Linear guard column (40 x 6 mm), three Waters Ultrahydrogel Linear columns (300 x 7.8 mm), and an Agilent 1260 refractive index detector. HPLC was performed using a Waters Alliance system eluting with 40/60 acetonitrile/water containing 1% trifluoroacetic acid, operated at 1.0 ml/min and 25 °C, with a Microsorb C18 column (250 x 4.6 mm), and Waters photodiode array (λ=480 nm) and fluorescence ($\lambda_{excitation}$=480 nm, $\lambda_{emission}$=580 nm) detectors. Fluorescence spectra were recorded on a Perkin-Elmer LS55 fluorescence spectrometer. UV-Vis absorption spectra were collected using PerkinElmer Lambda 25 and Shimadzu UV-2600 spectrometers. Dynamic light scattering (DLS) was performed using a Malvern Zetasizer NanoZS. Pendant drop interfacial tension (IFT) measurements were performed on a Marlin F131B IRF camera (Allied Vision Technologies) interfaced with MATLAB. Transmission electron microscopy (TEM) was performed on a JEOL JEM-2000FX microscope using samples prepared on PELCO® carbon-coated 300 mesh copper grids (Ted Pella, Inc.) or 400 square mesh carbon-coated copper grids (Electron Microscopy Sciences). Cryogenc-TEM (cryo-TEM) was performed on an FEI-Tecnai-T12 microscope equipped with a cryo-transfer holder using samples prepared on carbon-coated 400 mesh copper grids and vitrified in liquid ethane. Vitrification of cryo-TEM samples was performed using an FEI Vitrobot™. Lower critical solution temperature (LCST) measurements were performed

using a Hitachi U-3010 spectrophotometer operating at $\lambda = 550$ nm and equipped with a *t*2 temperature-controlled cuvette holder and a TC-1 temperature controller (Quantum Northwest). TMZ solution stability experiments were performed using a Shimadzu UV-2600 spectrometer equipped with a Quantum Northwest dual temperature-controlled cuvette holder and a TC-1 temperature controller. Surface tensiometry was performed using a Kibron MicrotroughX Langmuir instruments equipped with a Kibron DyneProbe (diameter = 0.51 mm) and custom cylindrical glass troughs (diameter = 1.5 cm, depth = 0.2 cm). Thiol-ene and thiol-yne reactions were performed in a UV box (model CL-1000L, UVP). Rheology was performed using a Malvern Kinexus Pro stress-controlled rheometer with a gap resolution of 0.1 µm, an environmental control range and resolution of -40-200 °C and 0.01 °C, respectively, a torque range in oscillatory mode of 0.05-200 µN·m with 0.1 nN·m resolution, and a frequency range of 6.28-942 rad/s. Fluorescence confocal micrographs were obtained using a Nikon A1 Resonant Scanning Confocal with Structured Illumination microscope equipped with a 60x objective lens. Flow cytometry experiments were performed using a BD DUAL LSRFortessa flow cytometer, and data was analyzed using FlowJo software (Flowjo, LLC). Viability measurements of glioblastoma cells treated with polyMPC-TMZ copolymers were performed using a FLUOstar OPTIMA plate reader (BMG LABTECH), and IC_{50} values were calculated using GraphPad Prism 7 software (GraphPad Software, Inc.).

7.3 Methods

- **Synthesis of poly(vinylmethylsiloxane) (PVMS) (P1)**

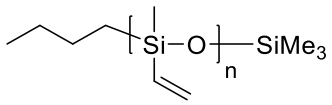

$D3^{v}$ (5.00 mL, 18.7 mmol) was dissolved in anhydrous THF (19 mL) in a flame-dried Schlenk flask charged with a stir bar. Polymerization was initiated by addition of 2.5 M *n*-butyllithium in hexanes (0.19 mL, 0.48 mmol), and the mixture was stirred under nitrogen at room temperature for 30 minutes. The polymerization was quenched with chlorotrimethylsilane (0.18 mL, 1.4 mmol). After stirring for an additional 10 minutes, the solution was transferred to a 1:1 mixture of pentane and water. The organic layer was isolated, and the aqueous layer was washed with an additional portion of pentane. The organic portions were combined, washed twice with water, and dried over sodium sulfate. Pentane was removed by rotary evaporation, and the residue was dialyzed against THF (or DMC) to remove monomer. The dialyzed polymer solution was passed through a 0.45 µm PTFE membrane, and solvent removed by rotary evaporation. The product was dried under high vacuum, and polymer **1** was isolated as a clear, viscous oil. Number-average degree of polymerization (X_n) and molecular weight (M_n) were determined by comparing the relative ^{1}H-NMR signal intensities of the pendent vinyl protons (5.73-6.06 ppm) and the terminal methyl protons (0.89 ppm). Yield: 75%. ^{1}H-NMR (500 MHz, $CDCl_3$, δ, ppm): -0.03-0.30 (m), 0.62 (t, 2H), 0.89 (t, 3H), 1.25-1.37 (m, 4H), 5.63-6.15 (m). ^{29}Si-NMR (99 MHz, $CDCl_3$, δ, ppm): -34.97 (s). $M_{n,\,NMR}$ = 7,500 g/mol, $M_{n,\,GPC}$ = 8,400 g/mol, PDI = 1.07.

- **General Procedure for the synthesis of poly(dimethylsiloxane)-*b*-PVMS (PDMS-*b*-PVMS) copolymers (P2-P4)**

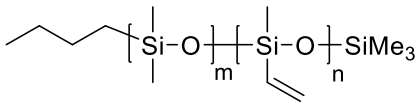

Block copolymers **P2-P4** were synthesized by a modified literature procedure.[2] D3 (2.33 g, 10.5 mmol) was distilled over calcium hydride under vacuum into an oven dried Schlenk flask charged with a stir bar, then dissolved in anhydrous THF (9.5 mL) under inert nitrogen. The polymerization was initiated by addition of a solution of 2.5 M *n*-butyllithium in hexanes (0.20 mL, 0.5 mmol) and the mixture was stirred at room temperature for 2 hour under nitrogen. $D3^{v}$ (2.80 mL, 10.5 mmol) was then added to the flask through a dry syringe and needle, and the reaction mixture was stirred under nitrogen at room temperature for 2 hours. The polymerization was quenched by the addition of chlorotrimethylsilane (0.19 mL, 1.5 mmol), and polymers **P2-P4** were isolated as clear, viscous oils in similar fashion to polymer **P1**. X_n of each block was determined by comparing the ^{1}H-NMR signal intensities at -0.06-0.10 ppm (Si—$(CH_3)_2$) (PDMS block) and 5.73-6.06 ppm (Si—$CH{=}CH_2$) (PVMS block) to that of the terminal methyl protons (0.89 ppm). Typical isolated yields were 70-80%. ^{1}H-NMR (500 MHz, $CDCl_3$, δ, ppm): -0.06-0.10 (m), 0.0-0.28 (m), 0.54 (t, 2H), 0.89 (t, 3H), 1.25-1.37 (m, 4H), 5.73-6.06 (m). ^{29}Si-NMR (99 MHz, $CDCl_3$, δ, ppm): -21.81 (s), -34.64 (s).

- **Synthesis of PC-thiol (PC-SH)**

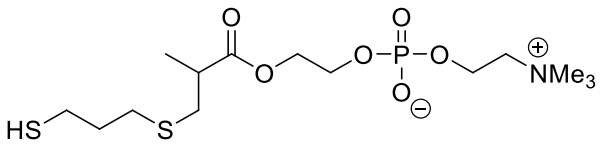

Compound **PC-SH** was synthesized following a modified literature procedure.[3] Chloroform (60 mL) was degassed with nitrogen in a flame-dried RB flask charged with a stir bar. MPC (10.0 g, 33.9 mmol) and 1,3-propanedithiol (5.10 mL, 50.9 mmol) were added to the chloroform to give a cloudy suspension. Diisopropylamine (0.20 mL, 1.4 mmol) was added, and the mixture was stirred under nitrogen for 24 hours at room temperature, noting that the solution gradually became clear and colorless. Solvent was removed by rotary evaporation, and **PC-SH** was isolated by precipitation into THF. The precipitate was triturated extensively against THF to removed unreacted dithiol, and **PC-SH** was isolated by centrifugation and dried under high vacuum to afford a white, tacky solid in 84% yield. ^{1}H-NMR (500 MHz, MeOD-d$_4$, δ, ppm): 1.24 (dd, J = 7.1, 1.1 Hz, 3H), 1.85 (m, 2H), 2.56-2.87 (m, 6H), 3.24 (s, 9H), 3.65 (q, J = 4-5 Hz, 2H), 4.08 (m, 2H), 4.29 (m, 4H). ^{13}C-NMR (125 MHz, MeOD-d$_4$, δ, ppm): 17.38, 23.87, 30.53, 31.70, 32.12, 34.76, 36.28, 41.74, 54.89, 60.57, 64.82, 65.44, 67.62, 176.86. ^{31}P-NMR (202 MHz, MeOD-d$_4$, δ, ppm): -0.42. HRMS-ESI (m/z): $[M+H]^+$ calculated for $C_{14}H_{30}NO_6PS_2$: 404.133, found: 404.131.

- **Synthesis of SB-thiol (SB-SH)**

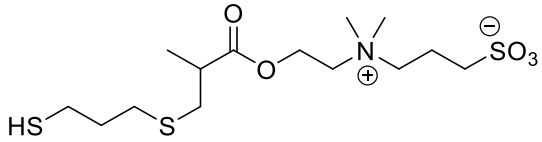

To a flame-dried RB flask charged with a stir bar was added SBMA (20.0 g, 71.6 mmol), 1,3-propanedithiol (14.40 mL, 143.2 mmol), and degassed MeOH (100 mL). To this clear solution catalytic diisopropylamine (0.40 mL, 2.9 mmol) was added, and the solution was stirred under nitrogen at room temperature for 24 hours. The mixture was concentrated by rotary evaporation, and the product precipitated into THF. The precipitate was triturated with THF, isolated by vacuum filtration, and washed with diethyl ether. The solid was dried under high vacuum, and **SB-SH** was isolated as a fine white powder in 67% yield. ^{1}H-NMR (500 MHz, MeOD-d_4, δ, ppm): 1.27 (d, J = 6.5 Hz, 3H), 1.85 (m, 2H), 2.24 (m, 2H), 2.58-2.72 (m, 4H), 2.78-2.91 (m, 4H), 3.18 (s, 6H), 3.61 (m, 4H), 3.75 (m, 2H), 4.58 (br, 2H). ^{13}C-NMR (125 MHz, MeOD-d_4, δ, ppm): 17.19, 20.16, 23.87, 31.74, 34.74, 36.20, 41.54, 52.14, 52.50, 56.96, 59.11, 64.14, 65.35, 66.74, 175.93. HRMS-ESI (m/z): $[M+H]^+$ calculated for $C_{14}H_{29}NO_5S_3$: 388.128, found: 388.131.

- **General procedure for the synthesis of zwitterionic polysiloxanes (P7-P14)**

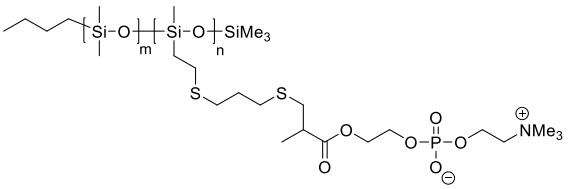

P7-P10

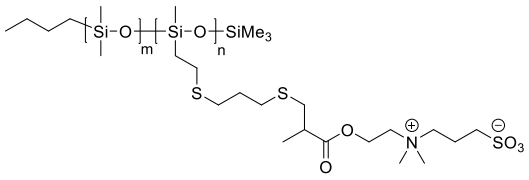

P11-P14

Polysiloxanes **P1-P4** were dissolved in THF in a glass scintillation vial charged with a stir bar. Thiols **PC-SH** and **SB-SH** (3 molar equivalents relative vinylsiloxane groups) were dissolved in MeOH and TFE, respectively. The desired thiol solution was added to the scintillation vial to afford a clear, colorless mixture. DMPA (0.3 molar equivalents relative to vinylsiloxane) was added to the vial as a solid. The mixture was degassed nitrogen for 15 minutes, then stirred and subjected to 365 nm light (~3.5 mW/cm^2) in a UV box for 1 hour at room temperature. The PC-substituted polysiloxanes (**P7-P10**) were purified by dialysis against MeOH and water, and isolated by lyophilization as fluffy, white solids. Typical yields were 85-90%. **P7**: ^{1}H-NMR (500 MHz, MeOD-d$_4$, δ, ppm): 0.24 (br, 3H), 0.97 (br, 2H), 1.27 (br, 3H), 1.88 (br, 2H), 2.48-2.90 (m, 9H), 3.26 (s, 9H), 3.68 (br, 2H), 4.08 (br, 2H), 4.17-4.38 (br, 4H). ^{31}P-NMR (202 MHz, MeOD-d$_4$, δ, ppm): -0.46. SB-containing polysiloxanes (**P11-P14**) were isolated by precipitation: THF was removed from the crude reaction mixture by rotary evaporation, and the polymer solution was precipitated into MeOH (repeated three times). The polymers were isolated by centrifugation and dried under high vacuum to afford off-white solids in 35-45% yield. **P11**: ^{1}H-NMR (500 MHz, TFE-d$_3$, δ, ppm): 0.06 (br, 3H), 0.82 (br, 2H), 1.14 (br, 3H), 1.73 (br, 2H), 2.11 (br, 2H), 2.32-2.89 (m, 11H), 3.00 (s, 6H), 3.40 (br, 2H), 3.51 (br, 2H), 4.41 (br, 2H).

- **Synthesis of the PPO macroinitiator (P15)**

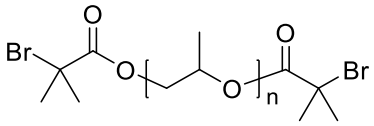

PPO macrointiator **P15** was synthesized using a modified literature procedure.[4] In a flame-dried round-bottom flask charged with a stir bar, PPO (24.12 g, 6.0 mmol) and anhydrous TEA (3.3 mL, 24.0 mmol) were dissolved in anhydrous THF (50 mL). The solution was cooled at 0 °C, and 2-bromoisobutyryl bromide (3.0 mL, 24.0 mmol) was added slowly using a syringe, resulting in the formation of a white precipitate. The suspension was allowed to warm to room temperature and stir under nitrogen for 48 hours, after which time the mixture was vacuum filtered. The precipitate was washed with diethyl ether (3 x 25 mL), and the filtrate was concentrated by rotary evaporation. The crude product mixture was dissolved in ethyl acetate (1500 mL) and washed with aqueous 1 M NaOH (5 x 100 mL) and saturated brine (2 x 100 mL). The organic layer was stirred over decolorizing carbon, filtered, concentrated by rotary evaporation, and dried under high vacuum to afford **P15** as an orange viscous oil in 73% yield. ^{1}H-NMR (500 MHz, MeOD-d_4, δ, ppm): 1.04-1.21 (br), 1.25 (t), 1.92 (s), 3.33-3.70 (m). ^{13}C-NMR (125 MHz, MeOD-d_4, δ, ppm): 17.75, 31.19, 31.22, 57.33, 57.36, 73.99, 74.01, 74.07, 74.09, 74.34, 74.38, 76.46, 76.60, 76.62, 76.73, 172.25, 172.26.

- **General procedure for the synthesis of PC-zwitteronics (P16-P20)**

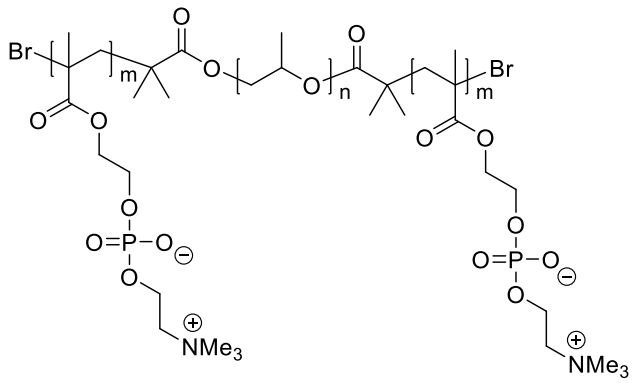

In a two-neck round-bottom flask charged with a stir bar, **P15** and MPC were dissolved in TFE ([monomer] = 0.5 M). The solution was cooled at 0 °C and degassed with bubbling nitrogen for 15 minutes, after which CuBr and Bipy were added under positive nitrogen pressure at $[\mathbf{P15}]_0$:$[CuBr]_0$:$[Bipy]_0$ = 1:2:4. The resulting mixture was degassed with nitrogen for 10 minutes and then was stirred at room temperature. Polymerization progress was monitored using ^{1}H-NMR spectroscopy. The polymerization was quenched by exposure to ambient atmosphere, and copper was removed by passing the crude polymer product through a silica gel plug eluting with MeOH. The polymer effluent was concentrated by rotary evaporation, centrifuged (10,000 rpm, 5 minutes), passed through a 0.45 μm PTFE membrane, and dialyzed against water. Lyophilization gave PC-zwitteronics **P16**-**P20** in yields of 42-78%. ^{1}H-NMR (500 MHz, MeOD-d_4, δ, ppm): 0.72-1.04 (br), 1.04-1.26 (s), 1.71-2.16 (m), 3.32 (s), 3.41-3.50 (br), 3.50-3.56 (br), 3.56-3.67 (br), 3.68-3.83 (br), 4.01-4.15 (br), 4.15-4.30 (br), 4.30-4.41 (br). ^{31}P-NMR (202 MHz, MeOD-d_4, δ, ppm): -0.51 ppm.

- **Synthesis of alkyne-substituted choline phosphate methacrylate (MCP) (1)**

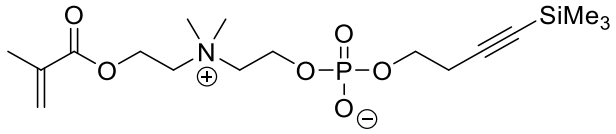

Alkyne-substituted MCP **1** was prepared following a previously described procedure.[5]

- **Synthesis polyMPC by reversible addition-fragmentation chain-transfer polymerization (RAFT) (P21)**

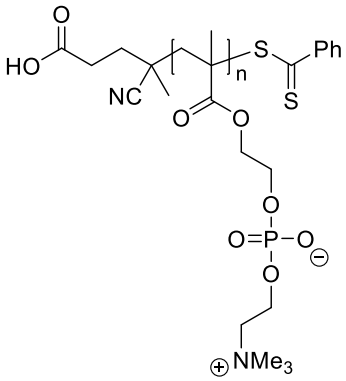

In a 20 mL glass vial charged with a stir bar, MPC (1.2034 g, 4.1 mmol), 4-cyano-4-(phenylcarbonothioylthio)pentanoic acid (8.7 mg, 0.031 mmol), and ACVA (2.1 mg, 0.0075 mmol) were dissolved in MeOH (3 mL). The resulting solution was degassed with bubbling nitrogen for 15 minutes and was heated at 70 °C. At a monomer conversion of 87%, estimated using ^{1}H-NMR spectroscopy, the polymerization was quenched by exposure to air, and the solution was precipitated in THF (35 mL). The crude polymer product was isolated by centrifugation (4000 rpm, 5 min) and was purified by dialysis against water. Lyophilization afforded polyMPC as a pink solid in a yield of 74%. ^{1}H-NMR (500 MHz, MeOD-d_4, δ, ppm): 0.66-1.34 (m, 3H), 1.65-2.20 (m, 2H), 3.26-3.36 (s,

9H), 3.64-3.78 (br, 2H), 3.96-4.12 (br, 2H), 4.12-4.26 (br, 2H), 4.26-4.38 (br, 2H). $M_{n,\,GPC}$ = 38,500 g/mol, PDI = 1.08.

- **Synthesis of functional zwitteronics (P22, P23)**

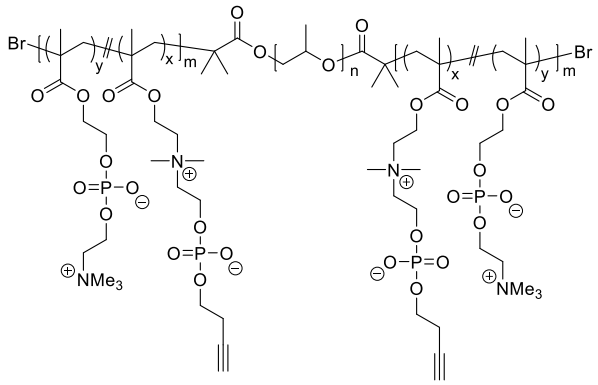

TMS-protected functional block copolymers **P22** and **P23** were prepared by macroinitiated-ATRP of MPC and monomer **1** using a similar procedure as polymers **P16**-**P20**. TMS-protected **P22** and **P23** were isolated in yields of 57%. TMS-protected **P23**: ^{1}H-NMR (500 MHz, MeOD-d$_4$, δ, ppm): 0.14 (s), 0.88-1.04 (br), 1.04-1.25 (br), 1.80-2.14 (br), 1.92 (s), 2.55-2.68 (br), 3.31 (s), 3.34-3.43 (br), 3.43-3.50 (br), 3.50-3.57 (br), 3.57-3.66 (br), 3.67-3.79 (br), 3.81-3.90 (br), 3.90-4.03 (br), 4.03-4.15 (br), 4.15-4.29 (br), 4.29-4.41 (br), 4.42-4.62 (br). ^{13}C-NMR (125 MHz, MeOD-d$_4$, δ, ppm): 0.23, 17.69, 22.96, 31.17, 46.09, 53.17, 54.80, 60.63, 64.32, 65.02, 67.42, 74.40, 76.66, 76.68, 76.79, 86.58, 104.42, 178.21, 179.10. ^{31}P-NMR (202 MHz, MeOD-d$_4$, δ, ppm): -0.50, -0.71. TMS-alkyne groups were removed by dissolving polymers **P22** and **P23** in solutions of MeOH containing 0.5 M KF (4 molar equivalents KF relative to TMS-alkyne groups). The solutions were stirred at 35 °C for 24 hours and then purified by dialysis against water. Lyophilization gave **P22** and **P23** as white solids in yields of 84 and 82%, respectively.

P23: ^{1}H-NMR (500 MHz, MeOD-d_4, δ, ppm): 0.78-1.03 (br), 1.03-1.26 (br), 1.82-2.16 (br), 1.93 (s), 2.39-2.52 (br), 2.52-2.64 (br), 3.32 (s), 3.35-3.43 (br), 3.43-3.51 (br), 3.51-3.58 (br), 3.58-3.68 (br). 3.68-3.82 (br), 3.82-3.91 (br), 3.91-4.04 (br), 4.04-4.16 (br), 4.16-4.28 (br), 4.28-4.45 (br), 4.47-4.64 (br). ^{13}C-NMR (125 MHz, MeOD-d_4, δ, ppm): 17.60, 21.52, 31.06, 45.92, 46.29, 54.65, 60.46, 64.15, 64.85, 64.89, 66.04, 67.29, 76.38, 76.51, 76.54, 76.64, 82.17, 178.07, 178.94. ^{31}P-NMR (202 MHz, MeOD-d_4, δ, ppm): -0.50, -0.72.

- **Crosslinking of P22 and P23 nanoparticles**

Shell-crosslinked nanoparticles were prepared from functional zwitteronics **P22** and **P23** by thiol-yne coupling. In 2 mL glass vials, aqueous suspensions containing Irgacure 2959, DTT, and alkyne-functionalized **P22** or **P23** were prepared at polymer concentration of 50 or 100 mg/mL with $[\text{Irgacure 2959}]_0$:$[\text{alkyne}]_0$:$[\text{thiol}]_0$ = 0.1:1:2. The suspensions were degassed with bubbling nitrogen for 10 minutes and then irradiated at 365 nm (~3.5 mW/cm^2) in a UV box for 1 hour.

- **Preparation of nanoparticle-crosslinked hydrogels from P22 and P23**

Nanoparticle-crosslinked hydrogels were prepared from alkyne-containing zwitteronics by UV-initiated thiol-yne crosslinking. Functional **P22** or **P23** were suspended in water at concentrations of 25, 50, or 100 mg/mL. Tetrafunctional PEO thiol and Irgacure 2959 were added at $[\text{Irgacure 2959}]_0$:$[\text{alkyne}]_0$:$[\text{thiol}]_0$ = 0.1:1:1, and the suspensions were degassed with bubbling nitrogen for 10 minutes in 7 mL glass vials. The degassed suspensions were irradiated at 365 nm (~3.5 mW/cm^2) in a UV box for 1 hour.

- **Rheology of nanoparticle-crosslinked hydrogels prepared from P22 and P23**

Rheological characterization of functional zwitteronic nanoparticle-crosslinked hydrogels previously swelled in water for 18-24 hours and a Pluronic F127 thermogel was performed using a Malvern Kinexus stress-controlled rheometer operated in strain-controlled oscillatory mode. A 20 mm diameter stainless steel parallel plate fixture equipped with a solvent trap was utilized for rheological characterization of the Pluronic F127 thermogel. Rheology of the 50 mg/mL **P22** hydrogel was performed using a 50 mm 2° cone-and-plate fixture. **P23** hydrogels and the 100 mg/mL **P22** hydrogel were characterized using an 8 mm diameter stainless steel parallel plate. For all gels, rheology was performed at 37°C, employing a frequency range of 1-100 rad/s. The strain amplitude used in the measurements was 0.1-1%, an amplitude range confirmed to be in the linear viscoelasticity region for all hydrogels using strain-sweep experiments; all frequency sweep measurements were thus performed under small amplitude oscillatory shear (SAOS).

For the Pluronic F127 thermogel, the 20 mm parallel plate fixture was mounted to the rheometer and allowed to equilibrate at 37°C. The gap was zeroed and then set to a value of 70 mm for sample loading. The Pluronic thermogel, previously prepared by heating a 200 mg/mL solution of Pluronic F127 in water at 37 °C, was transferred to the bottom plate of the rheometer using a stainless-steel spatula and taking care to prevent air bubble formation. The reservoir around the plate was filled with Milli-Q water. This reservoir does not contact the sample but is enclosed with the sample under the solvent trap. The top plate was then lowered to a gap of 0.81 mm, and the sample was trimmed using a nylon edge and a razor blade. Once the sample was trimmed, the gap was lowered

to 0.80 mm and the solvent trap was put into place. A similar procedure was used for the 50 mg/mL **P22** hydrogel, employing trimming and working gaps of 0.077 and 0.07 mm, respectively. The system was then allowed to equilibrate at 37°C for approximately 5 minutes before commencing rheological characterization. For the 100 mg/mL **P22** hydrogel and the **P23** hydrogels, the 8 mm parallel plate fixture was mounted to the rheometer and allowed to equilibrate at 37°C. The gap was zeroed and then set to a value of 70 mm for sample loading. After loading gels on the plate, the gap was adjusted gradually until the top plate made contact with the sample. The top plate was lowered in 0.1 mm increments until a normal force of 0.2-0.4 N was achieved; this protocol ensured that the top plate made homogenous contact with each hydrogel. Two frequency sweeps were performed in series for each gel.

- **Synthesis of polyMPC by atom transfer radical polymerization (P24)**

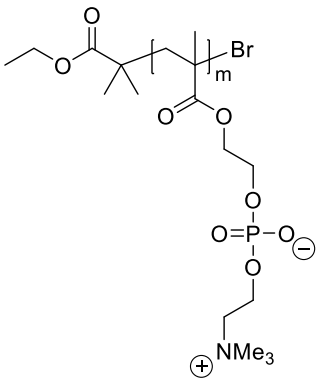

PolyMPC **P24** was prepared following a modified literature procedure.[7] MPC (3.01 g, 10.2 mmol) and EBiB (13.2 μL, 0.09 mmol) were dissolved in MeOH (6 mL) in a 2-neck, 25 mL RB flask charged with a stir bar and the solution was degassed with nitrogen. CuBr (13.2 mg, 0.09 mmol) and Bipy (28.0 mg, 0.18 mmol) were then added to the reaction vessel. The resulting mixture was degassed with nitrogen and then was stirred at room

temperature for 16 hours. The polymerization was quenched by exposure to ambient atmosphere, and residual copper was removed by the passing the solution through a plug of silica eluting with MeOH. Polymer effluent was concentrated by rotary evaporation, and polymer was precipitated in THF. Isolated polymer was dialyzed against water and lyophilized to give **P24** as a white, granular solid in typical yields of 66-75%. ^{1}H-NMR (500 MHz, MeOD-d_4, δ, ppm): 0.64−1.15 (br, 3H), 1.67−2.13 (br, 2H), 3.27 (s, 9H), 3.71 (br, 2H), 4.04 (br, 2H), 4.19 (br, 2H), 4.29 (br, 2H).

- **Synthesis of poly(MPC-*co*-hydrazine) (P25)**

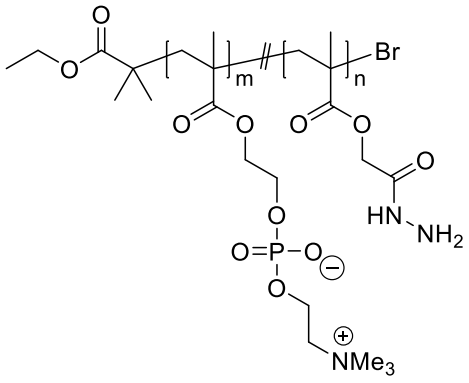

Poly(MPC-*co*-hydrazine) random copolymer (**P25**) was synthesized as described previously and isolated in typical yields greater than 80%.[8] Hydrazine content was estimated to be 22 mole percent using ^{1}H-NMR spectroscopy by comparing signal intensities at 3.72 ppm (—C*H*$_2$—N) (MPC) and 4.51 ppm (—C*H*$_2$—CONHNH$_2$). ^{1}H-NMR (500 MHz, MeOD-d_4, δ, ppm): 0.70-1.20 (br, 3H), 1.70-2.30 (br, 2H), 3.28 (s, 9H), 3.72 (br, 2H), 4.05 (br, 2H), 4.19 (br, 2H), 4.31 (br, 2H), 4.51 (br, 2H). $M_{n,\,GPC}$ = 25,000 g/mole, PDI = 1.44.

- **Synthesis of polyMPC-Dox prodrug (P26)**

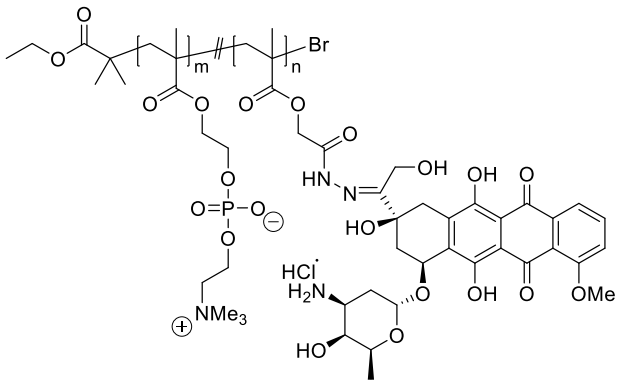

PolyMPC-Dox (**P26**) was synthesized and purified as described previously.[7,8] In an oven-dried 25 ml RB flask charged with a stir bar, **P25** (201.6 mg) and magnesium sulfate (204.6 mg) were suspended in anhydrous MeOH (5 ml). The suspension was acidified with glacial acetic acid (60 μL) and then Dox•HCl (58.1 mg) was added. The reaction vessel was sealed, and the red suspension was stirred under nitrogen, protected from the light, for 72 hours. The reaction mixture was passed through a column of Sephadex LH-20 size-exclusion media eluting with MeOH to separate the conjugate from unreacted Dox•HCl. The conjugate fraction was collected and concentrated by rotary evaporation. Conjugate residue was then dissolved in minimal water (2-3 mL) and passed through a Sephadex G-25 size-exclusion column eluting with pure water. Prodrug fractions were combined and lyophilized to give **P26** as a fluffy, red solid in yields over 84%.

- **Synthesis of TMZ-carboxylic acid (TMZ-COOH)**

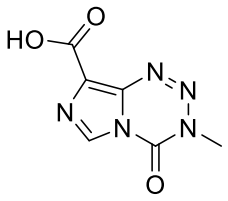

TMZ-carboxylic acid (**TMZ-COOH**) was prepared following a previously described procedure.[10] In a round-bottom flask charged with a stir bar and fitted with an addition funnel, TMZ (2.29 g, 11.8 mmol) was dissolved in concentrated sulfuric acid (23.6 mL), and the resulting yellow solution was cooled to 0 °C under nitrogen atmosphere. A solution of sodium nitrite (2.51 g, 36.4 mmol) in water (23.6 mL) was added dropwise over 45 minutes, noting the evolution of a brown gas during the addition. The mixture was allowed to warm to room temperature while protected from light. After stirring for 17 hours, the mixture was cooled to 0 °C and quenched with ice (61 g). Further stirring at 0 °C resulted in precipitation of a fine white solid, which was isolated by vacuum filtration, washed with cold water, and dried under vacuum to yield **TMZ-COOH** in 75% yield. ^{1}H-NMR (500 MHz, DMSO-d_6, δ, ppm): 3.88 (s, 3H), 8.82 (s, 1H), 13.33 (br, 1H). ^{13}C-NMR (125 MHz, DMSO-d_6, δ, ppm): 36.32, 127.78, 129.09, 136.48, 139.10, 161.85. HRMS-EI (*m*/*z*): $[M]^+$ calculated for $C_6H_5N_5O_3$: 195.0392, found: 195.0395.

- **Synthesis of TMZ-methacrylate (TMZ-MA)**

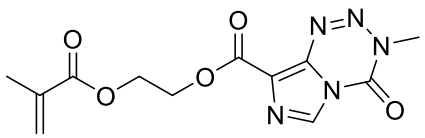

In a round-bottom flask charged with a stir bar, **TMZ-COOH** (592.5 mg, 3.05 mmol) was suspended in DCM (20 mL). HEMA (353 μL, 2.91 mmol) and catalytic DMAP (36.0 mg,

0.29 mmol) were added to the suspension, followed by EDC (674 mg, 3.51 mmol); the mixture became homogeneous and red. After stirring under nitrogen at room temperature for 14 hours, the mixture was filtered, and the filtrate was diluted with DCM (30 mL) and washed with aqueous 0.1 M HCl (5 × 50 mL). The organic layer was dried over sodium sulfate and concentrated by rotary evaporation. The resulting white solid was dried under high vacuum, protected from light, to yield **TMZ-MA** in 71% yield. ^{1}H-NMR (500 MHz, DMSO-d_6, δ, ppm): 1.87 (s, 3H), 3.88 (s, 3H), 4.43 (t, J = 5Hz, 2H), 4.62 (t, J = 5Hz, 2H), 5.68 (s, 1H), 6.04 (s, 1H), 8.85 (s, 1H). ^{13}C (125 MH, DMSO-d_6, δ, ppm): 17.93, 36.40, 62.49, 62.51, 126.15, 126.20, 129.41, 135.60, 136.87, 138.93, 160.29, 166.41. HRMS-FAB (m/z): $[M+H]^+$ calculated for $C_{12}H_{14}N_5O_5$: 308.0995, found: 308.0989.

- **General procedure for the synthesis of polyMPC-TMZ random copolymers (P27-P30)**

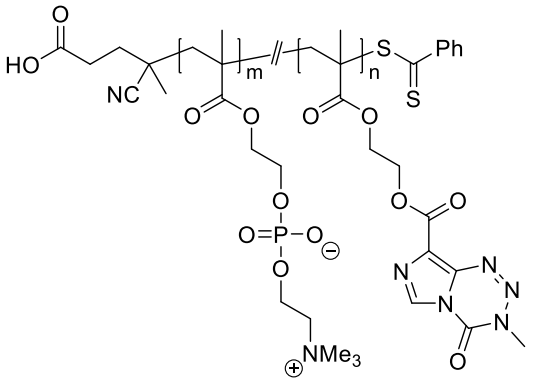

MPC and **TMZ-MA** were dissolved in TFE at a total monomer concentration of 1 M in a 20 mL vial charged with a stir bar. ACVA and 4-cyano-4-(phenylcarbonothioylthio)pentanoic acid were added as radical initiator (I) and chain-transfer agent (CTA), respectively, targeting $[monomer]_0$:$[CTA]_0$:$[I]_0$ of 102:1:0.2. The mixture was purged with nitrogen gas at 0 °C for 15 minutes, then stirred at 70 °C to initiate polymerization, judging monomer conversion by ^{1}H-NMR spectroscopy. At monomer

conversion >85%, the mixture was allowed to cool to room temperature then was quenched by exposure to air. The crude reaction mixture was precipitated from TFE into THF (this was repeated three times) to remove unreacted monomer, and the polymer was isolated by centrifugation. The isolated polymer was dissolved in aqueous 0.1 M HCl (10 mL), added to a centrifugal filter with a nominal molecular weight cutoff of 10 kDa, and centrifuged (4000 x g, 45 minutes, room temperature). The filtrate was discarded and centrifugal dialysis was repeated twice. The concentrated polymer was dissolved in aqueous 0.1 M HCl and lyophilization afforded polymers **P27**-**P30** as pink solids. Incorporation of **TMZ-MA** into the copolymer structure was estimated by ^{1}H-NMR spectroscopy by comparing relative signal intensities at 8.53 ppm (C—*H* in TMZ) and 2.86-3.29 ppm (N—(C*H*$_3$)$_3$ in MPC). Copolymer yields were 60-74%. ^{1}H-NMR (500 MHz, TFE-d$_3$, δ, ppm): 0.12-1.14 (br, 3H), 1.24-2.10 (br, 2H), 2.86-3.29 ppm (s, 9H), 3.60 (br, 2H), 3.92 (s, 3H), 4.01-4.26 (br, 4H), 4.39 (br, 2H), 4.48-4.76 (br, 4H), 8.53 (s, 1H). ^{13}C-NMR (125 MHz, TFE-d$_3$, δ, ppm): 18.48, 20.22, 38.22, 46.59, 47.05, 55.94, 62.60, 64.46, 65.02, 65.91, 66.97, 68.04, 128.44, 131.28, 138.79, 140.81, 162.60, 180.03. ^{31}P-NMR (202 MHz, TFE-d$_3$, δ, ppm): -2.36.

- **General procedure for the synthesis of a polyMPC macro-chain-transfer agent (macro-CTA) by RAFT (P31)**

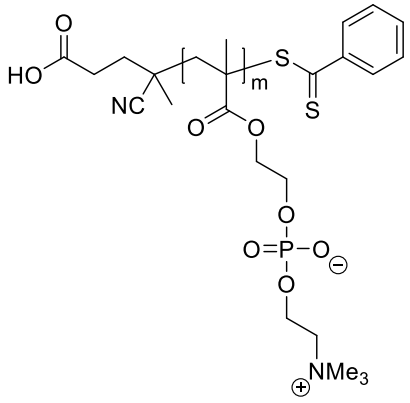

In a 20 mL vial charged with a stir bar, MPC (3.9038 g, 13.2 mmol), 4-cyano-4-(phenylcarbonothioylthio)pentanoic acid (74.3 mg, 0.27 mmol), and ACVA (15.6 mg, 0.056 mmol) were dissolved in MeOH (13.2 mL). The solution was degassed with bubbling nitrogen at 0 °C for approximately 20 minutes, and then was heated at 70 °C to initiate polymerization. Upon achieving a monomer conversion <80%, as estimated by ^{1}H-NMR spectroscopy, the polymerization was terminated by exposure to air, and the solution was precipitated in THF. The crude polymer was isolated by centrifugation (2000 rpm) and was dialyzed against water. Lyophilization afforded **P31** as a pink solid in yields >80%. M_n of the polyMPC macro-CTA was estimated using ^{1}H-NMR spectroscopy by comparing signal intensities at 3.66-3.82 ppm (CH_2—N) (PC methylene protons) to that of the terminal phenyl protons (7.40-7.96 ppm). ^{1}H-NMR (500 MHz, MeOD-d_4, δ, ppm): 0.73-1.22 (br, 3H), 1.68-2.17 (br, 2H), 3.23-3.38 (s, 9H), 3.66-3.82 (br, 2H), 4.00-4.15 (br, 2H), 4.15-4.29 (br, 2H), 4.29-4.41 (br, 2H), 7.40-7.95. ^{31}P-NMR (202 MHz, MeOD-d_4, δ, ppm): -0.45. $M_{n,\ NMR}$ = 15,100-19,800 g/mol, $M_{n,\ TFE\ GPC}$ = 20,900-21,900 g/mol, PDI = 1.05-1.13.

- **General procedure for the synthesis of polyMPC-TMZ block copolymers (P32-P34)**

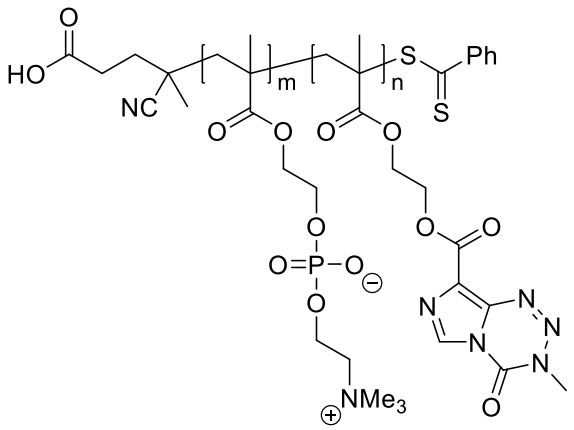

In a 7 mL vial charged with a stir bar, polyMPC macro-CTA **P31**, **TMZ-MA**, and ACVA were dissolved in TFE ([**TMZ-MA**] = 0.25 M), targeting $[ACVA]_0$:$[\mathbf{P31}]_0$: = 0.2:1 and $[\mathbf{TMZ\text{-}MA}]_0$:$[\mathbf{P31}]_0$ ranging from 17 to 37. The mixture was purged with nitrogen gas at 0 °C for 15 minutes, then stirred at 70 °C to initiate polymerization, judging monomer conversion by ^{1}H-NMR spectroscopy. At monomer conversion >90%, as judged using ^{1}H-NMR spectroscopy, the mixture was quenched in liquid nitrogen and was exposed to air. The crude reaction mixture was precipitated three times from TFE into THF, and the polymer was isolated by centrifugation. The isolated polymer was dissolved in aqueous 0.1 M HCl (10 mL), added to a centrifugal dialysis filter with a nominal molecular weight cutoff of 10 kDa, and centrifuged (4000 x g, 30 minutes, room temperature). The filtrate was discarded and centrifugal dialysis was repeated twice. The concentrated polymer was dissolved in aqueous 0.1 M HCl and lyophilization afforded polymers **P32**-**P34** as pink solids in yields >50%. Incorporation of **TMZ-MA** into the copolymer structure was estimated by ^{1}H-NMR spectroscopy by comparing relative signal intensities at 8.72 ppm (C—*H* in TMZ) and 2.78-3.22 ppm (N—(C*H*$_3$)$_3$ in MPC). ^{1}H-NMR (500 MHz, TFE-d$_3$, δ, ppm): 0.00-1.07 (br, 6H), 1.25-2.13 (br, 4H), 2.78-3.22 ppm (s, 9H), 3.53 (br, 2H), 3.88

(s, 3H), 3.93-4.26 (br, 4H), 4.34 (br, 2H), 4.43-4.75 (br, 4H), 8.53 (s, 1H). ^{13}C-NMR (125 MHz, TFE-d_3, δ, ppm): 18.47, 20.23, 38.51, 46.48, 46.95, 55.89, 62.81, 64.91, 65.94, 67.36, 67.88, 126.34, 131.34, 138.27, 140.01, 161.35, 179.79, 180.62. ^{31}P-NMR (202 MHz, TFE-d_3, δ, ppm): -2.79.

- **Synthesis of polyMPC-*b*-poly(butyl methacrylate) (polyMPC-BMA) (P35)**

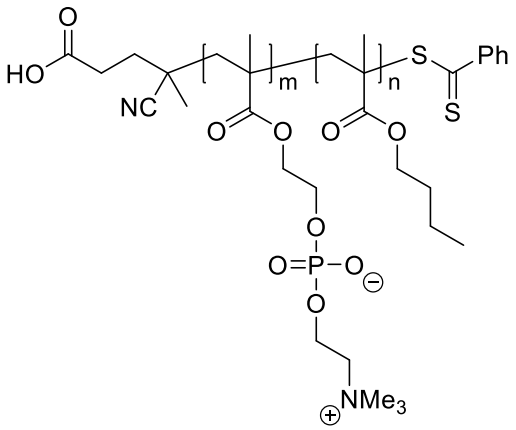

A polyMPC-*b*-poly(butyl methacrylate) (polyMPC-BMA) copolymer (**P35**) was prepared by chain extension using polyMPC macro-CTA **P31**. In a 7 mL vial charged with a stir bar, **P31** (439.3 mg, 0.022 mmol), BMA (140 µL, 0.88 mmol), and ACVA (1.23 mg, 0.0044 mmol) were dissolved in MeOH (1.76 mL). The solution was purged with nitrogen gas at room temperature for approximately 15 minutes, and was heated at 70 °C to initiate polymerization. After 18 hours, the solution was opened to ambient atmosphere and precipitated in THF (30 mL). The crude polymer was isolated by centrifugation (3000 rpm) and dialyzed against water. Lyophilization afforded block copolymer **P35** as a pink solid in 81% yield. Incorporation of BMA into the copolymer structure was estimated by ^{1}H-NMR spectroscopy by comparing relative signal intensities at 1.37-1.74 ppm (CH_2—CH_2 in BMA) and 3.66-3.84 ppm (N—CH_2 in MPC). ^{1}H-NMR (500 MHz, MeOD-d_4, δ,

ppm): 0.73-1.21 (m, 7H), 1.37-1.74 (m, 4H), 1.74-2.20 (b, 2H), 3.32 (s, 9H), 3.76 (br, 2H), 3.98 (br, 2H), 4.09 (br, 2H), 4.24 (br, 2H), 4.34 (br, 2H), 7.38-7.94. ^{31}P-NMR (202 MHz, MeOD-d_4, δ, ppm): -0.47. $M_{n,\ TFE\ GPC}$ = 29,400 g/mol, PDI = 1.16.

- **General procedure for the synthesis of fluorescent polyMPC-TMZ random copolymers (P36, P37)**

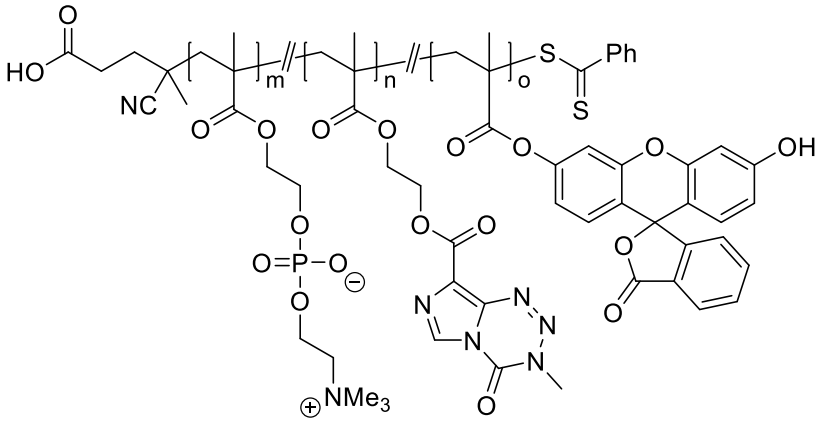

In a 7 mL vial charged with a stir bar, MPC and **TMZ-MA** were dissolved in TFE at a total monomer concentration of 0.75-1 M. Fluorescein *O*-methacrylate, 4-cyano-4-(phenylcarbonothioylthio)pentanoic acid (CTA), and ACVA were added to the solution, targeting $[monomer]_0$:$[fluorescein\ O\text{-}methacrylate]_0$:$[CTA]_0$:$[ACVA]_0$ of 102:1:1:0.2. The solution was degassed at 0 °C with nitrogen gas for approximately 15 minutes, and was heated at 70 °C, protected from light, to initiate polymerization. Upon reaching monomer conversion >75% (estimated using ^{1}H-NMR spectroscopy), the polymerization was quenched in liquid nitrogen and exposed to air. The crude polymer was purified by precipitation from TFE into THF (6 times), isolated by centrifugation (2000 rpm), and dried under vacuum. The polymer pellet was purified by centrifugal dialysis against 0.1 M HCl (aq) as described previously for polyMPC-TMZ copolymers **P27**-**P30**. Fluorescein-containing polymers **P36** and **P37** were isolated by lyophilization (protected from light)

and isolated as yellow and red solids, respectively, in yields of 55-59%. Incorporation of **TMZ-MA** into the copolymer structure was estimated by ^{1}H-NMR spectroscopy by comparing relative signal intensities at 8.58 ppm (C—*H* in TMZ) and 2.87-3.35 ppm (N—(C*H*$_3$)$_3$ in MPC). Fluorescein incorporation was estimated by fluorescence spectroscopy: **P36** = 0.067 weight percent; **P37** = 0.068 weight percent. **P36**: $M_{n,\ TFE\ GPC}$ = 37,300 g/mol, PDI = 1.19. **P37**: $M_{n,\ TFE\ GPC}$ = 37,000 g/mol, PDI = 1.20.

- **Synthesis of fluorescent polyMPC (P38)**

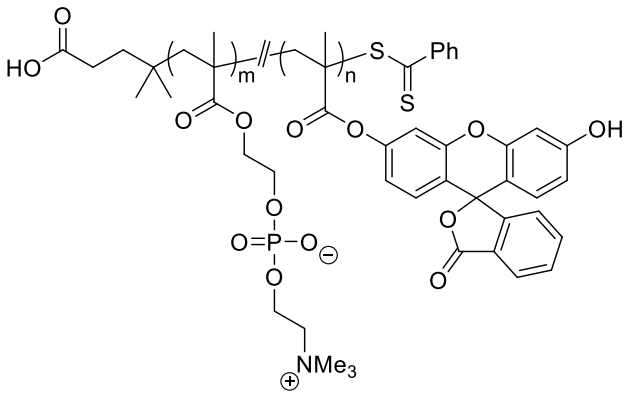

In a 7 mL vial charged with a stir bar, MPC (993.2 mg, 3.36 mmol), fluorescein *O*-methacrylate (14.0 mg, 0.035 mmol), 4-cyano-4-(phenylcarbonothioylthio)pentanoic acid (18.7 mg, 0.067 mmol), and ACVA (3.6 mg, 0.013 mmol) were dissolved in TFE (4.46 mL). The solution was purged at room temperature with nitrogen gas, and was heated at 70 °C, protected from light, to initiate polymerization. A monomer conversion of 67% was achieved in 5.5 hours, and the polymerization solution was quenched in liquid nitrogen and was exposed to air. The crude polymer was repeatedly precipitated into THF to remove unreacted monomer, and was isolated by centrifugation. The polymer was dialyzed against

water, protected from the light, and isolated by lyophilization. Fluorescent **P38** was isolated as a light-yellow solid in 38% yield. M_n of the polyMPC macro-CTA was estimated using ^{1}H-NMR spectroscopy by comparing signal intensities at 3.64-3.84 ppm (C*H*$_2$—N) (PC methylene protons) to that of the terminal phenyl protons (7.41-7.96 ppm). Fluorescein incorporation was estimated by fluorescence spectroscopy: **P38** = 0.32 weight percent. ^{1}H-NMR (500 MHz, MeOD-d$_4$, δ, ppm): 0.65-1.62 (br, 3H), 1.66-2.20 (br, 2H), 3.79-3.39 (s, 9H), 3.64-3.84 (br, 2H), 3.99-4.16 (br, 2H), 4.16-4.29 (br, 2H), 4.29-4.42 (br, 2H), 7.41-7.96. ^{31}P-NMR (202 MHz, MeOD-d$_4$, δ, ppm): -0.47 ppm. $M_{n,\ NMR}$ = 24,500 g/mol, $M_{n,\ TFE\ GPC}$ = 21,000, PDI = 1.13.

- **General procedure for the synthesis of fluorescent polyMPC-TMZ block copolymers (P39, P40)**

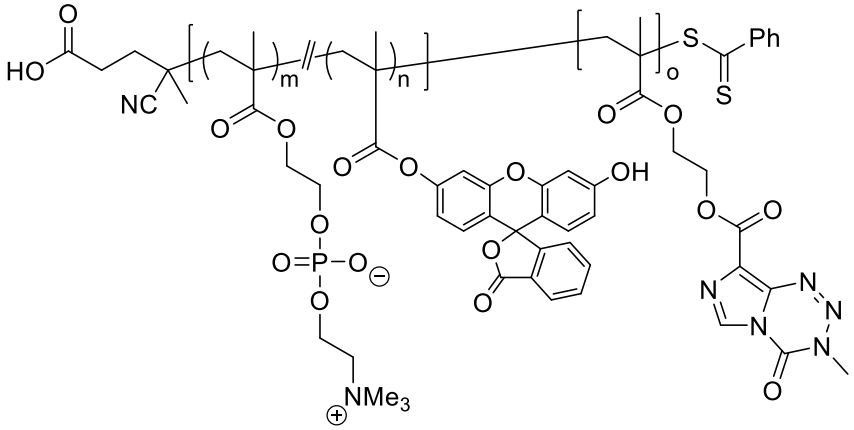

In a 7 mL vial charged with a stir bar, fluorescent polyMPC macro-CTA **P38**, **TMZ-MA**, and ACVA were dissolved in TFE ([**TMZ-MA**] = 0.25 M), targeting [ACVA]$_0$:[**P38**]$_0$: = 0.2:1 and [**TMZ-MA**]$_0$:[**P31**]$_0$ of 18 (**P39**) or 49 (**P40**). The mixture was purged with nitrogen gas at 0 °C for 15 minutes, then stirred at 70 °C, protected from the light, to initiate polymerization. At monomer conversion >85%, judged using ^{1}H-NMR spectroscopy, the

mixture was quenched in liquid nitrogen and was exposed to air. The crude polymers were then purified in similar fashion as block copolymers **P32**-**P34**. Lyophilization afforded polymers **P39** and **P40** in yields of 45-66%. Incorporation of **TMZ**-**MA** into the copolymer structure was estimated by ^{1}H-NMR spectroscopy by comparing relative signal intensities at 8.64 ppm (C—*H* in TMZ) and 2.88-3.49 ppm (N—(C*H*$_3$)$_3$ in MPC). Fluorescein incorporation was estimated by fluorescence spectroscopy: **P39** = 0.032 weight percent; **P40** = 0.021 weight percent. ^{1}H-NMR (500 MHz, TFE-d$_3$, δ, ppm): -0.33-1.58 (br, 6H), 1.61-2.30 (br, 4H), 2.88-3.49 ppm (s, 9H), 3.62 (br, 2H), 3.95 (s, 3H), 4.05-4.34 (br, 4H), 4.42 (br, 2H), 4.53-4.82 (br, 4H), 8.64 (s, 1H). ^{31}P-NMR (202 MHz, TFE-d$_3$, δ, ppm): -2.61.

- **Critical micelle concentration (CMC) measurements of P7-P11**

Polymer solutions of varying concentrations were prepared in water with a total volume of 1 mL. 5 µL of a stock solution of pyrene in acetone ([pyrene] = 1.2 x 10^{-4} M) was then added to each polymer solution (final [pyrene] = 6.0 x 10^{-7} M). Solutions were incubated for approximately 18 hours at room temperature. Excitation spectra were recorded from 300 to 360 nm, at a scan rate of 100 nm/s, with emission set to 394 nm. CMC values were determined by plotting that ratio of fluorescence intensities at 339 nm and 334 nm as a function of the log of the polymer concentration.

- **Critical aggregation concentration (CAC) measurements of P16-P20**

CAC values for PC-zwitteronics were estimated using a pyrene fluorescence assay.[6] A pyrene solution (10 µL) with a concentration of 120 µM was added to serial dilutions of

block copolymers **P16-P20** with concentrations ranging from 5 x 10^{-3} to 10 mg/mL and volumes of 2 mL. The resulting suspensions, with a pyrene concentration of ~0.6 µM, were incubated at room temperature for 16-18 hours protected from light. Using an excitation wavelength of 336 nm and a scanning rate of 600 nm/min, pyrene fluorescence emission spectra were recorded from 350-420 nm. CAC values were determined by plotting the ratio of fluorescence intensities for the first (I_1, λ_{em} ~ 374 nm) and third (I_3, λ_{em} ~ 385 nm) vibronic bands as a function of the log of the polymer concentration.

- **CAC measurements of P30 and P32-P34**

CAC values for polyMPC-TMZ copolymers were estimated using DLS.[11] Polymer suspensions with concentrations of 0.001-5 mg/mL were prepared in pH 7.4 PBS and passed through 0.45 µm cellulose acetate membranes into disposable cuvettes. The suspensions were analyzed by DLS at 37 °C using a fixed laser attenuator and position of 9 and 3.00 mm, respectively. Three measurements were made for each suspension, with each measurement consisting of 10 runs. CAC values were estimated by plotting scattering intensity as a function of polymer concentration.

- **Pendant drop IFT measurements of zwitterionic polysiloxanes P7-P11**

1 mg/mL solutions of zwitterionic siloxane polymers in water were prepared and added to glass cuvettes. For each polymer, a TCB droplet was dispensed into the solution using a syringe pump and the TCB droplet shape was recorded as a function of time. Interfacial tension was measured every 60 seconds for 1,800 seconds, and equilibrium surface tensions (γ_{eq}) were obtained by averaging the values from 1,500 to 1,800 seconds.

- **Surface tensiometry of PC-zwitteronics P16-P20**

Equilibrium room temperature surface tension values (γ_{eq}) were measured for polymer suspensions prepared in Milli-Q® ultrapure water (18.2 MΩ • cm) at concentrations of 0.1-10 mg/mL. Suspensions of the PPO starting material and **P16-P20** were cooled in an ice/water/sodium chloride bath prior to surface tension measurements to ensure complete polymer dispersion. The polymer suspensions (~350 µL) were added to clean glass troughs, and changes in surface tension (γ) were measured using a metal probe (diameter = 0.51 mm) inserted into each suspension. For each suspension, γ was allowed to equilibrate for at least 10 minutes and values were recorded every second. Reported values of γ_{eq} are the average of γ values over the final five minutes of each experiment.

- **DLS of zwitterionic polysiloxanes P7-P11**

1 mg/mL aqueous solutions of the zwitterionic polysiloxanes were filtered through 0.45 µm cellulose acetate membranes into clean, disposable cuvettes. DLS measurements were performed at 20 °C with an equilibration time of 1 minute. Solutions were measured three times, with each measurement consisting of 10 runs.

- **DLS of PC-zwitteronic block copolymers**

Zwitteronic block copolymer suspensions with concentrations of 1 mg/mL were cooled below their LCST in an ice/water/sodium chloride bath for 5 minutes to ensure complete polymer dispersion, and the cooled suspensions were quickly filtered through 0.45 µm membranes previously cooled at -20 °C into disposable cuvettes. Hydrodynamic diameters

were then estimated by DLS at 25 °C; three measurements consisting of 10 runs were performed for each suspension.

- **DLS of polyMPC 24 and polyMPC-Dox P26**

2 mg/ml solutions of **P24** and **P26** in pH 7.4 PBS were filtered through 0.45 μm cellulose acetate membranes into disposable cuvettes. These solutions were then analyzed by DLS at 25 °C, with an equilibration time of 1 minute. The suspensions were measured three times, with each measurement consisting of 10 runs.

- **DLS of polyMPC-TMZ copolymers P27-P30 and P32-P34**

1 mg/mL suspensions of polyMPC-TMZ copolymers **P27-P30** and **P32-P34** were prepared in pH 7.4 PBS. The suspensions were passed through 0.45 μm cellulose acetate filters into disposable cuvettes, and analyzed by DLS at 37 °C. Three measurements were made for each suspension, with measurements consisting of 10 runs each.

- **Lower critical solution temperature measurements for PC-zwitteronics P16-P20**

The LCST miscibility of PC-zwitteronic (**P16-P20**) suspensions was probed by measuring changes in turbidity as a function of temperature. Polymer suspensions with a concentration of 10 mg/mL were cooled in an ice/water/sodium chloride bath to ensure polymer dispersion and were added to glass cuvettes in a temperature-controlled holder. The suspensions were then cooled from 20 °C to -10 °C at a rate of 1 °C/min under a light nitrogen flow, and transmission at $\lambda = 550$ nm was recorded. LCST values are reported as the onset of increasing transmittance.

- **TEM of zwitterionic polysiloxanes**

Structures formed by the aqueous assembly of PC-containing siloxane block copolymers were visualized by TEM. Block copolymer solutions in pure water (at > CMC) were dropcast onto 400 square mesh carbon-coated copper grids, and allowed to dry under ambient conditions.

- **TEM of crosslinked, functional zwitteronic nanoparticles**

Aqueous suspensions of crosslinked **P22** and **P23** nanoparticles, with concentrations of 1 mg/mL, were dropcast onto PELCO® carbon-coated 300 mesh copper grids. Excess suspension was wicked away with filter paper, and the resulting films were allowed to dry overnight under ambient conditions.

- **Cryo-TEM of polyMPC-TMZ block copolymer P34**

Nanoparticles formed from polyMPC-TMZ block copolymer **P34** were visualized using cryo-TEM. A suspension of **P34** was prepared in pure water with a concentration of 1 mg/mL and was filtered through a 0.45 μm cellulose acetate filter. The suspension was cast onto a carbon-coated 400 mesh copper grid and blotted six times in a humidity controlled environment (~90% humidity) to remove excess suspension. The grid was plunged into liquid ethane and the vitrified **P34** nanoparticles were visualized at -180 °C using a liquid nitrogen cryo-transfer holder.

- **Measurement of Dox loading in polyMPC-Dox P26**

Dox loading in **P26** was determined using UV-Vis spectroscopy. Absorbances of aqueous solutions of Dox•HCl (0.01 mg/ml) and **P26** (0.1 mg/ml) were measured at 480 nm. Using the molar absorptivity of Dox•HCl in water, Dox concentration in the polymer prodrug was calculated using Beer-Lambert analysis.

- **Cell culture of SKOV-3 cells**

Human ovarian adenocarcinoma SKOV-3 cells were maintained in RPMI-1640 medium supplemented with 10% fetal bovine serum, 100U/mL penicillin, and 100μg/mL streptomycin at 37^{o}C under 5% CO_2.

- **Maximum tolerated dose of polyMPC P24 and polyMPC-Dox P26**

The maximum tolerated dose (MTD) is the greatest amount of drug that can be tolerated without evidence of toxicity. The MTD of the polymer carrier, **P24**, and the polymer-Dox conjugate, **P26**, were evaluated in 7-week-old NOD SCID mice. For polymer **P24**, three mice per treatment group were administered two lateral tail vein injections, at Day 0 and 17, of polymer solutions in HBSS at doses of 50, 100, 200, 400 or 800 mg/kg. Solutions of **P26** in HBSS at Dox equivalent doses of 10, 20, 30, 40 or 50 mg/kg (3 mice per group) was administered via a single lateral tail vein injection. Weight, appearance and behavior of the mice were monitored daily for a total of 35 days. Symptoms of toxicity were defined as weight loss greater than 15% or evidence of distress in appearance or behavior; animals exhibiting these criteria were euthanized prior to the end of the study. At the completion of the study, the remaining mice were euthanized. Necropsy was then performed to collect

tissues for histologic evaluation, following which paraffin embedded tissue samples were stained with hematoxylin and eosin (H&E).

- **Biodistribution of polyMPC-Dox P26**

The uptake and accumulation of Dox within tumor tissue and off-target organs was evaluated in four-week-old NOD SCID mice for free Dox and prodrug **P26**. SKOV-3 ovarian human adenocarcinoma subcutaneous xenografts were established following injection of $1x10^7$ cells in the right flanks of nine mice. Following tumor establishment and growth to a volume of 100-500mm^3 (calculated by length × width^2 / 2), mice were administered HBSS (control), prodrug **P26** (6 mg/kg Dox equivalent), or free Dox (6 mg/kg) by lateral tail vein injection (3 mice per group). Three days after the injections, the mice were euthanized and organs (liver, kidneys, spleen, heart, lungs) and tumor were resected, weighed, and then flash frozen in liquid nitrogen. All tissues were stored at -80°C prior to analysis.

Dox accumulation in the resected tissues was assessed by HPLC. Tumor and organs were homogenized in a 3 mL solution of acidified isopropanol (90% isopropanol + 75 mM HCl) using a BioSpec Tissue Tearor set at maximum speed. The homogenized suspensions were incubated at 4°C for approximately 24 hours and then were centrifuged at 1,500 x g for 15 minutes. 50 µL of each isolated supernatant was evaporated overnight under a stream of nitrogen and the residue was resuspended in 50 µL of HPLC mobile phase (40/60 acetonitrile/water + 1% trifluoroacetic acid). The suspensions were centrifuged at 12,000 rpm for 30 minutes at room temperature to precipitate residual

organic matter and the supernatants were analyzed by HPLC to determine Dox concentration.

- **Tumor Efficacy of polyMPC-Dox P26**

The therapeutic efficacy of prodrug **P26** was evaluated using a human ovarian tumor model in NOD SCID mice. Human ovarian tumors were established by injecting $1x10^7$ SKOV-3 cells subcutaneously in the right flanks of 24 four-week-old NOD SCID mice. Mice identified to have intramuscular tumors were excluded from analysis. Once tumors reached a volume of 250-500 mm^3, the mice were randomly divided into three groups (7-8 mice per group) and treated either with HBSS (control), half of the established MTD of free Dox (2 mg/kg),[9] or half of the experimentally determined Dox equivalent MTD of **P26** (5 mg/kg). Mice were treated via lateral tail vein injections every 7-8 days. Treatment was withheld if the animals exhibited significant weight loss approaching 20% or excessive injection site scarring prohibited further injections. The animals were evaluated every 24-48 hours for overall health, tumor volume and weight. Mice were removed from the study and euthanized if they experienced weight loss greater than 20%, exhibited signs of distress or if tumor volume exceeded 1,500 mm^3. At time of euthanasia, necropsy was performed and tumors and organs (liver, kidneys, spleen, heart and lungs) were collected for histologic evaluation, following which paraffin embedded tissue samples were stained with H&E.

- **Statistical analysis of the *in vivo* evaluations of polyMPC-Dox P26**

Statistical analysis was performed using GraphPad Prism Software (Prism, GraphPad Software, Inc., San Diego, CA). For the biodistribution study of, an unpaired T-test was used to compare Dox accumulation in the organs and tumors of mice treated with free Dox and polyMPC-Dox **P26**. For the tumor efficacy study, log-rank comparison (Mantel-Cox test) was first employed to compare survival curves of the three treatment groups, following which, pairwise comparisons between treatment groups were performed. Given the small sample sizes of the biodistribution and efficacy studies, $\alpha \leq 0.10$ was utilized as the threshold for statistical significance.

- **Measuring the solution stability of TMZ and polyMPC-TMZ copolymers P27-P30 and P32-P34**

The stability of TMZ and polyMPC-TMZ copolymers was evaluated at physiological conditions using UV-Vis spectroscopy. Solutions of TMZ and polyMPC-TMZ copolymers **P27**-**P30** and **P32**-**P34** were prepared in pH 7.4 PBS at a concentration of 1 mg/mL. The solutions were diluted to an approximate TMZ-equivalent concentration of 0.013 mg/mL and transferred to quartz cuvettes charged with stir bars. Solutions were incubated at 37 °C while stirring at 500 rpm in the UV-Vis spectrometer, and absorbance spectra (λ = 200-450 nm) were collected over a total of 6, 23, and 33 hours for TMZ, **P27**-**P30**, and **P32**-**P34**, respectively. The decrease in absorbance intensity at λ = 328-330 nm, corresponding to the urea of intact TMZ, was measured, and exponential decay curves were generated from plotting the normalized absorbance (A/A_0). Fitting these curves gave the decay constant, which was used to determine the $t_{1/2}$ of free TMZ and polyMPC-TMZ copolymers.

- **Cell culture of U87MG and T98G cells**

U87MG and T98G glioblastoma cells were cultured in DMEM supplemented with 10% FBS and 1x antibiotic-antimycotic solution at 37 °C under 5% CO_2.

- **Cellular uptake of fluorescent polyMPC-TMZ copolymers P36, P37, P39, and P40 in U87MG glioblastoma cells**

Cellular internalization of polyMPC-TMZ copolymers was evaluated in U87MG glioblastoma cells using confocal microscopy. U87MG cells were plated on 35 mm dishes with glass microwells and incubate overnight. The cells were then incubated at 37 °C with solutions of fluorescent polyMPC-TMZ copolymers (**P36**, **P37**, **P39**, **P40**) in DMEM containing 10% FBS at a 200 μM TMZ-equivalent concentration. Cells were also treated with a 0.35 mg/mL solution of fluorescent polyMPC **P38** in DMEM containing 10% FBS. After 3 hours, the cells were washed three times with pH 7.4 PBS and treated with 50 mM of Lysotracker® Red for 10 minutes to stain lysosomes. The cells were washed three times with PBS, fixed with paraformaldehyde (4% in pH 7.4 PBS) for 15 minutes, washed three times with PBS, and treated with aqueous DAPI to stain nuclei. The cells were visualized by fluorescence confocal microscopy using the following excitation and emission wavelengths: λ_{ex} = 405 nm, λ_{em} = 450 nm (DAPI); λ_{ex} = 488 nm, λ_{em} = 525 nm (fluorescein); λ_{ex} = 561 nm, λ_{em} = 595 nm (Lysotracker® Red).

- **Flow cytometry**

Cellular internalization of polyMPC-TMZ copolymers by U87MG glioblastoma cells was quantified using confocal microscopy. U87MG cells were grown in T-25 tissue culture

flasks and treated with solutions of fluorescein-labeled polyMPC-TMZ (**P36**, **P37**, **P39**, **P40**) at TMZ-equivalent doses of 200 μM in DMEM containing 10% FBS, or a 0.35 mg/mL solution of polyMPC **P38** in DMEM containing 10% FBS. Cells were incubated for 2 hours at 37 °C, then trypsinised and washed with PBS. Fluorescein fluorescence was then measured by flow cytometry.

- ***In vitro* cytotoxicity of polyMPC-TMZ copolymers P27-P30 and P32-P34**

The *in vitro* cytotoxicity of polyMPC-TMZ copolymers was evaluated in TMZ-sensitive U87MG and TMZ-resistant T98G glioblastoma cells. Cytotoxicity assays were performed by seeding and incubating approximately 1-2 x 10^3 cells in 96-well plates overnight. The cells were then incubated with solutions of TMZ (diluated from DMSO into a mixture of DMEM supplemented with 10% FBS) or polyMPC-TMZ copolymers in DMEM containing 10% FBS, respectively, at TMZ-equivalent concentrations ranging from 1 to 20,000 μM. As controls, cells were treated with a 25.9 mg/mL solution of polyMPC in DMEM containing 10% FBS. For cytoxicity experiments utilizing O^6-BG, O^6-BG was added to cells from a concentrated DMSO stock solution. After 6 days, cell viability was measured using a CellTiter-Glo® luminescence assay following manufacturer instructions. Luminescence was measured on a FLUOstar OPTIMA plate reader, and cell viability was calculated relative to untreated cells. Dose response curves and IC_{50} values were calculated using GraphPad Prism 7 software.

7.4 References

1. Wong, K. E.; Mora, M .C.; Skinner, M.; Page, S. M.; Crisi, G. M.; Arenas, R. B.; Schneider, S. S.; Emrick, T. Evaluation of PolyMPC-Dox Prodrugs in a Human Ovarian Tumor Model. *Mol. Pharmaceutics* **2016**, *13*, 1679-1687.

2. Boehm, P.; Mondeshki, M.; Frey, H. Polysiloxane-Backbone Block Copolymers in a One-Pot Synthesis: A Silicone Platform for Facile Functionalization. *Macromol. Rapid Commun*. **2012**, *33*, 1861-1867.

3. Goda, T.; Tabata, M.; Sanjoh, M.; Uchimura, M.; Iwasaki, Y.; Miyahara, Y. Thiolated 2-Methacryloyloxyethyl Phosphorylcholine for an Antifouling Biosensor Platform. *Chem. Commun.* **2013**, *49*, 8683-8685.

4. Robinson, K. L.; de Paz-Báñez, M. V.; Wang, X. S.; Armes, S. P. Synthesis of Well-Defined, Semibranched, Hydrophilic—Hydrophobic Block Copolymers Using Atom Transfer Radical Polymerization. *Macromolecules* **2001**, *34*, 5799-5805.

5. Hu, G.; Emrick, T. Functional Choline Phosphate Polymers. *J. Am. Chem. Soc.* **2016**, *138*, 1828-1831.

6. Kalyanasundaram, K.; Thomas, J. K. Environmental Effects on Vibronic Band Intensities in Pyrene Monomer Fluorescence and Their Application in Studies of Micellar Systems. *J. Am. Chem. Soc.* **1977**, *99*, 2039-2044.

7. Chen X, Parelkar S, Henchey E, Schneider S, Emrick T. PolyMPC-Doxorubicin Prodrugs. *Bioconjugate Chem*. **2012**, *23*, 1753-1763.

8. Page, S. M.; Henchey, E.; Chen, X.; Schneider, S.; Emrick, T. Efficacy of PolyMPC-DOX Prodrugs in 4T1 Tumor-Bearing Mice. *Mol. Pharmaceutics*. **2014**, *11*, 1715-1720.

9. Kratz, F.; Mansour, A.; Soltau, J.; Warnecke, A.; Fichtner, I.; Unger, C.; Drevs, J. Development of Albumin-Binding Doxorubicin Prodrugs that are Cleaved by Prostate-Specific Antigen. *Arch. Pharm.* **2005**, *338*, 462-472.
10. Arrowsmith, J.; Jennings, S. A.; Clark, A. S.; Stevens, M. F. G. Antitumor Imidazotetrazines. 41. Conjugation of the Antitumor Agents Mitozolomide and Temozolomide to Peptides and Lexitropsins Bearing DNA Major and Minor Groove-Binding Structural Motifs. *J. Med. Chem.* **2002**, *45*, 5458-5470.

11. Topel, O.; Çakir, A.; Budama, L.; Hoda, N. Determination of Critical Micelle Concentration of Polybutadiene-*block*-Poly(etheylene oxide) Diblock Copolymer by Fluorescence Spectroscopy and Dynamic Light Scattering. *J. Mol. Liq.* **2013**, *177*, 40-43.

BIBLIOGRAPHY

Adamson, C.; Kanu, O. O.; Mehta, A. I.; Di, C.; Lin, N.; Mattox, A. K.; Bigner, D. D. Glioblastoma Multiforme: A Review of Where We Have Been and Where We Are Going. *Expert. Opin. Investig. Drugs* **2009**, *18*, 1061-1083.

Aghi, M.; Rabkin, S.; Martuza, R. L. Effect of Chemotherapy-Induced DNA Repair on Oncolytic Herpes Simplex Viral Replication. *J. Natl. Cancer Inst.* **2006**, *98*, 38-50.

Alexandridis, P.; Athanassiou, V.; Fukuda, S.; Hatton, T. A. Surface Activity of Poly(ethylene oxide)-*block*-Poly(propylene oxide)-*block*-Poly(ethylene oxide) Copolymers. *Langmuir* **1994**, *10*, 2604-2612.

Alexandridis, P.; Hatton, T. A. Poly(ethylene oxide)-Poly(propylene oxide)-Poly(ethylene oxide) Block Copolymer Surfactants in Aqueous Solutions and at Interfaces: Thermodynamics, Structure, Dynamics, and Modeling. *Colloids Surfaces A: Physicochem. Eng. Aspects* **1995**, *96*, 1-46.

Almgren, M.; Brown, W.; Hvidt, S. Self-Aggregation and Phase-Behavior of Poly(ethylene oxide)-Poly(propylene oxide)-Poly(ethylene oxide) Block Copolymers in Aqueous Solution. *Colloid Polym. Sci.* **1995**, *273*, 2-15.

Alonso, M. M.; Gomez-Manzano, C.; Bekele, B. N.; Yung, W. K.; Fueyo, J. Adenovirus-Based Strategies Overcome Temozolomide Resistance by Silencing the O6-Methylguanine-DNA Methyltransferase Promoter. *Cancer Res.* **2007**, *67*, 11499-11504.

Amado, E.; Augsten, C.; Mäder, K.; Blume, A.; Kressler, J. Amphiphilic Water Soluble Triblock Copolymers Based on Poly(2,3-dihydroxypropyl methacrylate) and Poly(propylene oxide): Synthesis by Atom Transfer Radical Polymerization and Micellization in Aqueous Solutions. *Macromolecules* **2006**, *39*, 9486-9496.

Amiji, M.; Park, K. Prevention of Protein Adsorption and Platelet Adhesion on Surfaces by PEO/PPO/PEO Triblock Copolymers. *Biomaterials* **1992**, *13*, 682-692.

Appel, E. A.; Rowland, M. J.; Loh, X. J.; Heywood, R. M.; Watts, C.; Scherman, O. A. Enhanced Stability and Activity of Temozolomide in Primary Glioblastoma Multiforme Cells with Cucurbit[*n*]uril. *Chem. Commun.* **2012**, *48*, 9843-9845.

Armstrong, J. K.; Hempel, G.; Koling, S.; Chan, L. S.; Fisher, T.; Meiselman, H. J.; Garratty, G. Antibody Against Poly(ethylene glycol) Adversely Affects PEG-Asparginase Therapy in Acute Lymphoblastic Leukemia Patients. *Cancer* **2007**, *110*, 103-111.

Aroui, S.; Ram, N.; Appaix, F.; Ronjat, M.; Kenani, A.; Pirollet, F.; De Waard, M. Maurocalcin as a Non Toxic Drug Carrier Overcomes Doxorubicin Resistance in the Cancer Cell Line MDA-MB 231. *Pharm. Res.* **2009**, *26*, 836-845.

Arrowsmith, J.; Jennings, S. A.; Clark, A. S.; Stevens, M. F. G. Antitumor Imidazotetrazines. 41. Conjugation of the Antitumor Agents Mitozolomide and Temozolomide to Peptides and Lexitropsins Bearing DNA Major and Minor Groove-Binding Structural Motifs. *J. Med. Chem.* **2002**, *45*, 5458-5470.

Arrowsmith, J.; Jennings, S. A.; Langnel, D. A. F.; Wheelhouse, R. T.; Stevens, M. F. G. Antitumor Imidazotetrazines. Part 39. Synthesis of Bis(imidazotetrazine)s with Saturated Spacer Groups. *J. Chem. Soc., Perkin Trans. 1* **2000**, *1*, 4432-4438.

Babu, N. J.; Sanphui, P.; Nangia, A. Crystal Engineering of Stable Temozolomide Cocrystals. *Chem. Asian J.* **2012**, *7*, 2274-2285.

Baer, J. C.; Freeman, A. A.; Newlands, E. S.; Watson, A. J.; Rafferty, J. A.; Marglson, G. P. Depletion of O6-Alkylguanine-DNA Alkyltransferase Correlates with Potentiation of Temozolomide and CCNU Toxicity in Human Tumour Cells. *Br. J. Cancer* **1993**, *67*, 1299-1302.

Bahadur, P.; Riess, G. Block Copolymers: A Special Class of Surfactants. *Tenside Surfact. Det.* **1991**, *28*, 173-179.

Ballabh, P.; Braun, A.; Nedergaard, M. The Blood-Brain Barrier: An Overview: Structure, Regulation, and Clinical Implications. *Neurobiol. Dis.* **2004**, *16*, 1-13.

Barenholtz, Y. Doxil®—The First FDA-Approved Nano-Drug: Lessons Learned. *J. Control. Release* **2013**, *160*, 117-134.

Batrakova, E. V.; Kabanov, A. V. Pluronic Block Copolymers: Evolution of Drug Delivery Concept from Inert Nanocarriers to Biological Response Modifiers. *J. Control. Release* **2008**, *130*, 98-106.

Berrocal, A.; Perrez Segura, P.; Gil, M.; Balanã, C.; Garcia Lopez, J.; Yaya, R.; Rodríguez, J.; Reynes, G.; Gallego, O.; Iglesias, L. Extended-schedule Dose-dense Temozolomide in Refractory Gliomas. *J. Neuro-Oncol.* **2010**, *96*, 417-422.

Bertucci, A.; Prasetyanto, E. A.; Septiadi, D.; Manicardi, A.; Brognara, E.; Gambari, R.; Corradini, R.; De Cola, L. Combined Delivery of Temozolomide and Anti-miR221 PNA Using Mesoporous Silica Nanoparticles Induces Apoptosis in Resistant Glioma Cells. *Small* **2015**, *11*, 5687-5695.

Bhuchar, N.; Deng, Z.; Ishihara, K.; Narain, R. Detailed Study of the Reversible Addition-Fragmentation Chain Transfer Polymerization and Co-Polymerization of 2-Methacryloyloxyethyl Phosphorylcholine. *Polym. Chem.* **2011**, *2*, 632-639.

Bobola, M. S.; Tseng, S. H.; Blank, A.; Berger, M. S.; Silber, J. R. Role of O6-Methylguanine-DNA Methyltransferase in Resistance of Human Brain Tumor Cell Lines to the Clinically Relevant Methylating Agents Temozolomide and Streptozotocin. *Clin. Cancer Res.* **1996**, *2*, 735-741.

Boehm, P.; Mondeshki, M.; Frey, H. Polysiloxane-Backbone Block Copolymers in a One-Pot Synthesis: A Silicone Platform for Facile Functionalization. *Macromol. Rapid Commun*. **2012**, *33*, 1861-1867.

Braverman, O.; Feinshtein, R.; Weisman, A.; Kaspi, J. Temozolomide Storage System. U.S. Patent 20060222792 A1, October 5, 2006.

Bromberg, L. E.; Ron, E. S. Temperature-Responsive Gels and Thermogelling Polymer Matrices for Protein and Peptide Delivery. *Adv. Drug Deliv. Rev.* **1998**, *31*, 197-221.

Chang, C-C.; Letteri, R.; Hayward, R.; Emrick, T. Functional Sulfobetaine Polymers: Synthesis and Salt-Responsive Stabilization of Oil-in-Water Droplets. *Macromolecules* **2015**, *48*, 7843-7850.

Chen, C-Y.; Wang, H-L. Dual Thermo- and pH-Responsive Zwitterionic Sulfobetaine Copolymers for Oral Delivery System. *Macromol. Rapid Commun.* **2014**, *35*, 1534-1540.

Chen, M.; Briscoe, W. H.; Armes, S. P.; Klein, J. Lubrication at Physiological Pressures by Polyzwitterionic Brushes. *Science* **2009**, *323*, 1698-1701.

Chen, X.; McRae, S.; Parelkar, S.; Emrick, T. Polymeric Phosphorylcholine-Camptothecin Conjugates Prepared by Controlled Free Radical Polymerization and Click Chemistry. *Bionconjug. Chem.* **2009**, *20*, 2331-2341.

Chen, X.; Parelkar, S. S.; Henchey, E.; Schneider, S.; Emrick, T. PolyMPC-Doxorubicin Prodrugs. *Bioconjugate Chem.* **2012**, *23*, 1753-1763.

Chiappetta, D. A.; Sosnik, A. Poly(ethylene oxide)-Poly(propylene oxide) Block Copolymer Micelles as Drug Delivery Agents: Improved Hydrosolubility, Stability and Bioavailability of Drugs. *Eur. J. Pharm. Biopharm.* **2007**, *66*, 303-317.

Choi, H-J.; Brooks, E.; Montemagno, C. D. Synthesis and Characterization of Nanoscale Biomimetic Polymer Vesicles and Polymer Membranes for Bioelectronic Applications. *Nanotechnology* **2005**, *16*, S143-S149.

Choi, W. I.; Tae, G.; Kim, Y. H. One Pot, Single Phase Synthesis of Thermo-Sensitive Nano-Carriers by Photo-Crosslinking of a Diacrylated Pluronic. *J. Mater. Chem.* **2008**, *18*, 2769-2774.

Chojnowski, J.; Cypryk, M.; Fortuniak, W.; Rózga-Wijas, K.; Ścibiorek, M. Controlled Synthesis of Vinylmethylsiloxane-Dimethylsiloxane Gradient, Block and Alternate Copolymers by Anionic ROP of Cyclotrisiloxanes. *Polymer* **2002**, *43*, 1993-2001.

Custers, J. P. A.; van den Broeke, L. J. P.; Keurentjes, J. T. F. Phase Behavior and Micellar Properties of Carboxylic Acid End Group Modified Pluronic Surfactants. *Langmuir* **2007**, *23*, 12857-12863.

Dahanayake, M.; Rosen, M. J. *Structure/Performance Relationships in Surfactants*; **1984**; 49-59.

De Bonis, P.; Anile, C.; Pompucci, A.; Fiorentino, A.; Balducci, M.; Chiesa, S.; Maira, G.; Mangiola, A. Safety and Efficacy of Gliadel Wafers fo Newly Diagnosed and Recurrent Glioblastoma. *Acta Neurochir*. **2012**, *154*, 1371-1378.

Deng, C. C.; Brooks, W. L. A.; Abboud, K. A.; Sumerlin, B. S. Boronic Acid-Based Hydrogels Undergo Self-Healing at Neutral and Acidic pH. *ACS Macro Lett*. **2015**, *4*, 220-224.

Dolan, M. E.; Pegg, A. E. O^6-Benzylguanine and Its Role in Chemotherapy. *Clin. Cancer Res.* **1997**, *3*, 837-847.

Doncom, K. E. B.; Warren, N. J.; Armes, S. P. Polysulfobetaine-Based Diblock Copolymer Nano-Objects *via* Polymerization-Induced Self-Assembly. *Polym. Chem.* **2015**, *6*, 7264-7273.

Doncom, K. E. B.; Willcock, H.; O'Reilly, R. K. The Direct Synthesis of Sulfobetaine-Containing Amphiphilic Block Copolymers and Their Self-Assembly Behavior. *Eur. Polym. J.* **2017**, *87*, 497-507.

Donovan, M. S.; Sumerlin, B. S.; Lowe, A. B.; McCormick, C. L. Controlled/"Living" Polymerization of Sulfobetaine Monomers Directly in Aqueous Media via RAFT. *Macromolecules* **2002**, *35*, 8663-8666.

Du, J.; O'Reilly, R. K. Advances and Challenges in Smart and Functional Polymer Vesicles. *Soft Matter* **2009**, *5*, 3544-3561.

Du, Z.; Qin, J.; Wang, W.; Zhu, Y.; Wang, G. Synthesis, Surface Activities, and Aggregation Behaviors of Butynediol-ethoxylate Modified Polysiloxanes. *J. Phys. Chem. B* **2015**, *119*, 14180-14187.

Duffy, D. C.; McDonald, J. C.; Schueller, O. J.; Whitesides, G. M. Rapid Prototyping of Microfluidic Systems in Poly(dimethylsiloxane). *Anal. Chem.* **1998**, *70*, 4974-4984.

Duval, M.; Waton, G.; Schosseler, F. Temperature-Induced Growth of Wormlike Copolymer Micelles. *Langmuir* **2005**, *21*, 4904-4911.

El-Kamel, A. H. In Vitro and In Vivo Evaluation of Pluronic F127-based Ocular Delivery Systems for Timolol Maleate. *Int. J. Pharm.* **2002**, *241*, 47-55.

Engin, K.; Leeper, D. B.; Cater, J. R.; Thistlethwaite, A. J.; Tupchong, L.; McFarlane, J. D. Extracellular pH Distribution in Human Tumors. *Int. J. Hyperthermia*. **1995**, *11*, 211-216.

Fang, C.; Wang, K.; Stephen, Z. R.; Mu, Q.; Kievit, F. M.; Chiu, D. T.; Press, O. W.; Zhang, M. Temozolomide Nanoparticles for Targeted Glioblastoma Therapy. *ACS Appl. Mater. Interfaces* **2015**, *7*, 6674-6682.

FernLey, G. W. Zwitterionic Surfactants: Structure and Performance. *J. Am. Oil Chem. Soc.* **1978**, *55*, 98-103.

Filpula, D.; Zhao, H. Releasable PEGylation of Proteins with Customized Linkers. *Adv. Drug Deliv. Rev.* **2008**, *60*, 29-49.

Fourniols, T.; Randolph, L. D.; Staub, A.; Vanvarenberg, K.; Leprince, J. G.; Préat, V.; des Rieux, A.; Danhier, F. Temozolomide-Loaded Photopolymerizable PEG-DMA-Based Hydrogel for the Treatment of Glioblastoma. *J. Control. Release* **2015**, *210*, 95-104.

Fox, M. E.; Szoka, F. C.; Fréchet, J. M. J. Soluble Polymer Carriers for the Treatment of Cancer: The Importance of Molecular Architecture. *Acc. Chem. Res.* **2009**, *42*, 1141-1151.

Gal, Y-S.; Jin, S-H.; Lim, K. T.; Kim, S-H.; Koh, K. Synthesis and Electro-Optical Properties of Self-Doped Ionic Conjugated Polymers: Poly[2-ethynyl-*N*-(4-sulfobutyl)pyridinium betaine]. *Curr. Appl. Phys.* **2005**, *5*, 38-42.

Garay, R.P.; El-Gewely, R.; Armstrong, J. K.; Garratty, G.; Richette, P. Antibodies Against Polyethylene Glycol in Healthy Subjects and in Patients Treated with PEG-Conjugated Agents. *Expert Opin. Drug Deliv.* **2012**, *9*, 1319-1323.

Geldenhuys, W.; Mbimba, T.; Bui, T.; Harrison, K.; Sutariya, V. Brain-Targeted Delivery of Paclitaxel Using Glutathione-Coated Nanoparticles for Brain Cancers. *J. Drug Target* **2011**, *19*, 837-845.

Gelderblom, H.; Verweij, J.; Nooter, K.; Sparreboom, A. Cremophor EL: the Drawbacks of Vehicle Selection for Drug Formulation. *Eur. J. Cancer.* **2001**, *37*, 1590-1598.

Gilbert, M. R.; Wang, M.; Aldape, K. D.; Stupp, R.; Hegi, M. E.; Jaeckle, K. A.; Armstrong, T. S.; Wefel, J. S.; Won, M.; Blumenthanl, D. T.; Mahajan, A.; Schultz, C. J.; Erridge, S.; Baumert, B.; Hopkins, K. I.; Tzuk-Shina, T.; Brown, P. D.; Chakravarti, A.; Curran Jr., W. J.; Mehta, M. P. Dose-Dense Temozolomide for Newly Diagnosed Glioblastoma: A Randomized Phase III Clinical Trial. *J. Clin. Oncol*. **2013**, *31*, 4085-4091.

Goda, T.; Goto, Y.; Ishihara, K. Cell-Penetrating Macromolecules: Direct Penetration of Amphiphatic Phospolipid Polymers Across Plasma Membrane of Living Cells. *Biomaterials* **2010**, *31*, 2380-2387.

Goda, T.; Ishihara, K.; Miyahara, Y. Critical Update on 2-Methacryloyloxyethyl Phosphorylcholine (MPC) Polymer Science. *J. Appl. Polym. Sci.* **2015**, *132*, 41766.

Goda, T.; Konno, T.; Takai, M.; Moro, T.; Ishihara, K. Biomimetic Phosphorylcholine Polymer Grafting from Polydimethylsiloxane Surface Using Photo-Induced Polymerization. *Biomaterials* **2006**, *27*, 5151-5160.

Goda, T.; Tabata, M.; Sanjoh, M.; Uchimura, M.; Iwasaki, Y.; Miyahara, Y. Thiolated 2-Methacryloyloxyethyl Phosphorylcholine for an Antifouling Biosensor Platform. *Chem. Commun.* **2013**, *49*, 8683-8685.

Gonçalves, S.; Leirós, A.; van Kooten, T.; Dourado, F.; Rodrigues, L. R. Physicochemical and Biological Evaluation of Poly(ethylene glycol) Methacrylate Grafted Onto Poly(dimethylsiloxane) Surfaces for Prosthetic Devices. *Colloids Surf. B Biointerfaces* **2013**, *109*, 228-235.

Gou, P.; Liu, W.; Mao, W.; Tang, J.; Shen, Y.; Sui, M. Self-Assembling Doxorubicin Prodrug Forming Nanoparticles for Cancer Chemotherapy: Synthesis and Anticancer Study *In Vitro* and *In Vivo*. *J. Mater. Chem. B.* **2013**, *1*, 284-292.

Gouazé-Andersson, V.; Yu, J. Y.; Kreitenberg, A. J.; Bielawska, A.; Giuliano, A. E.; Cabot, M. C. Ceramide and Glucosylceramide Upregular Expression of the Multidrug Resistance Gene MDR1 in Cancer Cells. *Biochim. Biophys. Acta* **2007**, *1171*, 1407-1417.

Halacheva, S.; Rangelov, S.; Tsvetanov, C. Poly(glycidol)-Based Analogues to Pluronic Block Copolymers. Synthesis and Aqueous Solution Properties. *Macromolecules* **2006**, *39*, 6845-6852.

Halila, S.; Manguian, M.; Fort, S.; Cottaz, S.; Hamaide, T.; Fleury, E.; Driguez, H. Syntheses of Well-Defined Glyco-Polyorganosiloxanes by "Click" Chemistry and Their Surfactant Properties. *Macromol. Chem. Phys.* **2008**, *209*, 1282-1290.

Hasan, N.; Ohman, A. W.; Dinulescu, D. M. The Promise and Challenge of Ovarian Cancer Models. *Transl. Cancer. Res.* **2015**, *4*, 14-28.

Hassanzadeh, S.; Feng, Z.; Pettersson, T.; Hakkarainen, M. A Proof-of-Concept for Folate-Conjugated and Quercetin-Anchored Pluronic Mixed Micelles as Molecularly Modulated Polymeric Carriers for Doxorubicin. *Polymer* **2015**, *74*, 193-204.

Hayward, J. A.; Chapman, D. Biomembrane Surfaces as Models for Polymer Design: The Potential Haemocompatibility. *Biomaterials* **1984**, *5*, 135-142.

Hegi, M. E.; Diserens, A-C.; Gorlia, T.; Hamou, M-F.; de Tribolet, N.; Weller, M.; Kros, J. M.; Hainfellner, J. A.; Mason, W.; Mariani, L.; Bromberg, J. E. C.; Hau, P.; Mirimanoff, R. O.; Cairncross, J. G.; Janzer, R. C.; Stupp, R. *MGMT* Gene Silencing and Benefit from Temozolomide in Glioblastoma. *N. Engl. J. Med.* **2005**, *352*, 997-1003.

Houba, P. H. J.; Boven, E.; van der Meulen-Muileman, I. H.; Leenders, R. G. G.; Scheeren, J. W.; Pinedo, H. M.; Haisma, H. J. Pronounced Antitumor Efficacy of Doxorubicin When Given as the Prodrug DOX-GA3 in Combination with a Monoclonal Antibody β-Glucuronidase Conjugate. *Int. J. Oncol.* **2001**, *91*, 550-554.

Hoyle, C. E.; Bowman, C. N. Thiol-Ene Click Chemistry. *Angew. Chem. Int. Ed.* **2010**, *49*¸1540-1573.

Hu, G.; Emrick, T. Functional Choline Phosphate Polymers. *J. Am. Chem. Soc.* **2016**, *138*, 1828-1831.

Hu, G.; Parelkar, S. S.; Emrick, T. A Facile Approach to Hydrophilic, Reverse Zwitterionic, Choline Phosphate Polymers. *Polym. Chem.* **2015**, *6*, 525-530.

Injac, R.; Strukelj, B. Recent Advances in Protection Against Doxorubicin-Induced Toxicity. *Technol. Cancer Res. Treat.* **2008**, *7*, 497-516.

Ishihara, K. Highly Lubricated Polymer Interfaces for Advanced Artificial Hip Joints through Biomimetic Design. *Polym. J.* **2015**, *47*, 585-597.

Ishihara, K. New Polymeric Biomaterials—Phospholipid Polymers with a Biocompatible Surface. *Front Med. Biol. Eng.* **2000**, *10*, 83-95.

Ishihara, K.; Mu, M.; Konno, T.; Inoue, Y.; Fukazawa. The Unique Hydration State of. Poly(2-methacryloyloxyethyl phosphorylcholine). *J. Biomater. Sci. Polym. Ed.* **2017**, *28*, 884-899.

Ishihara, K.; Nomura, H.; Mihara, T.; Kurita, K.; Iwasaki, Y.; Nakabayashi, N. Why Do Phospholipid Polymers Reduce Protein Adsorption? *J. Biomed. Mater. Res.* **1998**, *39*, 323-330.

Ishihara, K.; Ueda, T.; Nakabayashi, N. Preparation of Phospholipid Polymers and Their Properties as Polymer Hydrogel Membranes. *Polym. J.* **1990**, *22*, 355-360.

Iwasaki, Y.; Ishihara, K. Cell Membrane-Inspired Phospholipid Polymers for Developing Medical Devices with Excellent Biointerfaces. *Sci. Tech. Adv. Mater.* **2012**, *13*, 064101.

Iwasaki, Y.; Ishihara, K. Phosphorylcholine-Containing Polymers for Biomedical Applications. *Anal. Bioanal. Chem.* **2005**, *381*, 534-546.

Jasinski, F.; Lobry, E.; Tarablsi, B.; Chemtob, A.; Croutxé-Barghorn, C.; Nouen, D. L.; Criqui, A. Light-Mediated Thiol-Ene Polymerization in Miniemulsion: A Fast Route to Semicrystalline Polysulfide Nanoparticles. *ACS Macro. Lett.* **2014**, *3*, 958-962.

Jauch, T.; Hau, P.; Bogdahn, U. Re-challenge with Temozolomide (TMZ) at Recurrence in High-Grade Gliomas (HGG). *J. Clin. Oncol*. **2007**, *25*, 2034.

Jeong, B.; Bae, Y. H.; Kim, S. W. Thermoreversible Gelation of PEG-PLGA-PEG Triblock Copolymer Aqueous Solutions. *Macromolecules* **1999**, *32*, 7064-7069.

Jerschow, P. *Silicone Elastomers*; Smithers Rapra: Schrewsbury, 2001; Vol. 12; p 5.

Johnston, T. P.; Punjabi, M. A.; Froelich, C. J. Sustained Delivery of Interleukin-2 from a Poloxamer 407 Gel Matrix Following Intraperitoneal Injection in Mice. *Pharm. Res.* **1992**, *9*, 425-434.

Joralemon, M. J.; McRae, S.; Emrick, T. PEGylated Polymers for Medicine: From Conjugation to Self-Assembled Systems. *Chem. Commun.* **2010**, *46*, 1377-1393.

Joshi, M.; Sodhi, K. S.; Pandey, R.; Singh, J.; Goyal, S.; Prasad, S.; Kaur, H.; Bhaskar, N.; Mahajan. Cancer Chemotherapy and Hepatotoxicity: An Update. *IAJPS*. **2014**, *4*, 2976-2984.

Kabanov, A. V.; Batrakova, E. V.; Miller, D. W. Pluronic® Block Copolymers as Modulators of Drug Efflux Transporter Activity in the Blood-Brain Barrier. *Adv. Drug Deliv. Rev.* **2003**, *55*, 151-164.

Kabanov, A. V.; Lemieux, P.; Vinogradov, S.; Alakhov, V. Pluronic® Block Copolymers: Novel Functional Molecules for Gene Therapy. *Adv. Drug Deliv. Rev.* **2002**, *54*, 223-233.

Kalyanasundaram, K.; Thomas, J. K. Environmental Effects on Vibronic Band Intensities in Pyrene Monomer Fluorescence and Their Application in Studies of Micellar Systems. *J. Am. Chem. Soc.* **1977**, *99*, 2039-2044.

Kamigaito, M.; Ando, T.; Sawamoto, M. Metal-Catalyzed Living Radical Polymerization. *Chem. Rev*. **2001**, *101*, 3689-3745.

Kannan, R.; Kuhlenkamp, J. F.; Jeandidier, E.; Trinh, H.; Ookhtens, M.; Kaplowitz, N. Evidence for Carrier-Mediated Transport of Glutathione Across the Blood-Brain Barrier in the Rat. *J. Clin. Invest.* **1990**, *85*, 2009-2013.

Kane, R. S.; Takayama, S.; Ostuni, E.; Ingber, D. E.; Whitesides, G. M. Patterning Proteins and Cells Using Soft Lithography. *Biomaterials* **1999**, *20*, 2363-2376.

Kanzawa, T.; Bedwell, J.; Kondo, Y.; Kondo, S.; Germano, I. M. Inhibition of DNA Repair for Sensitizing Resistant Glioma Cells to Temozolomide. *J. Neurosurg*. **2003**, *99*, 1047-1052.

Kanzawa, T.; Germano, I. M.; Kondo, Y.; Ito, H.; Kyo, S.; Kondo, S. Inhibition of Telomerase Activity in Malignant Glioma Cells Correlates with Their Sensitivity to Temozolomide. *Br. J. Cancer***2003**, *89*, 922-929.

Karim, R.; Palazzo, C.; Evrard, B.; Piel, G. Nanocarriers for the Treatment of Glioblastoma Multiforme: Current State-of-the-Art. *J. Control. Release* **2016**, *227*, 23-37.

Kato, M.; Kamigaito, M.; Sawamoto, M.; Higashimura, T. Polymerization of Methyl Methacrylate with the Carbon Tetrachloride/Dichlorotris-(Triphenylphosphine)ruthenium(II)/Methylaluminum Bis(2,6-di-tert-butylphenoxide) Initiating System: Possibility of Living Radical Polymerization. *Macromolecules* **1995**, *28*, 1721-1723.

Kevill, D. N.; Anderson, S. W. An Improved Scale of Solvent Nucleophilicity Based on the Solvolysis of the S-methyldibenzothiophenium Ion. *J. Org. Chem.* **1991**, *56*, 1845-1850.

Khandare, J.; Minko, T. Polymer-Drug Conjugates: Progress in Polymeric Prodrugs. *Prog. Polym. Sci.* **2006**, *31*, 359-397.

Kim, S-S.; Rait, A.; Kim, E.; DeMarco, J.; Pirollo, K. F.; Chang, E. H. Encapsulation of Temozolomide in a Tumor-Targeting Nanocomplex Enhances Anti-Cancer Efficacy and Reduces Toxicity in a Mouse Model of Glioblastoma. *Cancer Lett.* **2015**, *369*, 250-258.

King, S. M.; Heenan, R. K.; Cloke, V. M.; Washington, C. Neutron Scattering from a Poly(oxyethylene)-Poly(oxypropylene)-Poly(oxyethylene) Copolymers in Dilute Aqueous Solution under Shear Flow. *Macromolecules* **1997**, *30*, 6215-6222.

Kita-Tokarczyk, K.; Grumelard, J.; Haefele, T.; Meier, W. Block Copolymer Vesicles—Using Concepts from Polymer Chemistry to Mimic Biomembranes. *Polymer* **2005**, *46*, 3540-3569.

Ko, D. Y.; Patel, M.; Jung, B. K.; Park, J. H.; Jeong, B. Phosphorylcholine-Based Zwitterionic Biocompatible Thermogel. *Biomacromoelcules* **2015**, *16*, 3853-3862.

Kobayashi, M.; Terayama, Y.; Yamaguchi, H.; Terada, M.; Murakami, D.; Ishihara, K.; Takahara, A. Wettability and Antifouling Behavior on the Surfaces of Superhydrophilic Polymer Brushes. *Langmuir* **2012**, *28*, 7212-7222.

Konno, T.; Watanabe, J.; Ishihara, K. Enhanced Solubility of Paclitaxel Using Water-Soluble and Biocompatible 2-Methacryloyloxyethyl Phosphorylcholine Polymers. *J. Biomed. Mater. Res.* **2003**, *65A*, 209-214.

Kozlov, M. Y..; Melik-Nubarov, N. S.; Batrakova, E. V.; Kabanov, A. V. Relationship Between Pluronic Block Copolymer Structure, Critical Micellization Concentration and Partitioning Coefficients of Low Molecular Mass Solutes. *Macromolecules* **2000**, *33*, 3305-3313.

Kratz, F.; Mansour, A.; Soltau, J.; Warnecke, A.; Fichtner, I.; Unger, C.; Drevs, J. Development of Albumin-Binding Doxorubicin Prodrugs that are Cleaved by Prostate-Specific Antigen. *Arch. Pharm.* **2005**, *338*, 462-472.

Kratz, K.; Breitenkamp, K.; Hule, R.; Pochan, D.; Emrick, T. PC-Polyolefins: Synthesis and Assembly Behavior in Water. *Macromolecules* **2009**, *42*, 3227-3229.

Krumpfer, J. W.; McCarthy, T. J. Rediscovering Silicones: "Unreactive" Silcones React with Inorganic Surfaces. *Langmuir* **2011**, *27*, 11514-11519.

Kurzrock, R.; Goel, S.; Wheler, J.; Hong, D.; Fu, S.; Rezai, K.; Morgan-Linnell, S. K.; Urien, S.; Mani, S.; Chaudhary, I.; Ghalib, M. H.; Buchbinder, A.; Lokjec, F.; Mulcahy, M. Safety, Pharmacokinetics, and Activity of EZN-2208, a Novel Conjugate of Polyethylene Glycol and SN38, in Patients with Advanced Malignancies. *Cancer* **2012**, *118*, 6144-6151.

Landazuri, G.; Fernandez, V. V. A.; Soltero, J. F. A.; Rharbi, Y. Kinetics of the Sphere-to-Rod like Micelle Transition in a Pluronic Triblock Copolymer. *J. Phys. Chem. B.* **2012**, *116*, 11720-11727.

Larson, N.; Ghandehari, H. Polymeric Conjugates for Drug Delivery. *Chem. Mater.* **2012**, *24*, 840-853.

Laughlin, R. G. Fundamentals of the Zwitterionic Hydrophilic Group. *Langmuir* **1991**, *7*, 842-847.

Lee, S. Y. Temozolomide Resistance in Glioblastoma Multiforme. *Genes & Diseases* **2016**, *3*, 198-210.

Leng, C.; Hung, H-C.; Sun, S.; Wang, D.; Li, Y.; Jiang, S.; Chen, Z. Probing the Surface Hydration of Nonfouling Zwitterionic and PEG Materials in Contact with Proteins. *ACS Appl. Mater. Interfaces* **2015**, *7*, 16881-16888.

Li, D.; Li, C.; Wan, G.; Hou, W. Self-Assembled Vesicles of Amphiphilic Poly(dimethylsiloxane)-*b*-Poly(ethylene glycol) Copolymers as Nanotanks for Hydrophobic Drugs. *Colloids Surf. A* **2010**, *372*, 1-8.

Li, H.; Bian, S.; Huang, Y.; Liang, J.; Fan, Y.; Zhang, X. High Drug Loading pH-Sensitive Pullulan-DOX Conjugate Nanoparticles for Hepatic Targeting. *J. Biomed. Mater. Res. A.* **2014**, *102*, 150-159.

Li, Y.; Keefe, A. J.; Giarmarco, M.; Brault, N. D.; Jiang, S. Simple and Robust Approach for Passivating and Functionalizing Surfaces for Use in Complex Media. *Langmuir* **2012**, *28*, 9707-9713.

Liechty, W. B.; Kryscio, D. R.; Slaughter, B. V.; Peppas, N. A. Polymers for Drug Delivery Systems. *Annu. Rev. Chem. Biomol. Eng.* **2010**, *1*, 149-173.

Lin, Z.; Gao, W.; Hu, H.; Ma, K.; He, B.; Dai, W.; Wang, X.; Wang, J.; Zhang, X.; Zhang, Q. Novel Thermo-Sensitive Hydrogel System with Paclitaxel Nanocrystals: High Drug-loading, Sustained Drug Release and Extended Local Retention Guaranteeing Better Efficacy and Lower Toxicity. *J. Control. Release* **2014**, *174*, 161-170.

Liu, Y.; Lu, W-L.; Wang, J-C.; Zhang, X.; Zhang, H.; Wang, X-Q.; Zhou, T-Y.; Zhang, Q. Controlled Delivery of Recombinant Hirudin Based on Thermo-Sensitive Pluronic® F127 Hydrogel for Subcutaneous Administration: In Vitro and In Vivo Characterization. *J. Control. Release* **2007**, *117*, 387-395.

Lockman, P. R.; Oyewumi, M. O.; Koziara, J. M.; Roder, K. E.; Mumper, R. J.; Allen, D. D. Brain Uptake of Thiamine-Coated Nanoparticles. *J. Control. Release* **2003**, *93*, 271-282.

Lowe, A. B.; Billingham, N. C.; Armes, S. P. Synthesis and Properties of Low-Polydispersity Poly(sulfopropylbetaine)s and Their Block Copolymers. *Macromolecules* **1999**, *32*, 2141-2148.

Lowe, A. B.; Hoyle, C. E.; Bowman, C. N. Thiol-Yne Click Chemistry: A Powerful and Versatile Methodology for Materials Synthesis. *J. Mater. Chem.* **2010**, *20*, 4745-4750.

Lowe, A. B.; McCormick, C. L. Synthesis and Solution Properties of Zwitterionic Polymers. *Chem. Rev.* **2002**, *102*, 4177-4189.

Lu, C.; Mikhail, A. S.; Wang, X.; Brook, M. A.; Allen, C. Hydrogels Containing Core Cross-Linked Block Co-Polymer Micelles. *I. Biomater. Sci. Polym. Ed.* **2012**, *23*, 1069-1090.

Lunn, D. J.; Boott, C. E.; Bass, K. E.; Shuttleworth, T. A.; McCreanor, N. G.; Papadouli, S.; Manners, I. Controlled Thiol-Ene Functionalization of Polyferrocenylsilane-*block*-Polyvinylsiloxane Copolymers. *Macromol. Chem. Phys.* **2013**, *214*, 2813-2820.

Luxenhofer, R.; Schulz, A.; Li, S.; Bronich, T. K.; Batrakova, E. V.; Jordan, R.; Kabanov A. V. Doubly Amphiphilic Poly(2-oxazoline)s as High-Capacity Delivery Systems for Hydrophobic Drugs. *Biomaterials*. **2010**, *31*, 4972-4979.

Lv, C.; Su, Y.; Wang, Y.; Ma, X.; Sun, Q.; Jiang, Z. Enhanced Permeation Performance of Cellulose Acetate Ultrafiltration Membrane by Incorporation of Pluronic F-172. *J. Membrane Sci*. **2007**, *294*, 68-74.

Ma, I. Y.; Lobb, E. J.; Billingham, N. C.; Armes, S. P.; Lewis, A. L.; Lloyd, A. W. Synthesis of Biocompatible Polymers. 1. Homopolymerization of 2-Methacryloyloxyethyl Phosphorylcholine via ATRP in Protic Solvents: An Optimization Study. *Macromolecules* **2002**, *35*, 9306-9314.

Ma, Y.; Tang, Y.; Billingham, N. C.; Armes, S. P. Well-Defined Biocompatible Block Copolymers via Atom Transfer Radical Polymerization of 2-Methacryloyloxyethyl Phosphorylcholine in Protic Media. *Macromolecules* **2003**, *36*, 3475-3484.

Maeda, H.; Nakamura, H.; Fang, J. The EPR Effect for Macromolecular Drug Delivery to Solid Tumors: Improvement of Tumor Uptake, Lowering of Systemic Toxicity, and Distinct Tumor Imaging In Vivo. *Adv. Drug Deliv. Rev.* **2013**, *65*, 71-79.

Maeda, H.; Wu, J.; Sawa, T.; Matsumura, Y.; Hori, K. Tumor Vascular Permeability and the EPR Effect in Macromolecular Therapeutics: a Review. *J. Control. Release*. **2000**, *65*, 271-284.

Martino, A. D.; Kucharczyk, P.; Capakova, Z.; Humpolicek, P.; Sedlarik, V. Enhancement of Temozolomide Stability by Loading in Chitosan-Carboxylated Polylactice-Based Nanoparticles. *J. Nanopart. Res.* **2017**, *19*, 71-86.

Matsumura, Y.; Maeda, H. A New Concept for Macromolecular Therapeutics in Cancer Chemotherapy: Mechanism of Tumor Tropic Accumulation of Proteins and Antitumor Agents SMANCS. *Cancer Res.* **1986**, *46*, 6387-6392.

Matyjaszewski, K.; Xia, J. H. Atom Transfer Radical Polymerization. *Chem. Rev.* **2001**, *101*, 2921-2990.

McRae Page, S.; Martorella, M.; Parelkar, S.; Kosif, I.; Emrick, T. Disulfide Cross-Linked Phosphorylcholine Micelles for Triggered Release of Camptothecin. *Mol. Pharmaceutics* **2013**, *10*, 2684-2692.

Mellman, I.; Fuchs, R.; Helenius, A. Acidification of the Endocytic and Exocytic Pathways. *Annu. Rev. Biochem.* **1986**, *55*, 663-700.

Meng, Y.; Gu, D.; Zhang, F. Q.; Shi, Y. F.; Cheng, L.; Feng, D.; Wu, Z. X.; Chen, Z. X.; Wang, Y.; Stein, A.; Zhao, D. Y. A Family of Highly Ordered Mesoporous Polymer Resin and Carbon Structures from Organic-Organic Self-Assembly. *Chem. Mater*. **2006**, *18*, 4447-4464.

Mirzaei, S.; Khalilian, M. H.; Taherpour, A A. Mechanistic Study of the Hydrolytic Degradation and Protonation of Temozolomide. *RSC Adv.* **2015**, *5*, 41112-41119.

Miyata, R.; Ueda, M.; Jinno, H.; Konno, T.; Ishihara, K.; Ando, N; Kitagawa, Y. Selective Targeting by PreS1 Domain of Hepatitis B Surface Antigen Conjugated with Phosporylcholine-Based Amphiphilic Block Copolymer Micelles as a Biocompatible, Drug Delivery Carrier for Treatment of Human Hepatocellular Carcinoma with Paclitaxel. *Int. J. Cancer* **2009**, *15*, 2460-2467.

Mizerska, U.; Fortuniak, W.; Chojnowski, J.; Halasa, R.; Konopacka, A.; Werel, W. Polysiloxane Cationic Biocides with Imidazolium Salt (ImS) Groups, Synthesis and Antibacterial Properties. *Eur. Polym. J.* **2009**, *45*, 779-787.

Moad, G.; Rizzardo, E.; Thang, S. H. Radical Addition-Fragmentation Chemistry in Polymer Synthesis. *Polymer* **2008**, *49*, 1079-1131.

Moad, G.; Rizzardo, E.; Thang, S. H.; Toward Living Radical Polymerization. *Acc. Chem. Res.***2008**, *41*, 1133-1142.

Morisaku, T.; Watanabe, J.; Konno, T.; Takai, M.; Ishihara, K. Hydration of Phosphorylcholine Groups Attached to Highly Swollen Polymer Hydrogels Studied by Thermal Analysis. *Polymer* **2008**, *49*, 4652-4657.

Mortensen, K. Structural Studies of Aqueous Solutions of PEO-PPO-PEO Triblock Copolymers, Their Micellar Aggregates and Mesophases; a Small-Angle Neutron Scattering Study. *J. Phys.: Condens. Matter* **1996**, *8*, A103-A124.

Nair, D. P.; Podgórski, M.; Chatani, S.; Gong, T.; Xi, W.; Fenoli, C. R.; Bowman, C. N. The Thiol-Michael Addition Click Reaction: A Powerful and Widely Used Tool in Materials Chemistry. *Chem. Mater*. **2014**, *26*, 724-744.

National Cancer Institute. A Snapshot of Ovarian Cancer. http://www.cancer.gov/research/progress/snapshots/ovarian (accessed Sep 28, 2015).

Nardin, C.; Hirt, T.; Leukel, J.; Meier, W. Polymerized ABA Triblock Copolymer Vesicles. *Langmuir* **2000**, *16*, 1035-1041.

Newlands, E. S.; Blackledge, G. R. P.; Slack, J. A.; Rustin, G. J. S.; Smith, D. B.; Stuart, N. S. A.; Quarterman, C. P.; Hoffman, R.; Stevens, M. F. G.; Brampton, M. H.; Gibson, A. C. Phase I Trial of Temozolomide (CCRG 81045: M&B 39831: NSC 362856). *Br. J. Cancer* **1992**, *65*, 287-291.

Newlands, E. S.; Stevens, M. F. G.; Wedge, S. R.; Wheelhouse, R. T.; Brock, C. Temozolomide: A Review of its Discovery, Chemical Properties, Pre-Clinical Development and Clinical Trials. *Cancer Treat. Rev.* **1997**, *23*, 35-61.

Nguyen, L.; Hang, M.; Wang, W.; Tian, Y.; Wang, L.; McCarthy, T. J.; Chen, W. Simple and Improved Approaches to Long-Lasting, Hydrophilic Silicones Derived from Commercially Available Precursors. *ACS Appl. Mater. Interfaces* **2014**, *6*, 22876-22883.

Nicolson, P. C.; Vogt, J. Soft Contact Lens Polymers: An Evolution. *Biomaterials* **2001**, *22*, 3273-3283.

Nolan, S. L.; Phillips, R. J.; Cotts, P. M.; Dungan, S. R. Light Scattering Study on the Effect of Polymer Composition on the Structural Properties of PEO-PPO-PEO Micelles. *J. Colloid Interface Sci.* **1997**, *191*, 291-302.

Omuro, A.; DeAngeli, L. M. Glioblastoma and Other Malignant Gliomas. *JAMA* **2013**, *310*, 1842-1850.

O'Reilly, R. K.; Hawker, C. J.; Wooley, K. L. Cross-linked Block Copolymer Micelles: Functional Nanostructures of Great Potential and Versatility. *Chem. Soc. Rev.* **2006**, *35*, 1068-1083.

Ostrom, Q. T.; Gittleman, H.; Fulop, J.; Liu, M.; Blanda, R.; Kromer, C.; Wolinsky, Y.; Kruchko, C.; Barnholtz-Sloan, J. S. CBTRUS Statistical Report: Primary Brain and Central Nervous System Tumors Diagnosed in the United States in 2008-2012. *Neuro Oncol*. **2015**, *17*, iv1-iv62.

Özçam, A. E.; Efimenko, K.; Genzer, J. Effect of Ultraviolet/Ozone Treatment on the Surface and Bulk Properties of Poly(dimethylsiloxane) and Poly(vinylmethylsiloxane) Networks. *Polymer* **2014**, *55*, 3107-3119.

Page, S. M.; Henchey, E.; Chen, X.; Schneider, S.; Emrick, T. Efficacy of PolyMPC-DOX Prodrugs in 4T1 Tumor-Bearing Mice. *Mol. Pharmaceutics*. **2014**, *11*, 1715-1720.

Pasut, G.; Veronese, F. M. PEG Conjugates in Clinical Development or Use as Anticancer Agents: An Overview. *Adv. Drug Deliv. Rev.* **2009**, *61*, 1177-1188.

Patil, N.; Falentin-Daudré, C.; Jérôme, C.; Detrembleur, C. Mussel-Inspired Protein-Repelling Ambivalent Block Copolymers: Controlled Synthesis and Characterization. *Polym. Chem.* **2015**, *6*, 2919-2933.

Patil, R.; Portilla-Arias, J.; Ding, H.; Inoue, S.; Konda, B.; Hu, J.; Wawrowsky, K. A.; Shin, P. K.; Black, K. L.; Holler, E.; Ljubimova, J. Y. Temozolomide Delivery to Tumor Cells by a Multifunctional Nano Vehicle Based on Poly(β-L-malic acid). *Pharm. Res.* **2010**, *27*, 2317-2329.

Petrov, P.; Tsvetanov, C. B.; Jérôme, R. Two-Component "Onionlike" Micelles with a PPO Core, a PDMAEMA Shell and a PEO Corona: Formation and Crosslinking. *Polym. Int.* **2008**, *57*, 1258-1264.

Prhashanna, A.; Khan, S. A.; Chen, S. B. Micelle Morphology and Chain Conformation of Triblock Copolymers Under Shear: LA-DPD Study. *Colloids Surf., A* **2016**, *506*, 457-466.

Quinn, J. A.; Jiang, S. X.; Reardon, D. A.; Desjardins, A.; Vredenburgh, J. J.; Rich, J. N.; Gururangan, S.; Friedman, A. H.; Bigner, D. D.; Sampson, J. H.; McLendon, R. E.; Herndon II, J. E.; Walker, A.; Friedman, H. S. Phase II Trial of Temozolomide Plus O^6-Benzylguanine in Adults with Recurrent, Temozolomide-Resistant Malignant Glioma. *J. Clin. Oncol.* **2009**, *27*, 1262-1267.

Rahman, A. M.; Yusuf, S. W.; Ewer, M. S. Anthracycline-induced Cardiotoxicity and the Cardiac Sparing Effect of Liposomal Formulation. *Int. J. Nanomedicine*. **2007**, *2*, 567-583.

Rambarran, T.; Gonzaga, F.; Brook, M. A. Multifunctional Amphiphilic Siloxane Architectures Using Sequential, Metal-Free Click Ligations. *J. Polym. Sci. A Polym. Chem.* **2013**, *51*, 855-864.

Reddy, K. R.; Modi, M. W.; Pedder, S. Use of Peginterferon Alfa-2a (40KD) (Pegasys®) for the Treatment of Hepatitis C. *Adv. Drug Deliv. Rev.* **2002**, *54*, 571-586.

Rheingans, O.; Hugenberg, N.; Harris, J. R.; Fischer, K.; Maskos, M. Nanoparticles Built of Cross-Linked Heterotelechelic, Amphiphilic Poly(dimethylsiloxane)-*b*-Poly(ethylene oxide) Diblock Copolymers. *Macromolecules* **2000**, *33*, 4780-4790.

Richmond, A.; Su, Y. Mouse Xenograft Models vs GEM Models for Human Cancer Therapeutics. *Dis. Model Mech.* **2008**, *1*, 78-72.

Ringsdorf, H. Structure and Properties of Pharmacologically Active Polymers. *Journal of Polymer Science: Polymer Symposia* **1975**, *51*, 135-153.

Rivera, A. L.; Pelloski, C. E.; Gilbert, M. R.; Colman, H.; De La Cruz, C.; Sulman, E. P.; Bekele, B. N.; Aldape, K. D. MGMT Promoter Methylation is Predictive of Response to Radiotherapy and Prognostic in the Absence of Adjuvant Alkylating Chemotherapy for Giloblastoma. *Neuro Oncol*. **2010**, *12*, 116-121.

Robinson, K. L.; de Paz-Báñez, M. V.; Wang, X. S.; Armes, S. P. Synthesis of Well-Defined, Semibranched, Hydrophilic—Hydrophobic Block Copolymers Using Atom Transfer Radical Polymerization. *Macromolecules* **2001**, *34*, 5799-5805.

Rose, P. G. Pegylated Liposomal Doxorubicin: Optimizing the Dosing Schedule in Ovarian Cancer. *Oncologist*. **2005**, *10*, 205-214.

Rottenberg, D. A.; Ginos, J. Z.; Kearfott, K. J.; Junck, L.; Bigner, D. D. In Vivo Measurement of Regional Brain Tissue pH Using Positron Emission Tomography. *Ann. Neurol.* **1984**, *15*, S98-102.

Santa Chalarca, C. F.; Emrick, T. Reactive Polymer Zwitterions: Sulfonium Sulfonates. *J. Polym. Sci. A Poly. Chem.* **2017**, *55*, 83-92.

Sauvet, G.; Fortuniak, W.; Kazmierski, K.; Chojnowski, J. Amphiphilic Block and Statistical Siloxane Copolymers with Antimicrobial Activity. *J. Polym. Sci. A Polym. Chem.* **2003**, *41*, 2939-2948.

Schmolka, I. R. A Review of Block Polymer Surfactants. *J. Am. Oil Chem. Soc.* **1977**, *54*, 110-116.

Selan, L.; Palma, S.; Scoarughi, G. L.; Papa, R.; Veeh, R.; Clemente, D. D.; Artini, M. Phosphorylcholine Impairs Susceptibility to Biofilm Formation of Hydrogel Contact Lenses. *Am. J. Ophtholmal.* **2009**, *147*, 134-139.

Seo, J-H.; Matsuno, R.; Takai, M.; Ishihara, K. Cell Adhesion on Phase-Separated Surface of Block Copolymer Composed of Poly(2-methacryloyloxyethyl Phosphorylcholine) and Poly(dimethylsiloxane). *Biomaterials* **2009**, *30*, 5330-5340.

Shao, Q.; White, A. D.; Jiang, S. Difference in Hydration between Carboxybetaine and Sulfobetaine. *J. Phys. Chem. B* **2010**, *114*, 16625-16631.

She, W.; Li, N.; Luo, K.; Guo, C.; Wang, G.; Geng, Y.; Gu, Z. Dendronized Heparin-Doxorubicin Conjugate Based Nanoparticle as pH-Responsive Drug Delivery System for Cancer Therapy. *Biomaterials*. **2013**, *34*, 2252-2264.

Shim, G-s.; Manandhar, S.; Shin, D.; Kim, T-H.; Kwak, M-K. Acquisition of Doxorubicin Resistance in Ovarian Carcinoma Cells Accompanies Activation of the NRF2 Pathway. *Free Radic. Biol. Med.* **2009**, *47*, 1619-1631.

Silveira, C. P.; Apolinário, L. M.; Fávaro, W. J.; Paula, A. J.; Durán, N. Doxorubicin-Functionalized Silica Nanoparticles Incorporated into a Thermoreversible Hydrogel and Intraperitoneally Administered Result in High Prostate Antitumor Activity and Reduced Cardiotoxicity of Doxorubicin. *ACS Biomater. Sci. Eng.* **2016**, *2*, 1190-1199.

Singal, P.K.; Iliskovic, N. Doxorubicin-Induced Cardiomyopathy. *N. Engl. J. Med.* **1998**, *339*, 900-905.

Skinner, M.; Selhorst, R.; Emrick, T. Synthesis of Water-Soluble Zwitterionic Polysiloxanes. *J. Polym. Sci. A Polym. Chem.* **2016**, *1*, 127-134.

Skinner, M.; Ward, S. M.; Emrick, T. Versatile Synthesis of Polymer-Temozolomide Conjugates. *ACS Macro Lett.* **2017**, *6*, 215-218.

Smith, L.; Watson, M. B.; O'Kane, S. L.; Drew, P. J.; Lind, M. J.; Cawkwell, L. The Analysis of Doxorubicin Resistance in Human Breast Cancer Cells Using Antibody Microarrays. *Mol. Cancer Ther.* **2006**, *5*, 2115-2120.

Snow, S. A.; Fenton, W. N.; Owen, M. J. Synthesis and Characterization of Zwitterionic Silicone Sulfobetaine Surfactants. *Langmuir* **1990**, *6*, 385-391.

Song, H.; Zhang, J.; Wang, W.; Huang, P.; Zhang, Y.; Liu, J.; Li, C.; Kong, D. Acid-Responsive PEGylated Doxorubicin Prodrug Nanoparticles for Neuropilin-1 Receptor-Mediated Targeted Drug Delivery. *Colloids Surf., B.* **2015**, *136*, 365-374.

Stephen, Z. R.; Gebhart, R. N.; Jeon, M.; Blair, A. A.; Ellenbogen, R. G.; Silber, J. R.; Zhang, M. pH-Sensitive O6-Benzylguanosine Polymer Modified Magnetic Nanoparticles for Treatment of Glioblastomas. *Bioconjugate Chem.* **2017**, *28*, 194-202.

Stephen, Z. A.; Kievit, F. M.; Chiarelli, P. A.; Fang, C.; Wang, K.; Hatzinger, S. J.; Ellenbogen, R. G.; Silber, J. R.; Zhang, M. Redox-Responsive Magnetic Nanoparticle for Targeted Convection-Enhanced Delivery of O^6-Benzylguanine to Brain Tumors. *ACS Nano* **2014**, *8*, 10383-10395.

Stevens, M. F. G.; Hickman, J. A.; Langdon, S. P.; Chubb, D.; Vickers, L.; Stone, R.; Baig, G.; Goddard, C.; Gibson, N. W.; Slack, J. A.; Newton, C.; Lunt, E.; Fizames, C.; Lavelle, F. Antitumor Activity and Pharmacokinetics in Mice of 8-Carbamoyl-3-Methyl-Imidazo[5,1,*d*]-1,2,3,5-Tetrazin-4(3*H*)-One (CCRG 81045; M & B 39831), a Novel Drug with Potential as an Alternative to Dacarbazine. *Cancer Res.* **1987**, *47*, 5846-5852.

Strickley, R. G. Solubilizing Excipients in Oral and Injectable Formulations. *Pharmaceut. Res.* **2004**, *21*, 201-230.

Stupp, R.; Mason, W. P.; van den Bent, M. J.; Weller, M.; Fisher, B.; Taphoorn, M. J. B.; Belanger, K.; Brandes, A. A.; Marosi, C.; Bogdahn, U.; Curschmann, J.; Janzer, R. C.; Ludwin, S. K.; Gorlia, T.; Allgeier, A.; Lacombe, D.; Cairncross, G.; Eisenhauer, E.; Mirimanoff, R. O. Radiotherapy Plus Concomitant and Adjuvant Temozolomide for Glioblastoma. *N. Engl. J. Med.* **2005**, *352*, 987-996.

Sundy, J. S.; Baraf, H. S. B.; Yood, R. A.; Edwards, N. L.; Gutierrez-Urena, S. R.; Treadwell, E. L.; Vázquez-Mellado, J.; White, W. B.; Lipsky, P. E.; Horowitz, Z.; Huang, W.; Maroli, A. N.; Waltrip, R. W.; Hamburger, S. A.; Becker, M. A. Efficacy and Tolerability of Pegloticase for the Treatment of Chronic Gout in Patients Refractory to Conventional Treatment: Two Randomized Controlled Trials. *JAMA* **2011**, *306*, 711-720.

Takatori, Y.; Moro, T.; Ishihara, K.; Kamogawa, M.; Oda, H.; Umeyama, T.; Kim, Y. T.; Ito, H.; Kyomoto, M.; Tanaka, T. Clinical and Radiographic Outcomes of Total Hip Replacement with Poly(2-methacryloyloxyethyl phosphorylcholine)-Grafted Highly Cross-Linked Polyethylene Liners: Three-Year Results of a Prospective Consecutive Series. *Mod. Rheumatol*. **2015**, *25*, 286-291.

Tannock, I. F.; Rotin, D. Acid pH in Tumors and Its Potential for Therapeutic Exploitation. *Cancer Res.* **1989**, *49*, 4374-4384.

Tao, Y.; Han, J.; Ye, C.; Thomas, T.; Dou, H. Reduction-Responsive Gold-Nanoparticle-Conjugated Pluronic Micelles: An Effective Anti-Cancer Drug Delivery System. *J. Mater. Chem.* **2012**, *22*, 18864-18871.

Ten Tjie, A. J.; Verweij, J.; Loos, W. J.; Sparreboom A. Pharmacological Effects of Formulation Vehicles: Implications for Cancer Chemotherapy. *Clin. Pharmacokinet.* **2003**, *42*, 665-685.

Tolcher, A. W.; Gerson, S. L.; Denis, L.; Geyer, C.; Hammond, L. A.; Patnaik, A.; Goetz, A. D.; Schwartz, G.; Edwards, T.; Reyderman, L.; Statkevich, P.; Cutler, D. L.; Rowkinsky, E. K. *Br. J. Cancer* **2003**, *88*, 1004-1011.

Topel, O.; Çakir, A.; Budama, L.; Hoda, N. Determination of Critical Micelle Concentration of Polybutadiene-*block*-Poly(etheylene oxide) Diblock Copolymer by Fluorescence Spectroscopy and Dynamic Light Scattering. *J. Mol. Liq.* **2013**, *177*, 40-43.

Umeda, T.; Nakaya, T.; Imoto, M. The Convenient Preparation of a Vinyl Monomer Containing a Phospholipid Analogue. *Makromol. Chem., Rapid Commun.* **1982**, *3*, 457-459.

Uygun, M.; Tasdelen, M.; Yagci, Y. Influence of Type of Initiation on Thiol-Ene "Click" Chemistry. *Macromol. Chem. Phys.* **2010**, *211*, 103-110.

Veronese, F. M.; Schiavon, O.; Pasut, G.; Mendichi, R.; Andersson, L.; Tsirk, A.; Ford, J.; Wu, G.; Kneller, S.; Davies, J.; Duncan, R. PEG-Doxorubicin Conjugates: Influence of Polymer Structure on Drug Release, In Vitro Cytotoxicity, Biodistribution, and Antitumor Activity. *Bioconjugate Chem.* **2005**, *16*, 775-784.

Veyries, M. L.; Couarraze, G.; Geiger, S.; Agnely, F.; Massias, L.; Kunzil, B.; Faurisson, F.; Rouveix, B. Controlled Release of Vancomycin from Poloxamer 407 Gels. *Int. J. Pharm.* **1999**, *192*, 183-193.

Wang, D.; Kopečková, P.; Minko, T.; Nanayakkara, V.; Kopeček. Synthesis of Starlike *N*-(2-Hydroxypropyl)methacrylamide Copolymers: Potential Drug Carriers. *Biomacromolecules* **2000**, *1*, 313-319.

Wang, J-S.; Matyjaszewski, K. Controlled/"Living" Radical Polymerization. Atom Transfer Radical Polymerization in the Presence of Transition-Metal Complexes. *J. Am. Chem. Soc.* **1995**, *117*, 5614-5615.

Wang, L.; Yamauchi, Y. Block Copolymer Mediated Synthesis of Dendritic Platinum Nanoparticles. *J. Am. Chem. Soc.* **2009**, *131*, 9152-9153.

Wang, Y-C.; Xia, H.; Yang, X-Z.; Wang, J. Synthesis and Thermoresponsive Behaviors of Biodegradable Pluronic Analogs. *J. Polym. Sci. A Polym. Chem*. **2009**, *47*, 6168-6179.

Wedge, S. R.; Porteous, J. K.; May, B. L.; Newlands, E. S. Potentiation of Temozolomide and BCNU Cytotoxicity by O^6-Benzylguanine: A Comparative Study *In Vitro*. *Br. J. Cancer* **1996**, *73*, 482-490.

Wedge, S. R.; Porteous, J. K.; Newland, E. S. 3-Aminobenzamide and/or O^6-Benzylguanine Evaluated as an Adjuvant to Temozolomide or BCNU Treatment in Cell Lines of Variable Mismatch Repair Status and O^6-Alkylguanine-DNA Alkyltransferase Activity. *Br. J. Cancer* **1996**, *74*, 1030-1036.

Wei, L.; Cai, C.; Lin, J.; Chen, T. Dual-Drug Delivery System Based on Hydrogel/Micelle Composites. *Biomaterials* **2009**, *30*, 2606-2613.

Wei, Z.; Yang, J. H.; Zhou, J.; Xu, F.; Zrinyi, M.; Dussault, P. H.; Osada, Y.; Chen, Y. M. Self-Healing Gels Based on Constitutional Dynamic Chemistry and Their Potential Applications. *Chem. Soc. Rev.* **2014**, *43*, 8114-8131.

Wen, P. Y.; Kesari, S. Malignant Gliomas in Adults. *N. Engl. J. Med.* **2008**, *359*, 492-507.

Whelan, D. M.; van der Giessen, W. J.; Krabbendam, S. C.; van Vliet, E. A.; Verdouw, P. D.; Serruys, P. W.; van Beusekom, H. M. M. Biocompatibility of Phosphorylcholine Coated Stents in Normal Porcine Coronary Arteries. *Heart* **2000**, *83*, 338-345.

Wong, K. E.; Mora, M .C.; Skinner, M.; Page, S. M.; Crisi, G. M.; Arenas, R. B.; Schneider, S. S.; Emrick, T. Evaluation of PolyMPC-Dox Prodrugs in a Human Ovarian Tumor Model. *Mol. Pharmaceutics* **2016**, *13*, 1679-1687.

Woodfield, P. A.; Zhu, Y.; Pei, Y.; Roth, P. J. Hydrophobically Modified Sulfobetaine Copolymers with Tunable Aqueous UCST through Postpolymerization Modification of Poly(pentafluorophenyl acrylate). *Macromolecules* **2014**, *47*, 750-762.

Worm, M.; Kang, B.; Dingels, C.; Wurm, F. R. Acid-Labile Amphiphilic PEO-*b*-PPO-*b*-PEO Copolymers: Degradable Poloxamer Analogs. *Macrmol. Rapid Commun.* **2016**, *37*, 775-780.

Wick, A.; Felsberg, J.; Steinbach, J. P.; Herrlinger, U.; Platten, M.; Blaschke, B.; Meyermann, R.; Reifenberger, G.; Weller, M.; Wick, W. Efficacy and Tolerability of Temozolomide in an Alternating Weekly Regimen in Patients with Recurrent Glioma. *J. Clinc. Oncol.* **2007**, *25*, 3357-3361.

Wick, W.; Platten, M.; Weller, M. New (Alternative) Temozolomide Regimens for the Treatment of Glioma. *Neuro Oncol*. **2009**, *11*, 69-79.

Wick, W.; Steinbach, J. P.; Küker, W. M.; Dichgans, J.; Bamberg, M.; Weller, M. *Neurology* **2004**, *62*, 2113-2115.

Wu, A.; Loutherback, K.; Lambert, G.; Estévez-Salmerón, L.; Tlsty, T. D.; Austin, R. H.; Sturm, J. C. Cell Motility and Drug Gradients in the Emergence of Resistance to Chemotherapy. *Proc. Natl. Acad. Sci. U.S.A.* **2013**, *110*, 16103-16108.

Xiao, L.; Liu, C.; Zhu, J.; Pochan, D. J.; Jia, X. Hybrid, Elastomeric Hydrogels Crosslinked by Multifunctional Block Copolymer Micelles. *Soft Matter* **2010**, *6*, 5293-5297.

Xiao, L.; Zhu, J.; Londono, J. D.; Pochan, D. J.; Jia, X. Mechano-responsive Hydrogels Crosslinked by Block Copolymer Micelles. *Soft Matter* **2012**, *8*, 10233-10237.

Xiong, X. Y.; Tam, K. C.; Gan, L. H. Synthesis and Thermally Responsive Properties of Novel Pluronic F87/Polycaprolactone (PCL) Block Copolymers with Short PCL Blocks. *J. Appl. Polym. Sci.* **2006**, *100*, 4163-4172.

Yang, T-F.; Chen, C-N.; Chen, M-C. Lai, C-H.; Liang, H-F.; Sung, H-W. Shell-Crosslinked Pluronic L121 Micelles as a Drug Delivery Vehicle. *Biomaterials* **2007**, *28*, 725-734.

Yaseen, M.; Lu, J. R. The Structure of Zwitterionic Phosphocholine Surfactant Monolayers. *Langmuir* **2006**, *22*, 5825-5832.

Ye, S-H.; Johnson, C. A.; Woolley, J. R.; Murata, H.; Gamble, L. J.; Ishihara, K.; Wagner, W. R. Simple Surface Modification of a Titanium Alloy with Silanated Zwitterionic Phosphorylcholine or Sulfobetaine Modifiers to Reduce Thrombogenicity. *Colloids Surf. B Biointerfaces* **2010**, *79*, 357-364.

Yilgör, E.; Yilgör, I. Silicone Containing Copolymers: Synthesis, Properties and Applications. *Prog. Polym. Sci.* **2014**, *39*, 1165-1195.

Yoda, R. Elastomers for Biomedical Applications. *J. Biomater. Sci. Polym. Ed.* **1998**, *9*, 561-626.

Youngster, S.; Wang, Y. S.; Grace, M.; Bausch, J.; Bordens, R.; Wyss, D. F. Structure, Biology and Therapeutic Implications of Pegylated Interferon Alpha-2b. *Curr. Pharm. Des.* **2002**, *8*, 2139-2157.

Yuan, Y.; Zang, X.; Ai, F.; Zhou, J.; Shen, J.; Lin, S. Grafting Sulfobetaine Monomer onto Silicone Surface to Improve Haemocompatibility. *Polym. Int.* **2004**, *53*, 121-126.

Yusa, S-i; Fukuda, K.; Yamamoto, T.; Ishihara, K.; Morishima, Y. Synthesis of Well-Defined Amphiphilic Block Copolymers Having Phospholipid Polymer Sequences as a Novel Biocompatible Polymer Micelle Reagent. *Biomacromolecules* **2005**, *6*, 663-670.

Zhang, L.; Eisenberg, A. Multiple Morphologies and Characteristics of "Crew-Cut" Micelle-Like Aggregates of Polystyrene-*b*-Poly(acrylic acid) Diblock Copolymers in Aqueous Solutions. *J. Am. Chem. Soc.* **1996**, *118*, 3168-3181.

Zhang, J.; Stevens, M. F. G.; Bradshaw, T. D. Temozolomide: Mechanisms of Action, Repair and Resistance. *Curr. Mol. Pharmacol.* **2012**, *5*, 102-114.

Zhang, P.; Sun, F.; Liu, S.; Jiang, S. Anti-PEG Antibodies in the Clinic: Current Issues and Beyond PEGylation. *J. Control. Release* **2016**, *244*, 184-193.

Zhang, Q.; Tang, X.; Wang, T.; Yu, F.; Guo, W.; Pei, M. Thermo-Sensitive Zwitterionic Block Copolymers *via* ATRP. *RSC Adv*. **2014**, *4*, 24240-24247.

Zhang, X.; Dong, H.; Fu, S.; Zhong, Z.; Zhuo, R. Redox-Responsive Micelles with Cores Crosslinked via Click Chemistry. *Macromol. Rapid Commun*. **2016**, *37*, 993-997.

Zhang, Z.; Chao, T.; Liu, L.; Cheng, G.; Ratner, B. D.; Jiang, S. Zwitterionic Hydrogels: An In Vivo Implantation Study. *J. Biomater. Sci. Polym. Ed.* **2009**, *20*, 1845-1859.

Zhang, Z.; Chao, T.; Chen, S.; Jiang, S. Superlow Fouling Sulfobetaine and Carboxybetaine Polymers on Glass Slides. *Langmuir* **2006**, *22*, 10072-10077.

Zheng, P.; McCarthy, T. J. A Surprise from 1954: Siloxane Equilibration Is a Simple, Robust, and Obvious Polymer Self-Healing Mechanism. *J. Am. Chem. Soc.* **2012**, *134*, 2024-2027.